ISSN 0042-8469
e-ISSN 2217-4753
УДК 623 + 355/359

Вол. 68, бр. 4
2020

ВТГ

НАУЧНИ ЧАСОПИС МИНИСТАРСТВА ОДБРАНЕ И ВОЈСКЕ СРБИЈЕ

ВОЈНОТЕХНИЧКИ ГЛАСНИК

4 2020 ВОЈНОТЕХНИЧКИ ГЛАСНИК

втг.мо.упр.срб

www.vtg.mod.gov.rs

ISSN 0042-8469
e-ISSN 2217-4753
УДК 623 + 355/359

Том 68, № 4
2020

НАУЧНЫЙ ЖУРНАЛ МИНИСТЕРСТВА ОБОРОНЫ
И ВООРУЖЁННЫХ СИЛ РЕСПУБЛИКИ СЕРБИЯ

ВОЕННО-ТЕХНИЧЕСКИЙ ВЕСТНИК

ВТГ.МО.УПР.СРБ

www.vtg.mod.gov.rs

ВОЕННО-ТЕХНИЧЕСКИЙ ВЕСТНИК
4 2020

ISSN 0042-8469
e-ISSN 2217-4753
UDC 623 + 355/359

Vol. 68, Issue 4
2020

SCIENTIFIC JOURNAL OF THE MINISTRY OF DEFENCE AND SERBIAN ARMED FORCES

MILITARY TECHNICAL COURIER

4 2020 MILITARY TECHNICAL COURIER

ВТГ.МО.УПР.СРБ

www.vtg.mod.gov.rs

ISSN 0042-8469
e-ISSN 2217-4753
UDC 623 + 355/359

НАУЧНИ ЧАСОПИС МИНИСТАРСТВА ОДБРАНЕ И ВОЈСКЕ СРБИЈЕ

ВОЈНОТЕХНИЧКИ ГЛАСНИК

ВОЛУМЕН 68•БРОЈ 4•ОКТОБАР – ДЕЦЕМБАР 2020.

NAUČNI ČASOPIS MINISTARSTVA ODBRANE I VOJSKE SRBIJE

VOJNOTEHNIČKI GLASNIK

VOLUMEN 68•BROJ 4•OKTOBAR – DECEMBAR 2020.

ВТГ.МО.УПР.СРБ
www.vtg.mod.gov.rs
COBISS.SR-ID 4423938
DOI: 10.5937/VojnotehnickiGlasnik

ISSN 0042-8469
e-ISSN 2217-4753
UDC 623 + 355/359

НАУЧНЫЙ ЖУРНАЛ МИНИСТЕРСТВА ОБОРОНЫ И ВООРУЖЁННЫХ СИЛ РЕСПУБЛИКИ СЕРБИЯ

ВОЕННО-ТЕХНИЧЕСКИЙ ВЕСТНИК

ТОМ 68 • НОМЕР ВЫПУСКА 4 • ОКТЯБРЬ-ДЕКАБРЬ 2020.

SCIENTIFIC JOURNAL OF THE MINISTRY OF DEFENCE AND SERBIAN ARMED FORCES

MILITARY TECHNICAL COURIER

VOLUME 68 • ISSUE 4 • OCTOBER-DECEMBER 2020

ВТГ.МО.УПР.СРБ
www.vtg.mod.gov.rs
COBISS.SR-ID 4423938
DOI: 10.5937/VojnotehnickiGlasnik

Власници:
МИНИСТАРСТВО ОДБРАНЕ и ВОЈСКА СРБИЈЕ
Издавач:
УНИВЕРЗИТЕТ ОДБРАНЕ У БЕОГРАДУ
Ректор
Доц. др Горан Радовановић, генерал-потпуковник

Адреса редакције: ВОЈНОТЕХНИЧКИ ГЛАСНИК, Ветска Лукића Курјака 33, 11042 Београд
http://www.vtg.mod.gov.rs
http://aseestant.ceon.rs/index.php/vtg/issue/current
http://scindeks.nb.rs/journaldetails.aspx?issn=0042-8469
http://elibrary.ru/title_about.asp?id=53280
https://doaj.org/toc/2217-4753

e-mail: vojnotehnicki.glasnik@mod.gov.rs

Претплата на штампано издање: e-mail: vojnotehnicki.glasnik@mod.gov.rs; тел. 066/87-00-123

Рукописи се не враћају

Часопис излази тромесечно

Први штампани број *Војнотехничког гласника* објављен је 1. 1. 1953. године

Прво електронско издање *Војнотехничког гласника* на Интернету објављено је 1. 1. 2011. године

Војнотехнички гласник је лиценциран код EBSCO Publishing-a, највећег светског агрегатора часописа, периодике и осталих извора у пуном тексту. Комплетан текст *Војнотехничког гласника* доступан је у базама података EBSCO Publishing-a.

Штампа: Војна штампарија – Београд, Ресавска 40б, e-mail: vojna.stamparija@mod.gov.rs

Собственники:
МИНИСТЕРСТВО ОБОРОНЫ и ВООРУЖЁННЫЕ СИЛЫ РЕСПУБЛИКИ СЕРБИЯ
Издательство:
УНИВЕРСИТЕТ ОБОРОНЫ В Г. БЕЛГРАД
РЕКТОР
Генерал-лейтенант доц. д-р Горан Радованович

Адрес редакции: ВОЈНОТЕХНИЧКИ ГЛАСНИК, Ул. Велька Лукича Куряка 33, 11042 Белград,
Республика Сербия
http://www.vtg.mod.gov.rs
http://aseestant.ceon.rs/index.php/vtg/issue/current
http://scindeks.nb.rs/journaldetails.aspx?issn=0042-8469
http://elibrary.ru/title_about.asp?id=53280
https://doaj.org/toc/2217-4753
e-mail: vojnotehnicki.glasnik@mod.gov.rs
Подписка на печатную версию журнала: e-mail: vojnotehnicki.glasnik@mod.gov.rs; тел. +381 66 87 00 123
Присланные в редакцию журнала статьи не возвращаются.
Журнал выпускается ежеквартально.
Первый номер журнала «Военно-технический вестник» выпущен 1.1.1953 года.
Первая электронная версия журнала размещена на интернет странице 1.1.2011 года.
«Военно-технический вестник» включен в систему EBSCO – всемирная академическая база данных и сервисов.
Типография: Војна штампарија – Белград, Ресавска 40б, e-mail: vojna.stamparija@mod.gov.rs

Owners:
MINISTRY OF DEFENCE and SERBIAN ARMED FORCES

Publisher:
UNIVERSITY OF DEFENCE IN BELGRADE

Rector
Lieutenant General Goran Radovanović, PhD, Assistant Professor

Address: VOJNOTEHNIČKI GLASNIK/MILITARY TECHNICAL COURIER, Veljka Lukića Kurjaka 33, 11042 Belgrade, Republic of Serbia
http://www.vtg.mod.gov.rs/index-e.html
http://aseestant.ceon.rs/index.php/vtg/issue/current
http://scindeks.nb.rs/journaldetails.aspx?issn=0042-8469
http://elibrary.ru/title_about.asp?id=53280
https://doaj.org/toc/2217-4753

e-mail: vojnotehnicki.glasnik@mod.gov.rs

Subscription to print edition: e-mail: vojnotehnicki.glasnik@mod.gov.rs; Tel. +381 66 87 00 123

Manuscripts are not returned

The journal is published quarterly

The first printed issue of the *Military Technical Courier* appeared on 1st January 1953.

The first electronic edition of the *Military Technical Courier* on the Internet appeared on 1st January 2011.

Military Technical Courier has entered into an electronic licensing relationship with EBSCO Publishing, the world's most prolific aggregator of full text journals, magazines and other sources. The full text of Military Technical Courier can be found on EBSCO Publishing's databases.

Printed by Vojna štamparija – Belgrade, Resavska 40b, e-mail: vojna.stamparija@mod.gov.rs

С А Д Р Ж А Ј

ОРИГИНАЛНИ НАУЧНИ РАДОВИ

С О Д Е Р Ж А Н И Е

C O N T E N T S

ОРИГИНАЛНИ НАУЧНИ РАДОВИ
ОРИГИНАЛЬНЫЕ НАУЧНЫЕ СТАТЬИ
ORIGINAL SCIENTIFIC PAPERS

ON SOME F – CONTRACTION OF PIRI–KUMAM–DUNG–TYPE MAPPINGS IN METRIC SPACES

Jelena Z.Vujaković[a], *Stojan* N. Radenović[b]

[a] University of Priština, Faculty of Sciences and Mathematics, Kosovska Mitrovica, Republic of Serbia,
e-mail: jelena.vujakovic@pr.ac.rs,**corresponding author**,
ORCID iD: https://orcid.org/0000-0001-5361-7133

[b] University of Belgrade, Faculty of Mechanical Engineering, Belgrade, Republic of Serbia,
e-mail: radens@beotel.rs,
ORCID ID: https://orcid.org/0000-0001-8254-6688

DOI: 10.5937/vojtehg68-27385;https://doi.org/10.5937/vojtehg68-27385

FIELD: Mathematics
ARTICLE TYPE: Original scientific paper

Abstract:

Introduction/purpose: *This paper establishes some new results of Piri–Kumam–Dung-type mappings in a complete metric space.The goal was to improve the already published results.*

Methods: Using the property of a strictly increasing function as well as the known Lemma formulated in (Radenović et al, 2017), the authors have proved that a Picard sequence is a Cauchy sequence.

Results: New results were obtained concerning the F – contraction mappings of S in a complete metric space. To prove it, the authors used only property (W1).

Conclusion:The authors believe that the obtained results represent a significant improvement of many known results in the existing literature.

Key words: Banach principle, F–contractive mapping, metric space, fixed point.

ACKNOWLEDGMENT: The work of the first authoris supported by the Ministry of Education, Science and Technological Development of the Republic of Serbia, project TR-35030.

Introduction and preliminaries

It is well known that the Banach fixed point theorem is the most celebrated result in Nonlinear analysis, Functional analysis, Mathematical Analysis, Topology and other mathematical disciplines. It shows that in a complete metric space, each contractive mapping has a unique fixed point. This result is used as a main tool for the existence of solutions of many non–linear problems. A great number of generalizations of this famous results appear in the literature. On the one hand, the usual contractive condition is replaced by a weakly contractive condition, while, on the other hand, the action space is replaced by some generalization of a standard metric space (as $b-$metric space, partial metric space, partial $b-$metric space, $b-$metric like space, $G-$metric space, G_b-metric space, etc).

A fundamental role in the foundations of the constructions is played by the fixed point theorems in metric spaces. They have been intensively studied for quite some time. The Banach fixed point theorem (proved in 1922 (Banach, 1922)), provides a technique for solving a variety of problems in mathematical science and engineering.

In recent investigations, Wardowski (Wardowski, 2012) described a new contraction where the author proved fixed point results in a very general setting in a so–called $F-$contraction. Piri and Kumam (Piri & Kumam, 2014) refined his results by launching some weaker conditions on self–mapping regarding a complete metric space and over the mapping F. For more details see (Chen et al, 2016), (Cosentino & Vetro, 2015), (Cosentino et al, 2015), (Ćirić, 2003), (Dey et al, 2019), (Dung et al, 2015), (Goswami et al, 2019), (Gubran et al, 2021), (Kadelburg & Radenović, 2018), (Lukacs & Kajanto, 2018), (Luambano et al, 2019), (Minak et al, 2014), (Piri & Kumam, 2014, 2016), (Popescu & Stan, 2020); (Secelean, 2013, 2016), (Shukla et al, 2014), (Wardowski, 2012, 2018), (Wardowski & Dung, 2014).

In the further work we need the following notation.

Definition 1.1 (Wardowski, 2012) Let (Λ,ρ) be a metric space and $\Im$ be a family of mappings $F:(0,+\infty)\to(-\infty,+\infty)$ satisfying conditions:

(W1) F is strictly increasing, i.e. for all $a,b\in(0,+\infty)$, $a<b$ implies $F(a)<F(b)$;

(W2) for each sequence $\{a_n\}\subset(0,+\infty)$, $n\in\mathbb{N}$, $\lim_{n\to+\infty} a_n=0$ if and only if $\lim_{n\to+\infty} F(a_n)=-\infty$;

(W3) there exists $s\in(0,1)$ such that $\lim_{a\to0^+} a^s F(a)=0$.

A mapping $S:\Lambda\to\Lambda$ is said to be an $F-$contraction (or Wardowski function) on (Λ,ρ) if there exists $\theta>0$ such that for all $u,v\in\Lambda$, $\rho(Su,Sv)>0$ implies

$$\theta+F\left(\rho(Su,Sv)\right)\le F\left(\rho(u,v)\right). \tag{1.1}$$

Some examples of an $F-$contraction can be found, for instance, in (Wardowski, 2012). It is obvious, based on condition (**W1**) and inequality (1.1), that every $F-$contraction is necessarily continuous.

Remark 1.1 Let $F:(0,+\infty)\to(-\infty,+\infty)$ be a strictly increasing function. Then there are two possibilities:

1. $F(0+0)=\lim_{x\to0^+} F(x)=m, m\in\mathbb{R}$;
2. $F(0+0)=\lim_{x\to0^+} F(x)=-\infty$.

Hence, each strictly increasing function $F:(0,+\infty)\to(-\infty,+\infty)$ satisfies either 1. or 2. For more details, see (Aljančić, 1969, Proposition 1, Section 8). In the first case, we have that F satisfies (**W3**). Indeed, $\lim_{x\to0^+} x^k F(x)=0^k\cdot m=0$ for all $k\in(0,1)$. It is clear that in the second case F satisfies condition (**W2**).

Further, Wardowski in (Wardowski, 2012) proved some new fixed point result which was a proper generalization of the Banach contraction principle.

Theorem 1.1 (Wardowski, 2012) Let (Λ,ρ) be a complete metric space and $S:\Lambda\to\Lambda$ be an $F-$contraction. Then S has a unique fixed point $u^*\in\Lambda$ and for every $u\in\Lambda$ the sequence $\{S^n u\}, n\in\mathbb{N}$ converges to u^*.

This theorem played a significant role in the further research in the metric fixed point theory. Several authors, see (Chen et al, 2016), (Cosentino & Vetro, 2015), (Cosentino et al, 2015), (Ćirić, 2003), (Dey et al, 2019), (Dung et al, 2015), (Goswami et al, 2019), (Gubran et al, 2021), (Kadelburg & Radenović, 2018), (Lukacs & Kajanto, 2018), (Miculescu & Mihail, 2017), (Piri & Kumam, 2014, 2016), (Popescu & Stan, 2020), (Secelean, 2013, 2016), (Shukla et al, 2014), (Wardowski, 2012, 2018), (Wardowski & Dung, 2014) generalized it by introducing the various type of $F-$contractions in other general metric spaces, especially in $b-$metric spaces, partial metric spaces, etc. Others have considered Wardowski's approach in a multi–valued case for metric spaces and its generalizations.

In 2013, Secelean (Secelean, 2013) proved that condition (**W2**) in Definition 1.1 can be replaced by an equivalent condition

(A1) $\inf F = -\infty$, or

(A2) there exists a sequence $\{a_n\} \subset (0,+\infty)$, $n \in \mathbb{N}$ such that

$$\lim_{n\to+\infty} F(a_n) = -\infty.$$

Considering Theorem 1.1, with conditions (**A1**), (**A2**) and a new condition

(PK1) , F is continuous on $(0,+\infty)$,

Piri and Kumam (Piri & Kumam, 2014) introduced a new type of $F-$contraction, a so–called $F-$Suzuki contraction. With this notion, they generalized and extended the well–known fixed point results of Wardowski (Wardowski, 2012) and Secelean (Secelean, 2013).

Definition 1.2 (Piri & Kumam, 2014) Let (Λ,ρ) be a metric space. A mapping $S:\Lambda\to\Lambda$ is said to be an $F-$Suzuki contraction if there exists $\theta>0$ such that for all $u,v\in\Lambda$ with $\rho(Su,Sv)>0$, $\frac{1}{2}\rho(u,Su)<\rho(u,v)$ implies

$$\theta + F(\rho(Su,Sv)) \le F(\rho(u,v)),$$

where F satisfies (**W1**), (**A1**) and (**PK1**).

Theorem 1.2 (Piri & Kumam, 2014) Let $S:\Lambda\to\Lambda$ be a given mapping in a complete metric space (Λ,ρ). Suppose that $F:(0,+\infty)\to(-\infty,+\infty)$

satisfies conditions (**W1**), (**A1**) and (**PK1**), and let there exist $\theta > 0$ such that for all $u, v \in \Lambda$ with $\rho(Su, Sv) > 0$ holds

$$\theta + F\left(\rho(Su, Sv)\right) \leq F\left(\rho(u, v)\right).$$

Then, S has a unique fixed point $u^* \in \Lambda$ and for every $u \in \Lambda$ the sequences $\left\{S^n u\right\}$, $n \in \mathbb{N}$ converges to u^*.

Theorem 1.3 (Piri & Kumam, 2014) Let (Λ, ρ) be a complete metric space and $S : \Lambda \to \Lambda$ be an $F-$Suzuki contraction. Then S has a unique fixed point $u^* \in \Lambda$ and for every $u \in \Lambda$ the sequence $\left\{S^n u\right\}$, $n \in \mathbb{N}$ converges to u^*.

It is well known (see, for instance, (Cosentino & Vetro, 2014)) that the contraction conditions for the mappings $S : \Lambda \to \Lambda$ on the metric space (Λ, ρ) containing mainly the elements $\rho(u, v)$, $\rho(u, Su)$, $\rho(v, Sv)$, $\rho(u, Sv)$, $\rho(v, Su)$ can be complemented with $\rho\left(S^2 u, v\right)$, $\rho\left(S^2 u, Sv\right)$, $\rho\left(S^2 u, u\right)$ and $\rho\left(S^2 u, Su\right)$. This fact inspired Dung and Hang (Dung & Hang, 2015) to introduce a new concept, a generalized $F-$contraction, and to prove several fixed point theorems for such mapping.

Definition 1.3 (Dung & Hang, 2015) A mapping S of the metric space (Λ, ρ) into itself is said to be a generalized $F-$contraction on (Λ, ρ) if there exists $F : (0, +\infty) \to (-\infty, +\infty)$ satisfying conditions (**W1**), (**W2**), (**W3**) and $\theta > 0$ such that, for all $u, v \in \Lambda$, with $\rho(Su, Sv) > 0$ follows

$$\theta + F\left(\rho(Su, Sv)\right) \leq F\left(\Pi(u, v)\right),$$

where

$$\Pi(u, v) = \max\left\{\rho(u, v), \rho(u, Su), \rho(v, Sv), \frac{\rho(u, Sv) + \rho(v, Su)}{2}, \right.$$
$$\left. \frac{\rho\left(S^2 u, u\right) + \rho\left(S^2 u, Sv\right)}{2}, \rho\left(S^2 u, Su\right), \rho\left(S^2 u, v\right), \rho\left(S^2 u, Sv\right)\right\}.$$

Theorem 1.4 (Dung & Hang, 2015) Let (Λ,ρ) be a complete metric space and let $S:\Lambda\to\Lambda$ be a generalized $F-$contraction. If S or F is continuous, then S has a unique fixed point $u^*\in\Lambda$ and for every $u\in\Lambda$ the sequence $\{S^n u\}$, $n\in\mathbb{N}$ converges to u^*.

In this article, we will prove Theorem 1.2, Theorem 1.3 and Theorem 1.4 in the easier way: using only condition (**W1**) and the following Lemma.

Lemma 1.1 (Radenović et al, 2017) Let $\{u_n\}$, $n\in\mathbb{N}$ be a sequence in the metric space (Λ,ρ) such that $\lim_{n\to+\infty}\rho(u_n,u_{n+1})=0$. If $\{u_n\}$ is not a Cauchy in (Λ,ρ), then there exists $\xi>0$ and two sequences $\{n_k\}$ and $\{m_k\}$ of positive integers such that $n_k>m_k>k$ and the sequences

$$\{\rho(u_{n_k},u_{m_k})\},\{\rho(u_{n_k+1},u_{m_k})\},\{\rho(u_{n_k},u_{m_k-1})\},\{\rho(u_{n_k+1},u_{m_k-1})\},\{\rho(u_{n_k+1},u_{m_k+1})\},\ldots$$

tend to ξ^+ as $k\to+\infty$.

Remark 1.2 Notice, that if the condition of Lemma 1.1 is satisfied, then the sequences $\{\rho(u_{n_k+s},u_{m_k})\}$ and $\{\rho(u_{n_k+s},u_{m_k+1})\}$ also converge to ξ^+ when $k\to+\infty$, where $s\in\mathbb{N}$.

Results

We begin this section with the theorem which generalizes and improves Theorem 1.2. In our result, the function $F:(0,+\infty)\to(-\infty,+\infty)$ satisfies only condition (**W1**).

Theorem 2.1 Let (Λ,ρ) be a complete metric space and $S:\Lambda\to\Lambda$ be a $F-$contraction mapping with property (**W1**), that is, let there exist $\theta>0$ such that

$$\theta+F(\rho(Su,Sv))\le F(\rho(u,v)), \tag{2.1}$$

for all $u,v\in\Lambda$ with $Su\neq Sv$.

Then S has a unique fixed point, say, u^* and for all $u\in\Lambda$ the sequence $\{S^n u\}$, $n\in\mathbb{N}$ converges to u^*.

Proof. Firstly, from condition (**W1**), there are both $\lim_{c\to d^-} F(c) = F(d-0)$ and $\lim_{c\to d^+} F(c) = F(d+0)$ for all $d \in (0,+\infty)$, because it is known from mathematical analysis that the following is true

$$F(d-0) \le F(d) \le F(d+0),\ d \in (0,+\infty). \tag{2.2}$$

Further, from the assumption that S is an $F-$contraction, it follows that S is contractive ($u \neq v$ implies $\rho(Su,Sv) < \rho(u,v)$). This means that the mapping S is continuous. Besides, $F-$contractive condition (**W1**) implies the uniqueness of the fixed point if it exists.

We will show that S has a fixed point. Let u_0 be an arbitrary point in Λ. Consider the sequence $\{u_n\}, n \in \mathbb{N} \cup \{0\}$ with $u_{n+1} = Su_n$. If $u_k = u_{k+1}$ for some $k \in \mathbb{N} \cup \{0\}$ then u_k is a unique fixed point of S and the conclusion of the Theorem follows. Therefore, suppose that $u_n \neq u_{n+1}$ for all $n \in \mathbb{N} \cup \{0\}$. Based on $F-$contractive condition (2.1) of the mapping S, we get

$$F(\rho(u_n,u_{n+1})) < \theta + F(\rho(u_n,u_{n+1})) \le F(\rho(u_{n-1},u_n)), \tag{2.3}$$

for all $n \in \mathbb{N}$, that is, in accordance with property (**W1**), it follows

$$\rho(u_n,u_{n+1}) < \rho(u_{n-1},u_n) \text{ for all } n \in \mathbb{N}.$$

This further means that $\rho(u_n,u_{n+1}) \to \rho^* \ge 0$ as $n \to +\infty$, as well as $\rho(u_n,u_{n+1}) > \rho^*$ for all $n \in \mathbb{N} \cup \{0\}$. If we chose now that $\rho^* > 0$, then the relation

$$\theta + F(\rho(u_n,u_{n+1})) \le F(\rho(u_{n-1},u_n)), \tag{2.4}$$

implies

$$\theta + F(\rho^* + 0) \le F(\rho^* + 0), \tag{2.5}$$

which is a contradiction. Thus, $\rho^* = 0$, i.e., $\lim_{n\to+\infty} \rho(u_n,u_{n+1}) = 0$.

Next, we show that $\{u_n\}, n \in \mathbb{N} \cup \{0\}$ is a Cauchy sequence by assuming the contrary. If we put $u = u_{n_k}$ and $v = u_{m_k}, k \in \mathbb{N}$ in $F-$contractive condition (2.1), we obtain

$$\theta + F\left(\rho\left(u_{n_k+1}, u_{m_k+1}\right)\right) \le F\left(\rho\left(u_{n_k}, u_{m_k}\right)\right). \tag{2.6}$$

Since, according to Lemma 1.1, both $\rho\left(u_{n_k+1}, u_{m_k+1}\right)$ and $\rho\left(u_{n_k}, u_{m_k}\right)$ tend to ξ^+ as $k \to +\infty$, we have

$$\theta + F\left(\xi^+ + 0\right) \le F\left(\xi^+ + 0\right), \tag{2.7}$$

which is wrong. We conclude that $\{u_n\}$, $n \in \mathbb{N} \cup \{0\}$ is a Cauchy sequence, hence it converges to some $u^* \in \Lambda$ as (Λ, ρ) is complete. Since S is continuous, it follows that $Su^* = u^*$, i.e., u^* is a unique fixed point of S and the Theorem is proved.

Now we state one consequence that can be obtained concerning the $F-$contractive self–mapping S which satisfies one of five conditions.

Corolarry 2.1 Let (Λ, ρ) be a complete metric space and let $S : \Lambda \to \Lambda$ be a self-mapping such that there exists $\theta_i > 0, i = 1,2,3,4,5$ so for all $u, v \in \Lambda$ with $\rho(Su, Sv) > 0$, the following contractive conditions holds:

$$\theta_1 + \rho(Su, Sv) \le \rho(u, v),$$

$$\theta_2 - \frac{1}{\rho(Su, Sv)} \le -\frac{1}{\rho(u, v)},$$

$$\theta_3 - \frac{1}{\rho(Su, Sv)} + \rho(Su, Sv) \le -\frac{1}{\rho(u, v)} + \rho(u, v),$$

$$\theta_4 + \frac{1}{1 - e^{\rho(Su, Sv)}} \le \frac{1}{1 - e^{\rho(u, v)}},$$

$$\theta_5 + \frac{1}{e^{-\rho(Su, Sv)} - e^{\rho(Su, Sv)}} \le \frac{1}{e^{-\rho(u, v)} - e^{\rho(u, v)}}.$$

Then, in each of these cases, S has a unique fixed point $u^* \in \Lambda$ and for all $u \in \Lambda$ the sequence $\{S^n u\}$, $n \in \mathbb{N}$ converges to u^*.

Proof. As each of the functions $F_1(r) = r$, $F_2(r) = -\frac{1}{r}$, $F_3(r) = -\frac{1}{r} + r$, $F_4(r) = \frac{1}{1 - \exp r}$ and $F_5(r) = \frac{1}{\exp(-r) - \exp r}$, where $r = \rho(u, v) > 0$, is

strictly increasing on $(0,+\infty)$, the proof immediately follows by Theorem 2.1.

The following result is related to the generalization and the improvement of Theorem 1.2.

Theorem 2.2 Let (Λ,ρ) be a complete metric space and let $S:\Lambda\to\Lambda$ is an $F-$Suzuki contraction mapping where F satisfies condition (**W1**), that is, there exists $\theta>0$ such that $\frac{1}{2}\rho(u,Su)<\rho(u,v)$ implies

$$\theta+F\left(\rho(Su,Sv)\right)\le F\left(\rho(u,v)\right), \tag{2.8}$$

for all $u,v\in\Lambda$ with $\rho(Su,Sv)>0$.

Then S has a unique fixed point $u^*\in\Lambda$ and for each $u\in\Lambda$ the sequence $\{S^n u\}$, $n\in\mathbb{N}$ converges to u^*.

Proof. It is easily seen that relation (2.8) implies the uniqueness of the fixed point if it exists. Indeed, if we suppose that there are two distinct fixed points u^* and v^* of S, then it is clear that from $\frac{1}{2}\rho(u^*,Su^*)<\rho(u^*,v^*)$ follows

$$\theta+F\left(\rho(Su^*,Sv^*)\right)\le F\left(\rho(u^*,v^*)\right), \text{ i.e.}$$

$$\theta+F\left(\rho(u^*,v^*)\right)\le F\left(\rho(u^*,v^*)\right),$$

which is a contradiction.

Now we show the existence of the fixed point. Let $u_0\in\Lambda$ be an arbitrary point and $\{u_n\}$, $n\in\mathbb{N}\cup\{0\}$ is the corresponding Picard sequence, i.e. $u_n=S^n u_0$ with an initial value $u_0=S^0u_0$. If $u_k=u_{k+1}$ for some $k\in\mathbb{N}\cup\{0\}$, then u_k is an unique fixed point and the proof is complete.

Therefore, suppose $u_n\neq u_{n+1}$ for all $n\in\mathbb{N}\cup\{0\}$. In this case $\frac{1}{2}\rho(u_n,u_{n+1})<\rho(u_n,u_{n+1})$ holds true for all $n\in\mathbb{N}\cup\{0\}$, so from (2.8) we have

$$\theta + F\left(\rho\left(u_{n+1}, u_{n+2}\right)\right) \le F\left(\rho\left(u_n, u_{n+1}\right)\right),$$

that is, according to condition (**W1**) we get

$$\rho\left(u_{n+1}, u_{n+2}\right) < \rho\left(u_n, u_{n+1}\right), \text{ for all } n \in \mathbb{N} \cup \{0\}.$$

As in the proof of Theorem 2.1, we obtain that $\rho\left(u_n, u_{n+1}\right) \to 0$ as $n \to +\infty$. Since $\rho\left(u_n, u_{n_k+1}\right) \to 0$ and $\rho\left(u_{n_k}, u_{m_k}\right) \to \xi^+$ as $k \to +\infty$ it follows that there is some $k_1 \in \mathbb{N}$ such that $\frac{1}{2}\rho\left(u_{n_k}, u_{m_k+1}\right) < \rho\left(u_{n_k}, u_{m_k}\right)$, for all $k \in \mathbb{N}$ with $k \ge k_1$. Then, for $k \ge k_1$, we have

$$\theta + F\left(\rho\left(u_{n_k+1}, u_{m_k+1}\right)\right) \le F\left(\rho\left(u_{n_k}, u_{m_k}\right)\right),$$

that is $\theta + F\left(\xi^+ + 0\right) \le F\left(\xi^+ + 0\right)$, which is a contradiction because $\theta > 0$.

Hence we conclude that $\{u_n\}$, $n \in \mathbb{N} \cup \{0\}$ is a Cauchy sequence. The completeness of the metric space (Λ, ρ) guarantees the existence of some point $u^* \in \Lambda$ such that $\lim_{n \to +\infty} \rho\left(u_n, u^*\right) = 0$. The rest of the proof is analogous to the proof of Theorem 1.3 from (Piri & Kumam, 2014) on page 7. One can find that following inequalities hold

$$\frac{1}{2}\rho\left(u_n, Su_n\right) < \rho\left(u_n, u^*\right), \text{ or } \frac{1}{2}\rho\left(Su_n, S^2u_n\right) < \rho\left(Su_n, u^*\right),$$

for all $n \in \mathbb{N} \cup \{0\}$.

Further, from relation (2.8), it follows

$\theta + F\left(\rho\left(Su_n, Su^*\right)\right) \le F\left(\rho\left(u_n, u^*\right)\right)$, or $\theta + F\left(\rho\left(S^2u_n, Su^*\right)\right) \le F\left(\rho\left(Su_n, u^*\right)\right)$, i.e.,

$$\theta + F\left(\rho\left(u_{n+1}, Su^*\right)\right) \le F\left(\rho\left(u_n, u^*\right)\right), \text{ or}$$

$$\theta + F\left(\rho\left(u_{n+2}, Su^*\right)\right) \le F\left(\rho\left(u_{n+1}, u^*\right)\right). \quad (2.9)$$

Finally, using condition (**W1**), we can write inequalities (2.9) in the form

$$\rho\left(u_{n+1}, Su^*\right) \le \rho\left(u_n, u^*\right), \text{ or } \rho\left(u_{n+2}, Su^*\right) \le \rho\left(u_{n+1}, u^*\right). \quad (2.10)$$

This proves that u^* is a unique fixed point of S, i.e., $Su^* = u^*$.

The immediate consequence of Theorem 2.2 is the following result.

Corollary 2.2 Let (Λ,ρ) be a complete metric space and let $S:\Lambda\to\Lambda$ be self–mapping such that there exists $\theta_i>0,\ i=1,2,3,4,5,6$ so for all $u,v\in\Lambda$ with $\rho(Su,Sv)>0$ the following implications hold true: $\frac{1}{2}\rho(u,Su)<\rho(u,v)$ implies

$$\theta_1+\rho(Su,Sv)\le\rho(u,v),\ \text{or}$$

$$\theta_2-\frac{1}{\rho(Su,Sv)}\le-\frac{1}{\rho(u,v)},\ \text{or}$$

$$\theta_3-\frac{1}{\rho(Su,Sv)}+\rho(Su,Sv)\le-\frac{1}{\rho(u,v)}+\rho(u,v),\ \text{or}$$

$$\theta_4+e^{\rho(Su,Sv)}\le e^{\frac{1}{\rho(Su,Sv)}},\ \text{or}$$

$$\theta_5+\frac{1}{1-e^{\rho(Su,Sv)}}\le\frac{1}{1-e^{\rho(u,v)}},\ \text{or}$$

$$\theta_6+\frac{1}{e^{-\rho(Su,Sv)}-e^{\rho(Su,Sv)}}\le\frac{1}{e^{-\rho(u,v)}-e^{\rho(u,v)}}.$$

Then in each of these cases, S has a unique fixed point $u^*\in\Lambda$ and for all $u\in\Lambda$ the sequence $\{S^nu\}$, $n\in\mathbb{N}$ converges to u^*.

After all, we give the proof of Theorem 1.4 in an easier way: using only condition (**W1**) and Lemma 1.1.

Theorem 2.3 Let (Λ,ρ) be a complete metric space and $S:\Lambda\to\Lambda$ is a generalized $F-$contraction which satisfies condition (**W1**), that is, there exists $\theta>0$ such that for all $u,v\in\Lambda$ with $\rho(Su,Sv)>0$ follows

$$\theta+F\big(\rho(Su,Sv)\big)\le F\big(\Pi(u,v)\big),\tag{2.11}$$

where

$$\Pi(u,v)=\max\Big\{\rho(u,v),\rho(u,Su),\rho(v,Sv),\frac{\rho(u,Sv)+\rho(v,Su)}{2},$$
$$\frac{\rho(S^2u,u)+\rho(S^2u,Sv)}{2},\rho(S^2u,Su),\rho(S^2u,v),\rho(S^2u,Sv)\Big\}.$$

If S or F is continuous, then S has a unique fixed point $u^* \in \Lambda$ and for every $u \in \Lambda$ the sequence $\{S^n u\}$, $n \in \mathbb{N}$ converges to u^*.

Proof. Since $\rho(Su, Sv) > 0$ it follows that contractive condition (2.11) is well defined. Further, condition (2.11) implies the uniqueness of the fixed point if it exists. In order to show that S has a fixed point, suppose that u_0 is an arbitrary point in Λ and define a sequence $\{u_n\} \in \Lambda, n \in \mathbb{N} \cup \{0\}$ by $u_{n+1} = Su_n$. If we chose $u_k = u_{k+1}$ for some $k \in \mathbb{N} \cup \{0\}$, then u_k is a unique fixed point of S and the proof of the Theorem is completed.

Therefore, suppose that $\rho(u_n, u_{n+1}) > 0$ for all $n \in \mathbb{N} \cup \{0\}$. Using generalized $F-$contractive condition (2.11), of the mapping S, we obtain

$$F\left(\rho(u_n, u_{n+1})\right) < \theta + F\left(\rho(u_n, u_{n+1})\right) \leq F(\Pi(u_{n-1}, u_n), \tag{2.12}$$

where

$$\Pi(u_{n-1}, u_n) = \max\Big\{\rho(u_{n-1}, u_n), \rho(u_{n-1}, u_n), \rho(u_n, u_{n+1}), \frac{\rho(u_{n-1}, u_{n+1}) + 0}{2}, \frac{\rho(u_{n+1}, u_{n-1}) + 0}{2}, \rho(u_{n+1}, u_n), \rho(u_{n+1}, u_n), 0\Big\}$$

$$= \max\left\{\rho(u_{n-1}, u_n), \rho(u_n, u_{n+1}), \frac{\rho(u_{n-1}, u_{n+1})}{2}\right\}$$

$$\leq \max\left\{\rho(u_{n-1}, u_n), \rho(u_n, u_{n+1})\right\}.$$

It is clear that $\max\{\rho(u_{n-1}, u_n), \rho(u_n, u_{n+1})\} = \rho(u_{n-1}, u_n)$, otherwise, we get a contradiction. This further means that $\lim_{n \to +\infty} \rho(u_n, u_{n+1}) = 0$.

Next, we prove that $\{u_n\}, n \in \mathbb{N} \cup \{0\}$ is a Cauchy sequence by supposing it is not. Putting $u = u_{n_k}$ and $v = u_{m_k}$ in generalized $F-$contractive condition (2.11) we have

$$\theta + F\left(\rho(u_{n_k+1}, u_{m_k+1})\right) \leq F\left(\rho(u_{n_k}, u_{m_k})\right), \tag{2.13}$$

where

$$\Pi(u_{n_k}, u_{m_k}) = \max\left\{\rho(u_{n_k}, u_{m_k}), \rho(u_{n_k}, u_{n_k+1}), \rho(u_{m_k}, u_{m_k+1}),\right.$$

$$\frac{\rho\left(u_{n_k},u_{m_k+1}\right)+\rho\left(u_{m_k},u_{n_k+1}\right)}{2},\frac{\rho\left(u_{n_k+2},u_{n_k}\right)+\rho\left(u_{n_k+2},u_{m_k+1}\right)}{2},$$
$$\rho\left(u_{n_k+2},u_{n_k+1}\right),\rho\left(u_{n_k+2},u_{m_k}\right),\rho\left(u_{n_k+2},u_{m_k+1}\right)\Big\}.$$

According to Lemma 1.1, one can find that $\lim_{k\to+\infty}\Pi\left(u_{n_k},u_{m_k}\right)=\xi^{+}$.

Therefore, from (2.13), it follows that $\theta+F\left(\xi^{+}+0\right)\le F\left(\xi^{+}+0\right)$, which is a contradiction so we can conclude that the sequence $\{u_n\}$, $n\in\mathbb{N}\cup\{0\}$ is a Cauchy sequence. Since (Λ,ρ) is a complete metric space, it converges to some $u^{*}\in S$. Finally, if S is continuous, then $Su^{*}=u^{*}$ and the theorem is proved.

Suppose now that F is continuous and let $\rho\left(u^{*},Su^{*}\right)>0$. Putting $u=u_n$ and $v=u^{*}$ in condition (2.11) we get

$$\theta+F\left(\rho\left(u_{n+1},u^{*}\right)\right)\le F\left(\Pi\left(u_n,u^{*}\right)\right) \tag{2.14}$$

where

$$\Pi\left(u_n,u^{*}\right)=\max\Big\{\rho\left(u_n,u^{*}\right),\rho\left(u_n,u_{n+1}\right),\rho\left(u^{*},Su^{*}\right),$$
$$\frac{\rho\left(u_n,Su^{*}\right)+\rho\left(u^{*},u_{n+1}\right)}{2},\frac{\rho\left(u_{n+2},u_n\right)+\rho\left(u_{n+2},Su^{*}\right)}{2},$$
$$\rho\left(u_{n+2},u_{n+1}\right),\rho\left(u_{n+2},u^{*}\right),\rho\left(u_{n+2},Su^{*}\right)\Big\}.$$

Since $F\left(\rho\left(u_{n+1},Su^{*}\right)\right)\to F\left(\rho\left(u^{*},Su^{*}\right)\right)$ and $\Pi\left(u_n,u^{*}\right)\to\rho\left(u^{*},Su^{*}\right)$ as $n\to+\infty$, taking the limit in (2.13), when n tends to infinity, we obtain

$$\theta+F\left(\rho\left(u^{*},Su^{*}\right)\right)\le F\left(\rho\left(u^{*},Su^{*}\right)\right),$$

which is in contradiction with $\theta>0$. Therefore, the assumption $\rho\left(u^{*},Su^{*}\right)>0$ is wrong. This means that $\rho\left(u^{*},Su^{*}\right)=0$, i.e., u^{*} is a unique fixed point of the generalized $F-$contraction S and the proof is finished.

From the previous theorem, one consequence can be obtained assuming some strictly increasing function instead of F.

Corollary 2.3 Let (Λ,ρ) be a complete metric space and let $S:\Lambda\to\Lambda$ is a generalized $F-$contraction such that there is $\theta_i>0, i=1,2,3$ and that for all $u,v\in\Lambda$ with $\rho(Su,Sv)>0$ the following implication holds true

$$\theta_1+\rho(Su,Sv)\le\Pi(u,v),$$

$$\theta_2-e^{\frac{1}{\rho(Su,Sv)}}+e^{\rho(Su,Sv)}\le-e^{\frac{1}{\Pi(u,v)}}+e^{\Pi(u,v)},$$

$$\theta_3-\frac{1}{\rho(Su,Sv)}+\rho(Su,Sv)\le-\frac{1}{\Pi(u,v)}+\Pi(u,v),$$

where

$$\Pi(u,v)=\max\left\{\rho(u,v),\rho(u,Su),\rho(v,Sv),\frac{\rho(u,Sv)+\rho(v,Su)}{2},\right.$$
$$\left.\frac{\rho(S^2u,u)+\rho(S^2u,Sv)}{2},\rho(S^2u,Su),\rho(S^2u,v),\rho(S^2u,Sv)\right\}.$$

Then S has a unique fixed point $u^*\in\Lambda$ and for all $u\in\Lambda$ the sequence $\{S^nu\}$, $n\in\mathbb{N}\cup\{0\}$ converges to u^*.

Proof. Putting $F_1(r)=r$, $F_2(r)=-e^{\frac{1}{r}}+e^r$ and $F_3(r)=-\frac{1}{r}+r$ in relation to (2.12), the results follows.

Conclusion

In this article we get some new results concerning the $F-$ contraction mappings of S in a complete metric space. To prove it, we used only property (**W1**). We believe that this is a significant improvement of the known results in the existing literature.

References

Aljančić, S. 1969. *Uvod u realnu i funkcionalnu analizu*. Beograd: Naučna knjiga (in Serbian).

Banach, S. 1922. Sur les opérations dans les ensembles abstraits et leur applications aux équations intégrales. *Fundamenta Mathematicae,* 3, pp.133-181 (in French). Available at: https://doi.org/10.4064/fm-3-1-133-181.

Chen, C., Wen, L. & Gu, Y. 2016. Fixed point theorems for generalized F-contractions in b-metric-like spaces. *Journal of Nonlinear Sciences and Applications*, 9(5), pp.2161-2174. Available at: http://dx.doi.org/10.22436/jnsa.009.05.21.

Cosentino, M., Jleli, M., Samet, B. & Vetro, C. 2015. Solvability of integradifferential problems via fixed point theory in b-metric spaces. *Fixed Point Theory and Application*, art.num:70. Available at: https://doi.org/10.1186/s13663-015-0317-2.

Cosentino, M. & Vetro, P. 2014. Fixed point result for F-contractive mappings of Hardy-Rogers-Type. *Filomat*, 28(4), pp.715-722. Available at: https://doi.org/10.2298/FIL1404715C.

Ćirić, Lj. 2003. *Some recent results in metrical fixed point theory*. Belgrade: University of Belgrade.

Dey, L.K., Kumam, P. & Senapati, T. 2019. Fixed point results concerning α-F-contraction mappings in metric spaces. *Applied General Topology*, 20(1), pp.81-95. Available at: https://doi.org/10.4995/agt.2019.9949.

Dung, N.V. & Hang, V.T.L. 2015. A fixed point theorem for generalized F-contractions on complete metric space. *Vietnam Journal of Mathematics*, art.num:13, pp.743-753. Available at: https://doi.org/10.1007/s10013-015-0123-5.

Goswami, N., Haokip, N. & Mishra, V.N. 2019. F-contractive type mappings in b-metric spaces and some related fixed point results. *Fixed Point Theory and Application*, art.num:13. Available at: https://doi.org/10.1186/s13663-019-0663-6.

Kadelburg, Z. & Radenović, S. 2018. Notes on some recent papers concerning F-contractions in b-metric spaces. *Constructive Mathematical Analysis*, 1(2), pp.108-112. Available at: https://doi.org/10.33205/cma.468813.

Luambano, S., Kumar, S. & Kakiko, G. 2019. Fixed point theorem for F-contraction mappings in partial metric spaces. *Lobachevskii Journal of Mathematics*, 40(2), pp.183-188. Available at: https://doi.org/10.1134/S1995080219020094.

Lukacs, A. & Kajanto, S. 2018. Fixed point theorems for various types of F-contractions in complete b-metric spaces. *Fixed Point Theory*, 19(1), pp.321-334. Available at: https://doi.org/10.24193/fpt-ro.2018.1.25.

Miculescu, R. & Mihail, A. 2017. New fixed point theorems for set-valued contractions in b-metric spaces. *Journal of Fixed Point Theory and Application*, 19(3), pp.2153-2163. Available at: https://doi.org/10.1007/s11784-016-0400-2.

Minak, N., Helvaci, A. & Altun, I. 2014. Ćirić type generalized$F$-contractions on complete metric spaces and fixed point results.*Filomat*, 28(6), pp.1143-1151. Available at:https://doi.org/10.2298/FIL1406143M.

Piri, H. & Kumam, P. 2014. Some fixed point theorems concerning $F-$ contraction in complete metric spaces. *Fixed Point Theory and Application*, 210. Available at: https://doi.org/10.1186/1687-1812-2014-210.

Piri, H. & Kumam, P. 2016. Fixed point theorems for generalized F-Suzuki-contraction mappings in complete b-metric spaces. *Fixed Point Theory and Application*, art.num:90. Available at: https://doi.org/10.1186/s13663-016-0577-5.

Popescu, O. & Stan, G. 2020. Two fixed point theorems concerning F-contraction in complete metric spaces. *Symmetry*, 12(1), pp.1-10. Available at:https://doi.org/10.3390/sym12010058.

Radenović, S., Vetro, F. & Vujaković, J. 2017. An alternative and easy approach to fixed point results via simulation functions. *Demonstratio Mathematica*, 50(1), pp.223-230. Available at:https://doi.org/10.1515/dema-2017-0022.

Secelean, N. A. 2013. Iterated function system consisting of F-contractions. *Fixed Point Theory and Applications*, art.num:277. Available at: https://doi.org/10.1186/1687-1812-2013-277.

Secelean, N. A. 2016. Weak F-contractions and some fixed point results. *Bulletin of the Iranian Mathematical Society*, 42(3), pp.779-798 [online]. Available at: http://bims.iranjournals.ir/article_812.html [Accessed: 01 July 2020].

Shukla, S., Radenović, S. & Kadelburg, Z. 2014. Some fixed point theorems for ordered F-generalized contractions in 0-f-orbitally complete partial metric spaces.*Theory and Applications of Mathematical and Computer Science*, 4(1), pp.87-98 [online]. Available at: https://uav.ro/applications/se/journal/index.php/TAMCS/article/view/95 [Accessed: 01 July 2020].

Wardowski, D. 2012. Fixed points of a new type of contractive mappings in complete metric spaces. *Fixed Point Theory and Applications*, art.num:94. Available at: https://doi.org/10.1186/1687-1812-2012-94.

Wardowski, D. 2018. Solving existence problems via F-contractions. *Proceeding of American Mathematical Society*, 146(4), pp.1585-1598. Available at: https://doi.org/10.1090/proc/13808.

Wardowski, D. & Van Dung, N. 2014. Fixed points of F-weak contractions on complete metric spaces. *Demonstratio Mathematica*, 47(1), pp.146-155. Available at: https://doi.org/10.2478/dema-2014-0012.

О НЕКОТОРЫХ *F* - СЖИМАЮЩИХ ОТОБРАЖЕНИЯХ ТИПА ПИРИ-КУМАН-ДУНГА В МЕТРИЧЕСКИХ ПРОСТРАНСТВАХ

Елена З. Вуякович[а], **корреспондент**, *Стоян* Н. Раденович[б]

[а] Приштинский университет, Естественно-математический факультет, г. Косовска Митровица, Республика Сербия

[б] Белградский университет, Машиностроительный факультет, г. Белград, Республика Сербия

РУБРИКА ГРНТИ: 27.00.00 МАТЕМАТИКА;
27.39.27 Нелинейный функциональный анализ
ВИД СТАТЬИ: оригинальная научная статья

Резюме:

Введение/цель: В данной статье представлены некоторые из новейших результатов отображений типа Пири-Кумама-Дунга в полном метрическом пространстве. Целью работы было улучшение опубликованныхранее результатов.

Методы: Используя свойство строго возрастающей функции, а также известную лемму, сформулированную в исследовании (Radenović et al, 2017) было доказано, что данная последовательность является последовательностью Пикара − Коши.

Результаты: В данной статье представлено несколько новых результатов, полученных путем наблюдения F − сжимающих отображений S в полном метрическом пространстве. В качестве доказательства использовалось исключительно свойство (W1).

Выводы: Авторы считают, что полученные ими результаты представляют собой значительный вкладв данную область науки.

Ключевые слова: Принцип Банаха, F − сжимающее отображение, метрическое пространство, неподвижная точка.

О НЕКИМ F–КОНТРАКТИВНИМ ПРЕСЛИКАВАЊИМА ПИРИ-КУМАМ-ДУНГОВОГ ТИПА У МЕТРИЧКИМ ПРОСТОРИМА

Јелена З. Вујаковић[а], **аутор за преписку**, *Стојан* Н. Раденовић[б]

[а] Универзитет у Приштини, Природно–математички факултет, Косовска Митровица, Република Србија

[б] Универзитет у Београду, Машински факултет, Београд, Република Србија

ОБЛАСТ: математика
ВРСТА ЧЛАНКА: оригинални научни рад

Сажетак:

Увод/циљ: У чланку су успостављени нови резултати за пресликавања Пири–Кумам–Дунговог типа у комплетном метричком простору. Циљ рада јесте да се побољшају већ објављени резултати.

Методе: Користећи својство строго растуће функције, као и познату лему формулисану у (Radenović et al, 2017), доказано је да је Пикаров низ у ствари Кошијев.

Резултати: Добијено је неколико нових резултата посматрајући F–контрактивна пресликавања од S у комплетном метричком простору. У доказу је коришћена само особина (W1).

Закључак: Аутори верују да добијени резултати представљају значајан допринос досадашњим познатим резултатима.

Кључне речи: Банахов принцип, F–контрактивно пресликавање, метрички простор, непокретна тачка.

Paper received on / Дата получения работы / Датум пријема чланка: 05.07.2020.
Manuscript corrections submitted on / Дата получения исправленной версии работы / Датум достављања исправки рукописа: 13.07.2020.
Paper accepted for publishingon / Дата окончательного согласования работы / Датум коначног прихватања чланка за објављивање: 15.07.2020.

RELATING GRAPH ENERGY WITH VERTEX-DEGREE-BASED ENERGIES

Ivan Gutman
University of Kragujevac, Faculty of Science,
Kragujevac, Republic of Serbia,
e-mail: gutman@kg.ac.rs,
ORCID iD: https://orcid.org/0000-0001-9681-1550

DOI: 10.5937/vojtehg68-28083; https://doi.org/10.5937/vojtehg68-28083

FIELD: Mathematics (Mathematics Subject Classification: primary 05C50, secondary 05C07)
ARTICLE TYPE: Original Scientific Paper

Abstract:

Introduction/purpose: The paper presents numerous vertex-degree-based graph invariants considered in the literature. A matrix can be associated to each of these invariants. By means of these matrices, the respective vertex-degree-based graph energies are defined as the sum of the absolute values of the eigenvalues.

Results: The article determines the conditions under which the considered graph energies are greater or smaller than the ordinary graph energy (based on the adjacency matrix).

Conclusion: The results of the paper contribute to the theory of graph energies as well as to the theory of vertex-degree-based graph invariants.

Keywords: energy (of a graph), vertex-degree-based graph invariant, vertex-degree-based graph energy.

Introduction

This paper is concerned with simple graphs, i.e. with graphs without multiple, directed, or weighted edges, and without loops. Let *G* be such a graph with *n* vertices, labeled as $v_1, v_2, \ldots, v_n$. Two vertices connected by an edge are said to be adjacent. The degree of the vertex v_i, denoted by $\deg(v_i)$, is the number of the first neighbors of v_i.

The energy of a graph *G* was defined in 1978 as (Gutman, 1978), (Li et al, 2012)

$$E = E(G) = \sum_{i=1}^{n} |\lambda_i|$$

where $\lambda_1, \lambda_2, \ldots, \lambda_n$ are the eigenvalues of the adjacency matrix of *G.* Recall that the adjacency matrix *A*(*G*) is a symmetrix square matrix of the order *n*, whose (*i,j*)-entry is

$$A(G)_{ij} = \begin{cases} 1 & if\ v_i\ and\ v_j\ are\ adjacent \\ 0 & if\ v_i\ and\ v_j\ are\ not\ adjacent \\ 0 & if\ \ i = j \end{cases}$$

In the mathematical (Cruz et al, 2015), (Das et al, 2018), (Furtula et al, 2013), (Liu et al, 2019), (Rada & Cruz, 2014), (Zhong & Xu, 2014) and chemical (Todeschini & Consonni, 2009) literature, several dozens of vertex-degree-based graph invariants (usually referred to as "topological indices") have been introduced and extensively studied. Their general formula is

$$VDBI = VDBI(G) = \sum_{1 \le i < j \le n} F\left(\deg(v_i), \deg(v_j)\right)$$

where $F(x, y)$ is some function with the property $F(x, y) = F(y, x)$. In particular,

If $F(x, y) = x + y$, then *VDBI* = first Zagreb index;

if $F(x, y) = xy$, then *VDBI* = second Zagreb index;

if $F(x, y) = |x - y|$, then *VDBI* = Albertson index,

if $F(x, y) = \frac{1}{2}\left(\frac{x}{y} + \frac{y}{x}\right)$, then *VDBI* = extended index;

if $F(x, y) = (x - y)^2$, then *VDBI* = sigma index,

if $F(x, y) = 1/\sqrt{xy}$, then *VDBI* = Randić index;

if $F(x, y) = 2/(x + y)$, then *VDBI* = harmonic index;

if $F(x, y) = \sqrt{(x + y - 2)/(xy)}$, then *VDBI* = ABC index;

if $F(x,y)=\sqrt{xy}$, then *VDBI* = reciprocal Randić index;

if $F(x,y)=1/\sqrt{x+y}$, then *VDBI* = sum-connectivity index;

if $F(x,y)=\sqrt{x+y}$, then *VDBI* = reciprocal sum-connectivity index;

if $F(x,y)=x^2+y^2$, then *VDBI* = forgotten index;

if $F(x,y)=2\sqrt{xy}/(x+y)$, then *VDBI* = geometric-arithmetic index;

if $F(x,y)=(x+y)/(2\sqrt{xy})$, then *VDBI* = arithmetic-geometric index; and

if $F(x,y)=xy/(x+y)$, then *VDBI* = inverse sum indeg index.

There are several more such graph invariants; see in (Das et al, 2018), (Kulli, 2020), where also bibliographic data can be found.

For each function $F(x,y)$ and each graph *G,* a symmetric square matrix $\Phi=\Phi(G)$ of the order *n* can be defined, whose (*i,j*)-entry is

$$\Phi(G)_{ij}=\begin{cases} F\left(\deg(v_i),\deg(v_j)\right) & \textit{if } v_i \textit{ and } v_j \textit{ are adjacent} \\ 0 & \textit{if } v_i \textit{ and } v_j \textit{ are not adjacent} \\ 0 & \textit{if } i=j \end{cases}$$

Recall that if v_i and v_j are adjacent, then $\deg(v_i)\geq 1$, $\deg(v_j)\geq 1$.

The respective vertex-degree-based graph energy (of the graph *G*) is equal to the sum of absolute values of the eigenvalues of $\Phi=\Phi(G)$. We will denote it by $E_F=E_F(G)$.

For some of the above given functions $F(x,y)$, the condition $0<F(x,y)\leq 1$ holds for all $x\geq 1$, $y\geq 1$. Such are the functions pertaining to the Randić, harmonic, sum-connectivity, and geometric-arithmetic indices. For some of the above given functions, $F(x,y)\geq 1$

holds for all $x \geq 1$, $y \geq 1$. Such are those related to the first and second Zagreb, extended, forgotten, and arithmetic-geometric indices, as well as for some reciprocal and inverse indices. For such functions, we prove the following:

Theorem 1.

(a) If $0 < F(x, y) \leq 1$ holds for all $x \geq 1$, $y \geq 1$, and if *G* is a bipartite graph, then $E_F(G) \leq E(G)$.

(b) If $F(x, y) \geq 1$ holds for all $x \geq 1$, $y \geq 1$, and if *G* is a bipartite graph, then $E_F(G) \geq E(G)$.

The equality cases will be considered later.

In order to prove Theorem 1, we need some preparations.

Preliminary considerations

Let

$$P(x) = \sum_{k \geq 0} c_k \, x^{n-k}$$

be a polynomial with all zeros real. Then its energy satisfies (Mateljević et al, 2010)

$$E(P) = \frac{1}{\pi} \int_0^{\infty} \frac{dx}{x^2} \ln \left[\left(\sum_{k \geq 0} (-1)^k c_{2k} x^{2k} \right)^2 + \left(\sum_{k \geq 0} (-1)^k c_{2k+1} x^{2k+1} \right)^2 \right]$$

If the zeros of *P*(*x*) are symmetric w.r.t. *x*=0, i.e., if $c_{2k+1} = 0$ for all $k \geq 0$, then

$$E(P) = \frac{2}{\pi} \int_0^{\infty} \frac{dx}{x^2} \ln \sum_{k \geq 0} (-1)^k c_{2k} x^{2k}$$

As well known, a graph is bipartite if and only if it does not contain cycles of odd size. The characteristic polynomial of a bipartite graph is of the form

$$\phi(G, x) = \sum_{k \geq 0} c_{2k} x^{n-2k}$$

Analogously, the characteristic polynomial of $\Phi = \Phi(G)$ conforms to the relation

$$\phi_F(G,x) = \sum_{k\geq 0} c_{2k}^{(F)} x^{n-2k}$$

The respective energies are then

$$E(G) = \frac{2}{\pi}\int_0^\infty \frac{dx}{x^2} \ln \sum_{k\geq 0} (-1)^k c_{2k} x^{2k} \qquad (1)$$

and

$$E_F(G) = \frac{2}{\pi}\int_0^\infty \frac{dx}{x^2} \ln \sum_{k\geq 0} (-1)^k c_{2k}^{(F)} x^{2k} \qquad (2)$$

Proving Theorem 1

We apply the Sachs coefficient theorem (Cvetković et al, 2010), (Gutman, 2017a). Recall that a Sachs graph is a graph consisting of vertices of degree one and/or two, i.e., all its components are isolated edges and/or cycles.

The application of the Sachs theorem to the coefficients of $\phi_F(G,x)$ yields:

$$c_{2k}^{(F)} = \sum_{s\in S_{2k}(G)} (-1)^{p(s)}\, 2^{q(s)}\, w(s)$$

where *s* is a Sachs graph and $S_{2k}(G)$ is the set of all (*2k*)-vertex Sachs graphs that are as subgraphs contained in the graph *G*, and where

p(*s*) = number of components of *s,*
q(*s*) =number of cyclic components of *s*, and
w(*s*) = weight of *s*.

The weight of *s* is equal to the product of the weights of all edges contained in the cycles of *s*, times the product of the squares of the weights of the isolated edges of *s.* The weight of a particular edge is equal to the respective element of the matrix $\Phi(G)$. For the proof of

Theorem 1(a), it is only important that $w(s) \leq 1$.

Let *G* be a bipartite graph, and let the Sachs graph $s \in S_{2k}(G)$ contain α isolated edges, β cycles of the size 4*i*+2, and γ cycles of the size 4*i*.Then,

$$p(s) = \alpha + \sum_i \beta_i + \sum_i \gamma_i$$

and

$$2k = 2\alpha + \sum_i (4i+2)\beta_i + \sum_i (4i)\gamma_i \,.$$

Therefore,

$$p(s) + k = 2\left(\alpha + \sum_i (i+1)\beta_i + \sum_i i\,\gamma_i \right) \alpha + \sum_i \gamma_i$$

implying

$$p(s) + k \equiv \sum_i \gamma_i \pmod 2 \,.$$

In view of the above, the contribution of the Sachs graph *s* to the term

$(-1)^{p(s)}\, 2^{q(s)}\, w(s)$ is:

positive if *s* contains no cycles of size divisible by 4,
negative if *s* contains an odd number of cycles of a size divisible by 4, and
positive if s contains an even number of cycles of a size divisible by 4.

Suppose first that $\sum_i \gamma_i$ is zero or even. Then, the contribution of the Sachs graph $s \in S_{2k}(G)$ to $E_F(G)$, Eq. (2), is positive, and because of $w(s) \le 1$, it is not greater than the respective contribution of *s* to $E(G)$, Eq. (1). In this case, $E_F(G) \le E(G)$, with equality if all non-zero elements of $\Phi(G)$ are equal to unity.

There remains a case when $\sum_i \gamma_i$ is an odd integer. Then, *s* has at least one cycle whose size is divisible by 4. Let, for the sake of simplicity, this be a single 12-membered cycle, whose edges are $e_1, e_2, e_3, e_4, e_5, e_6, e_7, e_8, e_9, e_{10}, e_{11}, e_{12}$. Then, in addition to *s*, there exist

two more Sachs graphs $s', s'' \in S_{2k}(G)$ in which instead of the 12-membered cycle, there are 6 isolated edges, $e_1, e_3, e_5, e_7, e_9, e_{11}$ and $e_2, e_4, e_6, e_8, e_{10}, e_{12}$, respectively. The total contribution of the three Sachs graphs $s, s', s'' \in S_{2k}(G)$ is then

$$-2\prod_{i=1}^{12} w(e_i) + \prod_{i=1}^{6} w(e_{2i-1})^2 + \prod_{i=1}^{6} w(e_{2i})^2$$

plus the (necessarily positive) contribution coming from the other (mutually identical) fragments of s, s', s''. The above expression is equal to

$$\left(\prod_{i=1}^{6} w(e_{2n-1}) - \prod_{i=1}^{6} w(e_{2i}) \right)^2$$

which is non-negative. Because of $w(e) \le 1$, this term is also less than or equal to unity.

Thus, also in this case, the joint contribution of the Sachs graphs s, s', s'' to $E_F(G)$ is positive but not greater than their contribution to $E(G)$.

This completes the proof of Theorem 1(a).

The proof of Theorem 1(b) is analogous. Note that the special case of Theorem 1(b), pertaining to extended energy, was earlier communicated in (Gutman, 2017b).

Discussion

If the graph *G* is not bipartite, then it contains odd cycles. Then, of course, some Sachs graphs also contain odd cycles. Consequently, some of the coefficients c_{2k+1} and $c_{2k+1}^{(F)}$ are non-zero. Besides, the sign of the coefficients c_{2k} and $c_{2k}^{(F)}$ cannot be predicted in the general case. For these reasons, it is not easy to extend Theorem 1 to non-bipartite graphs, and we leave this for some later moment or some more skilled colleague.

From the definitions of $E(G)$ and $E_F(G)$, it is evident that the equality $E_F(G) = E(G)$ will hold if all non-zero elements of the matrix $\Phi(G)$ are equal to unity. Whether this is an "if and only if" condition remains a (difficult) open problem.

In the case of regular graphs, for which $\deg(v_i) = r$, $i=1,2,\ldots,n$, the relation between $E(G)$ and $E_F(G)$ is significantly simplified. $E_F(G) = E(G)$ holds for the extended, geometric-arithmetic, and arithmetic energies. In addition, $E_F(G) = 2rE(G)$ holds for the first Zagreb energy, $E_F(G) = r^2E(G)$ for the second Zagreb energy, $E_F(G) = 2r^2E(G)$ for the forgotten energy, $E_F(G) = \frac{1}{r}E(G)$ for the Randić and harmonic energies, etc. Interestingly but evidently, the Albertson and sigma energies of regular graphs are equal to zero. On the other hand, for the class of stepwise irregular graphs (Gutman, 2018), the Albertson and sigma matrices coincide with the adjacency matrix, and for such graphs the Albertson and sigma energies are equal to the ordinary graph energy.

References

Cruz, R., Pèrez, T. & Rada, J. 2015. Extremal values of vertex-degree-based topological indices over graphs. *Journal of Applied Mathematics and Computing*, 48(1-2), pp.395-406. Available at: https://doi.org/10.1007/s12190-014-0809-y.

Cvetković, D., Rowlinson, P. & Simić, K. 2010. *An Introduction to the Theory of Graph Spectra*. Cambridge: Cambridge University Press. ISBN: 9780521134088.

Das, K.C., Gutman, I., Milovanović, I., Milovanović, E. & Furtula, B. 2018. Degree-based energies of graphs. *Linear Algebra and its Applications,* 554, pp.185-204. Available at: https://doi.org/10.1016/j.laa.2018.05.027.

Furtula, B., Gutman, I. & Dehmer, M. 2013. On structure-sensitivity of degree-based topological indices. *Applied Mathematics and Computation,* 219(17), pp.8973-8978. Available at: https://doi.org/10.1016/j.amc.2013.03.072.

Gutman, I. 1978. The energy of a graph. *Berichte der Mathematisch-Statistischen Sektion im Forschungszentrum Graz*, 103, pp.1-22.

Gutman, I. 2017a. *Selected Theorems in Chemical Graph Theory*. Kragujevac: University of Kragujevac.

Gutman, I. 2017b. Relation between energy and extended energy of a graph. *International Journal of Applied Graph Theory*,1(1), pp.42-48.

Gutman, I. 2018. Stepwise irregular graphs. *Applied Mathematics and Computation*, 325, pp.234-238. Available at: https://doi.org/10.1016/j.amc.2017.12.045.

Kulli, V.R. 2020. Graph indices. In: Pal, M., Samanta, S. & Pal, A. (Eds.), *Handbook of Research of Advanced Applications of Graph Theory in Modern Society*, pp.66-91. Hershey, USA: IGI Global. Available at: https://doi.org/10.4018/978-1-5225-9380-5.ch003.

Li, X., Shi, Y. & Gutman, I. 2012. Introduction. In: *Graph Energy*, pp.1-9. New York, NY: Springer Science and Business Media LLC. Available at: https://doi.org/10.1007/978-1-4614-4220-2_1.

Liu, M., Xu, K. & Zhang, X.-D. 2019. Extremal graphs for vertex-degree-based invariants with given degree sequences. *Discrete Applied Mathematics,* 255, pp.267-277. Available at: https://doi.org/10.1016/j.dam.2018.07.026.

Mateljević, M., Božin, V. & Gutman, I. 2010. Energy of a polynomial and the Coulson integral formula. *Journal of Mathematical Chemistry*, 48(4), pp.1062-1068. Available at: https://doi.org/10.1007/s10910-010-9725-z.

Rada, J. & Cruz, R. 2014. Vertex-degree-based topological indices over graphs. *MATCH Communications in Mathematical and in Computer Chemistry*, 72(3), pp.603-616 [online]. Available at: http://match.pmf.kg.ac.rs/electronic_versions/Match72/n3/match72n3_603-616.pdf [Accessed: 15 August 2020].

Todeschini, R. & Consonni, V. 2009. *Molecular Descriptors for Chemoinformatics*. Weinheim: Wiley-VCH. ISBN: 978-3-527-31852-0.

Zhong, L. & Xu, K. 2014. Inequalities between vertex-degree-based topological indices. *MATCH Communications in Mathematical and in Computer Chemistry,* 71(3), pp.627-642 [online]. Available at: http://match.pmf.kg.ac.rs/electronic_versions/Match71/n3/match71n3_627-642.pdf [Accessed: 15 August 2020].

ВЗАИМОСВЯЗЬ ЭНЕРГИИ ГРАФОВ С ЭНЕРГИЕЙ СТЕПЕНИ УЗЛОВ

Иван Гутман

Крагуевацкий университет, Естественно-математический факультет, г. Крагуевац, Республика Сербия

РУБРИКА ГРНТИ: 27.00.00 МАТЕМАТИКА;
27.29.19 Краевые задачи и задачи на собственные значения для обыкновенных дифференциальных уравнений и систем уравнений

ВИД СТАТЬИ: оригинальная научная статья

Резюме:

Введение/цель: На основании анализа существующей литературы, в статье представлены многочисленные инварианты графов, зависимые от степени узлов. К каждому из этих инвариантов подключается соответствующая матрица, с помощью которой считывается энергия графа, как сумма абсолютных величин собственных значений данных матриц.

Результаты: В статье определены условия, при которых вычисленные энергии графа были больше или меньше средней энергии графа (на основании матрицы смежности).

Выводы: Результаты данной статьи вносят вклад в теорию энергии графов, а также в теорию инвариантов графов, основанных на степени узлов.

Ключевые слова: энергия (графа); инварианты, зависящие от степени узлов; энергия, зависящая от степени узлов.

РЕЛАЦИЈЕ ИЗМЕЂУ ЕНЕРГИЈЕ ГРАФА И ЕНЕРГИЈА ЗАСНОВАНИХ НА СТЕПЕНИМА ЧВОРОВА

Иван Гутман

Универзитет у Крагујевцу, Природно-математички факултет,
Крагујевац, Република Србија

ОБЛАСТ: математика
ВРСТА ЧЛАНКА: оригинални научни рад

Сажетак:

Увод/циљ: У раду су приказане бројне, у литератури постојеће, графовске инваријанте зависне од степена чворова. Овим инваријантама придружују се одговарајуће матрице, преко којих се израчунава енергија као збир апсолутних вредности сопствених вредности ових матрица.

Резултати: Одређени су услови под којима су испитиване веће, односно мање енергије од обичне енергије графа (засноване на матрици суседства).

Закључак: Рад доприноси теорији графовских енергија, као и теорији графовских инваријанти зависних од степена чворова.

Кључне речи: енергија (графа), инваријанте зависне од степена чворова, енергије зависне од степена чворова.

Paper received on / Дата получения работы / Датум пријема чланка: 21.08.2020.
Manuscript corrections submitted on / Дата получения исправленной версии работы / Датум достављања исправки рукописа: 28.08.2020.
Paper accepted for publishing on / Дата окончательного согласования работы / Датум коначног прихватања чланка за објављивање: 30.08.2020.

EXISTENCE AND UNIQUENESS OF THE SOLUTIONS OF SOME CLASSES OF INTEGRAL EQUATIONS C*-ALGEBRA-VALUED *b*-METRIC SPACES

Esad Jakupović[a], *Hashem* P. Masiha[b], *Zoran* D. Mitrović[c], *Seyede* S. Razavi[d], *Reza* Saadati[e]

[a]Academy of Sciences and Arts of the Republic of Srpska, Banja Luka, Republic of Srpska, Bosnia and Herzegovina,
e-mail: esadjakupovic50@gmail.com,
ORCID ID: https://orcid.org/0000-0003-2354-5532

[b]K. N. Toosi University of Technology, Faculty of Mathematics, Tehran, Islamic Republic of Iran,
e-mail: masihahp@kntu.ac.ir,
ORCID ID: https://orcid.org/0000-0001-9751-6828

[c]University of Banja Luka, Faculty of Electrical Engineering, Banja Luka, Republic of Srpska, Bosnia and Herzegovina,
e-mail: zoran.mitrovic@etf.unibl.org, **corresponding author,**
ORCID ID: https://orcid.org/0000-0001-9993-9082

[d]K. N. Toosi University of Technology, Faculty of Mathematics, Tehran, Islamic Republic of Iran,
e-mail: ssrazavi@kntu.ac.ir,
ORCID ID: https://orcid.org/0000-0002-9772-1140

[e]Iran University of Science and Technology, School of Mathematics, Narmak, Tehran, Islamic Republic of Iran,
e-mail: rsaadati@iust.ac.ir,
ORCID ID: https://orcid.org/0000-0002-6770-6951

DOI: 10.5937/vojtehg68-28632; https://doi.org/10.5937/vojtehg68-28632

FIELD: Mathematics

ARTICLE TYPE: Original scientific paper

Abstract:

Introduction/purpose: The aim of the paper is to establish some coupled fixed point results in C-algebra-valued b-metric spaces. Moreover, the obtained results are used to define the sufficient conditions for the existence of the solutions of some classes of integral equations.*

Methods: The method of coupled fixed points gives the sufficient conditions for the existence of the solution of some classes of integral equations.

*Results: New results were obtained on coupled fixed points in C * -algebra-valued b-metric space.*

Conclusion: The obtained results represent a contribution in the fixed point theory and open new possibilities of application in the theory of differential and integral equations.

Key words: Coupled fixed point, C-algebra, integral equation.*

Basic definitions

In this section, we review some facts of the C*-algebras which are needed in this paper. The references (Ali Abou Bakr, 2019), (Bai, 2016), (Bonsal, 1962), (Hussain et al, 2018), (Huang et al, 2018), (Hussain&Mitrović, 2017), (Kadelburg et al, 2016), (Kadelburg&Radenović, 2016), (Kongban&Kumam, 2018), (Ma et al, 2014), (Ma&Jiang, 2015), (Mitrović et al, 2019), (Radenović et al, 2017), (Radenović et al, 2019), (Vujaković et al, 2019), (Zoto et al, 2019), (Wu&Zhao, 2018), (Cao&Xin, 2016) and (Todorčević, 2019) are useful.

We denote $\mathcal{A}$ as a unital C*-algebra with the unit $1_{\mathcal{A}}$.

Let

$$\mathcal{A}_h = \{t \in \mathcal{A} : t = t^*\}.$$

We say $t \in \mathcal{A}$ a positive element, showed it by $t \succeq 0_{\mathcal{A}}$ if $t \in \mathcal{A}_h$ and $\sigma(t) \subseteq [0, \infty)$, where $0_{\mathcal{A}}$ is the zero element in $\mathcal{A}$ and $\sigma(t)$ is the spectrum of t.

On the set $\mathcal{A}_h$ we have a partial ordering given by $v \succeq u$ if and only if $v - u \succeq 0_{\mathcal{A}}$. Also, we will denote

$$\mathcal{A}_+ = \{t \in \mathcal{A} : t \succeq 0_{\mathcal{A}}\}$$

and

$$\mathcal{A}' = \{t \in \mathcal{A} : tk = kt \text{ for all } k \in \mathcal{A}\}.$$

Definition 1. *Assume that $\mathcal{X} \neq \emptyset$. As usual suppose that $\delta : \mathcal{X} \times \mathcal{X} \to \mathcal{A}$ is a function fulfilling:*

(1) $\delta(u, v) \succeq 0_{\mathcal{A}}$ for each u and v in $\mathcal{X}$;

(2) $\delta(v, u) = 0_{\mathcal{A}}$ if $v = u$;

(3) $\delta(u, v) = \delta(v, u)$ for each u and v in $\mathcal{X}$;

(4) $\delta(u, v) \preceq \delta(u, t) + \delta(t, v)$ for each u, v and $t \in \mathcal{X}$.

Then δ is a C-algebra-valued metric (shortly, C*-AV-M).*

Definition 2. *Assume that $\mathcal{X} \neq \emptyset$. Suppose that $b \in \mathcal{A}'$ such that $||b|| \geq 1$. A function $\delta_b : \mathcal{X}^2 \to \mathcal{A}$ is said to be a C*-algebra-valued b-metric (in short C*-AV-BM) on $\mathcal{X}$ if for every $u, v, t \in \mathcal{A}$:*

(1) $\delta_b(u, v) \succeq 0_{\mathcal{A}}$ for each u and v in $\mathcal{X}$ and $\delta_b(u, v) = 0$ if $u = v$;

(2) $\delta_b(u, v) = \delta_b(v, u)$;

(3) $\delta_b(u, v) \preceq b[\delta_b(u, t) + \delta_b(t, v)]$.

Then $(\mathcal{X}, \mathcal{A}, \delta_b)$ is a C-AV-BM space with the coefficient b.*

Example 1 (Ma&Jiang (2015)). Assume that $\mathcal{X} = \mathbb{R}$ and $\mathcal{A} = M_n(\mathbb{R})$. Now, we define

$$\delta(u, v) = diag(c_1|u - v|^p, c_2|u - v|^p, \ldots, c_n|u - v|^p),$$

where $diag$ denotes a diagonal matrix, and where $u, v \in \mathbb{R}$, $c_1, \ldots, c_n$ positive constants and $p \in (1, +\infty)$. It can be shown that $(\mathcal{X}, \mathcal{A}, \delta)$ is a complete C*-AV-BM. We only prove the third statement of Definition 2. For this we have:

$$|u - v|^p \leq 2^p(|u - t|^p + |t - v|^p),$$

then $\delta(u, v) \preceq A[\delta(u, t) + \delta(t, v)]$ for every $u, v, t \in \mathcal{X}$, where $A = 2^p I \in \mathcal{A}'$ and $A > I$ by $2^p > 1$. Since $|u - v|^p \leq |u - t|^p + |t - v|^p$ is impossible for all $u \succ t \succ v$, $(\mathcal{X}, M_n(\mathbb{R}), \delta)$ is not a C*-AV-M space.

Definition 3. *Assume that $(\mathcal{X}, \mathcal{A}, \delta_b)$ is a C*-AV-BM space. $(u, v) \in \mathcal{X} \times \mathcal{X}$ is called a coupled fixed point (shortly FP) of the function $\psi : \mathcal{X} \times \mathcal{X} \to \mathcal{X}$ if $\psi(u, v) = u$ and $\psi(v, u) = v$.*

For some useful applications, see (Kongban&Kumam, 2018) and (Ali Abou Bakr, 2019).

Main results

The following theorem is one of our main results.

Theorem 1. *Assume that $(\mathcal{X}, \mathcal{A}, \delta_b)$ is a C*-AV-BM space and suppose that $\psi : \mathcal{X}^2 \to \mathcal{X}$ is a function satisfying*

$$\delta_b(\psi(u, v), \psi(t, s)) \preceq a^* \delta_b(u, t)a + a^* \delta_b(v, s)a, \tag{1}$$

for every $u, v, t, s \in \mathcal{X}$, in which $a \in \mathcal{A}$ with $||a|| < \frac{1}{\sqrt{2}}$. Then ψ has a unique coupled FP. Moreover, ψ has a unique FP in $\mathcal{X}$.

Proof. Let $u_0, v_0 \in \mathcal{X}$. Set $u_1 = \psi(u_0, v_0)$ and $v_1 = \psi(v_0, u_0)$. We obtain two sequences $\{u_n\}$, $\{v_n\}$ in $\mathcal{X}$ such that $u_{n+1} = \psi(u_n, v_n)$ and $v_{n+1} = \psi(v_n, u_n)$ if we continue the above process. From (1) we have

$$\begin{aligned}\delta_b(u_n, u_{n+1}) &= \delta_b(\psi(u_{n-1}, v_{n-1}), \psi(u_n, v_n)) \\ &\preceq a^*\delta_b(u_{n-1}, u_n)a + a^*\delta_b(v_{n-1}, v_n)a \\ &\preceq a^*(\delta_b(u_{n-1}, u_n) + \delta_b(v_{n-1}, v_n))a.\end{aligned} \tag{2}$$

Similarly,

$$\begin{aligned}\delta_b(v_n, v_{n+1}) &= \delta_b(\psi(v_{n-1}, u_{n-1}), \psi(v_n, u_n)) \\ &\preceq a^*\delta_b(v_{n-1}, v_n)a + a^*\delta_b(u_{n-1}, u_n)a \\ &\preceq a^*(\delta_b(v_{n-1}, v_n) + \delta_b(u_{n-1}, u_n))a.\end{aligned} \tag{3}$$

Let

$$\delta_n = \delta_b(u_n, u_{n+1}) + \delta_b(v_n, v_{n+1}).$$

From (2) and (3), we have

$$\begin{aligned}\delta_n &= \delta_b(u_n, u_{n+1}) + \delta_b(v_n, v_{n+1}) \\ &\preceq a^*(\delta_b(u_{n-1}, u_n) + \delta_b(v_{n-1}, v_n))a + a^*(\delta_b(v_{n-1}, v_n) + \delta_b(u_{n-1}, u_n))a \\ &= 2(a^*(\delta_b(u_{n-1}, u_n) + \delta_b(v_{n-1}, v_n))a) \\ &\preceq (\sqrt{2}a)^*(\delta_b(u_{n-1}, u_n) + \delta_b(v_{n-1}, v_n))(\sqrt{2}a) \\ &\preceq (\sqrt{2}a)^*\delta_{n-1}(\sqrt{2}a).\end{aligned}$$

Due to the following property: (if $t, k \in \mathcal{A}_h$, then $t \preceq k$ implies $u^*tu \preceq u^*ku$), we can obtain for any $n \in \mathbb{N}$,

$$0_{\mathcal{A}} \preceq \delta_n \preceq (\sqrt{2}a)^*\delta_{n-1}(\sqrt{2}a) \preceq \ldots \preceq ((\sqrt{2}a)^*)^n\delta_0(\sqrt{2}a)^n.$$

If $\delta_0 = 0_{\mathcal{A}}$, then from (2) of Definition 2 we know (u_0, v_0) is a coupled FP of F.

Now, by letting $\delta_0 \preceq 0_{\mathcal{A}}$, we can obtain for $m, n \in \mathbb{N}$, $n > m$

$$\begin{aligned}\delta_b(u_n, u_m) &\preceq b(\delta_b(u_n, u_{n-1}) + \delta_b(u_{n-1}, u_m)) \\ &\preceq b\delta_b(u_n, u_{n-1}) + b^2\delta_b(u_{n-1}, u_{n-2}) + b^2\delta_b(u_{n-2}, u_m) \\ &\preceq b\delta_b(u_n, u_{n-1}) + b^2\delta_b(u_{n-1}, u_{n-2})\end{aligned}$$

$$
\begin{aligned}
&+ b^3\delta_b(u_{n-2}, u_{n-3}) + \ldots + b^{n-m}\delta_b(u_{m+1}, u_m) \\
&\preceq b\delta_b(u_n, u_{n-1}) + b^2\delta_b(u_{n-1}, u_{n-2}) + \ldots \\
&+ b^{n-m-1}\delta_b\left(u_{m+2}, u_{m+1}\right) + b^{n-m-1}\delta_b\left(u_{m+1}, u_m\right).
\end{aligned}
$$

Similarly,

$$
\begin{aligned}
\delta_b(v_n, v_m) \quad \preceq \quad & b\delta_b(v_n, v_{n-1}) + b^2\delta_b(v_{n-1}, v_{n-2}) + \ldots + \\
& b^{n-m-1}\delta_b\left(v_{m+2}, v_{m+1}\right) + b^{n-m-1}\delta_b\left(v_{m+1}, v_m\right).
\end{aligned}
$$

Therefore,

$$
\begin{aligned}
\delta_b(u_n, u_m) + \delta_b(v_n, v_m) \preceq\ & b(\delta_b(u_n, u_{n-1}) + \delta_b(v_n, v_{n-1})) \\
& + b^2(\delta_b(u_{n-1}, u_{n-2}) + \delta_b(v_{n-1}, v_{n-2})) \\
& + \ldots + b^{n-m-1}\left(\delta_b\left(u_{m+2}, u_{m+1}\right) + \delta_b\left(v_{m+2}, v_{m+1}\right)\right) \\
& + b^{n-m}\left(\delta_b\left(u_{m+1}, u_m\right) + \delta_b\left(v_{m+1}, v_m\right)\right) \\
& \preceq b\delta_{n-1} + b^2\delta_{n-2} + \ldots + b^{n-m}\delta_m \\
& \preceq b((2^{\frac{1}{2}}a)^*)^{n-1}\delta_0(2^{\frac{1}{2}}a)^{n-1} + b^2((2^{\frac{1}{2}}a)^*)^{n-2}\delta_0(2^{\frac{1}{2}}a)^{n-2} \\
& + \ldots + b^{n-m}((2^{\frac{1}{2}}a)^*)^m\delta_0(2^{\frac{1}{2}}a)^m \\
& \preceq \sum_{k=n-1}^{m} b^{n-k}((2^{\frac{1}{2}}a)^*)^k\delta_0(2^{\frac{1}{2}}a)^k.
\end{aligned}
$$

Therefore,

$$
\begin{aligned}
||\delta_b(u_n, u_m) + \delta_b(v_n, v_m)|| &\leq \sum_{k=n-1}^{m} ||b||^{n-k}||\sqrt{2}a||^{2k}\delta_0 \\
&\leq \sum_{k=n-1}^{\infty} ||b||^{n-k}||\sqrt{2}a||^{2k}\delta_0 \\
&\leq \frac{||b||||\sqrt{2}a||^{2(n-1)}}{1 - ||b||^{-1}||\sqrt{2}a||^2}\delta_0 \\
&= \frac{||b||}{1 - ||b||^{-1}||\sqrt{2}a||^2}||\sqrt{2}a||^{2(n-1)}\delta_0.
\end{aligned}
$$

Since $||a|| < \frac{1}{\sqrt{2}}$, we have

$$||\delta_b(u_n, u_m) + \delta_b(v_n, v_m)|| \leq \frac{||b||}{1 - ||b||^{-1}||\sqrt{2}a||^2}||\sqrt{2}a||^{2(n-1)}\delta_0 \longrightarrow 0,$$

$$\delta_b(u_n, u_m) \preceq \delta_b(u_n, u_m) + \delta_b(v_n, v_m),$$

and

$$\delta_b(v_n, v_m) \preceq \delta_b(v_n, v_m) + \delta_b(u_n, u_m),$$

yields that $\{u_n\}$ and $\{v_n\}$ are Cauchy sequences in $\mathcal{X}$, so we can find u and v in $\mathcal{X}$ such that $\lim_{n\to\infty} u_n = u$ and $\lim_{n\to\infty} v_n = v$. Now, we prove that $\psi(u, v) = u$ and $\psi(v, u) = v$.

From the triangle inequality and (1), we obtain

$$\begin{aligned}\delta_b(\psi(u, v), u) &\preceq b[\delta_b(\psi(u, v), u_{n+1}) + \delta_b(u_{n+1}, u)] \\ &\preceq b[\delta_b(\psi(u, v), \psi(u_n, v_n)) + \delta_b(u_{n+1}, u)] \\ &\preceq b[a^*\delta_b(u, u_n)a + a^*\delta_b(v, v_n)a + \delta_b(u_{n+1}, u)],\end{aligned}$$

taking $n \to \infty$, we have that $\delta_b(\psi(u, v), u) = 0_{\mathcal{A}}$, and consequently $\psi(u, v) = u$. In the same way $\psi(v, u) = v$. Therefore, a coupled FP of ψ is (u, v).

Assume that another coupled FP of ψ is (u', v'), so

$$\delta_b(u, u') = \delta_b(\psi(u, v), \psi(u', v')) \preceq a^*\delta_b(u, u')a + a^*\delta_b(v, v')a,$$

$$\delta_b(v, v') = \delta_b(\psi(v, u), \psi(v', u')) \preceq a^*\delta_b(v, v')a + a^*\delta_b(u, u')a,$$

and hence

$$\delta_b(u, u') + \delta_b(v, v') \preceq (\sqrt{2}a)^*(\delta_b(u, u') + \delta_b(v, v'))(\sqrt{2}a).$$

The above inequality with $||\sqrt{2}a|| < 1$ yields that

$$||\delta_b(u, u') + \delta_b(v, v')|| \leq ||\sqrt{2}a||^2||\delta_b(u, u') + \delta_b(v, v')||.$$

The above inequality holds only when $||\delta_b(u, u') + \delta_b(v, v')|| = 0$, which gives $(u', v') = (u, v)$. So the coupled FP is unique.

Now, we prove that $u = v$ to show that ψ has a unique FP. Note that

$$\delta_b(u, v) = \delta_b(\psi(u, v) + \psi(v, u)) \preceq a^*\delta_b(u, v)a + a^*\delta_b(v, u)a,$$

and hence

$$||\delta_b(u, v)|| \leq ||a||^2||\delta_b(u, v)|| + ||a||^2||\delta_b(v, u)||$$

$$\leq 2||a||^2||\delta_b(u,v)||.$$

In fact, from $||a|| < \frac{1}{\sqrt{2}}$ we get $||\delta_b(u,v)|| = 0$, thus $u = v$. □

Lemma 1. *(Ma et al, 2014)*

1) If $u \in \mathcal{A}_+$ with $||u|| < \frac{1}{2}$, then $1_\mathcal{A} - u$ is invertible.

2) If $u, v \in \mathcal{A}_+$ with $uv = vu$, then $uv \succeq 0_\mathcal{A}$.

3) If $u, v \in \mathcal{A}_h$ and $t \in \mathcal{A}'_+$, then $u \preceq v$ deduces $tu \preceq tv$, where $\mathcal{A}'_+ = \mathcal{A}_+ \cap \mathcal{A}'$.

Theorem 2. *Assume that $(X, \mathcal{A}, \delta_b)$ is a complete C*-AV-BM space and suppose that the function $\psi : \mathcal{X}^2 \to \mathcal{X}$ satisfies*

$$\delta_b(\psi(u,v), \psi(t,s)) \preceq a\delta_b(\psi(u,v), u) + b\delta_b(\psi(t,s), t), \ \forall u, v, t, s \in \mathcal{X} \quad (4)$$

in which $a, b, c, \in \mathcal{A}'_+$ with $||a|| + ||b|| < 1$, $||ac|| + ||bc|| < 1$, $||c|| > 1$. Then ψ has a unique coupled FP. Also, ψ has a unique FP in $\mathcal{X}$.

Proof. As in Theorem 1, choose $\{u_n\}$ and $\{v_n\}$ in $\mathcal{X}$ and set $u_{n+1} = \psi(u_n, v_n)$ and $v_{n+1} = \psi(v_n, u_n)$. Then from (4),

$$\begin{aligned}\delta_b(u_n, u_{n+1}) &= \delta_b(\psi(u_{n-1}, v_{n-1}), \psi(u_n, v_n)) \\ &\preceq a\delta_b(\psi(u_{n-1}, v_{n-1}), u_{n-1}) + b\delta_b(\psi(u_n, v_n), u_n) \\ &= a\delta_b(u_n, u_{n-1}) + b\delta_b(u_{n+1}, u_n),\end{aligned}$$

Thus,

$$(1_\mathcal{A} - b)\delta_b(u_n, u_{n+1}) \preceq a\delta_b(u_n, u_{n-1}),$$

Similarly,

$$(1_\mathcal{A} - b)\delta_b(v_n, v_{n+1}) \preceq a\delta_b(v_n, v_{n-1}),$$

Since $a, b \in \mathcal{A}'_+$ with $||a|| + ||b|| < 1$, then $1_\mathcal{A} - b$ is invertible and $(1_\mathcal{A} - b)^{-1}a \in \mathcal{A}'_+$. Therefore

$$\delta_b(u_n, u_{n+1}) \preceq (1_\mathcal{A} - b)^{-1}a\delta_b(u_n, u_{n-1}),$$

$$\delta_b(v_n, v_{n+1}) \preceq (1_\mathcal{A} - b)^{-1}a\delta_b(v_n, v_{n-1}),$$

Then

$$||\delta_b(u_n, u_{n+1})|| \leq ||(1_\mathcal{A} - b)^{-1}a||||\delta_b(u_n, u_{n-1})||,$$

$$||\delta_b(v_n, v_{n+1})|| \leq ||(1_{\mathcal{A}} - b)^{-1}a||||\delta_b(v_n, v_{n-1})||,$$

It follows from the fact

$$||(1_{\mathcal{A}} - b)^{-1}a|| \leq ||(1_{\mathcal{A}} - b)^{-1}||||a|| \leq \sum_{k=0}^{\infty} ||b||^k||a|| = \frac{||a||}{1 - ||b||} < 1.$$

Hence $\{u_n\}$ and $\{v_n\}$ are Cauchy sequences in $\mathcal{X}$. By the completeness of $\mathcal{X}$, there are $u, v \in \mathcal{X}$ such that $\lim_{n\to\infty} u_n = u$ and $\lim_{n\to\infty} v_n = v$. As

$$\begin{aligned}
\delta_b(\psi(u, v), u) &\preceq c[\delta_b(u_{n+1}, \psi(u, v)) + \delta_b(u_{n+1}, u)] \\
&= c\delta_b(\psi(u_n, v_n), \psi(u, v)) + c\delta_b(u_{n+1}, u) \\
&\preceq ca\delta_b(\psi(u_n, v_n), u_n) + cb\delta_b(\psi(u, v), u) + c\delta_b(u_{n+1}, u) \\
&\preceq ca\delta_b(u_{n+1}, u_n) + cb\delta_b(\psi(u, v), u) + c\delta_b(u_{n+1}, u),
\end{aligned}$$

which deduces that

$$\delta_b(\psi(u, v), u) \preceq (1_{\mathcal{A}} - cb)^{-1}ca\delta_b(u_{n+1}, u_n) + (1_{\mathcal{A}} - cb)^{-1}c\delta_b(u_{n+1}, u).$$

like above

$$||(1_{\mathcal{A}} - cb)^{-1}ca|| \leq ||(1_{\mathcal{A}} - cb)^{-1}||||ca|| \leq \sum_{k=0}^{\infty} ||cb||^k||ca|| = \frac{||ca||}{1 - ||cb||} < 1.$$

$$||(1_{\mathcal{A}} - cb)^{-1}c|| \leq ||(1_{\mathcal{A}} - cb)^{-1}||||c|| \leq \sum_{k=0}^{\infty} ||cb||^k||c|| = \frac{||c||}{1 - ||cb||} < 1.$$

Then $\delta_b(\psi(u, v), u) = 0_{\mathcal{A}}$ or equivalently $\psi(u, v) = u$. In the same way, $\psi(v, u) = v$. Now if (u', v') is another coupled FP of ψ, then from (4), we get

$$\begin{aligned}
\delta_b(u, u') &= \delta_b(\psi(u, v), \psi(u', v')) \\
&\preceq a\delta_b(u', \psi(u', v')) + b\delta_b(u, \psi(u, v)) = 0_{\mathcal{A}},
\end{aligned}$$

Hence $\delta_b(u', u) = 0_{\mathcal{A}}$, and then$u' = u$. In the same way, we can obtain that $v' = v$. That is, (u, v) is the unique coupled FP of ψ. Now, we prove the uniqueness of FPs of ψ. Using (4), we obtain

$$\begin{aligned}
\delta_b(u, v) &= \delta_b(\psi(u, v), \psi(v, u)) \\
&\preceq a\delta_b(\psi(u, v), u) + b\delta_b(\psi(v, u), v) \\
&= a\delta_b(u, u) + b\delta_b(v, v) = 0_{\mathcal{A}}.
\end{aligned}$$

This yields that $u = v$. □

Theorem 3. *Assume that* $(\mathcal{X}, \mathcal{A}, \delta_b)$ *is a complete C*-AV-BM space and let the function* $F : \mathcal{X}^2 \to \mathcal{X}$ *hold*

$$\delta_b(\psi(u,v),\psi(t,s)) \preceq a\delta_b(\psi(u,v),t) + b\delta_b(\psi(t,s),u),\ \forall u,v,t,s \in \mathcal{X} \tag{5}$$

where $a, b, c \in \mathcal{A}'_+$ *with* $||a|| + ||b|| < 1$, $||ac|| + ||bc|| < 1$, $||c|| > 1$. *then* ψ *has a unique coupled FP. Also,* ψ *has a unique FP in* $\mathcal{X}$.

Proof. Similar to Theorem 2, choose two sequences $\{u_n\}$ and $\{v_n\}$ in $\mathcal{X}$ and set $u_{n+1} = \psi(u_n, v_n)$ and $v_{n+1} = \psi(v_n, u_n)$. Then from (5) we obtain

$$\begin{aligned}
\delta_b(u_n, u_{n+1}) &= \delta_b(\psi(u_{n-1}v_{n-1}), \psi(u_n, v_n)) \\
&\preceq a\delta_b(\psi(u_{n-1}, v_{n-1}), u_n) + b\delta_b(\psi(u_n, v_n), u_{n-1}) \\
&= a\delta_b(u_n, u_n) + b\delta_b(u_{n+1}, u_{n-1}) \\
&= b\delta_b(u_{n+1}, u_{n-1}) \\
&\preceq cb(\delta_b(u_{n+1}, u_n) + \delta_b(u_n, u_{n-1})) \\
&= cb\delta_b(u_{n+1}, u_n) + cb\delta_b(u_n, u_{n-1}),
\end{aligned}$$

Thus,

$$(1_{\mathcal{A}} - cb)\delta_b(u_n, u_{n+1}) \preceq cb\delta_b(u_n, u_{n-1}). \tag{6}$$

By the symmetry in (5),

$$\begin{aligned}
\delta_b(u_{n+1}, u_n) &= \delta_b(\psi(u_n v_n), \psi(u_{n-1}, v_{n-1})) \\
&\preceq a\delta_b(\psi(u_n, v_n), u_{n-1}) + b\delta_b(\psi(u_{n-1}, v_{n-1}), u_n) \\
&= a\delta_b(u_{n+1}, u_{n-1}) + b\delta_b(u_n, u_n) \\
&= a\delta_b(u_{n+1}, u_{n-1}) \\
&\preceq ca(\delta_b(u_{n+1}, u_n) + \delta_b(u_n, u_{n-1})) \\
&= ca\delta_b(u_{n+1}, u_n) + ca\delta_b(u_n, u_{n-1}),
\end{aligned}$$

that is,

$$(1_{\mathcal{A}} - ca)\delta_b(u_n, u_{n+1}) \preceq ca\delta_b(u_n, u_{n-1}). \tag{7}$$

Now, from (6) and (7) we obtain

$$(1_{\mathcal{A}} - \frac{ca+cb}{2})\delta_b(u_n, u_{n+1}) \preceq \frac{ca+cb}{2}\delta_b(u_n, u_{n-1}).$$

Since $a, b, c \in \mathcal{A}'_+$ with $||ca+cb|| \leq ||ca||+||cb|| < 1$, then $(1_{\mathcal{A}} - \frac{ca+cb}{2})^{-1} \in \mathcal{A}'_+$, which together with [3, Lemma 1] yields that

$$\delta_b(u_n, u_{n+1}) \preceq (1_{\mathcal{A}} - \frac{ca+cb}{2})^{-1} \frac{ca+cb}{2} \delta_b(u_n, u_{n-1}).$$

Let $t = (1_{\mathcal{A}} - \frac{ca+cb}{2})^{-1} \frac{ca+cb}{2}$, then $||t|| = ||(1_{\mathcal{A}} - \frac{ca+cb}{2})^{-1} \frac{ca+cb}{2}|| < 1$.

By using the same argument of Theorem 2, we obtain $\{u_n\}$ which is a Cauchy sequence in X. Also, one can show that $\{v_n\}$ is a Cauchy sequence in $\mathcal{X}$. Therefore by the completeness of $\mathcal{X}$, there are $u, v \in \mathcal{X}$ such that $\lim_{n\to\infty} u_n = u$ and $\lim_{n\to\infty} v_n = v$. Now, we obtain that $\psi(u, v) = u$ and $\psi(v, u) = v$. To do this, we have

$$\begin{aligned}
\delta_b(\psi(u,v), u) &\preceq c[\delta_b(u_{n+1}, \psi(u,v)) + \delta_b(u_{n+1}, u)] \\
&= c\delta_b(\psi(u_n, v_n), \psi(u,v)) + c\delta_b(u_{n+1}, u) \\
&\preceq ca\delta_b(\psi(u_n, v_n), u) + cb\delta_b(\psi(u,v), u_n) + c\delta_b(u_{n+1}, u) \\
&\preceq ca\delta_b(u_{n+1}, u) + cb\delta_b(\psi(u,v), u_n) + c\delta_b(u_{n+1}, u),
\end{aligned}$$

and then

$$||\delta_b(\psi(u,v), u)|| \leq ||ca||||\delta_b(u_{n+1}, u)||+||cb||||\delta_b(\psi(u,v), u_n)||+||c||||\delta_b(u_{n+1}, u)||,$$

by the continuity of the metric and the norm, we get

$$||\delta_b(\psi(u,v), u)|| \leq ||cb||||\delta_b(\psi(u,v), u)||.$$

Since $||cb|| < 1$, it implies that $||\delta_b(\psi(u,v), u)|| = 0$, and then $\psi(u, v) = u$. In the same way, $\psi(v, u) = v$, which implies that (u, v) is a coupled FP of ψ. By the same reasoning in Theorem 2, we obtain $u = v$, which means that ψ has a unique FP in $\mathcal{X}$. □

Existence and uniqueness

Consider the next equation:

$$x(m) = \int_{\mathcal{E}} (T_1(m,n) + T_2(m,n))(\alpha(n, x(n)) + \beta(n, x(n))dn + J(m), \ \ m \in \mathcal{E} \tag{8}$$

for the Lebesgue measurable set of $\mathcal{E}$ in which $m(\mathcal{E}) < \infty$.

In what follows, we always let $\mathcal{X} = L^{\infty}(\mathcal{E})$ denote a class of essentially bounded measurable functions on $\mathcal{E}$, where $\mathcal{E}$ is a Lebesgue measurable set such that $m(\mathcal{E}) < \infty$.

Now, we consider the functions T_1, T_2, α, β fulfill the following assumptions:

(i) T_1 from $\mathcal{E} \times \mathcal{E}$ to $\mathbb{R}^{\geq 0}$, T_2 from $\mathcal{E} \times \mathcal{E}$ to $\mathbb{R}^{\leq 0}$. Also, two integrable functions α and β are from $\mathcal{E} \times \mathbb{R}$ to $\mathbb{R}$, and $J \in L^{\infty}(\mathcal{E})$;

(ii) there exists $\ell \in (0, \frac{1}{2})$ such that

$$0 \leq \alpha(m, x) - \alpha(m, y) \leq \ell(x - y)$$

and

$$-\ell(x - y) \leq \beta(m, x) - \beta(m, y) \leq 0$$

for $m \in \mathcal{E}$ and $x, y \in \mathbb{R}$;

(iii) $\sup_{m \in \mathcal{E}} \int_{\mathcal{E}} (T_1(m, n) - T_2(m, n)) dn \leq 1$.

Theorem 4. *Suppose that assumptions (i)-(iii) hold. Then the integral equation (8) has a unique solution in* $L^{\infty}(\mathcal{E})$.

Proof. Let $\mathcal{X} = L^{\infty}(\mathcal{E})$ and $B(L^2(\mathcal{E}))$ be the set of bounded linear operators on a Hilbert space $L^2(\mathcal{E})$. We endow $\mathcal{X}$ with the b-metric $\delta_b : \mathcal{X} \times \mathcal{X} \to B(L^2(\mathcal{E}))$ defined by

$$\delta_b(\alpha, \beta) = M_{|\alpha - \beta|^p}$$

where $M_{|\alpha-\beta|^p}$ is the multiplication operator on $L^2(\mathcal{E})$. Hence $(\mathcal{X}, B(L^2(\mathcal{E})), \delta_b)$ is a complete C*-AV-BM space. Define the self-mapping $\Psi : \mathcal{X} \times \mathcal{X} \to \mathcal{X}$ by

$$\begin{aligned}\Psi(x, y)(m) = &\int_{\mathcal{E}} T_1(m, n)(\alpha(n, x(n)) + \beta(n, y(n)))dn \\ &+ T_2(m, n)(\alpha(n, y(n)) + \beta(n, x(n)))dn + J(m),\end{aligned}$$

for all $m \in \mathcal{E}$. Now, we have

$$\delta_b(\Psi(x, y), \Psi(u, v)) = M_{|\Psi(x,y) - \Psi(u,v)|^p}.$$

We obtain,

$$|(\Psi(x, y) - \Psi(u, v))(m)|^p = |\int_{\mathcal{E}} T_1(m, n)(\alpha(n, x(n)) + \beta(n, y(n)))dn$$

$$
\begin{aligned}
&+ \int_{\mathcal{E}} T_2(m,n)(\alpha(n,y(n))+\beta(n,x(n)))dn - \int_{\mathcal{E}} T_1(m,n)(\alpha(n,u(n)) \\
&+ \beta(n,v(n)))dn - \int_{\mathcal{E}} T_2(m,n)(\alpha(n,v(n))+\beta(n,u(n)))dn|^p \\
&= (|\int_{\mathcal{E}} T_1(m,n)(\alpha(n,x(n))-\alpha(n,u(n))+\beta(n,y(n))-\beta(n,v(n)))dn| \\
&+ |\int_{\mathcal{E}} T_2(m,n)(\alpha(n,y(n))-\alpha(n,v(n))+\beta(n,x(n))-\beta(n,u(n)))dn|)^p \\
&\leq (\int_{\mathcal{E}} T_1(m,n)|\alpha(n,x(n))-\alpha(n,u(n))+\beta(n,y(n))-\beta(n,v(n))|dn \\
&- \int_{\mathcal{E}} T_2(m,n)|\alpha(n,y(n))-\alpha(n,v(n))+\beta(n,x(n))-\beta(n,u(n))|dn)^p \\
&\leq (\sup_{n\in\mathcal{E}}[\ell|x(n)-u(n)|+\ell|y(n)-v(n)|]\times\int_{\mathcal{E}}(T_1(m,n)-T_2(m,n))dn)^p \\
&\leq ([\ell||x-u||_\infty+\ell||y-v||_\infty]\sup_{m\in\mathcal{E}}\int_{\mathcal{E}}(T_1(m,n)-T_2(m,n))dn)^p \\
&\leq (\ell||x-u||_\infty+\ell||y-v||_\infty)^p \\
&\leq \ell(||x-u||_\infty+||y-v||_\infty)^p.
\end{aligned}
$$

Therefore,

$$
\begin{aligned}
||\delta_b(\Psi(x,y),\Psi(u,v))|| &= ||M_{|\Psi(x,y)-\Psi(u,v)|^p}|| \\
&= \sup_{||\varphi||=1}(M_{|\Psi(x,y)-\Psi(u,v)|^p}\varphi,\varphi) \\
&= \sup_{||\varphi||=1}\int_{\mathcal{E}}|(\Psi(x,y)-\Psi(u,v))(m)|^p\varphi(m)\varphi(\bar{m})dm \\
&\leq \sup_{||\varphi||=1}\int_{\mathcal{E}}|\varphi(m)|^2dt(\ell||x-u||_\infty+\ell||y-v||_\infty)^p \\
&\leq (\ell||x-u||_\infty+\ell||y-v||_\infty)^p \\
&\leq \ell(||x-u||_\infty+||y-v||_\infty)^p.
\end{aligned}
$$

Set $a=\sqrt{\ell}1_{B(L^2(\mathcal{E}))}$, then $a\in B(L^2(\mathcal{E}))$ and $||a||=|\sqrt{\ell}|<\frac{1}{\sqrt{2}}$. Hence by applying Theorem 1, we get the desired result. □

Funding

No funding was received.

Competing interests

The authors declare that they have no competing interests.

Authors' contributions

All authors contributed to the study, participated in its design and coordination, drafted the manuscript, participated in the sequence alignment, and read and approved the final manuscript.

References

Ali Abou Bakr, S. M. 2019. Common fixed point of generalized cyclic Banach algebra contractions and Banach algebra Kannan types of mappings on cone quasi metric spaces. *Journal of Nonlinear Sciences and Applications (JNSA)*, 12(10), pp.644-655. Available at: http://dx.doi.org/10.22436/jnsa.012.10.03.

Bai, C. 2016. Coupled fixed point theorems in C^*-algebra-valued b-metric spaces with application. *Fixed Point Theory and Applications*, art.number:70. Available at: https://doi.org/10.1186/s13663-016-0560-1.

Bonsal, F.F. 1962. *Lectures On Some Fixed Point Theorems Of Functional Analysis.* Bombay, India: Tata Institute Of Fundamental Research [online]. Available at: http://www.math.tifr.res.in/~publ/ln/tifr26.pdf. [Accessed: 25 September 2020].

Cao, T. and Xin, Q. 2016. Common coupled fixed point theorems in C^*-algebra-valued metric spaces. *arXiv:1601.07168v1[math.OA]*, 26 January [online]. Available at: https://arxiv.org/abs/1601.07168 [Accessed: 25 September 2020].

Huang, H., Došenović, T. and Radenović, S. 2018. Some fixed point results in b-metric spaces approach to the existence of a solution to nonlinear integral equations. *Journal of Fixed Point Theory and Applications*, 20(art.number:105). Available at: https://doi.org/10.1007/s11784-018-0577-7.

Hussain, A., Kanwal, T., Mitrović, Z. D. and Radenović, S., 2018. Optimal Solutions and Applications to Nonlinear Matrix and Integral Equations via Simulation Function. *Filomat*, 32(17), pp.6087-6106. Available at: https://doi.org/10.2298/FIL1817087H.

Hussain, N. and Mitrović, Z. D. 2017. On multi-valued weak quasi-contractions in b-metric spaces. *Journal of Nonlinear Sciences and Applications (JNSA)*, 10(7), pp.3815-3823. Available at: http://dx.doi.org/10.22436/jnsa.010.07.35.

Kadelburg, Z., Nastasi, A., Radenović, S. and Vetro, P. 2016. Fixed points of contractions and cyclic contractions on $C*$-algebra-valued b-metric spaces. *Advances in Operator Theory*, 1(1), pp.92-103. Available at: https://doi.org/10.22034/aot.1610.1030.

Kadelburg, Z. and Radenović, S., 2016. Fixed point results in $C*$-algebra-valued metric spaces are direct consequences of their standard metric counterparts. *Fixed Point Theory and Applications*, art.number:53(2016). Available at: https://doi.org/10.1186/s13663-016-0544-1.

Kongban, C. and Kumam, P. 2018. Quadruple random common fixed point results of generalized Lipschitz mappings in cone b-metric spaces over Banach algebras. *Journal of Nonlinear Sciences and Applications (JNSA)*, 11(1), pp.131-149. Available at: http://dx.doi.org/10.22436/jnsa.011.01.10.

Ma, Z. and Jiang, L. 2015. C^*-Algebra-valued b-metric spaces and related fixed point theorems. *Fixed Point Theory and Applications* , art.number:222(2015). Available at: https://doi.org/10.1186/s13663-015-0471-6.

Ma, Z.H., Jiang, N. and Sun, H.K. 2014. C^*-Algebra-valued metric spaces and related fixed point theorems. *Fixed Point Theory and Applications*, art.number:206(2014). Available at: https://doi.org/10.1186/1687-1812-2014-206.

Mitrović, Z.D., Aydi, H., Md Noorani, M.S. and Qawaqneh, H. 2019. The weight inequalities on Reich type theorem in b-metric spaces. *Journal of Mathematics and Computer Science (JMCS)*, 19(1), pp.51–57. Available at: http://dx.doi.org/10.22436/jmcs.019.01.07.

Radenović, S., Vetro, P., Nastasi, A. and Quan, L.T. 2017. Coupled fixed point theorems in $C*$-algebra-valued b-metric spaces. *Scientific Publications of the State University of Novi Pazar Series A: Applied Mathematics, Informatics and mechanics*, 9(1), pp.81-90. Available at: https://doi.org/10.5937/SPSUNP1701081R.

Radenović, S., Zoto, K., Dedović, N., Šešum Čavić, V. and Ansari, A.H. 2019. Bhaskar-Guo-Lakshmikantam-Ćirić type results via new functions with applications to integral equations. *Applied Mathematics and Computation*, 357(C), pp.75-87. Available at: https://doi.org/10.1016/j.amc.2019.03.057.

Todorčević, V. 2019. *Harmonic Quasiconformal Mappings and Hyperbolic Type Metrics*. Springer Nature Switzerland AG. ISBN: 978-3-030-22591-9.

Vujaković, J., Kishore, G.N.V., Rao, K.P.R., Radenović, S. and Sadik, S.K. 2019. Existence and Unique Coupled Solution in S_b-Metric Spaces by Rational Contraction with Application. *Mathematics*, 7(4), p.313. Available at: https://doi.org/10.3390/math7040313.

Zoto, K., Rhoades, B.E. and Radenović, S. 2019. Common fixed point theorems for a class of (s, q)-contractive mappings in b-metric-like spaces and applications to integral equations. *Mathematica Slovaca*, 69(1), pp.233-247. Available at: https://doi.org/10.1515/ms-2017-0217.

Wu, X. and Zhao, L. 2019. Fixed point theorems for generalized $\alpha - \psi$ type contractive mappings in b-metric spaces and applications,. *Journal of Mathematics and Computer Science (JMCS)*, 18(1), pp.49–62. Available at: http://dx.doi.org/10.22436/jmcs.018.01.06.

СУЩЕСТВОВАНИЕ И ЕДИНСТВЕННОСТЬ РЕШЕНИЙ НЕКОТОРЫХ КЛАССОВ ИНТЕГРАЛЬНЫХ УРАВНЕНИЙ С*-АЛГЕБРЫ В *b*-МЕТРИЧЕСКИХ ПРОСТРАНСТВАХ

Есад Якупович[а], *Хашем* П. Масиха[б], *Зоран* Д. Митрович[в], **корессподент**, *Сеиде* С. Разави[б], *Реза* Саадати[г]

[а]Академия наук и художеств Республики Сербской, г. Баня-Лука, Республика Сербская, Босния и Герцеговина

[б]Технологический университет «К. Н. Тооси», математический факультет, г. Тегеран, Исламская Республика Иран

[в]Университет в г. Баня-Лука, электротехнический факультет, г. Баня-Лука, Республика Сербская, Босния и Герцеговина

[г]Иранский научно-технологический университет, математический колледж, Нармак, г. Тегеран, Исламская Республика Иран

РУБРИКА ГРНТИ: 27.00.00 МАТЕМАТИКА:
27.25.17 Метрическая теория функций,
27.33.00 Интегральные уравнения,
27.39.29 Приближенные методы функционального анализа

ВИД СТАТЬИ: оригинальная научная статья

Резюме:

*Введение/цель: Цель данной статьи заключается в выявлении сопряженных неподвижных точек C *-алгебры в b-метрических пространствах. На основании полученных результатов обсуждается существование решений интегральных уравнений.*

Методы: С помощью методов сопряжения неподвижных точек представлены необходимые условия для существования решений некоторых классов интегральных уравнений.

*Результаты: Получены новые результаты о сопряженных неподвижных точках C *-алгебры в b-метрическом пространстве.*

Выводы: Полученные результаты вносят вклад в теорию неподвижных точек и открывают новые возможности применения в теории дифференциальных и интегральных уравнений.

*Ключевые слова: сопряженная неподвижная точка, C *-алгебра, интегральное уравнение.*

ЕГЗИСТЕНЦИЈА И ЈЕДИНСТВЕНОСТ РЈЕШЕЊА НЕКИХ КЛАСА ИНТЕГРАЛНИХ ЈЕДНАЧИНА У *b*-МЕТРИЧКИМ ПРОСТОРИМА НАД C*-АЛГЕБРАМА

Есад Јакуповић[а], *Hashem* P. Masiha[б], *Зоран* Д. Митровић[в], **аутор за преписку**, *Seyede* S. Razavi[б], *Reza* Saadati[г]

[а]Академија наука и умјетности Републике Српске, Бања Лука, Република Српска, Босна и Херцеговина

[б]Технолошки универзитет „K. N. Toosi", Математички факултет, Техеран, Исламска Република Иран

[в]Универзитет у Бањој Луци, Електротехнички факултет, Бања Лука, Република Српска, Босна и Херцеговина

[г]Ирански научно-технолошки универзитет, Колеџ математике, Нармак, Техеран, Исламска Република Иран

ОБЛАСТ: математика
ВРСТА ЧЛАНКА: оригинални научни рад

Сажетак:

*Увод/циљ: Циљ овог рада јесте да се добију одређени резултати о придруженим непокретним тачкама у C *-алгебра b-метричким просторима. Користећи ове резултате дати су довољни услови за егзистенцију рјешења неких класа интегралних једначина.*

Методе: Коришћењем методе придружених фиксних тачака дати су довољни услови за егзистенцију рјешења неких класа интегралних једначина.

Резултати: Добијени су нови резултати о придруженим фиксним тачкама у b-метричком простору над C-алгебром.*

Закључак: Добијени резултати представљају допринос теорији фиксних тачака и отварају нове могућности за примене у теорији диференцијалних и интегралних једначина.

*Кључне речи: придружена фиксна тачка, C *-алгебра, интегрална једначина.*

Paper received on / Дата получения работы / Датум пријема чланка: 30.09.2020.
Manuscript corrections submitted on / Дата получения исправленной версии работы / Датум достављања исправки рукописа: 15.10.2020.
Paper accepted for publishing on / Дата окончательного согласования работы / Датум коначног прихватања чланка за објављивање: 16.10.2020.

Jakupović, E. et al, Existence and uniqueness of the solutions of some classes of integral equations C*-algebra-valued b-metric spaces, pp.726–742

CUTTING TESTING COSTS BY THE POOLING DESIGN

Dimitrije D. Čvokić

University of Banja Luka, Faculty of Sciences and Mathematics, Banja Luka, Republic of Srpska, Bosnia and Herzegovina,
e-mail: dimitrije.cvokic@pmf.unibl.org,
ORCID ID: https://orcid.org/0000-0001-7975-4224

DOI: 10.5937/vojtehg68-28078; https://doi.org/10.5937/vojtehg68-28078

FIELD: Mathematics
ARTICLE TYPE: Original scientific paper

Abstract:
Introduction/purpose: The purpose of group testing algorithms is to provide a more rational resource usage. Therefore, it is expected to improve the efficiency of large–scale COVID-19 screening as well.

Methods: Two variants of non–adaptive group testing approaches are presented: Hwang's generalized binary–splitting algorithm and the matrix strategy.

Results: The positive and negative sides of both approaches are discussed. Also, the estimations of the maximum number of tests are given. The matrix strategy is presented with a particular modification which reduces the corresponding estimation of the maximum number of tests and which does not affect the complexity of the procedure. This modification can be interesting from the applicability viewpoint.

Conclusion: Taking into account the current situation, it makes sense to consider these methods in order to achieve some resource cuts in testing, thus making the epidemiological measures more efficient than they are now.

Key words: pooling design, group testing, Hwang's generalized binary-splitting algorithm, matrix strategy, COVID-19, SARS-CoV-2.

Introduction

The COVID-19 pandemic, caused by the SARS-CoV-2 virus, has posed a challenge to many countries when it comes to detecting infected people as a basis for implementing appropriate epidemiological measures. The high $R_0 = 5.7$ value of the SARS-CoV-2 virus (Sanche et al, 2020) affected the increased demand for tests (Pfeiffer et al, 2020), which was, according to some media reports in Serbia (Blic, 2020), also accompanied by the distribution problems. In other words, testing can quickly become a *bottleneck* in the event of a massive disease outbreak.

Modern epidemiological measures are proactive. In order to control the spread of infection, it is important to detect:

- pre–symptomatic cases;
- infected persons who have many high-risk social contacts (e.g., medical staff, geriatric center workers, teachers, etc.).

The mass testing allows observing and tracking epidemiological patterns as the infection spreads. The situation mentioned above in which testing becomes a bottleneck certainly requires some optimization.

Among the SARS-CoV-2 virus infection tests, the most well–known methods are RT-(q)PCR and serological antibody tests. The RT-(q)PCR test is considered the most accurate (the most reliable). On the other hand, these tests are more expensive and complex when it comes to equipment, time, trained personnel, and procedural complexity.

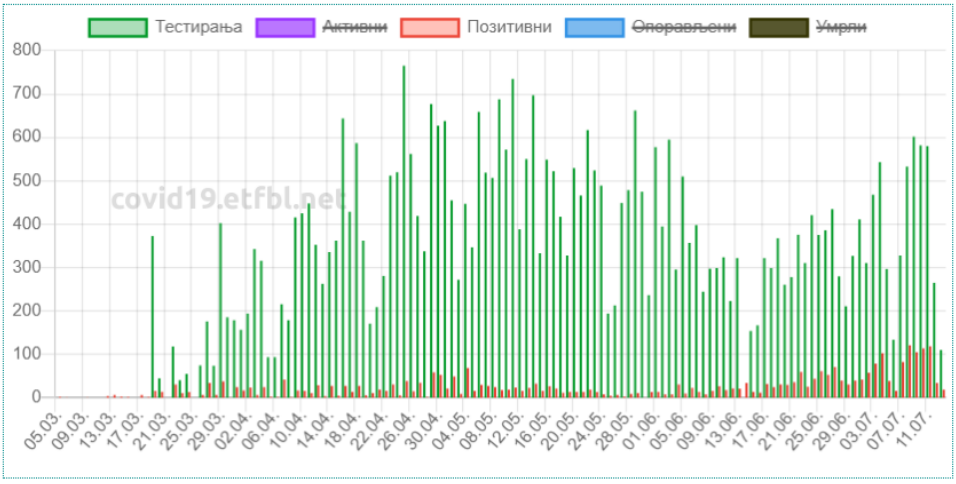

Figure 1 – Total number of tested (green) and confirmed (red) cases per day, for Republic of Srpska, until July 11th, 2020 (Faculty of Electrical Engineering in Banja Luka, 2020)

Рис. 1 – Общее количество протестированных (зеленый цвет) и подтвержденных (красный цвет) случаев на ежедневной основе в Республике Сербской, до 11 июля 2020 года (Faculty of Electrical Engineering in Banja Luka, 2020)

Слика 1 – Преглед односа укупног броја тестираних (зелена боја) и потврђених (црвена боја) случајева по данима, за Републику Српску, до 11. јула 2020. (Faculty of Electrical Engineering in Banja Luka, 2020)

According to the reports of the official portal of the Government of Republic of Srpska (Government of Republic of Srpska, 2020), in the Republic of Srpska the percentage of confirmed cases (relative to the number of tests, daily) took an upward trend. In Figure 1, there is a time series bar plot depicting values that correspond to the number of confirmed cases (red) and the number of conducted tests (green), until July 11th, 2020. Given the test cost and the increased workload of laboratory technicians, it is reasonable to consider some strategies that will save both the testing kits and time.

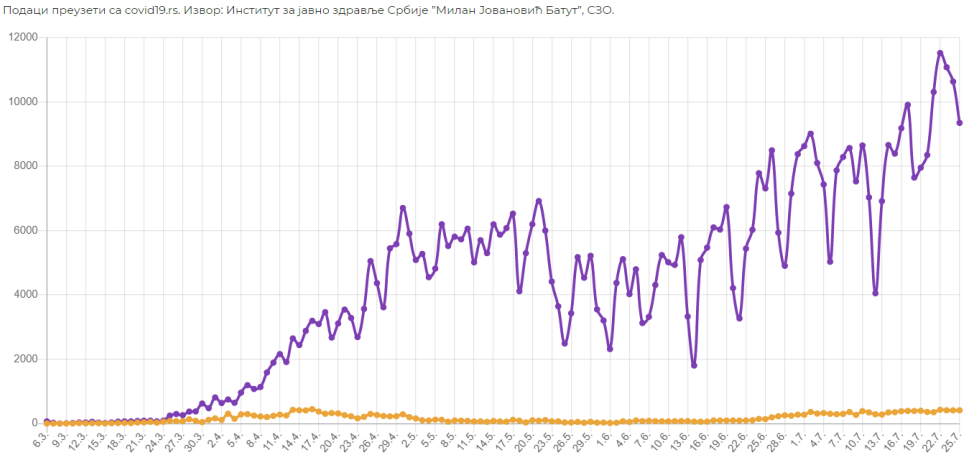

Figure 2 – Total number of tested (purple) and confirmed cases (orange) on daily basis, for Serbia, until July 25th, 2020 (Government of Republic of Serbia, 2020)
Рис. 2 –Общее количество протестированных (фиолетовый цвет) и подтвержденных (оранжевый цвет) случаев на ежедневной основе в Республике Сербия, до 25 июля 2020 года (Government of Republic of Serbia, 2020)
Слика 2 – Преглед односа укупног броја тестираних (љубичаста боја) и потврђених случајева (наранџаста боја) по данима, за Србију, до 25. јула 2020. (Government of Republic of Serbia, 2020)

In Serbia, the percentage of confirmed cases is not as high as in the Republic of Srpska, but the growth of tested, infected, and deceased is quite noticeable from the data provided by (Government of Republic of Serbia, 2020). Figure 2 shows a graphical representation of values corresponding to the number of confirmed cases (orange) and the number of conducted cases (purple), until July 25th, 2020.

As previously mentioned, the rest of the world has not been spared from the testing kit shortage. Therefore, new protocols have been developed worldwide to reduce the scope of testing without affecting (at least not significantly) the quality and accuracy of the procedures (Eberhardt et al, 2020), (Mallapaty, 2020).

As a combinatorial procedure, group testing breaks down the identification task (identifying the defects in equipment, downtime in the use of communication channels, infected persons, etc.) into group tests instead of individual checks. Dorfman (Dorfman, 1943) was the first to describe this problem. Since then, different test schemes have been designed, including different types of tests as testing phases alternate (the so–called adaptive procedures). The idea itself has many applications in almost all areas of science: biology, computing, medicine, electrical engineering, data protection, etc. Interest in group testing was renewed after the launch of the famous Human Genome Project (Colbourn & Dinitz, 2007) Some prominent examples where group testing is used in medicine are an examination of donated blood from American Red Cross donors (Dodd et al, 2002), testing for chlamydia and gonorrhea (Gaydos, 2005), and monitoring the mosquitoes which transmit the West Nile virus (White et al, 2001). Moreover, when it comes to testing for SARS-CoV-2 virus infection, (Gollier & Gossner, 2020) have shown that even a very simplified approach, based on the bisection method, provides significant economic benefits.

This paper presents two simpler variants of non–adaptive group testing based on swab–sample aggregation, also known as *the pooling design*. Firstly, Hwang's generalized binary–splitting algorithm is presented. Afterward, the so–called matrix strategy is described. In the end, concluding remarks are given, reviewing the current situation.

Hwang's generalized binary–splitting algorithm

Here we will present Hwang's generalized binary–splitting algorithm. The pseudo–code is given in Algorithm 1. This approach can be used to cut resource costs in testing for SARS-CoV-2 infection (Ding-Zhu & Hwang, 1993). The input variables are a statistical prediction of the number of people that will be tested n and a statistical prediction of the number of confirmed cases z. The result should be a smaller number of tests needed to identify all infected individuals.

According to (Ding-Zhu & Hwang, 1993), the maximum number of tests M_t when Algorithm 1 is used is

$$M_t = \begin{cases} n, \text{ for } n \leq 2m-2 \\ (s+2)z + p - 1, \text{ otherwise} \end{cases} \tag{1}$$

where $p < z$ is a unique nonnegative integer such that $m = 2^s z + 2^s p + \theta$, $0 \leq \theta < 2^s$. If $\frac{n}{z}$ increases we have that $M_t \to z \log_2 \frac{n}{z}$.

Algorithm 1: Hwang's generalized binary–splitting algorithm

Data: n, z
Result: resource savings
while $n > 2z - 1$ **do**
  $m \leftarrow n - z + 1$
  $s \leftarrow \lfloor \log_2 \frac{m}{z} \rfloor$
  $u \leftarrow$ group of 2^s samples
  $t \leftarrow$ result of testing the group u
  if t *negative* **then**
    label all corresponding cases as negative
    $n \leftarrow n - 2^s$
  end
  else
    $P \leftarrow$ the number of positive cases obtained by the bisection method
    $N \leftarrow$ the number of negative cases obtained by the bisection method
    $n \leftarrow n - 1 - N$
    $z \leftarrow z - P$
  end
end
test separately each reminding sample

Example 1. Let there be a statistical forecast for the next day which says that the laboratory would need to take $n = 100$ swab–samples. Consider two cases:

($z = 20$) according to the Eq. (1) we have an estimation that 79 test will be needed at most, i.e. the laboratory will save at least 21 testing kits.

$(z = 2)$ according to Eq. (1) we have an estimation that 14 test will be needed at most, i.e. the laboratory will save at least 86 testing kits, much more compared to the previous case. △

The downside of Hwang's generalized binary–splitting algorithm is that it may require more swabs from one individual. If we have a situation like in the case of $(z = 20)$, in Example 1, we can see from the the Algorithm 1 that it will be necessary to combine the swab–samples of four people at the beginning. Suppose, for simplicity, that only one is infected in the group. This means that the identification of the infected one will be based on the bisection method. In other words, our tests to identify an infected person have the following order:

1. test the group of 4 samples;
2. test two groups of 2 samples;
3. in the positive group test each sample separately.

As it can be noticed, it will be necessary to take three swabs from one person. The situation is getting complicated even more if the number of infected is very high, and z is much lower than n. As often, laboratories cannot send technicians several times to take swabs, and it is not convenient for potentially infected people to come to the laboratory. Hwang's general binary–splitting algorithm can create certain operational problems. Moreover, taking three swabs from each person is already pushing the bounds of practicality. For this reason, a matrix strategy has been devised, in which two swabs are taken from each individual.

Remark 1. In case the estimated percentage of confirmed cases exceeds 50%, it is not possible to make any resource cuts. Each swab–sample must be tested separately.

Remark 2. The presented Algorithm 1 does not take into account the accuracy of tests, i.e., the likelihood of obtaining false positive or false negative results is not considered.

Remark 3. The presented Algorithm 1 does not take into account whether there is a change in the accuracy of tests if a large number of samples are grouped.

Matrix strategy

Another way to reduce the total number of tests, which will be presented here, is based on the so-called matrix (tabular) strategy. We can, for the sake of simplicity, assume that the number of people n is the square of some natural number k, i.e., $n = k^2$. Phatarfod & Sudbury (1994) were the first to propose this idea for high–throughput screening.

Basic matrix strategy (Algorithm 2). We take 2 (two) swab–samples from each person and form a square matrix of M samples. Each entry $m_{i,j}$ of the matrix M corresponds to one person, more precisely to a pair of swab–samples of that person. Rows and columns form groups of combined samples. With this, we have $2k$ groups for the first phase of testing, which is $\frac{1}{2}k$ times less than the number in the case of individual checks. After the first phase (lines 1-2), we move on to the second phase (line 3).

Algorithm 2: Basic Matrix Strategy

Data: matrix of pairs of swab–samples
Result: identification of confirmed cases
1 test column–groups and label the positive ones
2 test row–groups and label the positive ones
3 apply Algorithm 3 on a set of marked rows and columns

The following two situations are possible for the second phase if we get at least one positive result:

(1) if only one sample is positive, it is uniquely determined by the intersection of the positive column and the positive row;

(2) otherwise, the swab–samples of the individuals from the intersection of the positive columns and rows are retested.

The second case is the reason why it is necessary to take two swab–samples from each person.

The obvious problem with this approach, unlike with Hwang's generalized binary–splitting algorithm, is a possibility of a diagonal arrangement of samples of infected individuals (a technician is not aware of this because he/she does not know who is infected). Let's say that at the positions $m_{i,i}$, for $i \in \{1 \ldots, k\}$, everyone is infected. The total number of infected is k. Each column–group and row–group will be positive on the test of pooled

samples. It follows from the previously described basic matrix strategy that we have to test all swab–samples on the intersections separately. In this case, it means all matrix entries. In other words, we need to test all swab–samples again, which in no way reduces the costs. Therefore, the maximum number of the basic matrix strategy tests for $n = k^2$ persons is $k^2 + 2k$.

Algorithm 3: Retesting

Data: labeled rows and columns of samples' matrix
Result: detected positive cases
if *only one column and one row are positive* **then**
    the infected person is at the intersection of this particular column and row
end
else
    test separately all swab–samples that correspond to the intersections of all positive columns and rows
end

The basic matrix strategy can be improved by taking into account the experience of epidemiologists. For example, according to epidemiological analyses and field experience, swab–samples are classified into likely positive and likely negative ones. The use of additional information of this type was first studied by McMahan et al (2012). They considered two approaches:

- spiral design;
- gradient design.

This paper will present only the first approach– spiral design, particularly, its simplified variant.

The first probably positive sample pairs are clustered along one of the matrix "corners" – say the upper left, (in the above notation: $m_{1,1}$). Put the first pair of probably positive swab–samples at $m_{1,1}$. We put the other three in the positions $m_{2,1}, m_{2,2}, m_{1,2}$. Then, the next five are placed at positions $m_{3,1}, m_{3,2}, m_{3,3}, m_{2,3}, m_{1,3}$. The procedure is repeated until a set of probably positive samples is exhausted.

As it can be observed, this procedure leads to more expressed heterogeneity of the matrix. Then, moving from right to left, the first column–groups of the matrix will most likely show that they are negative, which gives us the right to write off their samples from further consideration. We stop at

the first group–column that tests positive. Then we continue with the rows, from bottom to top, using the same idea. This can, roughly, eliminate a significant number of sample pairs. The described idea is represented by Algorithm 4.

Algorithm 4: Elimination of Probably Negative Cases

Data: the set of $n = k^2$ swab–sample pairs
Result: elimination of probably negative swab–samples
$P \leftarrow$ probably positive swab–sample pairs
$N \leftarrow$ probably negative swab–sample pairs
cluster the swab–sample pairs from P around $m_{1,1}$ in spiral fashion
arrange the remaining swab–sample pairs (i.e., those from N) so that a matrix is created
$j \leftarrow k$ //eliminations starts from the last column
$t \leftarrow 0$
while $t = 0$ **do**
    $t \leftarrow$ test result of column–group j
    if $t = 0$ **then**
        remove column //everyone is negative
    end
    $j \leftarrow j - 1$
end
$i = k$ //elimination starts from the bottom row
$t \leftarrow 0$
while $t = 0$ **do**
    $t \leftarrow$ test result of row–group j
    if $t = 0$ **then**
        remove row //everyone is negative
    end
    $i \leftarrow i - 1$
end

In Algorithm 4, the variables P and N are introduced, denoting sets of probably positive and probably negative samples, respectively. The variable t has a binary domain, taking the value 0 if the test shows no infection (negative result) and 1 if it shows SARS-CoV-2 virus infection (positive result).

Remark 4. In a gradient design, i.e, probably positive swab–sample pairs are clustered as columns, the elimination is performed only from right to left.

The diagonal elimination algorithm is applied to the rest of the matrix, obtained after the application of Algorithm 4. Before we describe the changes, we note that Algorithm 4 does not have to leave us a square matrix, i.e., the endpoint values of i and j do not have to be equal. Again, for simplicity, we consider a sub–matrix M' positioned along the upper left corner of the format $k' \times k'$, where $k' = \min\{i, j\}$, for i and j as values returned by Algorithm 4.

Algorithm 5: Diagonal Elimination

Data: set of remaining swab–sample pairs; i, j obtained by Algorithm 4
Result: identification of positive cases

$k' \leftarrow \min\{i, j\}$
create a sub–matrix of samples M' with dimension $k' \times k'$
foreach $i \in \{1, \ldots, k'\}$ **do**
    $t_{i,i} \leftarrow$ test the result of one swab–sample corresponding to the position $m_{i,k'}$
    if $t_{i,i} = 0$ **then**
        $t_{k'-i,i} \leftarrow$ test the result of one swab–sample corresponding to the position $m_{k'-i,i}$
        $t_{i,k'-i} \leftarrow$ test the result of one swab–sample corresponding to the position $m_{i,k'-i}$
    end
end
for each positive test result in the previous testing, label the corresponding columns and rows as positive
apply Algorithm 3 to the labeled rows and columns

In the first *phase* of eliminating diagonals, we test samples from one of the diagonals, say the main one. For each negative result at the position $m_{i,i}$ we test one sample from the corresponding positions on the counter–diagonal: $m_{k'-i,i}$ and $m_{i,k'-i}$. For each positive result, label the corresponding column and row as positive. Then test swab–samples from the intersec-

tions of all positively labeled rows and columns (Algorithm 3). An overview of this procedure is given in Algorithm 5.

Here, too, as in the previous algorithm, the variable $t_{i,j}$ $(\forall i, j \in \{1, \ldots, k'\})$ has a binary domain — takes the value 0 if the test shows no infection (negative result), and 1 if the test shows SARS-KoV-2 virus infection (positive result).

Remark 5. However, although this procedure should remove swab–samples of infected persons from a diagonal, we can observe that, if the statistical prediction of the percentage of infected persons is low enough, random distribution of samples of probably infected persons would rarely get into an undesirable situation. However, even the partial diagonal arrangement is unfavorable.

From the rest of all untested swab–sample pairs (including those that did not enter M'), a new matrix M'' is formed. The diagonal elimination process can be repeated. How many times this will be done depends on the protocol of a particular laboratory and the costs cut estimate, given the daily scope of testing. This means that the elimination of diagonals can also be omitted.

Remark 6. After eliminating rows and columns in the first phase, the rest of the matrix does not necessarily have to be a square matrix, but we choose the largest quadratic sub–matrix.

Combining the previously described as a whole, we get Algorithm 6 — *improved matrix strategy*. However, the proposed improvement of the basic matrix strategy does not bring the maximum number of tests below k^2, although such a large number is not expected in practice, especially if the percentage of infected concerning the number of tested is low. In other words, Hwang's generalized binary–splitting algorithm is theoretically a better approach than the matrix strategy. However, in practice, a matrix approach is used due to a smaller sampling volume.

Remark 7. The matrix strategy can be generalized to a multiphase tensor strategy, but this could lead to a rather impractical taking of many swab–samples from each person.

Algorithm 6: Improved matrix strategy algorithm

Data: swab–sample pair matrix , chosen protocol
Result: detected positive cases alongside with possible cost cuts

apply Algorithm 4
$i \leftarrow 0$
while *protocol about diagonal elimination* **do**
    apply Algorithm 5
    from the rest of *all* untested swab–sample pairs create a matrix M_i'
    $i \leftarrow i + 1$
end
apply the *basic matrix strategy* on the rest of swab–samples

Remark 8. The initial matrix does not have to be square, but the case is considered in the algorithm, for simplicity. Otherwise, the natural choice for the matrix format is that the sum of columns and rows is the smallest possible.

Remark 9. Additional improvements may be considered, but are likely to affect applicability in practice.

Remark 10. The presented Algorithm 6 does not take into account the accuracy of the tests, i.e. the likelihood of obtaining false–positive or false–negative results.

Remark 11. The presented Algorithm 6 does not take into account whether there is a change in the accuracy of tests if a large number of samples are combined.

Concluding remarks

The algorithms above provide a way to cut the resource costs if the number of confirmed cases is low enough compared to the number of conducted tests. The lower the percentage of infected, the more resources can be saved. However, this does not mean that timely action will not be useful if the percentage is high. On the contrary, even in that situation, adequate actions to save the resources are of considerable benefit.

Theoretically, more significant rationalization of resources is expected, first of all, when using Hwang's generalized binary–splitting algorithm, but

it is not very practical due to possible excessive taking of swabs. Its use depends on situation assessment. In a way, the combination of both approaches could give satisfactory results, i.e. lead to considerable savings. In that case, we would have an adaptive approach.

Considering the current situation and a noticeable increase in those infected with the SARS-CoV-2 virus, it makes sense to consider the presented type of resource rationalization to increase the effectiveness of epidemiological measures. Also, it is essential to notice that these approaches are not exclusively related to RT-(q)PCR testing. They can be used equally successfully in mass serological testings.

References

-Blic. 2020. Nema testova, ima testova, u čemu je problem? *Blic*, 4 July [online]. Available at: www.blic.rs/vesti/drustvo/pcr-test-korona-virus-uzice-beograd-dr-predrag-kon/kbb68g9 (in Serbian) [Accessed 15 July 2020].

Colbourn, C.J. & Dinitz, J.H. 2007. *Handbook of Combinatorial Designs (2nd ed.)*. Boca Raton: Chapman & Hall/ CRC. p. 574, Section 46: Pooling Designs

Ding-Zhu, Du. & Hwang, F.K. 1993. *Combinatorial group testing and its applications.* Singapore: World Scientific. ISBN 978-9810212933.

Dodd, R., Notari, E. & Stramer, S. 2002. Current prevalence and incidence of infectious disease markers and estimated window-period risk in the American Red Cross blood donor population. *Transfusion*, 42(8), pp.975-979. Available at: https://doi.org/10.1046/j.1537-2995.2002.00174.x.

Dorfman, R. 1943. The Detection of Defective Members of Large Populations. *Annals of Mathematical Statistics*, 14(4), pp.436-440. Available at: https://doi.org/10.1214/aoms/1177731363.

Eberhardt, J.N., Breuckmann, N.P. & Eberhardt, C.S. 2020. Multi-Stage Group Testing Improves Efficiency of Large-Scale COVID-19 Screening. *Journal of Clinical Virology*, 128(art.number:104382). Available at: https://doi.org/10.1016/j.jcv.2020.104382.

-Faculty of Electrical Engineering in Banja Luka. 2020. *Ukupan broj slučajeva u Republici Srpskoj* [online]. Available at: https://covid19.etfbl.net/ (in Serbian) [Accessed 15 July 2020].

Gaydos, C.A. 2005. Nucleic Acid Amplification Tests for Gonorrhea and Chlamydia: Practice and Applications. *Infectious Disease Clinics of North America*, 19(2), pp.367-386. Available at: https://doi.org/10.1016/j.idc.2005.03.006.

Gollier, C. & Gossner, O. 2020. Group testing against Covid-19. *Covid Economics*, 1(2), pp.32-42 [online]. Available at: https://www.tse-fr.eu/sites/default/files/TSE/documents/doc/by/gollier/covid_economics.pdf [Accessed: 21 August 2020].

-Government of Republic of Serbia. 2020. *COVID19 Statistics in Serbia* [online] Available at: https://covid19.data.gov.rs/?locale=en [Accessed 25 July 2020].

-Government of Republic of Srpska. 2020. *Zeljkovic: Nastavlja se trend pogoršanja epidemiološke situacije* [online]. Available at: https://koronavirususrpskoj.com/nastavlja-se-trend-pogorsanja-epidemioloske-situacije/ (in Serbian) [Accessed 25 July 2020] (In the original: -Влада Републике Српске. 2020. *Зељковић: Наставља се тренд погоршања епидемиолошке ситуације*).

Mallapaty, S. 2020. *The Mathematical Strategy That Could Transform Coronavirus Testing*. *Nature*, 10 July [online]. Available at: https://www.nature.com/articles/d41586-020-02053-6 [Accessed 15 July 2020].

McMahan, C.S., Tebbs, J.M. & Bilder, C.R. 2012. Two-Dimensional Informative Array Testing. *Biometrics*, 68(3), pp.793-804. Available at: https://doi.org/10.1111/j.1541-0420.2011.01726.x.

Pfeiffer, S., Anderson, M. & van Woerkom, B. 2020. Despite Early Warnings, U.S. Took Months To Expand Swab Production For COVID-19 Test. *NPR* [online]. Available at: https://www.npr.org/2020/05/12/853930147/despite-early-warnings-u-s-took-months-to-expand-swab-production-for-covid-19-te [Accessed 15 July 2020].

Phatarfod, R.M. & Sudbury, A. 1994. The use of a square array scheme in blood testing. *Statistics in Medicine*, 13(22), pp.2337-2343. Available at: https://doi.org/10.1002/sim.4780132205.

Sanche, S., Lin, Y., Xu, C., Romero-Severson, E., Hengartner, N. & Ke, R. 2020. High Contagiousness and Rapid Spread of Severe Acute Respiratory Syndrome Coronavirus 2. *Emerging Infectious Diseases* 26(7), pp.1470-1477. Available at: https://dx.doi.org/10.3201/eid2607.200282.

White, D., Kramer, L., Backenson, P., Lukacik, G., Johnson, G., Oliver, J., Howard, J., Means, R., Eidson, M., Gotham, I., Kulasekera, V. & Campbell, S. 2001. Mosquito surveillance and polymerase chain reaction detection of West Nile Virus, New York state. *Emerging Infectious Diseases*, 7(4), pp.643-649. Available at: https://dx.doi.org/10.3201/eid0704.017407.

Čvokić, D., Cutting testing costs by the pooling design, pp.743–759

ЭКОНОМИЯ РЕСУРСОВ ДЛЯ ТЕСТИРОВАНИЯ ПУТЕМ ОБЪЕДИНЕНИЯ ОБРАЗЦОВ

Димитрие Д. Чвокич

Университет в г. Баня-Лука, Факультет естественных наук и математики, г. Баня-Лука, Республика Сербская, Босния и Герцеговина

РУБРИКА ГРНТИ: 27.00.00 МАТЕМАТИКА:
27.47.19 Исследование операций,
27.47.17 Математическая теория информации,
27.41.41 Алгоритмы решения задач вычислительной и дискретной математики
ВИД СТАТЬИ: оригинальная научная статья

Резюме:

Введение/цель: Цель алгоритмов группового тестирования заключается в обеспечении рационального использования ресурсов. Вследствие такого подхода можно надеяться на повышение эффективности массового скрининга методом RT(q)PCR для выявления зараженных вирусом САРСКоВ2.

Методы: В данной статье представлены два варианта неадаптивных групповых подходов к тестированию: обобщенный алгоритм двоичного расщепления Венга и стратегическая матрица.

Результаты: В статье обсуждаются положительные и отрицательные стороны обоих подходов и даны оценки максимального количества тестов. Стратегическая матрица представлена с определенной модификацией, которая снижает вышеупомянутую оценку, но не сильно влияет на сложность процедуры, что делает ее особенно пригодной для применения.

Выводы: Учитывая текущую ситуацию, имеет смысл рассмотреть этот вид рационализации ресурсов с целью повышения эффективности противоэпидемических мероприятий.

Ключевые слова: экономия путем объединения образцов, групповое тестирование, обобщенный алгоритм двоичного расщепления Венга, стратегическая матрица, COVID19, SARSCoV2.

УШТЕДА ТЕСТОВА УДРУЖИВАЊЕМ УЗОРАКА

Димитрије Д. Чвокић

Универзитет у Бањој Луци, Природно-математички факултет,
Бања Лука, Република Српска, Босна и Херцеговина

ОБЛАСТ: математика

ВРСТА ЧЛАНКА: оригинални научни рад

Сажетак:

Увод/циљ: Сврха алгоритама групног тестирања јесте да обезбједе рационализацију ресурса. Стога, очекује се да се њиховим коришћењем могу, такође, остварити одређене уштеде при масовном тестирању RT(q)PCR методом ради идентификације заражених вирусом САРСКоВ2.

Методе: Предочена су два приступа неадаптивног групног тестирања заснованог на удруживању узорака, у англојезичној литератури познатом као pooling design: Хвангов алгоритам уопштеног цијепања и матрична стратегија.

Резултати: Уз дискусију добрих и лоших страна наведене су и оцјене максималног броја тестова. Матрична стратегија представљена је својеврсном модификацијом која смањује поменуту оцјену, а, с друге стране, не утиче много на комплексност процедуре, што је значајно за њену примјену у пракси.

Закључак: Узимајући у обзир тренутну ситуацију, има смисла разматрати овакву врсту рационализације ресурса, ради повећања ефикасности епидемиолошких мјера.

Кључне речи: уштеда удруживањем узорака, групно тестирање, Хвангова уопштена бисекција, матрична стратегија, COVID-19, САРС-КоВ-2.

Paper received on / Дата получения работы / Датум пријема чланка: 26. 08. 2020.
Manuscript corrections submitted on / Дата получения исправленной версии работы / Датум достављања исправки рукописа: 11. 10. 2020.
Paper accepted for publishing on / Дата окончательного согласования работы / Датум коначног прихватања чланка за објављивање: 13. 10. 2020.

A SOLUTION FOR THE OVER-THE-HORIZON-RADAR SIMULATOR

Bojan R. Džolić[a], *Mladen* Đ. Veinović[b], *Vladimir* D. Orlić[c], *Nikola* L. Lekić[d], *Nemanja* R. Grbić[e]

[a] Vlatacom Institute, Belgrade, Republic of Serbia; Singidunum University, Department for Electrical engineering and computing, Belgrade, Republic of Serbia, email: bojan.dzolic@vlatacom.com, **corresponding author**, ORCID iD: https://orcid.org/0000-0002-2169-2320

[b] Singidunum University, Belgrade, Republic of Serbia, email: mveinovic@singidunum.ac.rs, ORCID iD: https://orcid.org/0000-0001-6136-1895

[c] Vlatacom Institute, Belgrade, Republic of Serbia, email: vladimir.orlic@vlatacom.com, ORCID iD: https://orcid.org/0000-0002-5153-5115

[d] Vlatacom Institute, Belgrade, Republic of Serbia, email: nikola.lekic@vlatacom.com, ORCID iD: https://orcid.org/0000-0001-7543-3319

[e] Vlatacom Institute, Belgrade, Republic of Serbia, email: nemanja.grbic@vlatacom.com, ORCID iD: https://orcid.org/0000-0002-0540-3787

DOI: 10.5937/vojtehg68-26980; https://doi.org/10.5937/vojtehg68-26980

FIELD: Electronics, Telecommunications
ARTICLE TYPE: Original scientific paper

Abstract:

Introduction/purpose: The OTHR simulator presented in this paper is developed and used in practice, with the aim of emulating radar signal environment, but also optimizing the radar parameters in real applications such as: radiated power, antenna array gain, path loss, radar cross section, external interference, and noises.

Methods: In this paper, the methodology of mathematical modeling is used as well as simulations .

Results: Based on the performed analysis, the output data from the OTHR simulator is presented and discussed.

Conclusion: The usage of the presented OTHR simulator makes assessing the reliability of a potential radar at predetermined locations automated, controllable and efficient, with results closely matching radar behavior in real operation.

Key words: over-the-horizon-radar, radar cross-section, exclusive economic zone, radar simulator.

Introduction

The Over The Horizon Radar (OTHR) simulator presented in this paper is developed and designed in order to predict and analyze all external parameters that affect the OTHR functionality. The OTHR uses a surface wave component in order to achieve a huge coverage area. Detection and tracking of vessels with a maximal range up to 200 NM makes it suitable for application within a system for monitoring the Exclusive Economic Zone (EEZ). The EEZ is a sea belt of a certain width extending from the territorial waters in direction of the open seas, over which a coastal state has exclusive rights regarding the exploitation of biological and mineral resources of the sea (United Nations, 2011). To the best of our knowledge, there are only two ways to achieve complete EEZ monitoring. The first approach utilizes low range sensors, such as Electro – Optical (EO) camera systems and Micro-Wave (MW) radars, on the mobile platforms such as vessels and airplanes, thus avoiding sensor's limitations. The second approach uses a network of OTHR radars to ensure constant surveillance of a complete coastline well beyond the horizon. Since the price of the OTHR radar network is significantly lower than a combined cost of the aforementioned sensors and their platforms, it is clear why these radars became a sensor of choice for maritime surveillance (Sevgi & Ponsford, 1999), (Tošić et al, 2016).

The OTHR radar uses the frequency bandwidth from 3 to 30 MHz (HF) and utilizes vertically-polarized, surface electromagnetic waves which propagate above the sea or ocean surface. The usage of the surface wave OTHR is accompanied with specific issues, such as: influence of the sea state on electromagnetic wave propagation above the sea surface, impact of Earth's surface curvature on the characteristics of transmitting and receiving antenna stations, interference of other transmitting devices, atmospheric noise, space noise and man-made noise in the vicinity of OTHRs, along with the radar cross section (RCS) of targets that need to be detected and tracked (Skolnik, 1990), (Nikolić et al, 2016a), (Fabrizio, 2013), (Nikolic et al, 2018). All these issues should be taken into account properly when OTHR systems are planned for implementation. It is of great importance to analyze their effects at the early stage and calculate a corresponding system performance under the conditions of a specific deployment location. For that purpose, a computer - based simulator of the OTHR would be very practical in engineering tasks. One solution of this

simulator, developed in the Vlatacom Institute and used in our projects worldwide is presented in this paper.

The simulator allows the analysis of the environmental impact on the operation of OTHR radars, as defined by the user. It should keep track of all possible changes in radar conditions in the HF frequency band, and also allow different scenarios to be set. Thus, a proper flexibility in defining simulation parameters and specific scenarios for simulation should be provided. The simulator takes into consideration the change of the RCS to determine the signal to noise ratio (SNR) for each vessel defined by the scenario, which results in data comparable with real situations, as might be acquired by the radar in practical operation. The output data from the simulator should be provided in the format of the real OTHR radar sensor, in order to validate the data by comparing it with the real OTHR system, after installation. The OTHR Simulator solution described in this paper is commonly compared with vHF-OTHR radars (Vlatacom Institute, 2018), as being completely compatible with its model and data formats.

OTHR simulator concept

The main goal of the simulator is to estimate relevant capabilities of the detection of different sizes of vessels, which is the main benchmark for this kind of radar applications (Nikolic et al, 2016b). All estimations are made by taking into account the characteristics of the environment for potential locations, since many of parameters of interest in simulation are highly dependable on particular geo-location and surroundings.

The Simulator software has been developed in the Matlab and runs on Windows OS (Girault et al, 2017). The input parameters of the Simulator are given through the simulating scenario that includes: predicted paths of vessels, speed and size of vessels, season of the year, time of the day or night, sea conditions, wind directions, and geographical coordinates of potential sites. This scenario is represented in the form of an XML file. The output of the simulator represents detected targets in the table form, defined by the vHF-OTHR interface.

The simulator is designed for the following main tasks:

- Testing the software for the detection and tracking of vessels,
- Analyzing and estimating parameters of th OTHR radar, and
- Analysis and evaluation of location-specific conditions for OTHR deployment.

The main components of the Simulator, shown in Figure 1, are:

- Step Machine: a library for creating, reading and sorting input XML files for simulation,
- Radar Model: a library for calculating the signal to noise ratio of each simulated target,
- Detection engine: a library for the detection and tracking of simulated targets.

The block named "Step Machine" is used for designing a particular simulation scenario. It includes defining: the initial coordinates of vessels and their course and speed; the basic radar parameters (the latitude and longitude of the location, the output power); the environmental parameters (the time of the year - month, the time of the day, the state of the sea and the direction of the wind). The course of a ship can be set as straightforward, curvilinear or in accordance with the given scenario. These parameters are all given in the XML format.

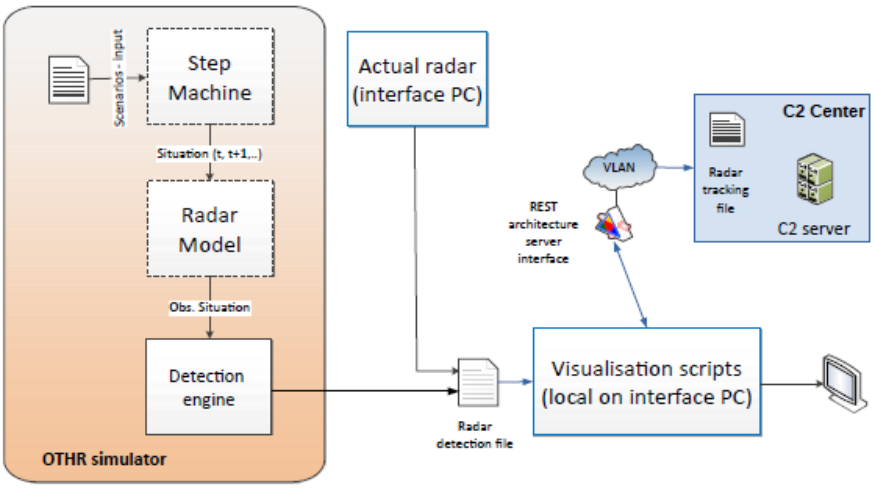

Figure 1 – Block diagram of the OTHR simulator
Рис. 1 – Блок-схема „OTHR“ симулятора
Слика 1 – Блок-шема „OTHR” симулатора

The block named “Radar Model” represents a function created in Matlab for calculating the maximum range, angular position relative to the true North and the signal to noise ratio (SNR) of potential targets. For all input data sets created by the step machine, the “Radar Model” creates a corresponding XML file with information about all potential radar targets.

This information represents an input for the last block - Detection and tracking engine.

The block named “Detection engine” imports the abovementioned information and creates a table of potential detections. In this way, the base of data sets is created in order to perform the testing of the radar tracking processes.

Usually, after the installation of the radar in practice (Actual radar block in Figure 1), the data obtained from the Simulator is compared with the data obtained from the real OTHR. All detection data obtained from installed, operational OTHR radars is sent to the Command and Control (C2) servers, via the communication network, Figure 1. The collected detection data passes through the top layer in the signal processing hierarchy – the tracking application (Stojković et al, 2016). This process of mutual comparison between simulated and real data is done and presented within Visualization scripts (Džolić et al, 2019b). In this way, additional calibration of the real OTHR radar can be performed if the results obtained in the field are different from those expected and an additional tuning of the radar system parameters is needed.

While the detection and tracking concept used in our research is already explained in detail, along with communication and data management for OTHR systems (Petrovic et al, 2020), in this paper we focus on describing the modeling process itself, which is the core of the Simulator and a true basis for all other features resulting from it. The solutions adopted in our radar model are of general importance: since they are not system-specific, they can be used within the performance analysis or simulation of any surface-wave over-the-horizon radar, of any vendor, in the manner completely independent from other blocks presented in Figure 1.

Radar model

The “Radar Model” is the most important block of the Simulator - it calculates the SNR for each target defined by a simulating scenario, shown in Figure 2.

The radar model used in the Simulator is based on the well-known radar equation, given by equation (1). This formula, unlike the classical radar equation, takes into account adaptation to the environment, frequency and waveform selection, RCS, external noises, interference, antenna gain, spatial resolution, and clutter (Skolnik, 1990).

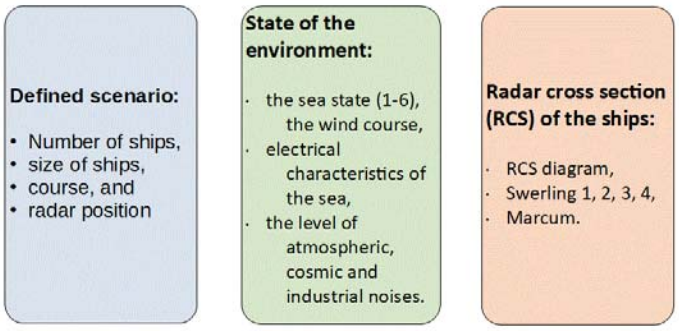

Figure 2 – Input scenario for the Radar Model function
Рис. 2 – Входной сценарий для функции модели радара
Слика 2 – Улазни сценарио за функцију радарског модела

$$S/N = \frac{P_{av} G_t G_r T \lambda^2 \sigma_{RCS} F_p}{N_0 L (4\pi)^3 R^4} \quad (1)$$

where:

- *S/N* stands for the signal to noise ratio,
- P_{av} stands for the average transmit power (W),
- G_t stands for the transmitted antenna gain,
- G_r stands for the received antenna gain,
- *T* stands for the effective processing time (s),
- λ stands for wavelength (m),
- σ_{RCS} stands for the radar cross section of a target (m^2),
- F_p stands for the propagation-path factor,
- N_o stands for the total noise power (W),
- *L* stands for transmission-path and system losses, and
- *R* stands for the distance between radar and target (m).

In practice, the S/N ratio is usually denoted in dB. The parameters from equation (1): σ_{RCS}, *L*, F_p and N_o are obtained from the radar model itself, as will be described later in the text. All other parameters are imported by the user.

In the considered radar model, the influence of external factors is calculated on the basis of the following sub-models:

- Sub-model 1: Sea surface propagation losses,
- Sub-model 2: Sea surface roughness impact,
- Sub-model 3: External noise, and
- Sub-model 4: Radar cross-section of vessels.

The sub-models listed above are fundamental for the simulation of the OTHR performance. While some system – specific parameters (like radiated power, antenna parameters, etc.) may vary from one particular radar unit to another, all the parameters generated through the listed sub-models are location – specific, fixed for predefined surrounding and environmental conditions, as described in detail in the rest of this section.

Sub-model1: Sea surface propagation losses

Since the OTHR radar operates in the HF band, frequencies between 4.6 and 7 MHz yield to the best range / cost performance. Moreover, with an increase in operating frequency values, signal propagation losses arise as well. The electrical characteristic of the propagation surface is mainly determined by the salinity level (ITU, 1992). Salty water when compared to dry land shows better conductivity characteristics, i.e. smaller propagation losses. This implies that OTHR radars can only operate at coastal areas (with installations close to the line of the waterfront), and are capable of monitoring large bodies of water.

For sea (salty) water, at 20 °C a value of 5 S/m is used as a world-wide average. Some areas of the Baltic Sea have a value of 1 S/m, while in the Red Sea the conductivity may exceed 6 S/m (ITU, 1992). The conductivity will however vary with both sea water salinity and temperature and it is given by:

$$\sigma_{SEA} = 0{,}18C^{0{,}93}\left[1 + 0{,}02(T - 20)\right]\frac{S}{m} \qquad (2)$$

where:

- C stands for salinity (grams of salt per liter),
- T stands for temperature (°C).

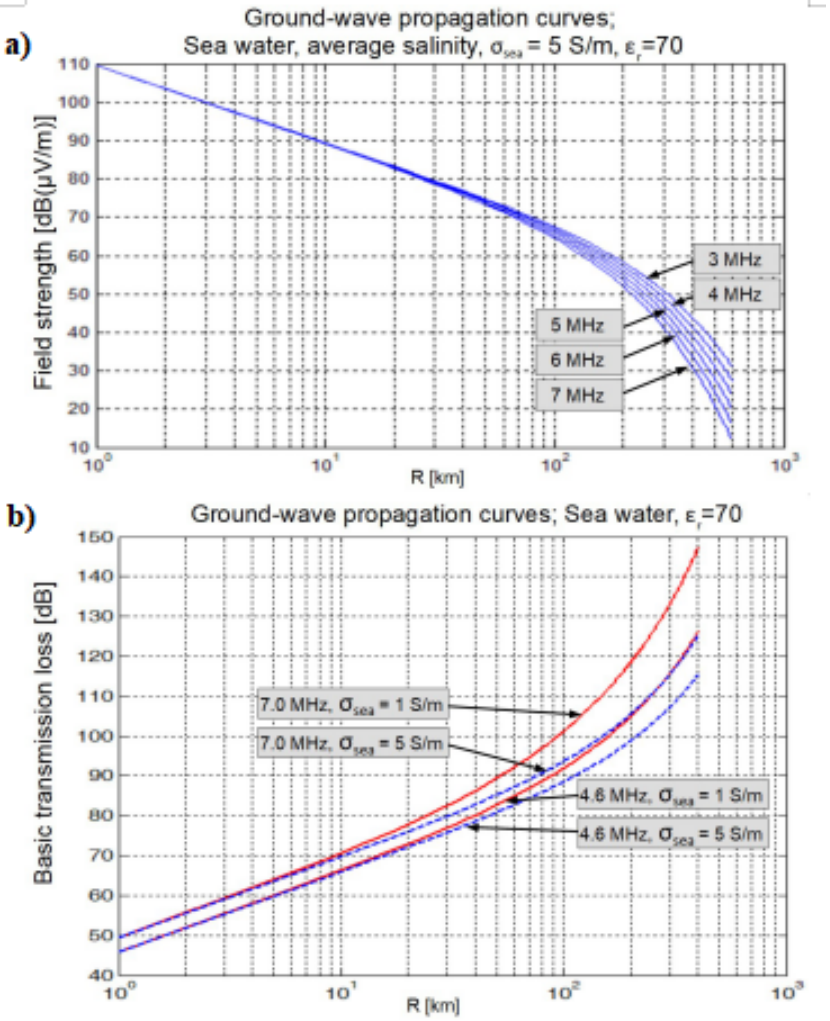

Figure 3 – Model of the signal propagation above the sea surface based on the GRWAVE software, a) Field strength, b) Transmission losses
Рис. 3 – Модель распространения сигнала над поверхностью моря на основе программного обеспечения „GRWAVE“, а) сила поля, б) потери при передаче
Слика 3 – Модел пропагације сигнала изнад морске површине заснован на софтверу „GRWAVE”, а) ниво поља, б) губици у пропагацији сигнала

The GRWAVE program (ITU, 2020) with linear interpolation between distance points is used to calculate propagation losses above the sea surface. This program uses a model that takes into account the curvature of the Earth's surface, as well as the electrical characteristics of the sea

surface and non-homogenous air causing refractions. The GRWAVE runs in the DOS environment, and the results are given in the form of an TXT file. The propagation curves for the frequencies from 3MHz to 8MHz are shown in Figure 3, on the basis of the values from the TXT file generated by the GRWAVE program, for the sea water propagation with the average salinity, the conductivity of 5 S/m and the relative permeability, $\varepsilon_{r,}$ of 70.The subfigure a) in Figure 3 shows the field strength of the electromagnetic (EM) wave at particular distances. This value was taken into account to calculate the basic transmission, L, from equation (1), (ITU, 2007). The subfigure b) in Figure 3 shows a variation of L in relation to the working frequency and the sea conductivity. The only input parameter for this function is a range (i.e. distance) of interest for loss calculation.

The values obtained from the GRWAVE are incorporated further in the Matlab code of the OTHR Simulator, and used for modeling the losses in propagation corresponding to this particular Sub-model.

Sub-model 2: Sea surface roughness impact

Apart from losses described within the *Sub-model 1,* additional losses in the propagation of HF surface waves are caused by wave ripples at the propagation surface. In other words, propagation losses are also dependent on roughness of the sea surface. Roughness of the sea surface, also known as the sea state, is most commonly described with the Douglas scale. By this scale, a sea state is expressed with digits from 0 to 9. A higher number on the scale corresponds to a higher wave height, which leads to higher losses in propagation. The analysis of the sea states from 0 to 6 shows that an increase in the wave height is proportional to an increase in propagation loss. A detailed analysis of this phenomenon could be found in (Barrick, 1970).

Another Matlab function is used to describe a propagation model which addresses the impact of the sea surface roughness. The maximum radar range, sea conditions and wind directions are defined as input parameters for this Matlab function, which generates an TXT file at the output. The values from the TXT file are used for the Calculation of the parameter “L” from the radar equation (1). Figure 4 shows the signal propagation losses for the sea states 3, 4, 5, and 6 when the wind direction is in the direction of the ship (red lines), as well as when the wind direction is normal to the course of the ship (blue lines). The calculations are made based on the values taken from empirical curves (Barrick, 1970) for the 7 MHz working frequency.

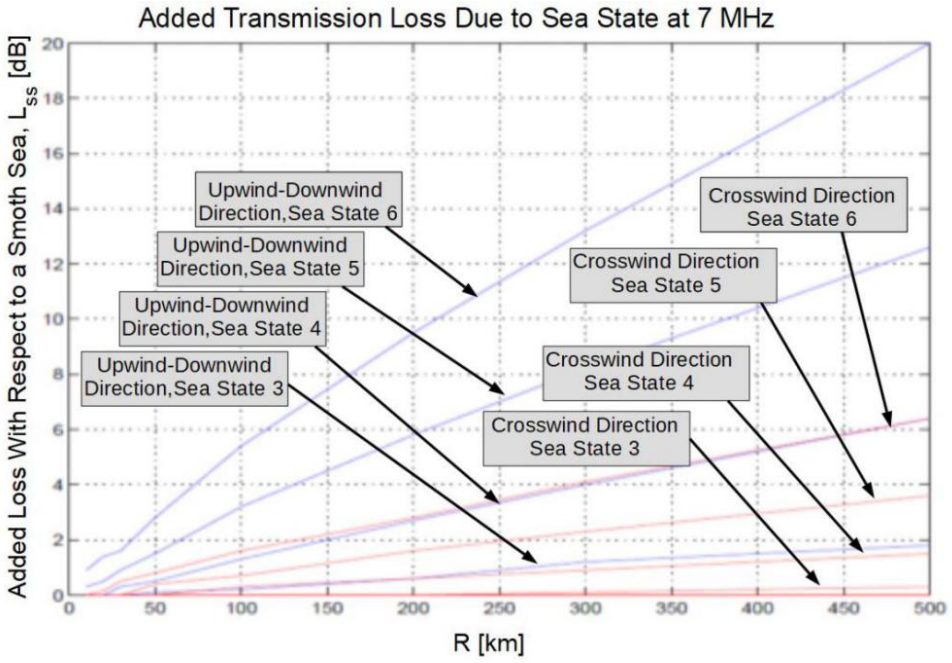

Figure 4 – Model of the signal loss due to roughness of the sea
Рис. 4 – Модель потери сигнала вследствие волнения моря
Слика 4 – Модел губитака у простирању сигнала изнад узбурканог мора

Sub-Model 3: External noise

The main difference for the calculation of the S/N between the MW radar and the HF-OTHR radar is the influence of external noises. For the MW radar, the S/N is defined by thermal noise, while for the OTHR the S/N is significantly affected by the level of external noise in the HF band. External noise consists of various types of noises, such as atmospheric, cosmic, and man - made noise (ITU, 2013).

Atmospheric noise predominantly depends on the geographic location and the season: winter, spring, summer or autumn, while cosmic noise depends only on the time of the day / night. From the HF point of view, there are 6 periods during 24 hours: 00h-04h, 04h-08h, 08h-12h, 12h-16h, 16h-20h, and 20h-24h (Spaulding & Washburn, 1985).

The characteristics of cosmic radio noise are similar to those of thermal noise. Being a phenomenon of the global nature, cosmic noise does not depend on a geographic location or a season. It depends only on the radar working frequency (Skolnik, 1990).

Artificial (man–made) noise varies by regions (rural zones, sub – urban or urban zones). A detailed description of atmospheric and cosmic noise could be found in (Spaulding & Washburn, 1985), while man – made noise mostly depends on the economic development of the area around the radar site, and is thus always analyzed in a very local manner, without a possibility to be covered with a global study. In general, the level of external noise is greater for lower operating frequencies. As shown in (Dzolic et al, 2019a), in some areas man – made noise is absolutely dominant in comparison with other noise sources.

The impact of external noise significantly limits a detection capability of the OTHR radar. The GH-NOISE (Hand, 2017) program is used to calculate the level of noise for different seasons and time of the day. The input for this software is given in the geographical coordinates of a potential radar site, a season, time interval (i.e. time slot, where the duration of the slot is 4 hours) during a day, and operating frequency for calculations.

The output of the GH-NOISE is stored in the form of an TXT file, used further by the Matlab function in order to correlate all types of noises that affect the maximum range of the radar. This function calculates the highest level of all noises (the level of dominant noise for a particular area), during all seasons and predefined time slots, and presents its variation as shown in Figure 5.

The Y axis values represent the noise power above the noise floor (−174 dBm//Hz). According to Figure 5, the average noise level varies between −125 and −112 dBm/Hz. Fam represents the median atmospheric noise power in dB above kTB, DL stands for how many dB below the median noise power exceeded 90% of the days of a month, and DU stands for how many dB above the median noise power exceeded 10% of the days of a month for a particular simulation point (parameter selection).

The value of the Fam is used for the N_0 in equation (1). All values are calculated for a site located in the Gulf of Guinea.

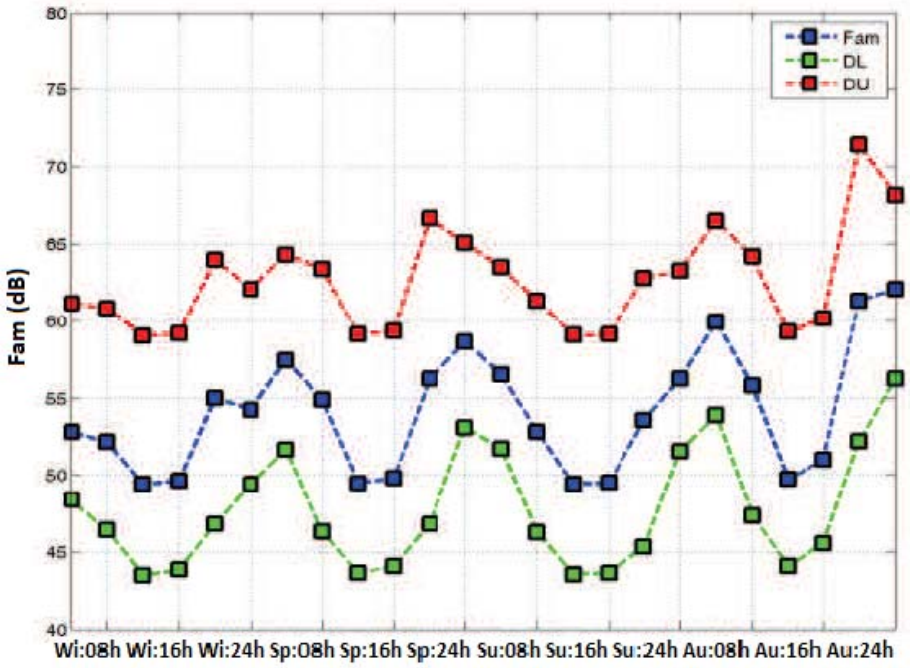

Figure 5 – Model of the external HF noises during all seasons (Wi—Winter, Sp—Spring, Su—Summer and Au—Autumn; 08 h, 16 h and 24 h represents the time of a day; the Y axis values represent the noise power level above the noise floor (−174 dBm/Hz);the values are plotted for 7 MHz operating frequency)

Рис. 5 – Модель внешних „HF“ шумов в течение всех времен года (Wi - зима, Sp - весна, Su - лето и Au - осень; 08 ч, 16 ч. и 24 ч. - время суток; значения по оси Y - уровень мощности шума над шумовым порогом (−174 dBm/Hz); приведены значения рабочей частоты 7 MHz)

Слика 5 – Модел екстерног HF шума током свих годишњих доба (Wi – зима, Sp – пролеће, лето, јесен; 08 ч, 16 ч и 24 ч означавају доба дана; вредности на Y оси представљају ниво снаге шума изнад прага шума (-174 dBm/Hz); вредности су приказане за радну фреквенцију 7 MHz)

Sub-Model 4: Radar cross-section of vessels

One of the most important parameters for the estimation of the radar performance is the RCS. The RCS has influence on the level of reflected signals and determines the signal to noise ratio (SNR). In the phase of the OTHR design, the knowledge about the RCS for different classes of ships is required in order to assess detection and tracking capabilities as objectively as possible. The RCS represents the projected area of a metal sphere that would return the same echo signal as the target does, in case when it would be replaced by the sphere (Skolnik, 1974). The

resulting echo from the conductive sphere is independent from the viewing angle, but the echo from a real target varies significantly with spatial orientation of the target (i.e. the angle between the radar and the observed target).

The RCS of the target depends on the following parameters:

- Geometrical shape and size of the vessel exposed to the radar beam,
- Electric properties of the vessel composing materials,
- Target position relative to the incident electromagnetic wave,
- The size of the vessel relative to the wavelength, and
- Antenna polarization with respect to the orientation of the vessel.

The OTHR simulator has the ability to scan the area in the angle width of ±60°around the predefined radar location. In order to detect the target, the receiving signal to noise ratio (SNR) of 10 dB is needed. Along with the OTHR system parameters, the environment parameters that affect detection (month, local time, sea state, man-made noise) are also taken into calculation. The target trajectory is given by target coordinates (latitude and longitude) which change depending on the vessel speed and course. For every point, the radar-vessel incident angle is calculated, which defines the RCS effect, Figure 6.

An analytic method for the calculation of the RCS is only possible for an elementary radar target form, such as a plate, disc, cylinder or thin wire structures. For a complex geometrical form, such as a vessel, analytic methods of the RCS calculation are not feasible. For this reason, professional software for electromagnetic modeling, WIPL-D (Kolundzija, 2005), is used to predict the RCS of vessels. The WIPL-D software enables electromagnetic modeling of antennas and scatters which represent a combination of wired and plate structures. This software uses the Method of Moment (MoM) approach to solve the starting integral equations for the assessment of unknown current distribution. This software solution is mainly used for antenna analysis, but offers a possibility to analyze mono-static and bi-static RCSs.

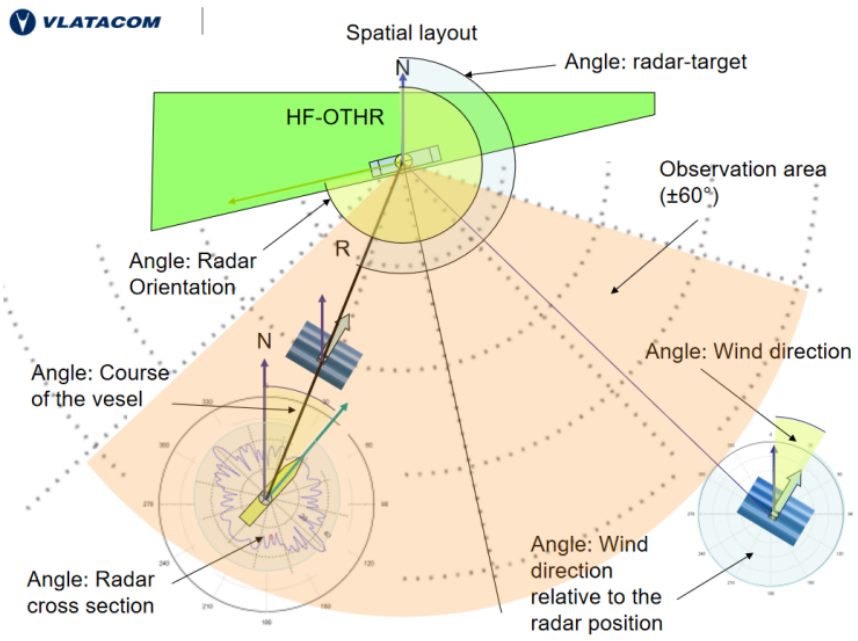

Figure 6 – Impact of the incident angle between the radar and the vessel

Рис. 6 – Влияние угла падения между радаром и судном

Слика 6 – Утицај инцидентног угла између радара и пловила

A model of the RCS implemented in the OTHR Simulator is shown in Figure 7.

This model consists of four important blocks. First of all, for the evaluation of the vessel's RCS, there is an empirical formula that represents a rough approximation only (Wilson & Leong, 2003):

$$\sigma_{RCS} = 52 * f^{\left(\frac{1}{2}\right)} * D^{\left(\frac{3}{2}\right)}, \qquad (3)$$

where *f* is frequency in MHz, and *D* is full-load displacement of the vessel in kilotons. The value σ_{RCS} calculated from this formula represents the maximum value of the RCS related to the vessel size and the working frequency only.

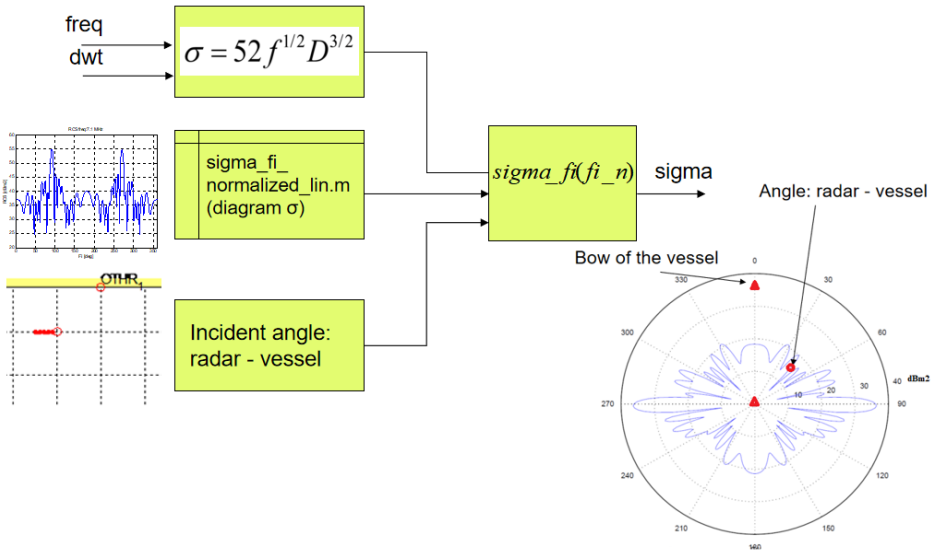

Figure 7 – Model of the radar cross section
Рис. 7 – Модель эффективной отражающей площади
Слика 7 – Модел радарске рефлексне површине

Another block is used for processing the output of the WIPL-D software. The maximum value of the signal is normalized with the signal value calculated by the previous block (empirical formula).

The calculation was made for the operating frequencies of 4.6MHz, 6.8MHz and 11MHz, as shown in Figure 8. The subfigure a) shows a vessel model designed in the WIPL-D and a table with variations due to incident angle change for the abovementioned working frequencies. The subfigures b), c) and d) show the RCS calculated from the WIPL-D for the working frequencies of 4.6MHz, 11 MHz, and 6 MHZ, respectively.

From the subfigure c), one can note that the minimum value of the RCS for the operating frequency of 11MHz, achieved in the situation where an incident wave falls upon the vessel bow, is lower for 26dB from the maximum value.

The highest side-lobes at this operating frequency are around 10dB under the maximum RCS value. For lower frequencies, a difference in the RCS values is smaller.

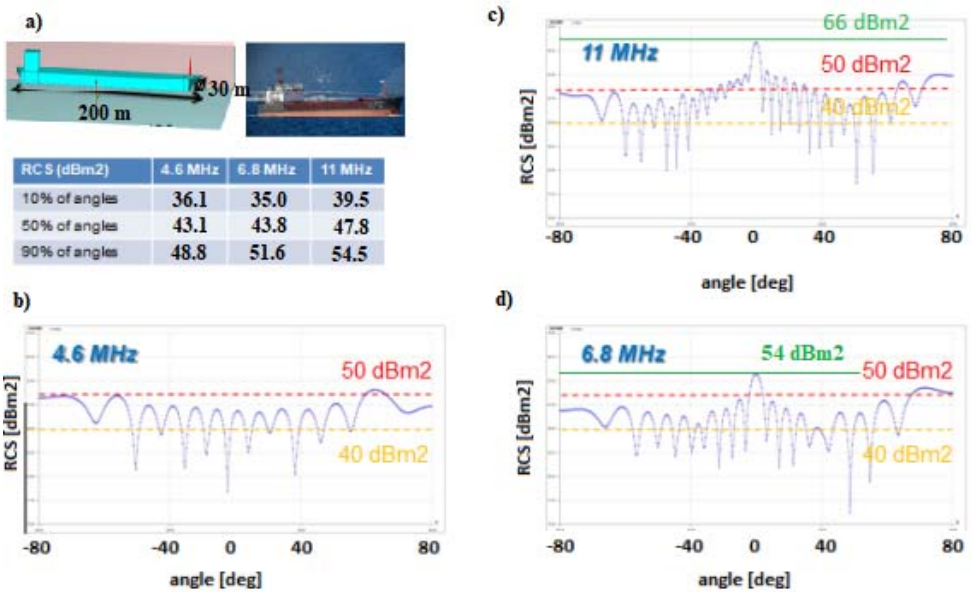

Figure 8 – RCS pattern of a vessel model generated with the OTHR Simulator a) WIPL-D model of the vessels and the table with the results of the RCS values for the simulated vessel, b) RCS calculated at 4.6MHz, c) RCS calculated at 11MHz, and d) RCS calculated at 6.8MHz

Рис. 8 – RCS модель судна, созданная с помощью OTHR симулятора. а)Модель судов WIPL-D и таблица с результатами значений RCS моделируемого судна, b) RCS, рассчитанная на 4,6 MHz, c) RCS, рассчитанная на 11 MHz, и d) RCS, рассчитанная на 6,8 MHz

Слика 8 – RCS расподела модела пловила срачуната помоћу OTHR симулатора. а) Модел пловила WIPL-D и табела са резултатима RCS вредности за симулирани брод, b) RCS израчунат на 4,6 MHz, c) RCS израчунат на 11 MHz и d) RCS израчунат на 6,8 MHz

From the third block (Figure 7), the user defines the incident angle between the radar and the vessel (Dzvonkovskaya & Rohling, 2010). Depending on the incident angle value, the RCS could change significantly, as shown in Figure 7, where the red triangle represents the course of the vessel, while the red circle represents the value of the RCS for the incident angle of the wave transmitted from the radar. From Figure 7, it can be also noticed that the RCS is attenuated for more than 20 dB, relative to the maximum value of the RCS for the incident angle of 90/270°.

The final block of this stage summarizes the values from the outputs of the previous three blocks, and generates a resulting σ_{RCS} value at its output depending on all the previously mentioned parameters. The data

obtained within this simulation can be easily exported to various file formats, which allows it to be imported into other software tools for further analysis. The generated RCS value, along with other basic parameters generated by the Simulator's specific blocks, provides a complete set of data necessary for the computer – based simulation of the OTHR.

A sample simulation

The paper presents the emulation of the sample system performances in the actual environment, carried out with the Simulator consisting of the described software components, executed in order to assess the coverage and test the vessel monitoring capabilities of the sample system. The system is fed with carefully prepared sets of inputs, with the aim of optimally illustrating the characteristics of the radar under various parameters in radar's own setup, targets, environment conditions and others. The flowchart of this sample simulation is shown in Figure 9.

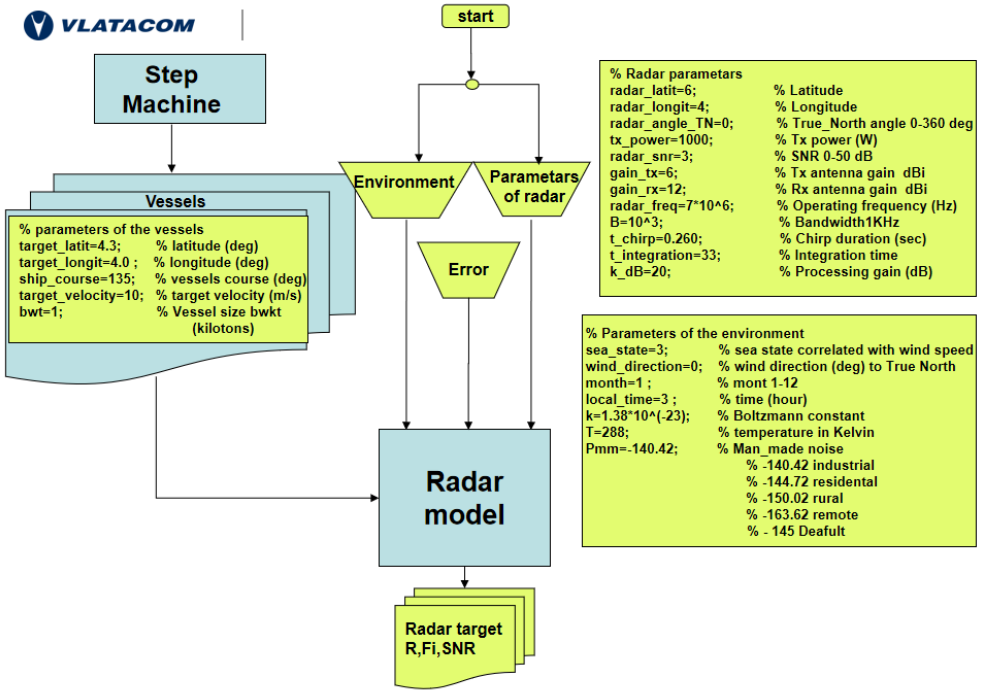

Figure 9 – Flowchart of the OTHR sample simulation
Рис. 9 – Блок-схема OTHR симулятора
Слика 9 – Дијаграм тока OTHR симулатора

Inputs for a simulation

The inputs for the simulation are provided through three important sets of parameters: Parameters of the radar, Environment parameters and Sample vessels. The block named “Error” gives an optional ability to analyze the impact of possible deviations of radar parameters, environment or target positions. A LAT and LON data from the step machine are converted into a radar coordinate system in relation to the LAT and LON positions of the radar in form of the distance (R), the angle (F_i), and the S/N corresponding with particular targets.

The distance (R) is used in modules 1 and 2 to calculate losses in the propagation of electromagnetic waves above the sea surface.

Parameters of the radar

The coordinates of the radar site were chosen in order to represent the situation as close as possible to realistic site locations that should be analyzed for potential deployment. Table 1 lists the main parameters of the radar.

Table 1 – Input parameters of the radar
Таблица 1 – Входные параметры радара
Табела 1 – Улазни параметри радара

NO	PARAMETER	UNIT	DEFAULT VALUE	VARIABLE
1	Radar latitude position	°	6.3	*radar_latit*
2	Radar longitude position	°	3.3	*radar_longit*
3	true_north-radar-antenna angle (main beam direction)	°	180	*radar_angle_TN*
4	Transmitted power	W	1000	*Tx_power*
5	SNR	dB	10	*Radar_snr*
6	Tx antenna gain	dBi	6	*gain_tx*
7	Rx antenna gain	dBi	12	*gain_rx*
8	Radar frequency	MHz	4.6	*radar_freq*
9	Bandwidth	kHz	1	*B*
10	Chirp duration	Sec	0.26	*t_chirp*
11	Integration time	Sec	33	*t_integration*

Environment parameters

Table 2 lists the environment parameters considered in the sample simulation.

Table 2 – Inputs for the environment estimation
Таблица 2 – Входные параметры оценки окружающей среды
Табела 2 – Улазни параметри за естимацију окружења

NO	PARAMETER	UNIT	DEFAULT VALUE	VARIABLE
1	Sea state 1-6		1	*sea_state*
2	Wind direction (°) to True North	°	0	*wind_direction*
3	Month 1-12		1	*month*
4	Time (Hour) 0-24		9	*local_time*

Sample vessels

A number of the parameters related to the vessels being directly of interest for the purpose of sample simulation are provided, describing the targets in a particular simulation scenario. These are shown in Table 3.

Table 3 – Input parameters for the sample vessels
Таблица 3 – Входные параметры по пробоотборникам
Табела 3 – Улазни параметри за симулиране бродове

NO	PARAMETER	UNIT	DEFAULT VALUE	VARIABLE
1	latitude (°)	°	5	*target_latit*
2	longitude (°)	°	5	*target_longit*
3	Vessel's course (°) TrueNorth	°	270	*ship_course*
4	Target velocity (m/s)	m/s	10	*target_velocity*
5	Ship size	kT	100	*bwt*

The estimations of the RCS surface used in this simulation, generated for the two system operating frequencies are shown in Table 4

Table 4. The values are classified for three categories of the vessels: Very large - VL, Medium – M, and Very small – VS (each category is defined by gross tones and the physical dimensions of the vessels (Grbić et al, 2018), as indicated in Table 4.

Table 4 – Estimated RCSs for 4.6 MHz and 7MHz, and the vessel size classification
Таблица 4 – Расчетное RCS для 4,6 MHz и 7 MHz и классификация размеров судов
Табела 4 – Процењени RCS за 4,6 MHz и 7 MHz и класификација величине бродова

	Very large – VL	Medium – M	Very small – VS
DWT(1000T)	300	50	5
Length (m)	400	200	50

	Very large – VL	Medium – M	Very small – VS
Width (m)	60	30	10
RCS- 4,6 MHz (m2)	579514.28	39430.95	1246.92
RCS- 4,6 MHz (dBm2)	57.63	45.96	30.96
RCS- 7 MHz (m2)	714881.81	48641.55	1538.18
RCS- 7 MHz (dBm2)	58.54	46.87	31.87

The results of the simulation

Two different scenarios are used to demonstrate the functionality of the described OTHR dedicated Simulator. The results from each simulation are compared with the realistic values achieved on the implemented OTHR system, and the obtained numerical results are forwarded to the presentation software tool for display and analysis.

The first scenario demonstrates the sea state effect on the vessel monitoring process, the second scenario demonstrates the vessel radial movement behavior in the context of detection performance, while the third scenario estimates the positioning error achieved in simulations. All the results are presented and explained, successively.

Scenario #1:Sea state effect on the vessel monitoring process

This scenario aims to show the sea state and the wind direction effect on the general system coverage area considered, for the vessels as defined. The hypothesis that a higher sea state value reduces the coverage of the system is under check with the simulation.

The radar targets in this scenario are created in the form of the group of 3 vessels of different classes. The vessel closest to the radar has the smallest class, while the distance from the radar is the biggest for the largest vessel. The movement of the group is linear, with a constant speed and the course normal to the radar receive array. The distance between successive vessels is fixed at 45 km. The observation zone for the simulation starts at 5km from the radar, and goes to 400km towards the open sea, with the coverage angle of 120° (±60° from the center axis of the radar array).

The scenario setup with the initial positions of the vessels and their bearings is presented in Figure 10. The main goal is to analyze the location of the potential site and, related to that geo-location, the X axis shows relative latitude, while the Y axis shows relative longitude of the observation area.

Integration time, the parameter defined in Table 1, represents the time needed for the radar simulator to complete acquisition of the data. Since the real radar takes 33s for the integration time, in this scenario the integration time will be set to 33s exactly. Chirp duration defined in Table 1 is 0.26s. For this scenario, 256 chirps are used, which represents a total simulation duration time of around 66s (0.26s *256). In total, eight data runs are executed: for each working frequency (2 data runs) and for each sea state (4 data runs) considered. Here, the considered sea state values are 1, 3, 5, and 6, with the vessel sizes of VS, M, VL observed in each simulation run. The operating frequencies considered are 4.6 MHz and 7 MHz.

The parameters for the sea state, the wind direction, the time of the year and the time of the day are defined in Table 2 and taken into account to calculate the maximum range of the detected targets. The "wind direction" parameter has a fixed value in all simulations.

The outputs of the radar simulator for scenario #1 are given in Table 5. The column “Expected Range” represents the values acquired from the previously installed (operational) radars in the field, while the “Actual Range” represents the values from the output of the OTHR simulator for a specific location. As it can be noticed from Table 5, the achieved results show that a higher sea state reduces the coverage of the OTHR system, as expected.

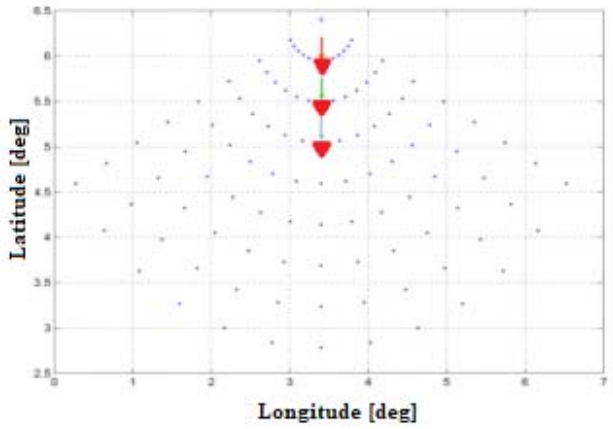

Figure 10 – Initial setup of scenario #01, the initial positions of the sample vessels are marked with coloured arrows.
Рис. 10 – Первоначальная настройка сценария № 01, начальные положения проботборников отмечены цветными стрелками.
Слика 10 – Иницијална поставка сценарија #01(почетне позиције пловила означене су обојеним стрелицама)

Table 5 – Achieved results for the analysis of the sea state effect on the vessel monitoring process, all range values presented in km units
Таблица 5 – Полученные результаты для анализа влияния состояния моря на процесс мониторинга судов, все значения приведены в км
Табела 5 – Постигнути резултати анализе утицаја стања мора на процес праћења пловила(све вредности су приказане у километрима)

Case	Radar freq. MHz	Sea State	Expected Range for **VS vessel**	Actual Range for **VS vessel**	Expected Range for **M vessel**	Actual Range for **M vessel**	Expected Range for **VL vessel**	Actual Range for **VL vessel**
1	4.6	1	215	222.75	300	313.25	370	387.75
2	4.6	3	215	225.75	300	317.25	370	392.75
3	4.6	5	190	197.25	260	275.75	320	340.25
4	4.6	6	170	176.25	220	245.75	280	302.75
5	7	1	120	129.75	180	196.25	240	253.25
6	7	3	115	127.75	160	191.25	230	245.25
7	7	5	100	103.75	140	154.75	180	197.75
8	7	6	90	92.25	120	135.25	160	172.75

From the columns “Actual Range” and “Expected Range” it can be noticed that the values for the maximum achieved range achieved via the simulation are very similar to those expected from the practical radar performance, and some existing small variations directly depend on the difference in the values of system parameters, as defined for the specific location.

Scenario #2: Vessel radial movement impact on the detection performance

In this scenario, the coverage area is observed for the vessels that are moving away from the radar, radially with a radiation pattern of the radar array, and with a difference between their courses of 10°. The hypothesis under check with this simulation is: that the achieved radar detection range is higher at the central lobe of the antenna array than at its boundaries, while the detection range for particular vessels varies depending on the size and working frequency (larger the vessel - higher the range, and lower the frequency - higher the range will be).

Figure 11 presents the initial positions of the vessels and their bearings for scenario #2.

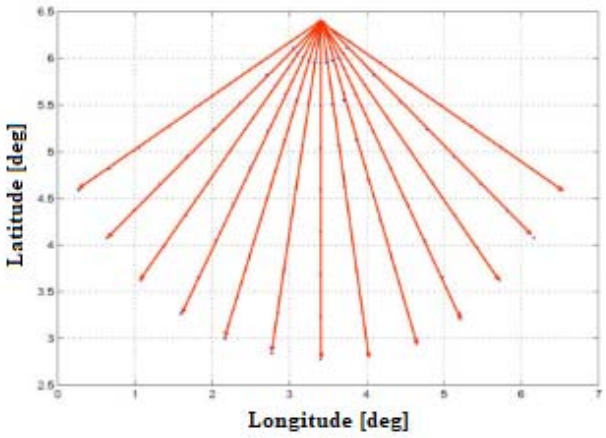

Figure 11 – Initial setup of scenario #02, the vessel trajectories presented with red lines
Рис. 11 – Начальная настройка сценария #02, траектории судна обозначены красными линиями
Слика 11 – Иницијална поставка сценарија #02(путање бродова приказане су црвеним линијама)

The radar targets are created in a form of the group of 13 vessels of the same classes, per one simulation run, while 3 different classes of vessels for different simulation runs will be demonstrated. The movement of the group is linear with a constant speed and course, radial to the radar receive array (radiation pattern). The observation zone for the simulation starts 5 km from the radar itself, and goes to 400 km towards the open sea, with the coverage angle of 120° (±60° from the center axis of the radar array).

The integration time is set to 33s, while the total duration time of the simulation is around 66s (in accordance with the comments already given for the previous scenario, above). In total, six data runs will be executed: for each working frequency (2 data runs) and for each class of the vessel (3 data runs) observed. The considered sea state value is 3, with the vessel sizes of VS, M, VL considered in each simulation run. The operating frequencies considered are 4.6 MHz and 7 MHz.

The resulting outputs of the radar simulator for scenario #2 are given in Table 6 and Table 7. The results are presented only for sectors 1-7 (corresponding with the angles from 60° down to 0°, with a decrement of 10°), since the values achieved in sectors 8-13 (corresponding with the angles from 0° up to -60°, with a decrement of 10°) are completely symmetrical with the ones presented. The ranges are given in km, where the fields marked with the letter “E” (Expected) represent the predicted

values from the output of the OTHR radar, based on the values from the previously installed (operational) radars, while the values marked with “A” (Actual) represent the values from the output of the OTHR simulator, for the considered, specific location.

Table 6 – Achieved maximum detection range in the scenario with the vessel radial movement, for the radar operating frequency of 4.6 MHz, all values presented in km units
Таблица 6 – Достигнута максимальная дальность обнаружения в сценарии с радиальным движением судна при рабочей частоте радара 4,6 MHz, все значения приведены в км
Табела 6 – Постигнути максимални домет детекције у сценарију са радијалним кретањем пловила за радну фреквенцију 4,6 MHz (све вредности су приказане у километрима)

Vessel size \ Sector	1E	1A	2E	2A	3E	3A	4E	4A	5E	5A	6E	6A	7E	7A
VS	180	188.2	185	189.2	195	202.2	200	209.7	205	218.7	215	221.7	220	222.7
M	275	276.2	280	289.2	290	299.2	295	304.7	300	309.7	305	311.7	310	312.7
VL	330	343.7	350	363.2	360	368.2	370	374.2	380	380.2	385	387.2	385	388.2

As it can be noticed from Table 6 and Table 7, the larger vessels are visible at greater distances from the radar, in comparison with smaller classes of vessels, as expected. Also, the vessels of the same size are visible at greater distances when detected with a lower operating frequency (4.6MHz) of the radar system. The absolute maximum range is achieved in the direction of the center axis of the radar array, while, by moving away from the direction of the angle center, the maximum range value decreases.

Table 7 – Achieved maximum detection range in the scenario with the vessel radial movement, for the radar operating frequency of 7 MHz, all values presented in km units
Таблица 7 – Достигнута максимальная дальность обнаружения в сценарии с радиальным движением судна при рабочей частоте радара 7 MHz, все значения прприведены в км
Табела 7 – Постигнути максимални домет детекције у сценарију са радијалним кретањем пловила за радну фреквенцију 7 MHz (све вредности су приказане у километрима)

Vessel size \ Sector	1E	1A	2E	2A	3E	3A	4E	4A	5E	5A	6E	6A	7E	7A
VS	90	106.7	95	114.7	110	124.7	115	127.7	120	128.7	125	129.7	125	129.7
M	160	168.7	170	177.7	180	187.2	185	191.2	190	192.2	195	195.2	195	195.2
VL	215	223.7	225	234.7	230	241.7	235	247.7	240	250.7	250	252.2	250	253.2

By comparing the columns “E” and “A”, it can be noticed that the OTHR simulator confirms the predicted ranges in a reasonable manner, and the variations that exist in the compared values directly depend on the input parameters (external noises) related to the specific location where the radar could be installed. Still, the magnitudes of detection range values for particular vessel classes, and the tendencies in their dynamics are simulated with proper correctness. This result represents another important confirmation of a proper performance of the developed Simulator, in terms of its practical usability.

Conclusion

In this paper, we presented a solution for the OTHR Simulator, based on software models for radar propagation and executed on a standard COTS computer. The solution is described in detail, and tested under characteristic parameters that verify its basic functionality and illustrate the properties of data achieved through the simulation. It was shown that the simulator allows the analysis of the environmental impact on the operation of OTHR radars, along with an impact of various system–specific parameters. The solution is flexible in possible interfacing with other computer–based tools, along with the real radar equipment for the comparison of the acquired data and a potential comparison for the purpose of real–system tuning. The Simulator solution was tested under various scenarios, with the aim to check its basic functionality, but also to make relevant comparisons of simulations with realistic measurements acquired in the field, from operational OTHR radars. As it was clearly shown, the achieved simulation results not only apply to the expected theoretical behavior, but also fit in quite a reasonable manner with the real data, thus confirming that the reliability of the simulations is at the level properly high for practical considerations. After the comprehensive tests, it may be concluded that the proposed simulator shows high reliability and represents an effective tool for the analysis and OTHR system planning, in spite of its simplicity in structure.

The implemented software solution of the OTHR Radar Simulator has enabled the further development of algorithms at a higher level of radar signal processing, like detection and tracking software. Also, various scenarios have been used with this Simulator for testing the capabilities of OTHR radars in real deployment. This was done by engineers in the Vlatacom Institute for the vHF-OTHR system installations on several locations worldwide, and the gained experience in assessing the real capabilities of OTHR radar systems was provided for

practical purpose. Finally, the described software solution can be used not only for research & development of radar systems, or for commercial applications strictly, but also for teaching purposes at higher education institutions which are covering the field of radar systems.

References

Barrick, D.E. 1970. *Theory of Ground-Wave Propagation Across A Rough Sea at Decameter Wavelengths*. Columbus, Ohio: Battelle Memorial Institute [online]. Available at: https://apps.dtic.mil/dtic/tr/fulltext/u2/865840.pdf [Accessed: 7 June 2020].

Dzolic, B., Tosic, N., Lekic, N., Orlic, V & Veinovic, M. 2019a. Transmitter's internal noise performance as limiting factor inHigh-Frequency Over-the-Horizon radars. In: *2019 14th International Conference on Advanced Technologies, Systems and Services in Telecommunications (TELSIKS),* Niš, Serbia, October 23-25. Available at: https://doi.org/10.1109/TELSIKS46999.2019.9002333.

Džolić, B., Tošić, N., Orlić, V. & Veinović, M. 2019b. Visualisation tools for design of Maritime Surveillance System. In: *Sinteza 2019 - International Scientific Conference on Information Technology and Data Related Research*, Belgrade, Serbia, April 20th. Available at: https://doi.org/10.15308/Sinteza-2019-546-552.

Dzvonkovskaya, A. & Rohling, H. 2010. Cargo ship RCS estimation based on HF radar measurements. In: *11th International Radar Symposium (IRS),* Vilnius, Lithuania, June 6-18 [online]. Available at: https://ieeexplore.ieee.org/document/5547445 [Accessed: 7 June 2020].

Fabrizio, G. 2013. *High Frequency Over-the-Horizon Radar: Fundamental Principles, Signal Processing, and Practical Applications*. New York: McGraw-Hill. ISBN: 9780071621274.

Girault, B., Narayanan, S., Ortega, A., Gonçalves, P. & Fleury, E. 2017. Grasp: A Matlab toolbox for graph signal processing. In: *2017 IEEE International Conference on Acoustics, Speech and Signal Processing (ICASSP),* New Orleans, USA, March 5-9. Available at: https://doi.org/10.1109/ICASSP.2017.8005300.

Grbić, N., Petrović, P., Stevanović, N., Džolić, B., Nikolić, D. & Lekić, N. 2018. Simulacija radarske površine brodova u kratkotalasnom frekventnom opsegu. In: *62nd ETRAN Conference*, Palić, Serbia, pp.126-129, June 11-14 (In Serbian) [online]. Available at: https://www.etran.rs/common/Zbornik%20ETRAN%20IC%20ETRAN-18-final.pdf [Accessed: 7 June 2020].

Hand, G.R. 2017. *Combination of Radio Noise modification* [online]. Available at: http://www.greg-hand.com/noise/ [Accessed: 15 April 2020].

-ITU (International Telecommunication Union). 1992. *Recommendation ITU-R P.527-3. Electrical characteristic of the surface of the earth* [online]. Available at: https://www.itu.int/dms_pubrec/itu-r/rec/p/R-REC-P.527-3-199203-S!!PDF-E.pdf [Accessed: 7 June 2020].

-ITU (International Telecommunication Union). 2007. *Recommendation P.368-9 (02/07) Ground-wave propagation curves for frequencies between 10 kHz and 30 MHz* [online]. Available at: https://www.itu.int/rec/R-REC-P.368-9-200702-I/en [Accessed: 7 June 2020].

-ITU (International Telecommunication Union). 2013. *Recommendation P.372-11 (09/2013) Radio noise* [online]. Available at: https://www.itu.int/rec/R-REC-P.372-11-201309-S/en [Accessed: 7 June 2020].

-ITU (International Telecommunication Union). 2020. *Software, Data and Validation examples for ionospheric and tropospheric radio wave propagation and radio noise, Ground-wave propagation (GRWAVE) ver.9.2, Software* [online]. Available at: https://www.itu.int/en/ITU-R/study-groups/rsg3/Pages/iono-tropo-spheric.aspx [Accessed: 15 April 2020].

Kolundzija, B.M., Ognjanovic, J.S.& Sarkar T.K. 2005. *WIPL-D Microwave: Software and User's Manual: Circuit and 3D EM Simulation for RF and Microwave Applications*. Norwood, Massachusetts: Artech House. ISBN: 978-1580539654.

Nikolić, D., Džolić. B., Tošić, N., Lekić, N., Orlić. V. & Todorović, B. 2016a. HFSW Radar Design: Tactical, Technological and Environmental Challenges. In: *OTEH 7th International Scientific Conference on Defensive Technologies*, Belgrade, Serbia, October 6-7.

Nikolic, D., Popovic, Z., Borenovic, M., Stojkovic, N., Orlic, V., Dzvonkovskaya, A. & Todorovic, B. 2016b. Multi-Radar Multi-Target Tracking Algorithm for Maritime Surveillance at OTHR Distances. In: *17th International Radar Symposium (IRS)*, Krakow, Poland, May 11-15.

Nikolic, D., Stojkovic, N. & Lekic, N. 2018. Maritime Over the Horizon Sensor Integration: HFSWR and AIS Data Integration Algorithm. *Sensors*, 18 (4), 1147. Available at: https://doi.org/10.3390/s18041147.

Petrovic, R., Simic, D., Drajic, D., Cica, Z., Nikolic, D. & Peric, M. 2020. Designing Laboratory for IoT Communication Infrastructure Environment for Remote Maritime Surveillance in Equatorial Areas Based on the Gulf of Guinea Field Experiences. *Sensors*, 20(5), 1349. Available at: https://doi.org/10.3390/s20051349

Sevgi, L. & Ponsford, A.M. 1999. An HF Radar Base Integrated Maritime Surveillance System. In: *3rd International Multiconference IMACS/IEEE CSCC'99*, Athens (Greece), pp.5801-5806, July 4-8 [online]. Available at: http://www.wseas.us/e-library/conferences/athens1999/Papers/580.pdf [Accessed: 7 June 2020].

Skolnik, M.I. 1974. An empirical formula for the radar cross section of the ships at grazing incidence. *IEEE Transactions on Aerospace and Electronic Systems*, AES-10(2), pp.292-292. Available at: https://doi.org/10.1109/TAES.1974.307935.

Skolnik, M.I. 1990. *Radar Handbook, Second Edition*. New York: McGraw-Hill. ISBN: 0-07-057913-X.

Spaulding, A.D. & Washburn, J.S., 1985. *Atmospheric Radio Noise: Worldwide Levels and Other Characteristics*. *NTIA Report 85-173.* U.S. Department of commerce.

Stojković, N., Nikolić, D., Džolić, B., Tošić, N., Orlić, V., Lekić, N. & Todorović, B. 2016. An Implementation of Tracking Algorithm for Over-The-Horizon Surface Wave Radar. In: *24th Telecommunications Forum (TELFOR)*, Belgrade, Serbia, November 22–23.

Tošić, N., Džolić, B., Nikolić, D., Lekić, N. & Todorović, B. 2016. Izazovi pri projektovanju HFSW radara. In: *60th ETRAN Conference*, Zlatibor, Serbia, June 13-16 (in Serbian).

-United Nations, 2011. *Law of the Sea, Part V—Exclusive Economic Zone* [online]. Available at: https://www.un.org/depts/los/convention_agreements/texts/unclos/part5.htm [Accessed: 7 June 2020].

-Vlatacom Institute. 2018. *Over the horizon radar: vOTHR, Product datasheet* [online]. Available at: https://www.vlatacominstitute.com/over-the-horizon-radar [Accessed: 7 June 2020].

Wilson, H. & Leong, H. 2003. An Estimation and Verification of Vessel Radar-Cross-Section for HF Surface Wave Radar. In: 2003 Proceedings of the International Conference on Radar (IEEE Cat. No.03EX695), Adelaide, Australia, September 3-5. Available at: https://doi.org/10.1109/RADAR.2003.1278830.

РАЗРАБОТКА СИМУЛЯТОРА ЗАГОРИЗОНТНОГО РАДИОЛОКАТОРА

Боян Р. Джолич[а,б], **корреспондент**, *Младен* Дж. Веинович[в], *Владимир* Д. Орлич[а], *Никола* Л. Лекич[а], *Неманя* Р. Грбич[а]

[а] Институт «Влатаком», г. Белград, Республика Сербия
[б] Университет «Сингидунум», кафедра электротехники и вычислительной техники, г. Белград, Республика Сербия
[в] Университет «Сингидунум», г. Белград, Республика Сербия

РУБРИКА ГРНТИ: 47.00.00 ЭЛЕКТРОНИКА. РАДИОТЕХНИКА:
47.49.00 Радиотехнические системы зондирования, локации и навигации,
47.49.29 Радиолокационные системы, станции
ВИД СТАТЬИ: оригинальная научная статья

Резюме:

Введение/цель: Симулятор загоризонтного радиолокатора, представленный в этой статье, разработан и используется на практике с целью имитации среды радиолокационного сигнала, а также для оптимизации параметров радара в реальном применении, таких как: излучаемая мощность, усиление антенной решетки, потери при передаче, эффективная отражающая площадь, внешние помехи и шумы.

Методы: В данной статье применен метод математического моделирования и симуляции.

Результаты: На основании проведенного анализа в статье представлены выходные данные симулятора загоризонтного радиолокатора.

Выводы: Применение описанного симулятора загоризонтного радиолокатора позволяет автоматизировать прогноз возможности использования радара на потенциальных локациях, при этом результаты симуляции превосходно согласованы с реальными данными.

Ключевые слова: загоризонтный радиолокатор, эффективная отражающая площадь, исключительная экономическая зона, симулятор радара.

ЈЕДНО РЕШЕЊЕ СИМУЛАТОРА ИЗАХОРИЗОНТСКОГ РАДАРА

Бојан Р. Џолић[а,б], **аутор за преписку**, *Младен* Ђ. Веиновић[в], *Владимир* Д. Орлић[а], *Никола* Л. Лекић[а], *Немања* Р. Грбић[а]

[а] Институт Влатаком, Београд, Република Србија
[б] Универзитет Сингидунум, Катедра за електротехнику и рачунарство, Београд, Република Србија
[в] Универзитет Сингидунум, Београд, Република Србија

ОБЛАСТ: електроника, телекомуникације
ВРСТА ЧЛАНКА: оригинални научни рад

Сажетак:

Увод/циљ: Симулатор изахоризонтског радара (ИХР), који је представљен у овом раду, развијен је и коришћен у пракси, са циљем да опонаша окружење радарског сигнала, али и да оптимизира параметре радара у стварној примени, као што су: зрачена снага, појачање антене, губитак пута, радарска рефлексна површина, спољне сметње и шум.

Методе: У раду се користи методологија математичког моделирања и симулација.

Резултати: На основу обављене анализе, излазни подаци из ИХР симулатора представљени су и разматрани.

Закључак: Примена описаног симулатора ИХР омогућава аутоматизовану процену могућности употребе радара на потенцијалним локацијама, док резултати симулације показују високо слагање са реалним подацима.

Кључне речи: изахоризонтски радар, радарска рефлексна површина, ексклузивна економска зона, радарски симулатор.

Paper received on / Дата получения работы / Датум пријема чланка: 09.06.2020.
Manuscript corrections submitted on / Дата получения исправленной версии работы / Датум достављања исправки рукописа: 03.08.2020.
Paper accepted for publishing on / Дата окончательного согласования работы / Датум коначног прихватања чланка за објављивање: 05.08.2020.

INTRUSION DETECTION BASED ON THE ARTIFICIAL IMMUNE SYSTEM

Danijela D. Protić
Serbian Armed Forces, General Staff,
Department for Telecommunication and Informatics (J-6),
Center for Applied Mathematics and Electronics,
Belgrade, Republic of Serbia,
e-mail: adanijela@ptt.rs,
ORCID iD: http://orcid.org/0000-0003-0827-2863

DOI: 10.5937/vojtehg68-27954; https://doi.org/10.5937/vojtehg68-27954

FIELD: Computer sciences
ARTICLE TYPE: Original scientific paper

Abstract:

Introduction/purpose: The artificial immune system is a computational model inspired by the biological or human immune system. Of particular interest in artificial immune systems is the way the human body reacts to new pathogens and adapts to remain immune for a long period after a disease has been combated, which refers to the recognition of known malicious attacks and the way the immune system identifies self-cells not to be reacted to, which refers to the anomaly detection.

Methods: Negative selection, positive selection, clonal selection, immune networks, danger theory, and dendritic cell algorithm are presented.

Results: A variety of algorithms and models related to artificial immune systems and two classification principles are presented; one based on the detection of a particular attack and the other based on anomaly detection.

Conclusion: Artificial immune systems are often used in intrusion detection since they are accurate and fast. Experiments show that the models can be used in both known attack and anomaly detection. Eager machine learning classifiers show better results in the decision, which is an advantage if runtime is not a significant parameter. Dendritic cell and negative selection algorithms show better results for real-time detection.

Key words: artificial immune system, intrusion detection.

Introduction

Artificial immune systems (AISs) are computational models inspired by the human immune system (HIS). The HIS is a complex, adaptive system of cells and molecules that protects the body against a variety of pathogens and distinguishes self- from non-self- cells. It recognizes, responds to and remembers the pathogens from previous attacks in order to force quicker fight against intruders in the future. The HIS consists of two different inter-related subsystems which act together. The innate immune system provides

a general protective mechanism present from birth and makes a quick response immediately after the exposure to the invader and its recognition (De Castro & Von Zuben, 1999, p.95). The adaptive response takes several weeks to become effective. Once activated, the components of the adaptive immune system proliferate and create mechanisms for the elimination of foreign substances called antigens (Timmis et al, 2008, pp.11-32). The cells responsible for adaptive immunity are B cells which originate in the bone marrow and T cells which originate in the thymus. AISs describe concepts of positive and negative selection, clonal selection, immune networks, and a variety of other concepts of immunology. In order to map the processes involved in the HIS to AISs, a few considerations have to be taken into account: how to represent antigens and antibodies, what are memory cells, how to calculate affinity, etc.

The goal of intrusion detection is to build a system which recognizes malicious attacks or unusual network behavior and generate alerts. There are two basic trends in intrusion detection: misuse detection, based on the knowledge accumulated from previous attacks and anomaly detection, based on search for deviation of usual computer network behavior. Of particular interest in AISs is the way the human body reacts to new pathogens and adapts to remain immune for a long period after a disease has been combated (misuse detection). Also of interest is the way the immune system identifies self-cells which are not to be reacted to (anomaly detection).

AIS concepts and algorithms

A distinction between what is self and what is not (non-self) is determined by an antibody that can be recognized by the antigen binding sites on other antibodies. If the HIS cannot perform this distinction, it may be triggered against self (Haag et al, 2007, pp.420-435).

Negative selection

In the HIS at birth, all new immature T-cells must undergo a process of negative selection in the thymus, where self-reactive T-cells binding with self-proteins are destroyed. Immature T cells, which react against self cells, are eliminated by the immune system through controlled cell death - apoptosis**.** Other T cells mature, leave the thymus and circulate throughout the body to perform protective functions against non-self antigens (Forrest et al 1994, pp.202-212). The negative selection algorithm (NSA) consists of two phases: generation of a detector set and monitoring with detection of new instances. The starting point of the NSA is to produce a set of self strings *S* that define the normal state of the system. The task is to generate a set of detectors *D* that only recognize the complement of *S*. The

candidates that match are eliminated while the rest are kept as detectors. In the detection stage, the detectors are applied to new data in order to classify them as being self or non-self (Ji & Dasgupta, 2007, pp.223-251). The matching rule can be defined as a distance between the detector and the data instance within the threshold such as the Hamming distance, or the Euclidean distance.

Positive selection

If the T cell recognizes self-molecules, it causes apoptosis and dies. If it does not react, it is tested with non-self molecules. If the T cell is not able to recognize them, it dies. T cells that can react with non-self molecules survive. This is positive selection (Sri Lakshmi, 2014, pp.367-372). T cells are selected because of their lack of recognition of self. Positive selection ensures removing lymphocytes with ineffective receptors allowing the effective antibodies the space to clone and survive, which maintains a controlled size of population (repertoire) (Haag et al, 2007, pp.420-435). T cells that can pass through the thymus react to non-self cells, but they are unable to react to self cells.

Clonal selection

Burnet (1959) proposed the clonal selection theory which describes the HIS basics. The immune response is made possible by the antigen-recognizing surface receptor molecules of both the B and T cells and is based on the complementarities between the antibody receptor and the antigen (De Castro & Timmis, 2002b). An antibody can potentially identify another antibody if their receptor arrangement matches. If the HIS cannot perform this distinction, it may be triggered against self (Haag et al, 2007, pp.420-435). As a response to an antigenic stimulus, the organism activates the cells that match a particular antigen which proliferate and secrete antibodies (De Castro & Timmis, 2002a, pp.669-674). Cells are stimulated to produce clones of themselves very quickly, thus producing more antibodies at high speed (Aickelin & Dasgupta, 2005). In 2002, De Castro & Von Zuben (De Castro & Von Zuben, 2002) presented the algorithm named CLONALG, developed to perform pattern recognition and optimization. The authors demonstrated the ability of the algorithm to learn a set of input patterns by "selecting, reproducing and mutating a set of artificial immune cells". They highlighted two important features of affinity maturation of B cells that can be applied in artificial immune systems: 1) proliferation of B cells is proportional to the affinity of the antigen that binds, and 2) mutations suffered by the antibody of a B cell are inversely proportional to the affinity of the antigen. When applied to pattern matching, a set of patterns S to be

matched are considered to be antigens. The task of CLONALG is then to produce a set of memory antibodies *M* that match *S*.

Immune network theory

The immune network theory (INT) proposed by Jerne (1974, pp.373-389) suggested that the HIS is composed of a regulated network of cells and molecules that recognize one another even in the absence of antigens (De Castro & Von Zuben, 2001). Jerne concluded that the immune system must display a behavior or activity resulting from interactions with itself and from these interactions immunological behavior such as tolerance and memory emerge. The discrete immune network model (DINM) is proposed by Timmis & Neal (2001, pp.121-130).

Danger theory

In 1994, Matzinger (Matzinger, 1994) proposed a new immunological danger model. The immune system does not concentrate to distinguish between self and non-self, but to danger and safe. The main idea is that the immune system should not react to "non-self but harmless" but to "self but harmful". The theory claims that an immune system response is triggered by alarm signals sent out when danger is "detected". The activated antigen presenting cells are able to provide the necessary co-stimulatory signal to the T helper cells that subsequently control the adaptive immune response. The danger signals are emitted by ordinary cells of the body that have been injured due to an attack by a pathogen. The main objective of the danger theory based system (DTBS) is to reduce false positive and negative errors and maintain high detection accuracy of the model.

Dendritic cell algorithm

In the danger theory, danger is measured by damage to cells indicated by distress signals sent out when cells die from unnatural causes (Aickelin & Cayzer, 2002, pp.141-148). The signals are detected by dendritic cells (DCs) that have three modes of operation: immature, semi-mature, and mature. In the immature state, a DC collects an antigen along with safe and danger signals from its local environment. DCs are able to integrate these signals to decide whether the environment is safe or dangerous. If safe, a DC becomes semi-mature and, upon presenting an antigen to T-cells, the DC causes T cell tolerance. If dangerous, the DC becomes mature and causes the T cell to become reactive on antigen-presentation. The DC algorithm (DCA) introduces the notion of danger signals as well as safe and pathogen-associated signals which all contribute to the context of a data signal at any given time.

Applications of AISs

Malicious attacks, hardware failure, or human errors can be considered anomalies. Detection of anomalies is based on irregularities in the pattern with respect to the normal pattern. Anomaly detection creates a model of normal behavior of the system and then looks for activities that differ from the created model. The main idea is to learn from examples of one class and generate the detectors of deviations. The HIS, by its nature, does not perform optimization. There are various optimization algorithms such as CLONALG, opt-aiNet, and B-cell algorithm, which are all based on the clonal selection principles. All the approaches use cloning, mutation, and selection to build a population of solutions. The earliest AIS algorithm for unsupervised clustering was aiNet, proposed by De Castro and van Zuben (2001).

AIS-based intrusion detection systems

Intrusion detection systems (IDSs) monitor computer network traffic in order to detect malice or anomalies. IDSs can be either network-based or host-based. The network-based IDS (NIDS) scans network packets at audits packet information and logs suspicious packets into the log file. The host-based IDS (HIDS) monitors information collected from individual computer systems. There are two basic advantages of an AIS over an IDS: 1) it provides passively proactive protection via negative detection, and 2) it is capable of adapting to dynamically changing environment.

Performances of the models

Performances of the models are often measured based on: true positive (*TP*), true negative (*TN*), false positive (*FP*), and false negative (*FN*), where *TP* represents the number of positive samples correctly classified as positive, *TN* represents correctly classified negatives as negative, *FN* represents the number of positive samples wrongly classified as negative, and *FP* represents the number of negative samples wrongly classified as positive. The key criterion which differentiates classifiers is prediction accuracy (*ACC*), which represents the ratio of the number of instances correctly classified to the total number of instances (Eq. 1).

$$ACC = \frac{TP + TN}{TP + TN + FP + FN}, \tag{1}$$

Researchers often use other measures such as the false positive rate (*FPR*) that is defined as the probability that a false alarm will be raised (Eq. 2),

$$FPR = \frac{FP}{TN + FP}. \quad (2)$$

or the false negative rate (*FNR*) which is the probability that a TP will be missed by the classifier (Protic, 2020, pp.603-605) (Eq. 3).

$$FNR = \frac{FN}{TP + FN} \quad (3)$$

Detection of a specific attack

Once an attack has been discovered, the signature of the attack is stored in the black-list used to check against the normal network traffic and to detect if an attack has happened. Newly discovered attacks are added to the dataset of known attacks. The disadvantages of misuse detection are dependence on the size and the efficiency of the black-list, and vulnerability to a zero-day attack. Publicly available datasets often used for the known attack detection are the KDD Cup '99 and the NSL-KDD dataset. The KDD Cup '99 dataset is collected by simulation of the operation of a typical US Air Force Local Area Network with attacks classified into four categories: 1) probe, 2) denial of service (DoS), 3) user to root (U2R), and 4) remote to local (R2L). The dataset contains 41 features which fall into the following categories: 1) basic, 2) traffic, 3) content, 4) host-related attack, and 5) normal behavior (Aggarwal & Sharma, 2015, pp.842-851). On the other hand, the KDD Cup '99 dataset contains redundant and duplicate records which prevent classifying the other records. To fix these issues, Tavallaee et al (2009) proposed the NSL-KDD dataset that consists of selected features from the KDD Cup'99 dataset excluding redundant records in the training set and duplicates in the test set (Protic, 2018, pp.585-586).

Many authors presented various results on the specific attack recognition. Al-Dabagh & Ali (2011, pp.381-390) presented the dendritic cell algorithm for the detection of DoS in the real time. Flow-based DoS detection schemes for high speed networks have been proposed by Wang et al (2012, pp.646-650) as an effective supplement to payload-based solutions. The existing flow-based solutions had serious limitations in detecting unknown attacks and efficiently identifying real attack flows buried into the background traffic, and had difficulty to adapt to attack dynamics. To address these issues, the authors proposed a flow-based DoS detection scheme based on Neighborhood Negative Selection (NNS) as the detection algorithm for unknown DoS attacks, and identified attack flows from massive traffic.

Anomaly detection

NIDSs are deployed at the computer network level and work by tracking network traffic. The aim of such systems is to detect if there was an attack or not. If an attack is detected, NIDSs rise an alert and create/respond to the log of attack (depending on the NIDS configuration). The anomaly-based NIDSs are deployed in the most critical parts of the computer network and learn from the network behavior. The longer the IDS is in the network, the more effective it will be. Any deviation from the normal traffic is considered an anomaly. The threshold level configured in the anomaly-based IDS will dictate the detection of anomalies. The main issue of such IDSs is a high level of FP. For that reason, the system has to be configured not to become insensitive to such alarms.

For the purpose of anomaly detection, the Kyoto 2006+ dataset is often used in experiments. It is built on real network traffic collected from 2006 to 2015 on five different computer networks inside and outside the Kyoto University. The records consist of 14 statistical features derived from the KDD Cup '99 dataset and 10 additional features which can be used for further analyses of systems. During the observation period, ~50 million sessions of normal traffic and ~43 million sessions of attacks and ~425 thousands sessions of unknown attacks were recorded.

One of the results on anomaly detection presented in this paper is based on NSA and the NSL-KDD dataset. The IDS proposed by Kumarvel (2016) that is based on the algorithm Elberfeld and Textor (2011, pp.534-542) shows lesser FP, lesser computational overhead and higher detection rates if compared with the literature. A Java application has four modules: 1) input (captures traffic from the input); two types of files are to be fed into the input module – the self file is used for training and generation of the detector set while the test file uses a packet of normal traffic that is to be monitored, 2) the network converter converts the data into binary strings, 3) the negative selection module generates detectors, and 4) classification. The Hamming distance, r-contiguous matching, and r-chunk matching are used to compute affinity (Kumarvel, 2016, pp.23-31). The testing of the IDS was based on the false alarm rates, the Receiver Operating Characteristics (ROC) analysis and the testing environment. Another example of anomaly detection based on NSA is proposed by Shen (2012, pp.18-48). The scheme consists of two weighted feature selection algorithms based on the Rough Set Algorithm (RSA) and Linear Genetic Programming (LGP). Weighting the contribution of the parameters in the IDS improved the performance of the algorithms. The results indicate that the proposed scheme outperforms most of the existing IDS on the same testing data set.

The aim of the research conducted by Murad & Mohd. Aizani, (2012, pp.147-154) was to address the impact of the feature reduction in designing an anomaly detection system based on the immune network theory to detect novel attacks. The results on anomaly detection show that the detection rate ranges from 80.25% to 82.25%, while the FPR ranges from 0.1975 to 0.1775.

AIS vs. machine learning

AIS and machine learning (ML) - based IDSs have advantages and disadvantages one over the other. AIS algorithms are easy to be used in classification (supervised learning) or clustering (unsupervised learning). The methods used in the AIS design include: 1) generation of antibodies, 2) diversity, 3) distributed systems, 4) dynamic systems, 5) self-organizing memory, and 6) noise/error tolerance. However, there are several issues that can occur during the evaluation of models, so several questions have to be answered: *How to determine antigens, antibodies and B cells?, How to define memory cells?, How to determine the similarity between an antigen and an antibody?, and What are the basic calculations in the AIS models?* It is obvious that both supervised and unsupervised learning can be used to develop AIS-based IDSs. The CLONALG and Hypermutation are instance-based models. Negative and positive selection algorithms are algorithms with regularization (positive selection) and clustering algorithms (negative selection). Immune networks are algorithms with regression or with associated rules. The danger theory is based on the decision tree, or the associated rules algorithms. Dendritic cell algorithms work in the similar way to the danger theory algorithms but the tolerance to the signal indicating danger has to be properly set.

The experiments presented in this paper are conducted to four data sets from the Kyoto 2006+ dataset. Each dataset consists of different number of instances (158572, 129651, 128740 and 136625). Of all instances, 70% were used for training and 30% were used for testing the models. Of 24 features from the Kyoto 2006+ dataset, nine features are used for classifiers': Flag, IDS_detection, Count, Same_srv_rate, Serror_rate, Srv_serror_rate, Dst_host_count, Dst_host_srv_count, Dst_host_same_src_port_rate, and Dst_host_serror_rate. The Label feature indicated whether the session was an attack or not. Features are chosen based on expert knowledge and the pre-processing algorithm which cuts all categorical features, removes statistical features, cuts all features which can be used for further analyses, cuts all features that cannot be normalized into the range [-1,1] and normalizes the remaining instances into the range [-1,1] by applying the tangent hyperbolic function (Protić & Stanković, 2018, p.43).

Four ML models are used for the binary classifications: the Decision tree (DT) (Sebastiani, 2012, p.13), the support vector machine (SVM) (Burges, 1998, p.291), the k-Nearest Neighbor (k-NN), and the weighted k-NN (wk-NN) (Hechenbichler & Schilep, 2004). The results show high accuracy for the k-NN and the wk-NN, followed by the DT and the SVM. The fastest model is the DT. The processing time (sum of training and testing time) is more than 100 times shorter than the processing time for all the other models (Table 1).

Table 1 – Accuracy and processing time
Таблица 1 – Точность и время обработки
Табела 1 – Тачност и време обраде

No	Size	Model	Accuracy	Processing time
1	158572	k-NN	98.3%	275.72s
		wk-NN	98.4%	277.32s
		SVM	98.1%	449.35s
		DT	97.2%	3.8452s
2	129651	k-NN	91.8%	175.84s
		wk-NN	91.8%	173.32s
		SVM	98.3%	254.32s
		DT	97.3%	3.3104s
3	128740	k-NN	98.2%	193.82s
		wk-NN	98.1%	194.81s
		SVM	97.8%	280.82s
		DT	97.2%	3.3033s
4	136625	k-NN	99.3%	194.83s
		wk-NN	99.4%	194.23s
		SVM	99.1%	217.32s
		DT	98.3%	8.3169s

As it can be seen, the wk-NN has the highest accuracy (up to 99.5%), while the accuracies of both k-NN and DT classifiers are much higher than the accuracy of the SVM. A significantly shorter processing time of the DT model is due to the Iterative Dichotomy 3 algorithm. The results point to the given pros and cons of the models. Eager ML models are very accurate but the training and testing time can be very long. This is not the characteristic that suits the real-time for detection of the attack such as DoS or Distributed DoS (DDoS). On the other hand, DT models are very fast but their accuracy is significantly low and corresponds to the accuracy of the IDS based on the immune network theory. NSAs are highly accurate but the processing time of these algorithms can be significantly slow if the number of the detectors is high and the threshold is not set well. Also, NSAs are mostly used in anomaly detection. ML models based on the SVM showed better results in the detection of U2R and R2L attacks. The results also showed that

the accuracy of the models trained and tested on the real data flow is higher than the accuracies of the model trained on the simulated data.

Conclusions

Artificial immune systems are accurate and fast computational models inspired by the human immune system. They are often used in intrusion detection. There are two trends in intrusion detection: signature and anomaly detection. The basic concepts of AIS are negative selection, positive selection, clonal selection, immune networks, danger theory, and dendritic cell algorithm. IDSs based on the AIS are often compared to IDSs based on ML. Experiments on different datasets show that the models can be used in both known attack and anomaly detection. Eager ML classifiers show better results in the decision, which is an advantage if processing time is not significant. Dendritic cell algorithms and negative selection algorithms show better results for real-time detection.

References

Aggarwal, P. & Sharma, S.K. 2015. Analysis of KDD Dataset Attributes –Class Wise for Intrusions Detection. *Procedia Computer Science*, 57, pp.842-851. Available at: https://doi.org/10.1016/j.procs.2015.07.490.

Aickelin, U. & Cayzer, S. 2002. The Danger Theory and Its Application to Artificial Immune Systems. In: *CARIS 2002: 1st International Conference on Artificial Immune Systems,* University of Kent at Canterbury, UK, pp.141-148, September 9-11. Available at: http://dx.doi.org/10.2139/ssrn.2832054.

Aickelin, U. & Dasgupta, D. 2005. Artificial Immune Systems. In: Burke, E. & Kendal, G. (Eds.) *Introductory Tutorials in Optimization, Decision Support and Search Methodology* [e-book section] Alphen aan den Rijn: Kluwer. Available at: http://eprints.nottingham.ac.uk/336/1/05intros_ais_tutorial.pdf [Accessed: 10 August 2020].

Al-Dabagh, N.B.I & Ali, I.A. 2011. Design and implementation of artificial immune system for detecting flooding attacks. In: *International Conference on High Performance Computing & Simulation (HPCS)*, Istanbul, pp.381-390, July 4-8. Available at: https://doi.org/10.1109/HPCSim.2011.5999850.

Burges, M. 1998. Computer Immunology. In: *Proceedings of the 12th Systems Administration Conference (LISA '98)*. Boston, MA, USA, pp.283-298, December 6-11 [online]. Avialble at: https://www.usenix.org/legacy/event/lisa98/full_papers/burgess/burgess_html/burgess.html [Accessed: 10 August 2020].

Burnet, F.M. 1959. *The clonal selection theory of acquired immunity.* Nashville, Tennessee, USA: Vanderbilt University Press. Available at: https://doi.org/10.5962/bhl.title.8281.

De Castro, L.N. & Timmis, J. 2002a. An artificial immune network for multimodal function optimization. In: *Proceedings of the 2002 Congress on Evolutionary Computation. CEC'02 (Cat. No.02TH8600),* Honolulu, HI, USA, pp.669-674, May 12-17. Available at: https://doi.org/10.1109/CEC.2002.1007011.

De Castro, L.N. & Timmis, J. 2002b. *Artificial Immune Systems: A New Computational Intelligence Approach.* London: Springer-Verlag Publishing. ISBN: 978-1-85233-594-6.

De Castro, L.N. & Von Zuben, F.J. 1999. Artificial Immune Systems: Part I – Basic Theory and Applications. *Technical Report TR - DCA 01/99,* pp.1-95.

De Castro, L.N. & Von Zuben, F.J. 2001. aiNet: An Artificial Immune Network for Data Analysis. In: Abbas, H.A., Sarker, R.A. & Newton, C. (Eds.) *Data Mining: A Heuristic Approach.* USA: Idea Group Publishing [online]. Available at: http://www.dca.fee.unicamp.br/~vonzuben/research/lnunes_dout/artigos/DMHA.PDF [Accessed: 10 August 2020].

De Castro, L.N. & Von Zuben, F.J. 2002. Learning and optimization using the clonal selection principle. *IEEE Transactions on Evolutionary Computation,* 6(3), pp.239-251. Available at: https://doi.org/10.1109/TEVC.2002.1011539.

Elberfeld, M. & Textor, J. 2011. Negative selection algorithms on strings with efficient training and linear-time classification. *Theoretical Computer Science*, 412(6), pp.534-542. Available at: https://doi.org/10.1016/j.tcs.2010.09.022.

Forrest, S., Perelson, A.S., Allen, L. & Cherukuri, R. 1994. Self-nonself discrimination in a computer. In: *Proceedings of 1994 IEEE Computer Society Symposium on Research in Security and Privacy,* Oakland, CA, pp.202-212, May 16-18. Available at: https://doi.org/10.1109/RISP.1994.296580.

Haag, C.R., Lamont, G.B., Williams, P.D. & Peterson, G.L. 2007. An artificial immune system-inspired multiobjective evolutionary algorithm with application to the detection of distributed computer network intrusions. In: *GECCO '07: Proceedings of the 9th annual conference companion on Genetic and evolutionary computation,* London, UK, pp.2717-2724, July. Available at: https://doi.org/10.1145/1274000.1274035.

Hechenbichler, K. & Schilep, K. 2004. Weighted k-Nearest Neighbor Techniques and Ordinal Classification. *Sonderforschungsbereich 386*, Paper 399, pp.1-16 [online]. Available at: https://epub.ub.uni-muenchen.de/1769/1/paper_399.pdf [Accessed: 10 August 2020].

Jerne, N.K. 1974. Towards a Network Theory of Immune System. *Ann Immunol (Paris),* 125C(1-2), pp.373-389. PMID: 4142565.

Ji, Z. & Dasgupta, D. 2007. Revisiting Negative Selection Algorithms. *Evolutionary Computation,* 15(2), pp.223-251. Available at: https://doi.org/10.1162/evco.2007.15.2.223.

Matzinger, P. 1994. Tolerance, danger, and the extended family. *Annual Review of Immunology,* 12, pp.991-1045. Available at: https://doi.org/10.1146/annurev.iy.12.040194.005015.

Murad, A.R. & Mohd. Aizani, M. 2012. Artificial Immune network Clustering Approach for Anomaly Intrusion Detection. *Journal of Advances in Information Technology,* 3(3), pp.147-154. Available at: https://doi.org/10.4304/jait.3.3.147-154.

Protić, D.D. 2018. Review of KDD CUP '99, NSL-KDD and KYOTO 2006+ Datasets. *Vojnotehnički glasnik/Military Technical Courier*, 66(3), pp.580-596. Available at: https://doi.org/10.5937/vojtehg66-16670.

Protić, D.D. 2020. Influence of preprocessing on anomaly-based intrusion detection. *Vojnotehnički glasnik/Military Technical Courier,* 68(3), pp.598-611. Available at: https://doi.org/10.5937/vojtehg68-27319.

Protić, D. & Stanković, M. 2018. Anomaly-Based Intrusion Detection: Feature Selection and Normalization Influence to the Machine Learning Models Accuracy. *European Journal of Formal Sciences and Engineering*, 2(3), pp.101-106. Available at: http://dx.doi.org/10.26417/ejef.v2i3.p101-106.

Sebastiani, F. 2002. Machine learning in automated text categorization. *ACM Computing Surveys,* 34(1), pp.1-47. Available at: https://doi.org/10.1145/505282.505283.

Shen, J. 2012. *Network intrusion detection by artificial immune system.* MA thesis. Melbourne, Australia: RMIT University - School of Engineering [online]. Available at: https://researchrepository.rmit.edu.au/discovery/fulldisplay?docid=alma9921863885901341&context=L&vid=61RMIT_INST:ResearchRepository&lang=en&search_scope=Research&adaptor=Local%20Search%20Engine&tab=Research&query=any,contains,Shen,%20J.%202012.%20Network%20Intrusion%20Detection%20By%20Artificial%20Immune%20System.&offset=0 [Accessed: 10 August 2020].

Sri Lakshmi, K. 2014. Implementation of Artificial Immune System Algorithms. *International Journal of Application or Innovation in Engineering and Management (IJAIEM),* 3(6), pp.367-372. Available at: https://www.ijaiem.org/Volume3Issue6/IJAIEM-2014-07-01-90.pdf.

Tavallaee, M., Bagheri, E., Lu, W. & Ghorbani, A.A. 2009. A detailed analysis of the KDD CUP 99 data set. In: *2009 IEEE Symposium on Computational Intelligence for Security and Defense Applications,* Ottawa, ON, Canada, July 8-10. Available at: https://doi.org/10.1109/CISDA.2009.5356528.

Timmis, J., Hone A., Stibor, T. & Clark, E. 2008. Theoretical advances in artificial immune systems. *Theoretical Computer Science,* 403(1), pp.11-32. Available at: https://doi.org/10.1016/j.tcs.2008.02.011.

Timmis, J. & Neal, M. 2001. A resource limited artificial immune system for data analysis. *Knowledge-Based Systems*, 14(3-4), pp.121-130. Available at: https://doi.org/10.1016/S0950-7051(01)00088-0.

Wang, D., He, L., Xue, Y. & Dong, Y. 2012. Exploiting Artificial Immune systems to detect unknown DoS attacks in real-time. In: *2012 IEEE 2nd International Conference on Cloud Computing and Intelligence Systems*, Hangzhou, China, pp.646-650, October 30 - November 1. Available at: https://doi.org/10.1109/CCIS.2012.6664254.

ОБНАРУЖЕНИЕ ВТОРЖЕНИЙ, ОСНОВАННОЕ НА ИСКУССТВЕННОЙ ИММУННОЙ СИСТЕМЕ

Даниела Д. Протич

Вооруженные силы Республики Сербия, Генеральный штаб,
Управление информатики и телекоммуникаций (J-6),
Центр прикладной математики и электроники,
г. Белград, Республика Сербия

РУБРИКА ГРНТИ: 20.00.00 ИНФОРМАТИКА:
20.15.05 Информационные службы, сети, системы в целом
ВИД СТАТЬИ: оригинальная научная статья

Резюме:

Введение/цель: Искусственная иммунная система − это вычислительная модель, вдохновленная биологической или человеческой иммунной системой, которая защищает организм от патогенов и различает собственные клетки от инородных. Особо интересным в искусственной иммунной системе является то, как человеческий организм реагирует на новые патогены и как он адаптируется, становясь невосприимчивым в течение длительного периода после борьбы с заболеванием, что относится к распознаванию уже известной атаки, и способу, которым иммунная система идентифицирует собственные клетки, на которые не реагирует и как обнаруживает аномалии.

Методы: В исследовании применялись следующие методы: отрицательный отбор, положительный отбор, клональный отбор, иммунные сети, теория опасности и алгоритм дендритных клеток.

Результаты: Представлены различные алгоритмы и модели, относящиеся к искусственным иммунным системам, и два принципа классификации: один основан на обнаружении конкретной атаки, а другой − на обнаружении аномалии.

Выводы: Искусственные иммунные системы часто используются для обнаружения вторжений в компьютерные сети, потому что они точные и быстрые. Эксперименты с различными наборами данных показывают, что модели можно использовать как для обнаружения атак, так и для обнаружения аномалий. Классификаторы на основе машинного обучения показывают лучшие результаты при принятии решений, что является большим преимуществом, если время обработки не является значимым параметром. Алгоритмы дендритных клеток и алгоритмы отрицательного отбора показывают лучшие результаты для обнаружения в реальном времени.

Ключевые слова: искусственная иммунная система, обнаружение вторжений.

ДЕТЕКЦИЈА НАПАДА ЗАСНОВАНА НА ВЕШТАЧКОМ ИМУНОМ СИСТЕМУ

Данијела Д. Протић

Војска Србије, Генералштаб, Управа за телекомуникације и информатику (J-6), Центар за примењену математику и електронику,
Београд, Република Србија

ОБЛАСТ: рачунарске науке, информационе технологије
ВРСТА ЧЛАНКА: оригинални научни рад

Сажетак:

Увод/циљ: Вештачки имуни систем (ВИС) инспирисан је биолошким имунолошким системом који разликује сопствене ћелије од оних које то нису. За ВИС је занимљив начин на који тело реагује на патогене и прилагођава се да остане имуно дужи период. То се односи на препознавање познатог напада и начин на који имуни систем идентификује сопствене ћелије на које не треба да реагује, и на откривање аномалије.

Методе: Приказане су методе негативне и позитивне селекције, затим клонирање, имуне мреже, теорија опасности и алгоритам дендритичних ћелија.

Резултати: Представљени су модели који се односе на ВИС и два принципа класификације – један заснован на детекцији одређеног напада, а други на детекцији аномалије.

Закључак: Вештачки имуни системи користе се у откривању упада у рачунарске мреже јер су тачни и брзи. Експерименти на различитим скуповима података показују да се модели могу користити у откривању напада или аномалија. Класификатори засновани на машинском учењу показују боље резултате у одлуци, што је велика предност ако време обраде није значајан параметар. Алгоритми дендритичких ћелија и алгоритми негативног одабира показују боље резултате за детекцију у реалном времену.

Кључне речи: вештачки имуни систем, детекција упада.

Paper received on / Дата получения работы / Датум пријема чланка: 10.08.2020.
Manuscript corrections submitted on / Дата получения исправленной версии работы / Датум достављања исправки рукописа: 10.10.2020.
Paper accepted for publishing on / Дата окончательного согласования работы / Датум коначног прихватања чланка за објављивање: 12.10.2020.

EXPLOSION OF THE BOUNDARY LAYER UPON ENTRY OF SPACECRAFT INTO DENSE LAYERS OF THE EARTH'S ATMOSPHERE

Leonid I. Gretchikhin
Belarusian State Academy of Communications,
Minsk, Republic of Belarus,
e-mail: gretchihin@yandex.ru,
ORCIDiD: https://orcid.org/0000-0002-5358-9037

DOI: 10.5937/vojtehg68-28605; https://doi.org/10.5937/vojtehg68-28605

FIELD: Mechanical engineering, Aerodynamics
ARTICLE TYPE: Original scientific paper

Abstract:

Introduction/purpose: A supersonic flow around a sphere with a radius of 1m at altitudes of 80 to 40 km was analysed.

Methods: The descent trajectory at the first cosmic velocity, similar to that of the Soyuz spacecraft with a duralumin structure without thermal protection, was taken into consideration.

Results: For the gas between the shock wave front and the surface of the descending spacecraft, data were obtained on the increase in density, pressure, and temperature behind the shock wave front as well as the shift of the shock wave from the surface of the descending spacecraft. The effective temperature of the shock-heated gas reaches its maximum value of 7340 K at an altitude of 60 km. At altitudes of 80 and 40 km, the effective temperature is 7000 K and 6400 K, respectively. Based on the obtained data on the thermodynamic state of the gas behind the shock wave every 10 km, calculations were made of energy fluxes to the surface of the spacecraft for convective and radiative heat transfer, as well as for the impact of electrons produced due to ionization of negative ions. Radiative heat transfer has proven to be the most significant.The burning mechanism of negative ions of triatomic molecules of aluminium with the formation of AlO molecules was determined, and data on pressure rise in the boundary layer on the spacecraft surface were obtained. At all considered altitudes, the pressure rises instantly: to 1.06×10^{10} Pa at an altitude of 80 km, 5.3×10^{9} Pa at an altitude of 60 km, and reaches the maximum value of 5.5×10^{10} Pa and an altitude of 40 km. A pressure of 10^{9} to 10^{10} Pa arises during explosion of various explosives. The energy flux reaches the spacecraft surface between explosions. At the moment of explosion, shock waves develop in the atmosphere surrounding the surface of the descending spacecraft, and compressive waves

develop in the entire structure of the spacecraft. The descending spacecraft cracks, and its entire structure breaks down into parts. The area of interaction increases sharply, and each subsequent explosion has a greater intensity and size. As a result, the last most intense explosion occurs at an altitude of approx. 40 km, after which individual fragments of the spacecraft fall to Earth.

Conclusion: The exploration of space with flight to other planets is possible only after a thorough study of explosive processes taking place on the surface of the spacecraft descending on other planets, and especially on Earth.

Keywords: explosion of explosives, supersonic motion, convective heat transfer, radiative heat transfer, electron flux effects, negative ions.

Introduction

During the exploration of space, there was a problem of retrieving spacecraft reentering the Earth's atmosphere at the first and, especially, the second cosmic velocity. The nature of the flow around flying objects at different altitudes is well defined. At very high altitudes starting from approx. 120 km and above, the flow around moving bodies corresponds to the free-molecular regime (Gretchikhin, 1986), (Gretchikhin, 2003). At altitudes below 120 km and up to approx. 100km, the transition flow regime takes place. Starting from altitudes below 100 km, the continual flow regime (i.e. the supersonic flight) takes place. In this flight regime, strong shock waves are formed with a sharp increase in high-temperature gas on the spacecraft surface, causing a noticeable heating of the surface of the descending spacecraft. Previously, it was assumed that heating of the surface occurs due to intense convective and radiative heat transfer.

Various heat-barrier materials were used to protect descending spacecraft from the effects of the emerging heat fluxes. For the first cosmic velocity, pyrolytic graphite with a thickness up to 5 cm was used in the front hemisphere.[1)] It was assumed that the temperature of the shock-compressed gas does not exceed 3500–4000 K. The burning behaviour of the thermal-protective coating at such temperatures could be studied in laboratory conditions. These studies were carried out, and a full analysis of the results taking into account the emission of negative ions from the surface was performed (Gretchikhin, 1986).

[1)] This thickness was sufficient, since the thermal-protective coating burned out no more than 3 cm.

Gretchikhin, L., Explosion of the boundary layer upon entry of spacecraft into dense layers of the earth's atmosphere, pp.804-822

In the supersonic flow regime, a mixture of air heated by the shock wave with debris of the thermal-protective coating emerges between the shock wave and the surface of the descending spacecraft. The chemical reactions taking place in such a mixture were beyond our vision.

With the development of rocket technology, intensive exploration of space began. A spacecraft re-entering the Earth's atmosphere at the first cosmic velocity has a speed of approx. 7.5 km/s, and at the second cosmic velocity – approx. 11.2 km/s or greater. Such flight conditions lead to the emergence of strong shock waves. The air behind the shock wave heats up to temperatures above 4000 K. The burning behaviour of the thermal-protective coating under such conditions remained unclear. The burning behaviour of the thermal-protective coating is even more complex when a spacecraft enters dense atmospheric layers at the second or greater cosmic velocity. In this case, the destruction of the thermal-protective coating will be more intense. How can a descending spacecraft be safely retrieved under such conditions? The temperature increases significantly in the emerging shock wave. Intense convective and radiative heat transfers occur. Without taking into account the effects of negative ions, the performed theoretical calculation has allowed to establish that the thickness of the burn-out of the thermal-protective coating during the continuous movement of the burning front can be approx. 2 cm. This result was shocking. Then the effects of negative ions had to be taken into account.

Ionization of negative ions produces an intense flux of electrons to the surface of the thermal-protective coating, and in combination with the radiative and convective heat flux, such a net energy flux is formed that an explosion of the surface layer occurs. At this moment, heat stops coming to the surface of the spacecraft. Specific evaluations showed that the thermal-protective coating at the second cosmic velocity should burn less when compared to the first cosmic velocity. After a circumlunar flight followed by the descent of the spacecraft at the second cosmic velocity, the thickness of the burned-out thermal-protective coating turned out to be approx. 2 cm, i.e. less than at the first cosmic velocity with a burn-out thickness of approx. 3 cm.

At the second cosmic velocity, heat-barrier materials do not burncontinuously, but with separate explosive pulses, which was proven demonstratively during the first studies of the effect of laser radiation (Gretchikhin&Minko, 1967) as well as with arc and spark discharge

cathode flares (Gretchikhin&Minko, 1967) and (Gretchikhin&Tyunina, 1967). The results of these studies are shown in Fig. 1.

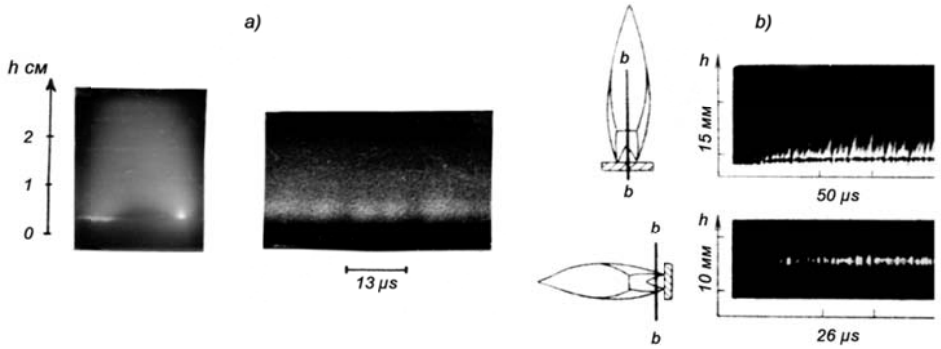

Figure 1 – Destruction pattern: a) electric arc discharge between carbon electrodes and explosive processes at the cathode at a power of $1.3 \cdot 10^9$ W/m^2; b) explosive processes during exposure of laser radiation with a power of $5 \cdot 10^{11}$ W/m^2 on: copper (top) and aluminium (bottom)

Рис. 1 – Схема разрушения: а) дуговой разряд между угольными электродами и взрывные процессы на катоде мощностью $1.3 \cdot 10^9$ W/m^2; б) взрывные процессы при воздействии лазерного излучения мощностью $5 \cdot 10^{11}$ W/m^2: медь (сверху) и алюминий (снизу)

Слика 1 – Образац деструкције: а) пражњење електричног лука између електрода угљеника и експлозивни процеси на катоди при снази $1{,}3 \times 10^9$ W/m^2; б) експлозивни процеси током излагања ласерском зрачењу снаге 5×10^{11} W/m^2 у бакру (горе) и алуминијуму (доле)

Experimental results indicate that the destruction of a solid at energy fluxes greater than 10^9 W/m^2 occurs in the form of successive explosions. The frequency of explosions at the cathode in the arc discharge between carbon electrodes is approx. 150 kHz with an energy flux of $1.3 \cdot 10^9$ W/m^2 (Gretchikhin&Tyunina, 1967), and approx. 290kHz when aluminium is exposed to laser radiation with an effective absorbed energy flux of $4.2 \cdot 10^{10}$ W/m^2 (Gretchikhin&Minko, 1967).

Thus, the gaseous products of destruction of the surface layer of the descending spacecraft mix with the ambient environment and react with air molecules. Depending on the type of the chemical reaction (endothermic or exothermic), additional cooling or heating of the heated air behind the shock wave takes place in the frontal part of the spacecraft. Exothermic reactions with the release of energy are

Gretchikhin, L., Explosion of the boundary layer upon entry of spacecraft into dense layers of the earth's atmosphere, pp.804-822

especially dangerous. Therefore, let us have a closer look at the dynamics of the destruction of the surface of the descending spacecraft determining the number of atoms and molecules that mix with the heated air behind the shock wave, and how much energy is released in various exothermic reactions. This posed the task of finding out what energy is absorbed by a moving object and how this affects the flight dynamics of the descending spacecraft. It is important to determine what processes occur in the shock-compressed gas area in the frontal part of space objects descending at the first and especially at the second cosmic velocity. In this work, we will consider in detail a spacecraft without thermal-protective coating descending at the first cosmic velocity[2)]. In order to achieve this objective, the following tasks must be solved:

♦ Determining the heating dynamics of the shock-compressed gas and the effective temperature of atoms and molecules in the area between the shock wave and the spacecraft surface at altitudes of 40 to 80km, where strong shock waves are formed,

♦ Developing an impact theory of convective heat transfer,

♦ Considering the structure of the exposed surface in radiative heat transfer,

♦ Developing a theory of energy transfer by electrons produced due to the ionization of negative ions, and

♦ Performing an analysis of the explosive processes taking place when various space objects enter dense layers of the Earth's atmosphere.

Now, let us consider these objectives one by one.

Effective temperature of the air compressed by the shock wave

When a spacecraft descends from the orbit, a shock wave begins to form at an altitude of approx. 100 km. As the altitude decreases, the speed increases slightly, and then drops sharply from an altitude of 40 km. The change in flight speed with altitude for a descending Soyuz series spacecraft is given in Table 1.

[2)] These conditions correspond to the re-entry conditions of the long-term orbital station MIR-1.

Table 1 – Parameters of the air behind the shock wave at the first cosmic velocity
Таблица 1 – Параметры воздуха за ударной волной при первой космической скорости
Табела 1 – Параметри ваздуха иза ударног таласа при првој космичкој брзини

Parameters	Altitude, km				
	40	50	60	70	80
First cosmic velocity, *Mach*	22.35	23.82	25.34	25.80	26.42
Density, ρ / ρ_∞	5.940	5.947	5.954	5.955	5.957
Pressure, P / P_∞	584	663	750.1	777.6	815
Shock wave shift distance, *m*	0.112	0.112	0.1119	0.1118	0.1118
Temperature at the wave front, *K*	25 746	27 532	29 357	28 595	28 057
Temperature of the shock-compressed gas, *K*	6437	6883	7339	7149	7014
Effective temperature of the compressed gas, *K*	6434	6880	7337	7146	7012
Convective heat transfer, W/m^2	$2.01\ 10^7$	$5.48\ 10^6$	$2.24\ 10^6$	$3.85\ 10^5$	$5.57\ 10^4$
Penetration depth, *m*	$7.51 \cdot 10^{-2}$	$1.98 \cdot 10^{-2}$	$7.81 \cdot 10^{-3}$	$1.36 \cdot 10^{-3}$	$2.00 \cdot 10^{-4}$
Radiative heat transfer, W/m^2	$4.86\ 10^6$	$6.35\ 10^6$	$8.21\ 10^6$	$7.39\ 10^6$	$6.85 \cdot 10^6$
Electron flux heat transfer, W/m^2	$2.56 \cdot 10^7$	$6.98\ 10^6$	$2.85\ 10^6$	$4.90\ 10^5$	$7.09 \cdot 10^4$
Pressure in the boundary layer, *Pa*	$5.485 \cdot 10^{10}$	$1.62 \cdot 10^{10}$	$5.938 \cdot 10^9$	$7.088 \cdot 10^9$	$1.059 \cdot 10^{10}$
Energy released on the surface, *J*	$4.477 \cdot 10^6$	$1.092 \cdot 10^6$	$1.096 \cdot 10^5$	$1.367 \cdot 10^5$	$1.921 \cdot 10^5$

Flight speeds are much higher than the speed of sound. In this case, the density, pressure and temperature of the gas in the shock wave can be determined by the formulas (Gretchikhin et al, 2012).

$$\rho = \rho_\infty \left(\frac{\gamma-1}{\gamma+1} + \frac{2}{\gamma+1}\frac{1}{M^2}\right)^{-1}; \rho = \rho_\infty \left(1 + \frac{2\gamma}{\gamma+1} M^2\right); T = T_0 \frac{\rho_\infty}{\rho}\frac{P}{P_\infty} \qquad (1)$$

where γ is the ratio of the specific heat capacities of the gas at constant volume and constant pressure; and *M* is the Mach number. Specific calculations for a sphere with a radius of 1 m at different altitudes are given in Table 1. At all altitudes, the temperature directly in the front

of the shock wave is relatively high, comparable to high-power pulsed electric discharge. The shift distance of the shock wave from the nose of a hypersonic vehicle of a given geometry for a direct shock wave in the first approximation can be determined as follows: (Gretchikhin et al, 2012)

$$\Delta = R\frac{\rho_\infty}{\rho}\left(1-\frac{\rho_\infty}{\rho}+\sqrt{\frac{8}{3}\frac{\rho_\infty}{\rho}}\right)^{-1} \quad (2)$$

High temperature behind the direct shock wave causes significant heating of the air atmosphere. Diatomic molecules of nitrogen and oxygen dissociate instantly and completely. Since this requires energy, the temperature in the shock wave decreases.

The number of particles doubles. Also, the ionization of oxygen and nitrogen atoms takes place, which leads to a decrease in the adiabatic index. Taking into account the dissociation process, the temperature of the air behind the shock wave (Zeldovich&Raizer, 2008) and (Kheiz&Probstin, 1962) is:

$$T_B = T_0\frac{\rho_\infty}{\rho}\frac{P}{P_\infty}\alpha \quad (3)$$

At temperatures above 10,000 K, nitrogen and oxygen molecules will dissociate completely, and then $\alpha = 0.5$. As a result of ionization, the air temperature will decrease due to the formation of plasma. Then (Zeldovich&Raizer, 2008) and (Kheiz&Probstin, 1962)

$$T_{eff.} \approx \frac{T_B}{3-\gamma} \quad (4)$$

For dry air at a temperature of 2000 K, the adiabatic index is $\gamma = 1.088$.

For higher temperatures, we can assume that $\gamma \approx 1$.

The results of calculation according to (4) are shown in Table 1. The temperature of the shock-compressed gas is sufficiently high, and such a gas should be considered as plasma. Charged particles are produced in plasma as a result of the ionization of predominantly negative ions. Therefore, thermal energy is transferred to the surface of the descending spacecraft due to convective and radiative heat transfer, as well as due to the flow of electrons when passing through the electrical double layer.

The input data on the energies of dissociation of diatomic molecules, detachment of atoms in triatomic molecules and electron affinity for aluminium are given in Table 2.

Table 2 – Energy of dissociation and detachment of an electron in a negative aluminium ion
Таблица 2 – Энергия диссоциации и отрыва электрона в отрицательном ионе алюминия
Табела 2 – Енергија дисоцијације и одвајање електрона у негативном јону алуминијума

Atoms, molecules	Energy, eV	
	dissociation	Electron detachment
Al_3^-	~ 0.406	~ 1.785
Al_2^-	2.0	2.42
Al^- (3P)	-	0.44
Al^- (1D2)	-	0.33
AlO -	5.14	3.6
AlO_2^-	~ 2.51	4.1

The "~" symbol means that this value is obtained by extrapolation

Convective heat transfer

In convective heat transfer, energy is transferred by the collision of heated gas particles with the surface of the spacecraft. Each solid is formed by an intercluster lattice structure.

The clusters themselves are formed by diatomic or triatomic molecules.

The structure of clusters of diatomic molecules with experimental confirmation is reported in (Gretchikhin et al, 2015a) and (Gretchikhin, 2008), of triatomic molecules – in (Gretchikhin et al, 2015b) and (Gretchikhin, 2008).

Aluminium clusters are formed by triatomic molecules as shown in Fig. 2.

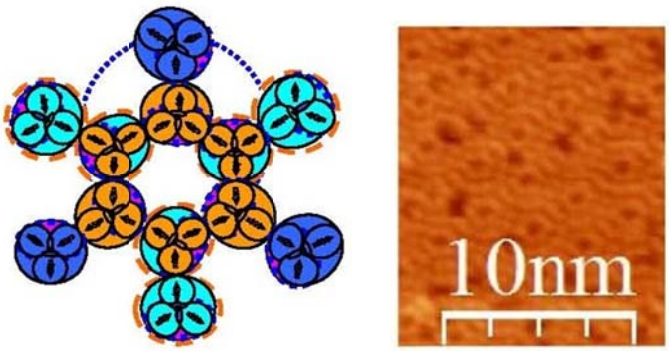

a) b)

Figure 2 – Cluster of triatomic molecules:
a) theoretical calculation; b) experimental confirmation
Рис. 2 – Кластер трехатомных молекул:
а) теоретический расчет; б) экспериментальное измерение
Слика 2 – Кластер триатомских молекула: а) теоријско израчунавање; б) експериментална потврда

The main cluster is highlighted in the center, and the highlighted triatomic molecules have broken bonds in diatomic molecules. As a result, some triatomic molecules in the center have an excess negative charge, and others – a positive charge. In Fig. 2, these molecules are shown in different colours. The clusters are flat and interact with each other by cohesion, and the solid resembles a layered cake. Clusters are formed as a result of the interaction of molecules of the first, second and third coordination layers (Gretchikhin et al, 2015b) and (Gretchikhin, 2008). The energy from the heated gas is transferred to the spacecraft surface by the collision of air molecules with the clusters of the solid. The thermal random velocity of the heated air

$$v_r = \sqrt{\frac{8k_bT_a}{\pi m_a}} \tag{5}$$

where k_b is the Boltzmann constant, T_a is the temperature of the shock-compressed air and m_a is the average weight of air molecules.

Only 1/6 of air molecules collide directly with the surface. Molecules collide with clusters of the solid. In convective heat transfer, only the surface layer of cluster formations is excited. Clusters of aluminium are formed by triatomic molecules, producing a face-centered crystalline structure. Since there is a hollow in the centre of a cluster, which does not receive the impacts of external particles, only 9/10 of the total flow of

external particles acting on the surface of the spacecraft is received. The second coordination layer of the cluster is destroyed before the melting temperature is reached, and the first coordination layer is destroyed after the melting temperature is reached. Near the boiling temperature, the number of molecules in a cluster is approx - 6 (Gretchikhin et al, 2015b). When air molecules collide with clusters on the surface of a solid, the energy transfer ratio is (Gretchikhin, 2008).

$$n = \frac{4m_a m_s}{(m_a+m_s)^2} \quad (6)$$

where m_b is the weight of a solid cluster, and m_S is the average effective mass of air molecules in the atomic form equal to approx. 29/2.

Taking into account (5) and (6), the convective energy flux to the solid surface is

$$J_c = \frac{9}{120}\rho v \frac{3}{T} n \quad (7)$$

where ρ is the density of the air behind the shock front.

The energy consumption of a single molecule of the solid:

$$E_m = \frac{10}{9} J_c \pi r_m^2 \quad (8)$$

The radius of a triatomic aluminium molecule $r_m \approx 2.155 r_a$, and r_a is the radius of an atom of the solid, obtained by the radiographic method, approx. 1.43Å. At each altitude, an aluminium object loses its weight to a depth

$$dh = 2r_a \frac{E_m}{E_{\text{св.}}} \quad (9)$$

where $E_{св.}$ is the molecular bond energy, which is determined by the boiling temperature. For aluminium, this value is $3.389 \cdot 10^{-20} J$. The results of the calculation of the depth of complete dissociation of the main clusters according to (13) are given in Table 1. It takes only ¾ of the total heat flux in convective heat transfer. The remaining part of the convective energy flux is absorbed by intercluster hollows preventing the destruction of the solid (see Fig. 2b).

As a result of destruction, the total number of triatomic aluminium molecules is formed as negative ions

$$N_{AI} = 2\pi r^2 dh \frac{\rho_{AI}}{m_b} \quad (10)$$

and the concentration of negative ions of triatomic aluminium molecules in the shock-compressed gas

$$n_{Al} = \frac{N_{AI}}{2\pi r^2 dh} \quad (11)$$

The temperature of the gas of triatomic aluminium molecules is equal to the boiling temperature, i.e. $T_{кип.}$ = 2770K.

Gretchikhin, L., Explosion of the boundary layer upon entry of spacecraft into dense layers of the earth's atmosphere, pp.804-822

The total number of air molecules in the shock-compressed air behind the shock wave

$$N_a = 2\pi r^2 dhp/m_a \quad (12)$$

and the molecules are at the temperature determined according to (4).

The average effective temperature will be

$$T_{eff.} = \left(\frac{T_{boiling}N_{Al}+T_0N_a}{N_{Al}+N_a}\right) \quad (13)$$

At this temperature, the following aluminium combustion reactions occur:

$$Al_3 + O \Leftrightarrow Al_2 + AlO + e + 1.134\ эВ;\ Al_2 + O \Leftrightarrow Al + AlO + 3.14\ эВ;$$
$$Al + O \Leftrightarrow AlO + 5.14\ эВ \quad (14)$$

The total energy released during the complete combustion of triatomic aluminium molecules is 9.41*4eV*, and the energy of the electron gas corresponds to the effective temperature of the plasma determined according to (13). The electron gas produced ionizes negative ions of aluminium molecules by electron impact:

$$Al_3 + e \Leftrightarrow Al_3 + 2e. \quad (15)$$

In this case, the temperature of the electron gas is (Gretchikhin, 1986)

$$T_e = 0.55 \cdot IA \cdot 11600K \quad (16)$$

where IA is the ionization energy of plasma particles in eV.

The electron gas produced from the ionization of negative ions is nonequilibrium. Consequently, the plasma of the shock-compressed gas at such temperatures of the electron gas and a sufficiently high temperature of the atomic gas has a very high radiation capacity, which is dangerous to eyesight. In this case, radiative heat transfer must be considered.

Radiative heat transfer

With a sufficiently dense plasma, the radiation of individual atoms and molecules from the inner layers is intensely absorbed inside the plasma, and thermal radiation can be considered as black body radiation, taking into account the emissivity factor. For evaluations, let us assume that the emissivity factor κ = 0.5. Then

$$J_L = K\sigma_S T_{эфф}^4 \quad (17)$$

where $\sigma_S = 5.67 \cdot 10^{-8}\ Bm \cdot M^{-2}K^{-4}$ is the Stefan constant.

The results of the obtained radiant energy fluxes at different altitudes are given in Table 1. The energy flux in radiative heat transfer penetrates through the solid to the skin layer depth. If the solid receives external radiation, then the thickness of the skin layer can be determined according to the formula (Gretchikhin, 2016):

$$\Delta r = \sqrt{\frac{\rho_э}{\pi f \mu}} \quad (18)$$

where f is the electromagnetic radiation frequency, μ is the magnetic permeability, and $\rho_э$ is the electrical conductivity of the solid.

In formula (18), the frequency of thermal radiation f corresponds to the maximum of the radiation flux density distribution function per unit frequency interval according to the Planck formula. Therefore, the obtained specific values of the absorption thickness are much smaller than the thickness of the aluminium cluster. This means that all incident radiation is completely reflected from an aluminium surface with a close-packed structure (Fig. 2*b*). The absorption of the radiant flux takes place at defects of the crystalline structure and the centres of cluster formations. For an ideal surface, absorption occurs only by the centres of cluster formations and is approximately 1/10, and as the surface transits to the liquid state, the ratio of the absorbed radiant flux energy increases, and the radiant flux contributes to the destruction of both a metal and a dielectric moving object.

With the emission of molecules with an electron affinity from the spacecraft surface, an electric double layer is formed. At some distance, negative ions are ionized, and the produced electrons, passing through the potential difference of the double electric layer, bombard the surface and additionally increase the energy flux to the spacecraft surface.

Electron impact energy flow

Negative ions from the aluminium surface are emitted in the form of triatomic molecules at the boiling temperature. The ionization of negative ions of aluminium molecules takes place due to the occurrence of reactions (14) and (15). Both reactions take place in the gas-vapour phase. As a result of the emission of negative ions from the aluminium surface, an electric double layer is formed. The potential difference in the electric double layer is determined by the molecular energy at the boiling temperature. For aluminium, the potential difference of the double layer

$$\Delta U = \frac{k_b T_{boiling}}{e} \cdot B \quad (19)$$

The flux of the energy carried by electrons to the aluminium surface will be

$$J_e = n_{Al}^{-} v_e k_b T_{boiling} \quad (20)$$

and the total energy transferred to the surface by electron impact will be

$$\Delta E_2 = J_e 2\pi r^2 dh. \quad (21)$$

The total energy to the metal surface of a solid entering dense atmospheric layers is the sum of convective, radiative and electronic heat transfer. The pressure that arises in the boundary layer is

$$P = \frac{\Delta E}{2\pi r^2 \, \Delta l} \quad (22)$$

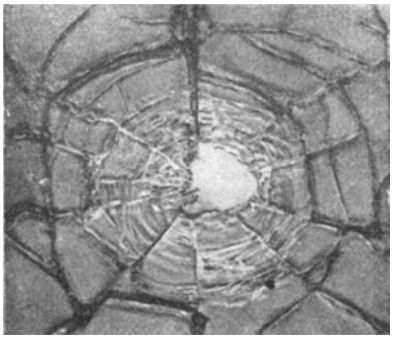

Figure 3 – Fracture pattern in a glass plate exposed to an explosion pressure of $2.8 \cdot 10^9$ Pa

Рис. 3 – Изображение разрушения стеклянной пластины под давлением взрыва $2.8 \cdot 10^9$ Pa

Слика 3 – Начин лома стаклене плоче изложене притиску експлозије од $2{,}8 \times 10^9$ Pa

The values of pressure arising in the boundary layer at different altitudes are given in Table 1. The obtained pressure values are typical for the explosion of explosives (Gretchikhin, 2008). The explosion in the boundary layer has such high intensity that the entire structure of the spacecraft breaks down into small parts. This process is shown in Fig. 3 (Gretchikhin, 2008). A sublimation spot appears in the centre of the explosion. An explosion on the surface of a solid causes not only sublimation, but also cracking of the entire array in the form of radial cracks, as well as a formation of cylindrical and spherical cracks inside the solid. Each explosion on the spacecraft surface causes an intensive sublimation of the flow of solid molecules, and, accordingly, blocks the flow of energy to the surface. As a result, a sequence of explosions occurs, causing breakdown of the solid monolith into separate small

parts. At the same time, the effective interaction surface between the solid and the shock-compressed air increases. The magnitude of the explosion energy is increasing in succession. The explosion fire cloud also expands. Finally, small fragments of the spacecraft fall onto Earth. This was experimentally confirmed when the long-term orbital station MIR-1, with the main structure made of duralumin without a thermal-protective coating, entered dense atmospheric layers.

Conclusion

From these studies, the following wasconcluded:

1. For the descent trajectory of the Soyuz series spacecraft with the structure made of duralumin without a thermal-protective coating at altitudes of 80 to 40 km, data were obtained on the increase in density, pressure and temperature behind the shock front, as well as the shift of the shock wave from the surface of the descending spacecraft.

2. The effective temperature of the shock-compressed gas reaches its maximum value of 7340 K at an altitude of 60 km. At altitudes of 80 and 40 km, it reaches 7000 K and 6400 K, respectively.

3. Calculations were made of the energy fluxes to the surface of the spacecraft for every 10 km in the altitude range of 40 to 80 km, for convective and radiative heat transfer, as well as for the impact of electrons produced due to the ionization of negative ions. Radiative heat transfer has proven to be the most significant.

4. The increase in pressure in the boundary layer at the spacecraft surface was calculated taking into account the burning of negative ions of triatomic molecules of aluminium with the formation of AlO molecules. At all considered altitudes, the pressure rises instantly to a value of 10^9 to 10^{10} Pa and more, which is typical for explosion of various explosives. Each subsequent explosion produces shock waves in the surrounding atmosphere and compressive waves in the entire structure of the spacecraft. The descending spacecraft cracks, and its entire structure breaks down into parts. The area of interaction increases sharply, and each subsequent explosion has a greater intensity and size. After each explosion, the energy flux to the surface stops due to shielding for all types of heat transfer. After the dispersion of the explosion products, an intense flux of energy reappears on the surface of the descending

Gretchikhin, L., Explosion of the boundary layer upon entry of spacecraft into dense layers of the earth's atmosphere, pp.804-822

spacecraft and a new explosion occurs. As a result, the last most intense explosion occurs at an altitude of approx. 40km, after which individual fragments of the spacecraft fall onto Earth. All of this was clearly observed during the reentry of the long-term orbital station MIR-1.

5. The situation is slightly better for spacecraft with thermal protection, but is still very dangerous. Descents must not be carried out at low g-forces. Even at the first cosmic velocity, the descent phase at an altitude of 80 to 40 km should be passed as quickly as possible.

6. When descending spacecraft and meteors enter the atmosphere at the second or greater cosmic velocity, the temperature of the shock-compressed gas reaches up to 15,000 K. At such temperature, the intensity of explosion increases by one order of magnitude or more. This results in falling of small debris and even individual dust particles onto Earth, which was observed when the Chelyabinsk meteor entered the Earth's atmosphere. We must not hurry into manned space exploration. It is necessary to carefully analyze the situation, think and think again! The Tunguska and Chelyabinsk meteor events were a serious warning!

References

Gretchikhin, L.I. 1986. *Neravnovesnoe opticheskoe izluchenie vozdushnyh i kosmicheskih letatel'nyh apparatov*. Ph.D. thesis. Minsk, Belarus: Belarusian Polytechnic Institute (in Russian). (In the original: Гречихин, Л.И. 1986. *Неравновесное оптическое излучение воздушных и космических летательных аппаратов.* Докторская диссертация. Минск, Беларусь: Белорусский политехнический институт).

Gretchikhin, L.I. 2003. Vzaimodejstvie tverdogo tela s okruzhajushhej sredoj v rezhime svobodnomolekuljarnogo obtekanija (jeffekt Gretchikhina). In *The First Belarusian Space Congress*, Minsk, Belarus, pp.31-33, October 28-30 (in Russian). (In th eoriginal: Гречихин, Л.И. 2003. Взаимодействие твердого тела с окружающей средой в режиме свободномолекулярного обтекания (эффект Гречихина). В: *Первый Белорусский космический конгресс*, г. Минск, Беларусь, с.31-33, 28-30 октября).

Gretchikhin, L.I. 2008. *Nanochasticy i nanotehnologii*. Minsk, Belarus: Pravo i jekonomika (in Russian). (In the original: Гречихин, Л.И. 2008. *Наночастицы и нанотехнологии*. Минск, Беларусь: Право и экономика).

Gretchikhin, L.I. 2016. *Osnovy radiosvjazi*. Minsk, Belarus: National Library of Belarus (in Russian). (In the original: Гречихин, Л.И. 2016. *Основы радиосвязи*. Минск, Беларусь: Национальная библиотека Беларуси).

Gretchikhin, L.I., Laptsevich, A.A. & Kuts, N.G. 2012. *Ajerodinamika letatel'nyh apparatov*. Minsk, Belarus: Pravo i ekonimka (in Russian). (In the original: Гречихин, Л.И., Лапцевич, А.А., Куць, Н.Г. 2012. *Аэродинамика летательных аппаратов*. Минск, Беларусь: Право и экономика).

Gretchikhin, L.I., Latushkina, S.D., Komarovskaya, V.M. & Shmermbekk, Yu. 2015a. Formation of a close-packed and cluster lattice structure of indium on a silicon surface. *Strengthening Technologies and Coatings*, 6, pp.3-12 (in Russian) [online]. Available at: http://www.mashin.ru/files/2015/up615_web1.pdf [Accessed: 20 September 2020]. (In the original: Гречихин, Л.И., Латушкина, С.Д., Комаровская, В.М., Шмермбекк, Ю. 2015a. Образование плотноупакованной и кластерной решеточной структуры индия на поверхности кремния. *Упрочняющие технологии и покрытия*, 6, с.3-12 [онлайн]. Доступно на: http://www.mashin.ru/files/2015/up615_web1.pdf [Дата посещения: 20 сентября 2020 г.]).

Gretchikhin, L.I., Latushkina, S.D., Komarovskaya, V.M. & Shmermbekk, Yu. 2015b. The cluster structure of silicon and its surface construction. *Strengthening Technologies and Coatings*, 9, pp.5-10 (in Russian) [online]. Available at: http://www.mashin.ru/files/2015/up_0915_01-48_min.pdf [Accessed: 20 September 2020]. (In the original: Гречихин, Л.И., Латушкина, С.Д., Комаровская, В.М., Шмермбекк, Ю. 2015b. Кластерная структура кремния и конструкция его поверхности. *Упрочняющие технологии и покрытия*, 9, с.5-10 [онлайн]. Доступно на: http://www.mashin.ru/files/2015/up615_web1.pdf [Дата посещения: 20 сентября 2020 г.]).

Gretchikhin, L.I. & Minko, L.Ya. 1967. Ob analogii fizicheskih processov protekajushhih v impul'snom razrjade i pri vozdejstvii koncentrirovannogo lazernogo izluchenija. *Zhurnal tehnicheskoj fiziki*, 37 (in Russian). (In the original: Гречихин, Л.И., Минько, Л.Я. 1967. Об аналогии физических процессов протекающих в импульсном разряде и при воздействии концентрированного лазерного излучения. *Журнал технической физики*, 37).

Gretchikhin, L.I. & Tyunina, E.S. 1967. Study of arc discharge electrode flares. 1967. *Physics and chemistry of materials treatment*, 11(3), in Russian. (In the original: Гречихин, Л.И., Тюнина, Е.С. 1967. Исследование электродных факелов дугового разряда. *Физика и химия обработки материалов,* 11(3)).

Kheiz, I.D. & Probstin, R.F. 1962. *Theory of hypersonic phenomena*. Moscow: Foreign Languages Publishing House (translation into Russian). (In the original: Хейз, И.Д., Пробстин, Р.Ф. 1962.*Теория гиперзвуковых явлений*. Москва: Издательство иностранной литературы, переведено с английского).

Zeldovich, Ya.B. & Raizer, Yu.P. 2008. *Fizika udarnyh voln i vysokotemperaturnyh gidrodinamicheskih javlenij: prakticheskoe posobie*. Moscow: Fizmatlit (in Russian). ISBN: 978-5-9221-0938-3. (In the original: Зельдович, Я.Б., Райзер, Ю.П. 2008. *Физика ударных волн и высокотемпературных гидродинамических явлений: практическое пособие*. Москва: Физматлит. ISBN: 978-5-9221-0938-3).

VOJNOTEHNIČKI GLASNIK / MILITARY TECHNICAL COURIER, 2020, Vol. 68, Issue 4

ВЗРЫВ ПОГРАНИЧНОГО СЛОЯ ПРИ ВХОЖДЕНИИ ЛЕТАТЕЛЬНЫХ АППАРАТОВ В ПЛОТНЫЕ СЛОИ ЗЕМНОЙ АТМОСФЕРЫ

Леонид И. Гречихин

Белорусская государственная академия связи,
Минск, Республика Беларусь

РУБРИКА ГРНТИ: 55.00.00 МАШИНОСТРОЕНИЕ:
55.49.03 Аэродинамика ракет и космических аппаратов
ВИД СТАТЬИ: оригинальная научная статья

Резюме:

Ведение/цель: Проведен анализ сверхзвукового обтекания шара радиусом 1 м на высотах полета 80 ÷ 40 км.

Методы: Траектория спуска при первой космической скорости использовалась та, которая соответствует аппарату «Союз» без теплозащиты с дюралюминиевой конструкцией.

Результаты: Для газа между фронтом ударной волны и поверхностью спускаемого аппарата получены данные по увеличению плотности, давления и температуры за фронтом ударной волны, а также отхода ударной волны от поверхности спускаемого аппарата. Эффективная температура ударно нагретого газа достигает своего максимального значения 7340 К на высоте 60 км. На высотах полета 80 и 40 км эффективная температура составляет соответственно 7000 К и 6400 К. На основании полученных данных о термодинамическом состоянии газа за ударной волной через каждых 10 км произведены расчеты потоков энергии на поверхность летательного аппарата при конвективном и лучистом теплообмене, а также при ударном воздействии электронами, которые получены при ионизации отрицательных ионов. Лучистый теплообмен оказался наиболее существенным. Установлен механизм горения отрицательных ионов трехатомных молекул алюминия с образованием молекул AlO и получены данные по увеличению давления в пограничном слое у поверхности летательного аппарата. На всех рассмотренных высотах полета давление повышается мгновенно до значения на высоте 80 км $1.06 \cdot 10^{10}$ Па, на высоте 60 км $5.3 \cdot 10^{9}$ Па и на высоте 40 км достигает максимального значения $5.5 \cdot 10^{10}$ Па. Давления $10^{9} \div 10^{10}$ Па возникают при подрыве разных взрывчатых веществ. Поток энергии на поверхность спускаемого аппарата поступает между взрывами. В момент взрыва у поверхности спускаемого аппарата возникают ударные волны в окружающей атмосфере и волны сжатия во всей конструкции летательного аппарата. Спускаемый аппарат растрескивается, и вся конструкция аппарата распадается на отдельные части. Резко возрастает

площадь взаимодействия, и каждый последовательный взрыв возрастает по своей мощности и соответственно в размерах. Последний самый мощный взрыв происходит на высоте ~ 40 км, после которого на Землю падают отдельные обломки летательного аппарата.

Вывод: Освоение космического пространства с полетом на другие планеты возможно только при тщательном изучении взрывных процессов у поверхности спускаемого аппарата на других планетах, а особенно при спусках на планету Земля.

Ключевые слова: взрыв взрывчатых веществ, сверхзвуковое движение, конвективный теплообмен, лучистый теплобмен, эффекты потока электронов, отрицательные ионы.

ЕКСПЛОЗИЈА ГРАНИЧНОГ СЛОЈА ПО УЛАСКУ СВЕМИРСКЕ ЛЕТЕЛИЦЕ У ГУСТЕ СЛОЈЕВЕ ЗЕМЉИНЕ АТМОСФЕРЕ

Леонид И. Гречихин

Белоруска државна академија за комуникације,
Минск, Република Белорусија

ОБЛАСТ: машинство
ВРСТА ЧЛАНКА: оригинални научни рад

Сажетак:

Увод/циљ: Анализиран је суперсонични ток око сфере полупречника 1м на висинама од 80 до 40 км.

Методе: Разматрана је силазна трајекторија при првој космичкој брзини, слична трајекторији свемирске летелице Сојуз с алуминијумском структуром без топлотне заштите.

Резултати: За гас између фронта ударног таласа и површине свемирске летелице при спуштању добијени су подаци о повећању густине, притиска и температуре иза фронта ударног таласа, као и о померању ударног таласа од површине свемирске летелице у фази спуштања. Ефективна температура гаса загрејаног услед удара достиже максималну вредност од 7340 К на висини од 60 км. На висинама од 80 и 40 км ефективна температура је 7000 К, односно 6400 К. На основу података о термодинамичком стању гаса иза ударног таласа на сваких 10 км, израчунати су флуксеви енергије ка површини свемирске летелице за пренос топлоте конвекцијом и радијацијом, као и за утицај електрона насталих услед јонизације негативних јона. Показало се да је пренос топлоте радијацијом најзначајнији. Утврђен је механизам сагоревања негативних јона триатомских молекула алуминијума са формирањем AlO молекула и добијени су подаци о

Gretchikhin, L., Explosion of the boundary layer upon entry of spacecraft into dense layers of the earth's atmosphere, pp.804-822

порасту притиска у граничном слоју на површини свемирске летелице. На разматраним висинама притисак тренутно расте на $1,06\times10^{10}$ Ра при висини од 80 км, на $5,3\times10^{9}$ Ра при висини од 60 км и достиже максималну вредност од $5,5\times10^{10}$Ра при висини од 40 км. Притисак од 10^{9} до 10^{10} ствара се током експлозија различитих типова експлозива. Флукс енергије стиже до површине свемирске летелице између експлозија. У тренутку експлозије стварају се ударни таласи у атмосфери око површине свемирске летелице која се спушта, а унутар њене целокупне структуре настају компресивни таласи. Свемирска летелица пуца при спуштању, а целокупна структура се распада. Убрзано се повећава област интеракције и свака наредна експлозија је снажнија и већа. Последња најинтензивнија експлозија настаје на висини од отприлике 40 км, праћена падом фрагмената свемирске летелице на Земљу.

Закључак: Истраживање свемира путем летова на друге планете могуће је само после исцрпног проучавања експлозивних процеса који се дешавају на површини свемирске летелице при спуштању на другу планету, а нарочито при спуштању на Земљу.

Кључне речи: експлозија експлозива, суперсонично кретање, пренос топлоте конвекцијом, пренос топлоте радијацијом, ефекти флукса електрона, негативни јони.

Paper received on / Дата получения работы / Датум пријема чланка: 29. 09. 2020.
Manuscript corrections submitted on / Дата получения исправленной версии работы / Датум достављања исправки рукописа: 17. 10. 2020.
Paper accepted for publishingon / Дата окончательного согласования работы / Датум коначног прихватања чланка за објављивање: 19. 10. 2020.

DETERMINATION OF THE CRITICAL DISTANCE IN THE PROCEDURE OF EXPLOSIVE WELDING

Miloš S. Lazarević[a], *Bogdan* P. Nedić[b,]
Jovica Đ. Bogdanov[c], *Stefan* V. Đurić[d]

[a] University of Kragujevac, Faculty of Engineering,
Kragujevac, Republic of Serbia,
e-mail: laky_boy_kg@hotmail.com,
ORCID iD: https://orcid.org/0000-0002-5441-4482

[b] University of Kragujevac, Faculty of Engineering,
Kragujevac, Republic of Serbia,
e-mail: nedic@kg.ac.rs, **corresponding author**,
ORCID iD: https://orcid.org/0000-0002-4236-3833

[c] University of Defence in Belgrade, Military Academy, Department for Military Chemical Engineering, Belgrade, Republic of Serbia,
e-mail: bjbogdanov@yahoo.com,
ORCID iD: http://orcid.org/0000-0001-7995-3004

[d] University of Kragujevac, Faculty of Engineering,
Kragujevac, Republic of Serbia,
e-mail: stefandjuric992@gmail.com,
ORCID iD: https://orcid.org/0000-0003-0660-7551

DOI: 10.5937/vojtehg68-26683; https://doi.org/10.5937/vojtehg68-26683

FIELD: Mechanical engineering
ARTICLE TYPE: Original scientific paper

Abstract:

Introduction/purpose: When performing the explosive welding procedure, for the safety of workers, it is necessary to take into account the minimum distance between the workers and the place of explosion at the time of explosion. Negligence can cause temporary hearing loss, rupture of the eardrum and in some cases even the death of workers. The aim of this paper is to determine the critical distance based on the mass of explosive charge required for explosive welding, provided that the limit pressure is 6.9 kPa in the case of temporary hearing loss and 35 kPa in the case of eardrum rupture. This paper does not take into account other effects of the explosion than those caused by the shock wave.

ACKNOWLEDGMENT: This paper presents the results of the research in Project TR35034: Research on the application of modern unconventional technologies in manufacturing companies with the aim of increasing efficiency, product quality, reducing costs and saving energy and materials, which is financially supported by the Ministry of Education, Science and Technological Development of the Republic of Serbia.

Methods: Depending on the type of explosion, the equivalent explosive mass was calculated. Based on the equivalent explosive mass and the limit pressure, the minimum distances were calculated using the Sadovsky and Kingery-Bulmash equations.

Results: The corresponding tables show the results of the calculation of the critical distance of workers from the place of the explosion when there may be temporary hearing loss or rupture of the eardrum. The calculated value of the critical explosion distance by the Kingery-Bulmash method, under the condition of the maximum pressure for temporary hearing loss, is 5.62% lower than the distance value obtained by the Sadovsky method while the value of the critical explosion distance calculated by the Kingery-Bulmash method, under the condition of the maximum pressure for eardrum rupture, is 7.83% lower than the value obtained by the Sadovsky method.

Conclusion: The results of the calculation showed that the critical distance from the explosion can be successfully calculated and that the obtained values have small differences depending on the applied calculation method.

Key words: explosion welding, critical distance, shock wave, eardrum damage, risk matrix.

Introduction

Explosive welding is a process in which the chemical energy of explosives is used to create a welded joint. Part of the internal energy of explosives is converted into kinetic energy of gaseous detonation products which cause metal particles to move and form a welded joint. This technological process is used to join two dissimilar materials that cannot otherwise be joined by classical welding processes or their joining is considerably more difficult (e.g. production of clad materials).

The advantage of this procedure is that cheap materials, e.g. aluminum and steel, can be used to form inexpensive materials with excellent mechanical and chemical characteristics. Also, with this procedure, it is possible to obtain multilayer materials of large areas. For this reason, this technology is increasingly used in shipbuilding for the manufacture of ship hulls, in chemical industry for manufacturing tanks and boilers, and for the manufacture of electrical contacts. Explosive welding is a process accompanied by certain hazards. With this in mind, all safety aspects of the application of this procedure must be taken into account.

When performing the explosive welding procedure, for the safety of workers, it is necessary to take into account the minimum distance between workers and the place of explosion at the time of explosion. Negligence can cause temporary hearing loss and rupture of the eardrum. Severe consequences and death are caused by damage to the lungs and other internal organs.

The aim of this work is to determine the critical distance based on the explosive charge mass and required for explosive welding under the condition of the maximum limit pressure for temporary hearing loss and the maximum limit pressure for eardrum rupture.

Explosive welding

Explosion of metals is achieved due to a very fast collision of metals under the action of detonation products, with the appearance of high pressure and plastic deformations in the waveform at the joint boundary and adiabatic local heating of metal surface layers (Pejčinović, 2000), (Ghomi, 2009), (Bataev et al, 2019).

The joining process consists of placing welded plates in parallel or at a certain angle at an appropriate distance from each other. An explosive charge of a certain thickness is placed on the plate to be pushed. Initiation is usually performed at a point on one of the sides of the explosive charge. After initiating the detonation process in an explosive charge, a very high pressure is created in the detonation products.

The detonation products suppress the upper plate (Figure 1), which collides with the lower plate at high speed. The collision is performed gradually, during which the pushed plate rotates and turns into a quasi-liquid state.

At the same time, a tangential component of the collision velocity appears in the direction of propagation of the detonation wave which makes the metal joint zone wavy during plastic deformation (Pejčinović, 2000), (Blazynski, 1983).

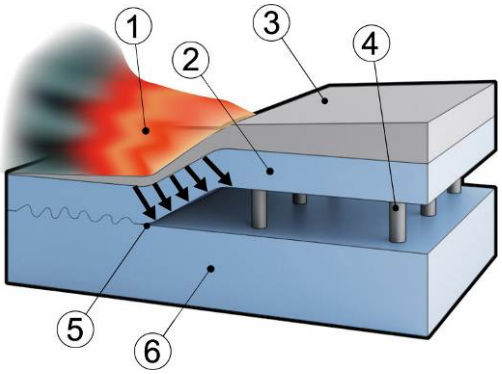

Figure 1 – Explosive welding scheme: 1 - Detonation products, 2 - coating for base material, 3 - explosive, 4 - spacers, 5 - connection point, 6 - base material (Manufacturing Guide, 2020)
Рис. 1 – Схема сварки взрывом: 1 - продукты детонации, 2 - покрытие для основного материала, 3 - взрывчатка, 4 - проставки, 5 - точка соединения, 6- основной материал (Manufacturing Guide, 2020)
Слика 1 – Шематски приказ експлозивног заваривања: 1 – продукти детонације, 2 – облога за основни материјал, 3 – експлозив, 4 – дистанцери, 5 – тачка спајања, 6 – основни материјал (Manufacturing Guide, 2020)

Hearing damage criteria

Hearing damage occurs due to the action of shock waves (UT) in the air as a consequence of the action of explosion. An explosion produces a primary wave (compression wave) and a secondary wave (dilution wave). Damage to the hearing organs under the action of the shock wave depends on the distance of the person from the center of the explosion, on the position of the hearing organs in relation to the shock wave, as well as on the previous condition of the damaged ear (presence of inflammatory processes, etc.) (Shangyuan, 2018), (Gan et al, 2016).

It has been found that temporary hearing loss can occur at a pressure level below 6.9 kPa (Beveridge, 2011), while the eardrum rupture threshold is at a pressure of 35 kPa that occurs during an explosion (Stewart, 2006).

Injuries caused by the explosion shock wave are proportional to the amount of explosive and inversely proportional to the distance from the place of explosion (Solomos et al, 2020). In the case of an explosion of 8 kg of TNT, at distances of 1-3.5 m, mortality is over 99% while at a distance of about 5 m, mortality is over 50%. At distances of 6-8.5 meters, mortality is over 20%, while at a distance of over 10 meters, mortality is lower than 5%. (Waldau et al, 2015)

It should be emphasized that the adopted critical values are conditional. In the works (BlackBox Biometrics, 2018), (Stamatović, 1995), data on shock wave overpressure values for different degrees of injuries can be found.

Explosive characteristics

Within this paper, a possible impact of Amonex 1 explosives was analyzed (Table 1). It is a powder explosive made on the basis of ammonium nitrate (AN) and TNT (TNT). The percentage of the chemical composition of Amonex 1 is 82% ammonium nitrate, 16% TNT, 0.6% carboxymethyl cellulose, 0.4% calcium stearate and 1% base paraffin oil (Trayal Corporation, 2008). It has low sensitivity to impact and friction, which makes this explosive safe to handle and transport. It is used, first of all, for mass mining blasting in underground and surface exploitation, and for blasting from soft to very hard rock masses where methane and explosive coal dust are not present (Trayal corporation, 2020). It is not water resistant, which is why it is used for blasting in dry and wet mine wells, so it is not suitable for blasting in wells with water.

Table 1 – Characteristics of AMONEX 1-4 powder explosives (Trayal corporation, 2020)
Таблица 1 – Характеристики порошковых взрывчатых веществ AMONEX 1-4 (Trayal corporation, 2020)
Табела 1 – Карактеристике прашкастих експлозива AMONEX 1-4 (Trayal corporation, 2020)

PROPERTY	Unit	Type of explosive			
		AMONEX 1	AMONEX 2	AMONEX 3	AMONEX 4
Density	g/cm^3	1.02-1.10	1.02-1.10	0.96-1.04	0.96-1.04
Velocity of detonation, min	m/s	4100	3900	3600	3200
Gas volume	dm^3/kg	975	984	993	1004
Oxigen balance	%	+ 0.13	+ 0.08	+ 0.10	+ 0.17
Heat of explosion	kJ/kg	4103	4082	4040	3892
Temperature of explosion	K	2740	2725	2707	2661
Presure of detonation	kbar	45	40	33	27
Initiation		blasting cap N°8			

Determination of theTNT equivalent

Most of the equations for calculating the shock wave and pulse are based on the TNT equivalent. Therefore, it is desirable to know their equivalent mass for different explosives.

The equivalent mass of the explosive charge is calculated on the basis of the expression (Jeremić, 2002):

$$M_{TNTe} = \frac{E_{deksp}}{E_{dTNT}} M_{eksp} \tag{1}$$

where:

M_{TNTe} – equivalent mass of trinitrotoluene (TNT) in g,
E_{deksp} – detonation energy of explosive in kJ/kg,
E_{dTNT} – TNT detonation energy of 4184 kJ/kg, and
M_{eksp} – mass of explosive in g.

More on the calculation of the equivalent mass and the TNT equivalent can be found in the papers (Bajić et al, 2009), (Panowicz et al, 2017).

The calculation of the TNT equivalent is usually based on the energy released during an explosion. Such energy can be determined in different ways. The most commonly used methods are based on hydrodynamic or thermodynamic parameters.

The explosive mass in individual experiments was determined on the basis of calculations (Ghomi, 2009) and on the basis of the plate dimensions of 200 × 150 mm. The mass of explosives in the range of 170-290 g satisfies all the criteria of the stated calculation. The experimental setup of explosive welding performed at the Technical Overhaul Institute in Kragujevac is shown in Figure 2.

Figure 2 – Experimental setting for explosive welding
Рис. 2 – Экспериментальная установка сварки взрывом
Слика 2 – Експериментална поставка експлозивног заваривања

The calculated values of the equivalent masses of AMONEX 1 explosives depending on the mass of the explosive charge for the required critical distance calculations within this paper are shown in Table 2.

Table 2 – Explosive charge mass and the equivalent mass of AMONEX 1
Таблица 2 – Масса заряда взрывчатого вещества и эквивалентная масса AMONEX 1
Табела 2 – Маса експлозивног пуњења и еквивалентна маса AMONEX 1

Type of explosive	Unit	AMONEX 1				
Experiment number N		1	2	3	4	5
Explosive charge mass M_{eksp}	g	170	190	220	250	290
TNT equivalent E_{deksp}/E_{dTNT}		0.981				
Equivalent mass of explosives M_{TNTe}	g	167	186	216	245	285
Double equivalent mass of explosives m_p	g	333	370	432	491	569

Determination of the critical distance of an explosion

The main characteristics of the shock wave are the overpressure at the front of the shock wave and the duration of the compression wave, the values of which depend on the type of explosive, the mass of the explosive and the distance from the place of the explosion.

In addition to Sadovsky's formula (Sadovsky, 1952), there are numerous newer relations for determining the overpressure at the shock wave front, such as the Brode formula (Brode, 1955), the Kinney-Graham formula (Kinney & Graham, 1985), the Kingery-Bulmash formula, (Kingery & Bulmash, 1984), etc. For the sake of simplicity, this paper will be based on Sadovsky's formula with two groups of the k_1, k_2, and k_3 coefficients (Table 3) and the Kingery-Bulmash method.

Based on the experimental results for spherical shock waves formed by a detonation of a certain mass of TNT, Sadovsky (Sadovsky, 1952) proposed an empirical equation for the calculation of overpressure at the shock wave front in the form:

$$\Delta p = k_1 \frac{m_e^{\frac{1}{3}}}{r} + k_2 \frac{m_e^{\frac{2}{3}}}{r^2} + k_3 \frac{m_e}{r^3}$$

By arranging the equation we get:

$$\Delta \mathrm{p} \cdot r^3 - k_1 m_e^{\frac{1}{3}} r^2 - k_2 m_e^{\frac{2}{3}} r - k_3 m_e = 0 \tag{2}$$

where:

Δp - overpressure at the shock wave front in bar (1 bar = 10^5 Pa),
m_e - mass of explosive charge in kg,
r - distance from the center of the explosion in m, and
k_1, k_2, k_3 - empirical coefficients depending on the type of explosive charge.

For TNT in the case of an above-ground explosion (at an infinite distance from the ground), the empirical coefficients can be adopted according to Table 3. In the following work, the results with different groups of k_1, k_2, and k_3 coefficients from Table 3 will be presented.

In the case of a surface explosion, the shock wave in the air propagates in the shape of a hemisphere (twice the volume), so the overpressure is higher in that case. Therefore, in equation (2), twice the mass value is taken as the mass of the explosive charge (Andreev et al, 2004).

Table 3 – Coefficients k_1, k_2, and k_3 in TNT above-ground explosions (Andreev et al, 2004), (Bajić et al, 2009).
Таблица 3 – Коэффициенты k_1, k_2, k_3, в зависимости от типа взрыва (Andreev et al, 2004), (Bajić et al, 2009).
Табела 3 – Коефицијенти k_1, k_2, k_3 у зависности од надземне експлозије TNT (Andreev et al, 2004), (Bajić et al, 2009).

Coefficient	Above-ground explosion (Andreev et al, 2004)	Above-ground explosion (Bajić et al, 2009)
k_1	0.84	1.02
k_2	2.7	4.36
k_3	7	14

As the surface explosion causes soil deformation, it is necessary to introduce a coefficient η that depends on the type of soil (Table 4), so that the equivalent (calculated) mass of explosives can be calculated using expression (3):

$$m_p = 2 \cdot \eta \cdot M_{TNTe} \tag{3}$$

Table 4 – Values of the coefficient η depending on the soil type (Andreev et al, 2004)
Таблица 4 – Значения коэффициента η в зависимости от типа почвы (Andreev et al, 2004)
Tabela 4 – Вредности коефицијента η у зависности од типа тла (Andreev et al, 2004)

Obstacle type	Steel plate	Reinforced concrete plate	Concrete, rock	Hard ground	Medium hard ground	Water
η	1	0.95-1	0.85-0.9	0.7-0.8	0.6-0.65	0.55-0.6

In this paper, the coefficients k_1, k_2, and k_3 are presented in Table 3 according to the work (Andreev et al, 2004) and according to the work (Bajić et al, 2009). Both cases assume that, in the calculation of explosive welding, twice the mass of explosive charge mp is adopted according to equation (3) and the coefficient η for the steel plate. Other values of the coefficient η will not be considered.

The solution of equation (2) is obtained by reducing it to the following form:

$$y^3 + p \cdot y + q = 0$$

where p and q have the following values:

$$p = -\frac{m_p^{\frac{2}{3}}(k_1^2 + 3k_2\Delta p_\varphi)}{3\Delta p_\varphi^2}$$

$$q = -\frac{m_p(27k_3 m_p \Delta p_\varphi^2 + 9k_1k_2\Delta p_\varphi + 2k_1^3)}{27\Delta p_\varphi^3}$$

The calculation of the discriminant D is performed according to the following equation:

$$D = \frac{q^2}{4} + \frac{p^3}{27}$$

Using the Cardano equation, the solutions are obtained by y:

$$y = \sqrt[3]{-\frac{q}{2} + \sqrt{D}} + \sqrt[3]{-\frac{q}{2} - \sqrt{D}}$$

To obtain the solution of the cubic equation, the following equation is used:

$$r = y - \frac{k_1 m_p^{\frac{1}{3}}}{3\Delta p_\varphi} \tag{4}$$

The dependence of a critical distance as a function of pressure (Sadovsky method) is shown in Figure 3.

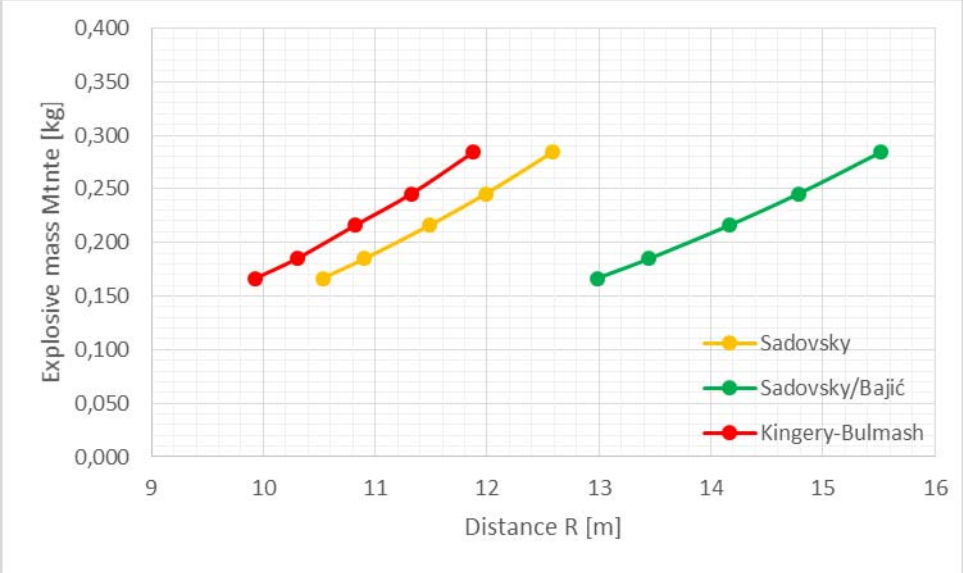

Figure 3 – Critical distance as a function of pressure
Рис. 3 – Критическое расстояние в зависимости от давления
Слика 3 – Критично растојање у зависности од притиска

In Figure 3, the solid lines denote the coefficients k_1, k_2, and k_3 according to the work (Andreev et al, 2004), while the dashed lines refer to the coefficients according to the work (Bajić et al, 2009) in Table 4.

In addition to the Sadovsky method, the Kingery-Bulmash method is also used in this paper. The Kingery-Bulmash method is used in international regulations (United Nations, 2015) and is more applicable in this case.

In the case of a surface explosion, the Kingery-Bulmash shock wave pressure polynomial is:

$$Y = C_0 + C_1U + C_2U^2 + C_3U^3 + ... + C_nU^n \tag{5}$$

$$U = K_0 + K_1T \tag{6}$$

$$T = log_{10}\left(R\sqrt[3]{M_{TNTe}}\right) \tag{7}$$

where:

T – Logarithm of distance with base ten, m,

K_0, K_1 – coefficients,
C_1 - C_9 – coefficients, and
R – distance, m.

These equations have an applicability range of 0.05 to 40 m.

The parameters of the Kingery-Bulmash pressure polynomial at the front of the shock wave are shown in Table 5.

Table 5 – Parameters of the Kingery-Bulmash polynomial for the pressure at the front of the shock wave (United Nations, 2015)
Таблица 5 – Параметры многочлена Кингери и Булмаша для давления во фронте ударной волны (United Nations, 2015)
Табела 5 – Параметри полинома Kingery-Bulmash-а за притисак на челу ударног таласа (United Nations, 2015)

Parameters	Numeric value
K_0	-0.214362789151
K_1	1.35034249993
C_1	2.78076916577
C_2	-1.6958988741
C_3	-0.154159376846
C_4	0.514060730593
C_5	0.0988534365274
C_6	-0.293912623038
C_7	-0.0268112345019
C_8	0.109097496421
C_9	0.00162846756311
C_{10}	-0.0214631030242
C_{11}	0.0001456723382
C_{12}	0.00167847752266

The numerical values for the constants "*C*" and "*K*" are the values for 1 kg of TNT equivalent.

For other explosives, it is required to first estimate the TNT equivalent.

Many states use rules regulating explosives, their quantity and distance from explosives where people are at risk. These rules are known as the quantity-distance criteria (Q-D), (NATO, 2010) and are based on the approach derived from the Hopkinson-Cranz scaling law which is further supplemented by a series of coefficients (equations 7 and 8). (United Nations, 2015)

This is the basis of much of the work on estimating the appropriate quantities and separation distances.

The dependence of a critical distance as a function of pressure (Kingery-Bulmash method) is shown in Figure 4.

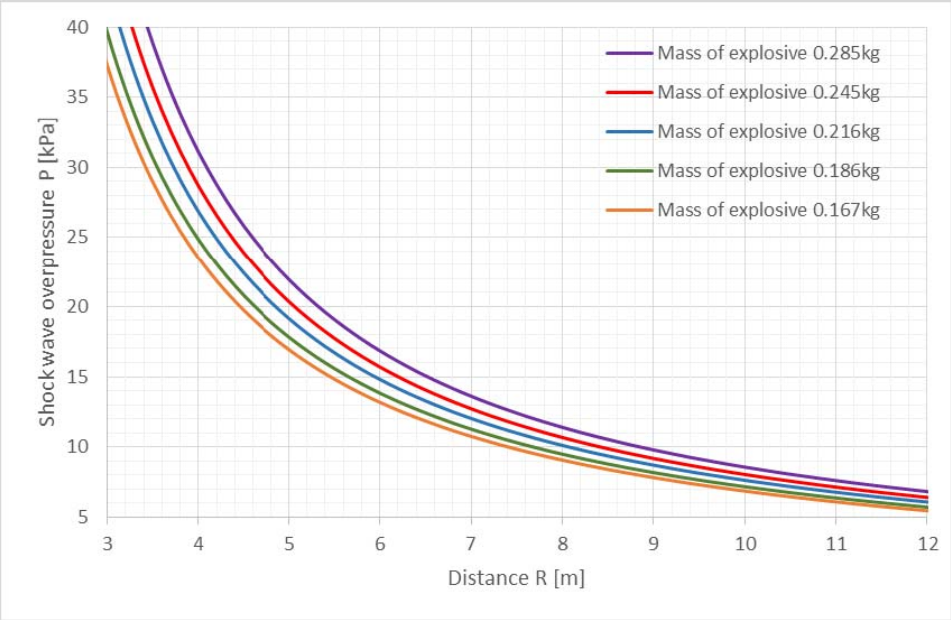

Figure 4 – Critical distance as a function of pressure in the case of temporary hearing loss
Рис. 4 – Критическое расстояние в зависимости от давления в случае временной потери слуха
Слика 4 – Критично растојање у зависности од притиска у случају привременог губитка слуха

Critical distance as a function of explosive charge mass

The paper gives a calculation for Amonex 1 explosive, because it is the strongest commercial explosive from that group (Table 2). Therefore, the critical distance will have the greatest value.

Critical distance determination was performed for two boundary cases:

- critical distance in a case of temporary hearing loss,
- critical distance in a case of rupture of the eardrum.

Both cases assume that an explosion during explosive welding occurs on a metal plate (coefficient η =1, Table 4). By including the coefficients k_1, k_2, and k_3 (Table 3), the equivalent masses of explosives obtained by equation (1) and the limit pressure in the case of temporary hearing loss of 6.9 kPa and 35 kPa in the case of eardrum rupture in equation (2), critical distance in a surface explosion is determined.

The methodology for determining the critical distance as a function of explosive charge mass by the Kingery-Bulmash method will be performed according to a similar principle.

By substituting the critical diameter *R* and the equivalent mass of MTNTe explosives into equation (7), the parameter *T* is obtained. By replacing the coefficients (Table 5) K_0, K_1, and equation (7) with equation (6), the parameter *U* is obtained. By subsituting equation (6) in equation (5), the pressure at the front of the shock wave is obtained depending on the distance.

Figure 5 shows the dependences of the critical distance as a function of the mass of the explosive, under the assumption of the limit pressure that causes temporary hearing loss.

In Figure 5, the yellow line represents the results of the calculation according to the work (Andreev et al, 2004), the green line refers to the work (Bajić et al, 2009) and the red line denotes the Kingery-Bulmash method.

Figure 6 shows the dependences of the critical distance as a function of the mass of the explosive, assuming the limit pressure that causes the eardrum to burst.

In Figure 6, the yellow line represents the results of the calculation according to the work (Andreev et al, 2004), while the green line represents those based on the work (Bajić et al, 2009). The red line refers to the Kingery-Bulmash method.

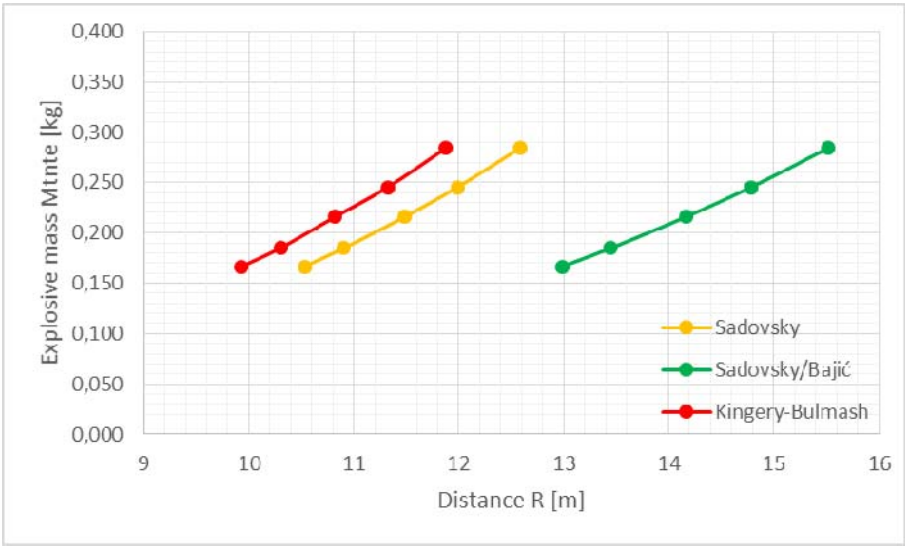

Figure 5 – Critical distance as a function of mass in the case of temporary hearing loss
Рис. 5 – Критическое расстояние в зависимости от массы в случае временной потери слуха
Слика 5 – Критично растојање у функцији масе у случају привременог губитка слуха

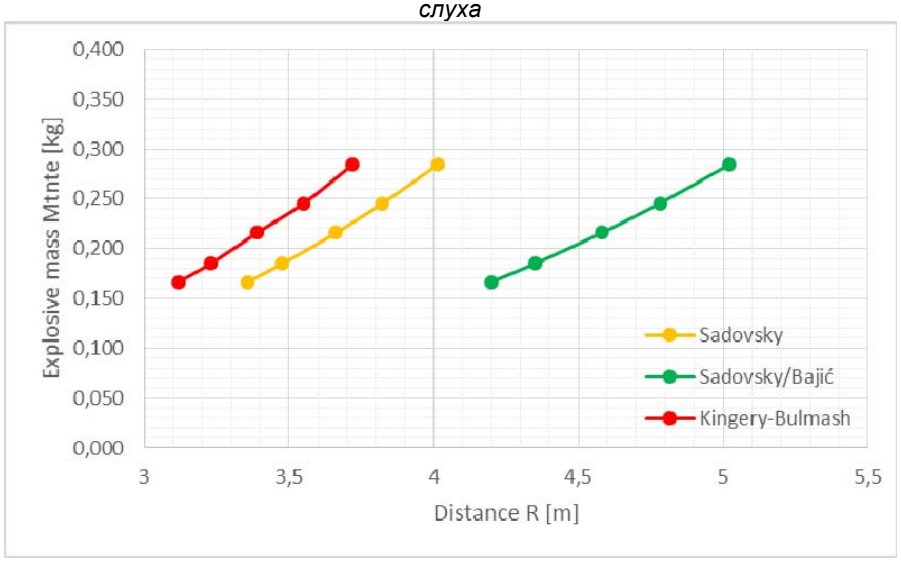

Figure 6 – Critical distance as a function of mass in the case of eardrum rupture
Рис. 6 – Критическое расстояние в зависимости от массы при разрыве барабанной перепонки
Слика 6 – Критично растојање у функцији масе у случају пуцања бубне опне

Risk matrix

Considering the stated results from the previous chapters, a risk matrix was formed. The risk matrix is shown in Figure 7. The maximum values of the critical distance were adopted to form the risk matrix. The critical distance obtained by the Sadovsky method in the case of the maximum equivalent mass of Amonex 1 explosives for the case of temporary hearing loss is 12.59 m and 15.52, while the critical distance in the case of the maximum equivalent mass of the Amonex 1 explosive for the case of eardrum rupture is 4.01 m and 5.02 m, respectively.

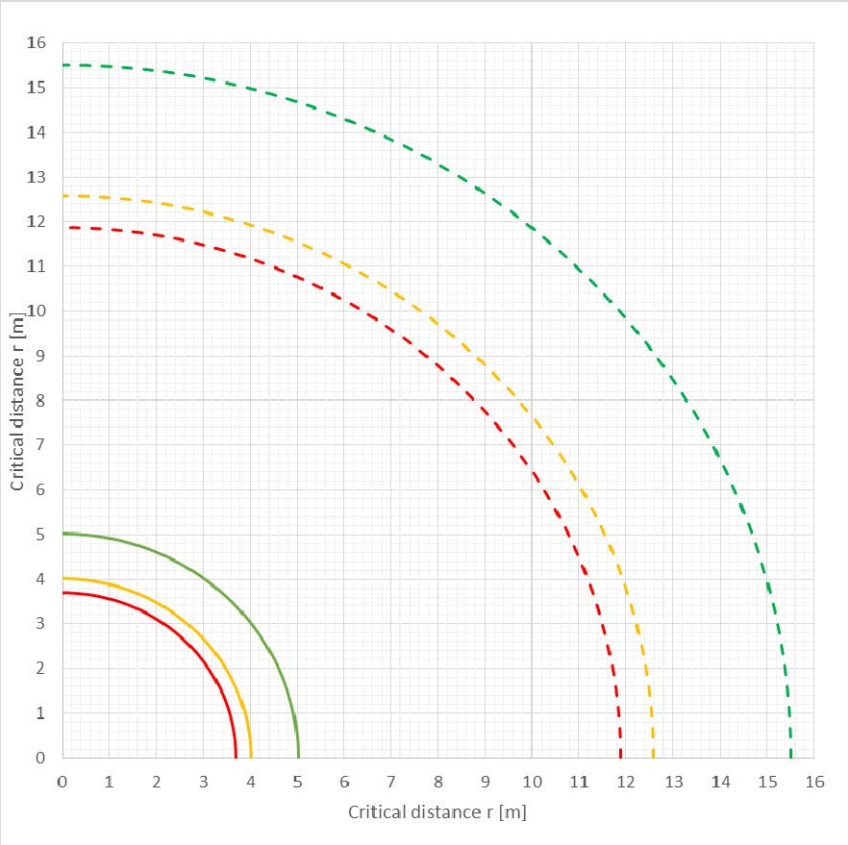

Figure 7 – Risk matrix of the critical distance
Рис. 7 – Матрица рисков критического расстояния
Слика 7 – Матрица ризика критичног растојања

The critical distance obtained by the Kingery-Bulmash method, in the case of the maximum equivalent mass of Amonex 1 explosives in the case of temporary hearing loss is 11.88 m, while the critical distance in the case of the maximum equivalent mass of Amonex 1 explosives in the case of eardrum rupture is 3.72 m.

In Figure 7, the red lines represent the critical distances obtained by the Kingery-Bulmash method. The green and orange lines represent the critical distances obtained by the Sadovsky method with the coefficients k_1, k_2, and k_3 according to the work (Andreev et al, 2004) and according to the work (Bajić et al, 2009), respectively. The solid lines represent the critical distances that would cause the eardrum to rupture, while the dashed lines represent the critical distances that would cause temporary hearing loss. More serious injuries can occur in the zone within the solid lines.

Table 7 shows the critical distances under the condition of the maximum pressure for temporary hearing loss or the maximum pressure for eardrum rupture, respectively.

Table 7 – Tabular view of the critical distances
Таблица 7 – Табличное отображение критического расстояния
Табела 7 – Табеларни приказ критичног растојања

Type of explosive	Unit	AMONEX 1				
Experiment number N		1	2	3	4	5
Critical distance R, Sadovsky method (Andreev et al, 2004) (6,9kPa)	m	10.53	10.90	11.48	11.98	12.59
Critical distance R, Sadovsky method (Bajić et al, 2009) (6,9kPa)	m	12.98	13.45	14.16	14.78	15.52
Critical distance R, Kingery-Bulmash method (6,9kPa)	m	9.93	10.30	10.82	11.32	11.88
Critical distance R, Sadovsky method (Andreev et al, 2004) (35kPa)	m	3.36	3.48	3.66	3.82	4.01
Critical distance R, Sadovsky method (Bajić et al, 2009) (35kPa)	m	4.20	4.35	4.58	4.78	5.02
Critical distance R, Kingery-Bulmash method (35kPa)	m	3.12	3.23	3.39	3.55	3.72

Conclusion

The critical distance of the explosion obtained by the Sadovsky method, under the condition of the maximum pressure for temporary hearing loss, is 12.59 m and 15.52 m, respectively. The critical distance of the explosion obtained by the Sadovsky method, under the condition of the maximum pressure for eardrum burst is 4.01 and 5.02 m, respectively.

The critical explosion distance obtained by the Kingery-Bulmash method, under the condition of the maximum pressure for temporary hearing loss is 11.88 m. The critical explosion distance obtained by the Kingery-Bulmash method, under the condition of the maximum pressure for the eardrum to burst is 3.72 m.

The calculated value of the critical explosion distance by the Kingery-Bulmash method, under the condition of the maximum pressure for temporary hearing loss, is 5.62% lower than the distance obtained by the Sadovsky method according to the coefficients from (Andreev et al, 2004) and 23.47% according to the coefficients from (Bajić et al, 2009).

The value of the critical explosion distance calculated by the Kingery-Bulmash method, under the condition of the maximum burst pressure, is 7.83% lower than the distance obtained by the Sadovsky method according to the coefficients from (Andreev et al, 2004) and 26.31% according to the coefficients from (Bajić et al, 2009).

The presented results refer to the maximum equivalent mass of explosives (experiment number 5) shown in Table 2.

Sadovsky's equation was originally developed for very large quantities of explosives, so its applicability in the considered cases is questionable.

The Kingerey-Bulmash method is used in international regulations and is more applicable in these cases as well.

References

Andreev, S.G., Babkin, A.V. & Baum, F.A. 2004. *Fizika vzryva* (Ed: Orlenko, L.P.). Moscow: Fizmatlit (in Russian). ISBN: 5-9221-0218-4. (In the original: Андреев, С.Г., Бабкин, А.В., Баум, Ф.А. 2004. *Физика взрыва* (ред: Орленко, Л.П.). Москва: Физматлит).

Bajić, Z., Bogdanov, J. & Jeremić, R. 2009. Blast Effects Evaluation Using TNT Equivalent. *Scientific Technical Review*, 59(3-4), pp.50-53 [online]. Available at: http://www.vti.mod.gov.rs/ntp/rad2009/34-09/7/7.pdf [Accessed: 18 February 2020].

Bataev, I., Tanaka, A.S., Zhou, Q., Lazurenko, D.V., Jorge Junior, A.M., Bataev, A.A., Hokamoto, K., Mori, A. & Chen, P. 2019. Towards better understanding of explosive welding by combination of numerical simulation and experimental study. *Materials & Design*, 169(art.number:107649). Available at: https://doi.org/10.1016/j.matdes.2019.107649.

Beveridge, A. 2011. *Forensic Investigation of Explosions*. Boca Raton, Florida: CRC Press. ISBN: 9781420087260.

-BlackBox Biometrics. 2018. *The Blast gauge System*. *Pressure thresholds: what your medic needs to know* [online]. Available at: http://quwdb2fvzocb4glqwropj20o-wpengine.netdna-ssl.com/wp-content/uploads/2018/10/White-Paper-Pressure-Thresholds-v4.pdf [Accessed: 18 February 2020].

Blazynski, T.Z. 1983. *Explosive Welding Forming and Compaction*. Dordrecht, NL: Springer. Online ISBN: 978-94-011-9751-9. Available at: https://doi.org/10.1007/978-94-011-9751-9.

Brode, H.L. 1955. Numerical solutions of spherical blast waves. *Journal of Applied Physics*, 26(6), pp.766–775. Available at: https://doi.org/10.1063/1.1722085.

Gan, R.Z., Nakmali, D.U., Ji, X.D., Leckness, K. & Yokell, Z. 2016. Mechanical damage of tympanic membrane in relation to impulse pressure waveform – A study in chinchillas. *Hearing Research*, 340, pp.25-34. Available at: https://doi.org/10.1016/j.heares.2016.01.004.

Ghomi, M.T. 2009. *Impact wave process modeling and optimization in high energy rate explosive welding*. Västerås, Sweden: Mälardalen University Press. Online ISBN: 978-91-86135-35-5 [online]. Available at: https://www.diva-portal.org/smash/get/diva2:232277/FULLTEXT03.pdf [Accessed: 21 January 2020].

Jeremić, R. 2002. *Eksplozivni procesi*. Belgrade: General Staff of the Yugoslav Army, Directorate for Education (in Serbian).

Kingery, C.N. & Bulmash, G. 1984. *Technical report ARBRL-TR-02555: Air blast parameters from TNT spherical air burst and hemispherical burst, AD-B082 713.* U.S. Army Ballistic Research Laboratory, Aberdeen Proving Ground, MD.

Kinney, G.F. & Graham, K.J. 1985. *Explosive Shocks in Air*. Berlin, Heidelberg: Springer-Verlag. Available at: https://doi.org/10.1007/978-3-642-86682-1.

-Manufacturing Guide. 2020. *Explosion Welding* [online]. Available at: https://www.manufacturingguide.com/en/explosion-welding [Accessed: 02 February 2020].

-NATO. 2010. *Manual of NATO safety principles for the storage of military ammunition and explosives, AASTP-1, Change 3* [online]. Available at: http://www.rasrinitiative.org/pdfs/AASTP-1-Ed1-Chge-3-Public-Release-110810.pdf [Accessed: 18 February 2020].

Panowicz, R., Konarzewski, M. & Trypolin , M. 2017. Analysis of Criteria for Determining a TNT Equivalent. *Strojniški vestnik - Journal of Mechanical Engineering*, 63(11), pp.666-672. Available at: https://doi.org/10.5545/sv-jme.2016.4230.

Pejčinović, M. 2000. *Analiza postupaka obrade eksplozijom*. Graduate thesis. Kragujevac: University of Kragujevac, Faculty of Engineering (in Serbian).

Sadovsky, M.A. 1952. Mehanicheskoe dejstvie vozdushnyh udarnyh voln vzryva po dannym jeksperimental'nyh issledovanij. In: Sadovsky, M.A. & Beljaev, A.F. (Eds.) *Fizika vzryva, Sbornik No. 1*, pp.20-110. Moscow: USSR Academy of Sciences Publishing House [online]. Available at: http://elib.biblioatom.ru/text/fizika-vzryva_1_1952/go,20/ (in Russian) [Accessed: 2 February 2020]. (In the original: Садовский, М.А. 1952. Механическое действие воздушных ударных волн взрыва по данным экспериментальных исследований. В: Садовский, М.А. и Беляев, А.Ф. (Ред.) *Физика взрыва, Сборник Но. 1,* с.20-110. Москва: Издательство Академии наук СССР [онлайн]. Доступно на: http://elib.biblioatom.ru/text/fizika-vzryva_1_1952/go,20/ [Дата посещения: 2 февраля 2020 г]).

Shangyuan, J. 2018. *Mechanical properties of human incudostapedial joint and tympanic membrane in normal and blast-damaged ears*. Ph.D. thesis. Norman, OK: University of Oklahoma [online]. Available at: https://hdl.handle.net/11244/299908 [Accessed: 02 February 2020].

Solomos, G., Larcher, M., Valsamos, G., Karlos, V. & Casadei, F. 2020. *A survey of computational models for blast induced human injuries for security and defence applications*. Luxembourg: Publications Office of the European Union. Online ISBN: 978-92-76-14659-9. Available at: https://doi.org/10.2760/685.

Stamatović, A. 1995. *Konstruisanje projektila.* Belgrade: Ivexy (in Serbian).

Stewart, C. 2006. Blast Injuries: Preparing for the Inevitable. *Emergency Medical Practic,* 8(4) [online]. Available at: http://www.storysmith.net/page5/files/Blast%20Injuries%200406.pdf [Accessed: 21 January 2020].

-Trayal corporation. 2008. *Technological procedure for making industrial powdered explosives.* Serbian Patent number WO2008009031A1 [online]. Available at: https://patents.google.com/patent/WO2008009031A1/en [Accessed: 18 February 2020].

-Trayal corporation. 2020. *Powder explosives* [online]. Available at: https://trayal.rs/en/products/explosives/explosives-and-initiating-devices/explosives/explosive-cartridges/#599 [Accessed: 02 February 2020].

-United Nations. 2015. *International Ammunition Technical Guideline - Formulae for ammunition management. IATG 01.80. Second ed.* [online]. Available at: https://s3.amazonaws.com/unoda-web/wp-content/uploads/2019/05/IATG-01.80-Formulae-for-Ammunition-Management-V.2.01.pdf [Accessed: 18 February 2020].

Waldau, B., Huang, J.H., Winn, H.R. & Grant, G.A. 2015. *Blast-Induced Neurotrauma, Chapter 337* [online]. Available at: https://clinicalgate.com/blast-induced-neurotrauma/ [Accessed: 18 February 2020].

ОПРЕДЕЛЕНИЕ КРИТИЧЕСКОГО РАССТОЯНИЯ ПРИ СВАРКЕ ВЗРЫВОМ

Милош С. Лазаревич[а], *Богдан* П. Недич[а], **корреспондент**,
Йовица Дж. Богданов[б], *Стефан* В. Джурич[а]

[а] Крагуевацкий университет, Факультет инженерных наук, г. Крагуевац, Республика Сербия

[б] Университет обороны в г. Белград, Военная академия, Департамент военного химического инжиниринга, г. Белград, Республика Сербия

РУБРИКА ГРНТИ: 55.00.00 МАШИНОСТРОЕНИЕ:
55.01.93 Условия труда, социально-бытовые мероприятия (услуги), охрана труда, техника безопасности

ВИД СТАТЬИ: оригинальная научная статья

Резюме:

Введение/цель: При проведении сварочных работ методом взрыва всем сотрудникам необходимо придерживаться техники безопасности, соблюдая все правила преосторожности, в первую очередь не нарушать критическое расстояние между рабочими и местом взрыва в момент взрыва. Небрежность или невнимательность могут привести к временной потере слуха, разрыву барабанной перепонки и, в некоторых случаях, даже к смерти сотрудников. Целью данной работы является определение критического расстояния на основании массы заряда взрывчатого вещества, необходимой для сварки взрывом, при условии, что предельное давление в случае временной потери слуха составляет 6,9 кПа, а в случае разрыва барабанной перепонки составляет 35 кПа. В данной статье не приведены иные методы, кроме взрыва, вызванного ударной волной.

Методы: Эквивалентные массы взрывчатых веществ рассчитываются в зависимости от типа взрыва. На основании эквивалентной массы взрывчатых веществ и предельного давления, применяя уравнение Садовского и Кингери и Булмаша рассчитывается минимально допустимое расстояние.

Результаты: В соответствующих таблицах приведены результаты расчета критического расстояния рабочих от места взрыва, который может вызвать временную потерю слуха или разрыв барабанной перепонки. Расчетное значение критического расстояния взрыва, вычисленное по методу Кингери и Булмаша при условии максимального давления, вызывающем временную потерю слуха составило на 7,83% меньше, чем расстояние, полученное методом Садовского, в то время как расчетное значение критического расстояния от

взрыва, вычисленное по методу Кингери и Булмаша при условии максимального давления разрыва барабанной перепонки составило на 7,83% меньше расстояния, полученного методом Садовского.

Вывод: Результаты расчета показали, что критическое расстояние от взрыва можно успешно рассчитать, а также, что полученные значения несущественно различаются вне зависимости от применяемого метода расчета.

Ключевые слова: сварка взрывом, критическое расстояние, ударная волна, повреждение барабанной перепонки, матрица риска.

ОДРЕЂИВАЊЕ КРИТИЧНОГ РАСТОЈАЊА У ПОСТУПКУ ЕКСПЛОЗИВНОГ ЗАВАРИВАЊА

Милош С. Лазаревић[а], *Богдан* П. Недић[а], **аутор за преписку**, *Јовица* Ђ. Богданов[б], *Стефан* В. Ђурић[а]

[а] Универзитет у Крагујевцу, Факултет инжењерских наука, Крагујевац, Република Србија

[б] Универзитет одбране у Београду, Војна академија, Катедра војнохемијског инжењерства, Београд, Република Србија

ОБЛАСТ: машинство
ВРСТА ЧЛАНКА: оригинални научни рад

Сажетак:

Увод/циљ: При извођењу поступка експлозивног заваривања потребно је водити рачуна о минималном растојању између запослених или извођача и места експлозије у тренутку експлозије. Немарност или нехат може проузроковати привремени губитак слуха, пуцање бубне опне, а у неким случајевима чак и смрт. Циљ овог рада је да се на основу масе експлозивног пуњења, која је потребна за експлозивно заваривање, одреди критично растојање под условом да је у случају привременог губитка слуха гранични притисак 6,9 kPa, а у у случају пуцања бубне опне 35 kPa. У раду се не узимају у обзир други ефекти експлозије осим они проузроковани ударним таласом.

Методе: У зависности од типа експлозије, прорачуната је еквивалентна маса експлозива. На основу ње и граничног притиска израчуната су минимална растојања применом једначине Садовског и Kingerey-Bulmash-a.

Резултати: У одговарајућим табелама приказани су резултати прорачуна критичног растојања радника од места експлозије

када може доћи до привременог губитка слуха, односно пуцања бубне опне. Критична удаљеност од експлозије израчуната методом Kingerey-Bulmash, под условом максималног притиска привременог губитка слуха, за 5,62% је мања од растојања добијеног методом Садовског, док је критична удаљеност од експлозије израчуната методом Kingerey-Bulmash-а, под условом максималног притиска пуцања бубне опне, за 7,83% мања од растојања добијеног методом Садовског.

Закључак: Резултати прорачуна су показали да се критична удаљеност од експлозије може успешно прорачунати и да добијене вредности имају мале разлике у зависности од примењене методе за прорачун.

Кључне речи: заваривање експлозијом, критично растојање, ударни талас, оштећење бубне опне, матрица ризика.

Paper received on / Дата получения работы / Датум пријема чланка: 21.05.2020.
Manuscript corrections submitted on / Дата получения исправленной версии работы / Датум достављања исправки рукописа: 01.08.2020.
Paper accepted for publishing on / Дата окончательного согласования работы / Датум коначног прихватања чланка за објављивање: 03.08.2020.

ANALYSIS OF INFLUENCING FACTORS THAT CAN CAUSE ERRORS IN THE APPLICATION OF MODERN METHODS OF SLIDING BEARING DIAGNOSTICS IN MACHINE AND ELECTRICAL SYSTEMS

Nikola P. Žegarac
Serbian Academy of Inventors and Scientists,
Belgrade, Republic of Serbia,
e-mail: zegaracnikola@vektor.net,
ORCID iD: https://orcid.org/0000-0002-1766-8184

DOI: 10.5937/vojtehg68-27265; https://doi.org/10.5937/vojtehg68-27265

FIELD: Mechanical engineering, Energetics, Shipbuilding
ARTICLE TYPE: Original scientific paper

Abstract:

Introduction/purpose: The paper presents the application of modern methods in the diagnostics of sliding bearings and the analysis of influencing factors that can cause errors in such an application. Possibilities to determine with certainty when and where problems affect sliding bearings during system operation are presented. It is also shown how the system will continue to function over time. Causes of failures and the manner of their elimination are predicted, as well as the time for planned maintenance of technical systems.

Method: The new method solves the problem of sliding bearing diagnostics by measuring the dynamic trajectories of the sleeve in the sliding bearing and by measuring vibration parameters on the inner and outer surfaces of the technical system. The dynamic trajectories of the bearing sleeve are measured with non-contact probes; therefore, the centering of probes in relation to the geometric center of the bearing is very important. Vibration parameters, directly related to the clearance in the sliding bearing, are measured on the inner and outer surfaces of the system. The choice of vibration parameters and measuring points is very important. This method has a number of advantages over other diagnostic methods, as it is easy to access measuring points.

ACKNOWLEDGEMENT: The author would like to express his sincere gratitude to world-renowned scientists and experts from many institutes and laboratories, in Serbia and abroad, for their successful and long-term collaboration. The author is especially grateful to General Branko Bilbija, a test pilot, who has flown on most modern military aircraft in many countries. With his considerable knowledge and experience of science and technology, he was of valuable support to the author's scientific and research work.

Results: By measuring the dynamic trajectory of the sleeves in the plain bearing and vibration parameters on the inner and outer surfaces, the bearing clearance quantities are determined, including: normal condition, initial clearance size, its further increase, bearing clearance sizes, and the moment when the condition parameters are close to the upper limit of the permissible bearing clearance.

Conclusion: New diagnostic methods and monitoring systems can be widely applied to: internal combustion engines, all piston machines, hydroelectric power plants, thermal power plants, processing plants, and many other systems.

Keywords: technical diagnostics, sliding bearing, bearing clearance, bearing wear, bearing sleeve, dynamic trajectory.

Introduction

Modern methods of technical diagnostics enable fast and reliable measurement of the size of clearance (bearing wear) in sliding bearings, measurement of vibration parameters, vibration analysis, measurement of speed, measurement of lubricating oil temperature, lubricating oil analysis, measuring coolant temperature, positioning the top dead center in the case of internal combustion engines, etc. Since these are multi-channel measuring systems, a large number of diagnostic parameters can be monitored and measured.

Based on the measured quantities, diagnostics of the condition of mechanical and electrical systems is performed. Data are obtained on the degree of wear and damage of machine elements (gears, shaft sleeves and shafts, sliding and roller bearings) as well as on imbalance which is very important for balancing the system in accordance with the prescribed standards. The selected failure symptoms mark relevant frequency components and create failure symptom sizes whose trend can be monitored. Alarm conditions can also be based on statistical estimates of the selected parameters.

During production, there are deviations from the manufacturing tolerances prescribed by the technical documentation due to various influences and installation errors. During operation, certain operating characteristics deviate more and more from the initial values so that proper operation is disrupted and the system working capacity is reduced. Therefore, it is very useful to pay special attention to these problems and do some research.

In recent years, there has been a significant increase in the share of diagnostics in the maintenance process, which is associated with safer operation, durability, reduced work, and maintenance costs.

According to some research (Miroshnikov, LV, & et al. 1977), (Genkin, MD, & Sokolova AG, 1987), (Vasil'ev, Yu.N., & et al. 1987), diagnostic works account for over 35% of the scope of technical maintenance work.

The largest number of papers in the field of technical diagnostics has been published in the Russian Federation, the USA and Japan, regardless of whether it is a vibration method or some other diagnostic method. In the professional literature of Western countries, specific studies are rarely given, although it is well known that a large number of manufacturers of internal combustion engines allocate huge financial resources for the development and research of engines. The basic principles (Cohn et al, 1975), (Zhdanovsky, NS 1966), (Thomson, 1983), (Fertis, 1973), (Schiffbänker & Gerhard, 1988) are usually presented so that data on the results and possibilities of application of technical diagnostics for engines are very scarce.

Since technical diagnostics needs increasing financial and other costs, expensive measuring equipment and automation, it is necessary to pay attention to the convenience for modern control and monitoring requirements in system development and design.

Increasing control convenience for which there must be evaluation indicators leads to a reduction in the diagnostic work scope, which means that it is necessary to ensure and improve the availability of diagnostics, comfort, ease and accuracy of measurement, unification of control points, number of control points, measuring equipment, diagnostic methods, continuous registration of measured values and collection of information on the technical condition of systems.

The technical condition of a plant is characterized by a large number of operating process parameters. At the same time, not all parameters of the operating process affect the state of the system equally. Therefore, it is necessary to take as many parameters as possible during control in order to more completely determine the condition of the plant. When choosing the diagnostic parameters of the plant, it is necessary to determine the character of their relation with the parameters of the technical condition. In order for the output process parameter to be applicable in technical diagnostics, it must meet certain requirements:

- uniformity,
- width of the field of application, and
- availability of parameter measurement.

Damage to plain bearings in operating conditions can be classified into the following groups:

- damage caused by material fatigue,
- damage due to increased bearing wear,
- damage caused by changing the size of the clearance between the sleeve and the plain bearing, and
- damage due to lack or interruption of the supply of bearing lubricating oil.

There are two concepts of monitoring systems in technical diagnostics:

The ON-line monitoring system intended for continuous measurement and analysis of technical conditions. Measuring sensors and systems are permanently installed on machine and electrical plants.

The OFF-line monitoring system intended for periodic measurements and analyses of technical conditions of plants. Some sensors are permanently built into the system (depending on which parameters are measured), and other sensors are placed together with the portable part of the monitoring system when measurements are to be performed.

Sliding bearing dynamics and vibration generation

Clearance in plain bearings occurs as an important indicator of the technical condition. It enables the assessment of significant movement of the sleeve when measuring dynamic trajectory and vibrations on the bearing housing. Related to this are the bearing structural parameters which include the shape, dimensions, clearances, material properties and other properties that characterize normal operation. The bearing-sleeve system must meet certain criteria so that the structural parameters of the assembly as a whole are within the prescribed limits, which determines the possibility of using the assembly.

Operation of a system with increased working clearance in the bearing causes a violation of lubrication conditions and increases the coefficient of friction, which is ultimately associated with damage to the bearing. Therefore, bearing wear is one of the basic parameters for diagnosing the technical condition. It is almost impossible to determine the laws of wear and tear exactly. It is possible to predict only one part of the type of wear based on the load forces on the sleeve and the sliding bearing.

The main types of wear observed during the system operation are adhesive and abrasive wear, material surface fatigue, and, to a lesser extent, wear due to erosion, fretting and corrosion. Normal wear and tear

occurs due to the damage caused by tribological processes, as inevitable companions of the work of sliding bearings, while extremely intensive material surface wear occurs in extreme cases. Complete elimination of damage due to wear is impossible. Researching relevant parameters and offering a constructive solution ensure the smallest possible impact of unknown quantities and reduce damage due to the wear process to the smallest possible extent, thus increasing the reliability and durability of bearings. An important constructional dimension when designing a bearing is bearing clearance.

The absolute clearance (diametrical bearing clearance) is denoted as the difference between the bearing diameter (D) and the sleeve diameter (d):

$$Z_D = D - d \tag{1}$$

The radial bearing clearance is defined as the difference between the bearing radius (R) and the sleeve radius (r):

$$Z = R - r \tag{2}$$

The relative bearing clearance (ψ) is the ratio of the clearance (Z_D) to the sleeve radius unit (d):

$$\psi = \frac{Z_D}{d} = \frac{D-d}{d} = \frac{R-r}{r} = \frac{Z}{r} \tag{3}$$

Small bearing clearances increase the thickness of the oil film, while too small clearance values reduce oil flow, increase temperature and significantly reduce oil viscosity, leading to mixed friction which causes the oil to overheat and ultimately damage the bearing.

Increased clearances reduce energy losses and contribute to lower oil temperatures, and in local bearing locations where the maximum hydrodynamic pressures are in the oil film, there is also an increase in bearing temperature. Figure 1 shows the influence of the relative clearance (ψ) on the minimum oil film thickness (h_0) for various oil inlet temperatures (ν).

The optimal values of the minimum oil film thickness are in the range ψ = (0,7 - 1,2) 0/00, which means that during the operation time the

values of the oil film thickness in the bearing will decrease, although the bearing construction was performed optimally at the very beginning.

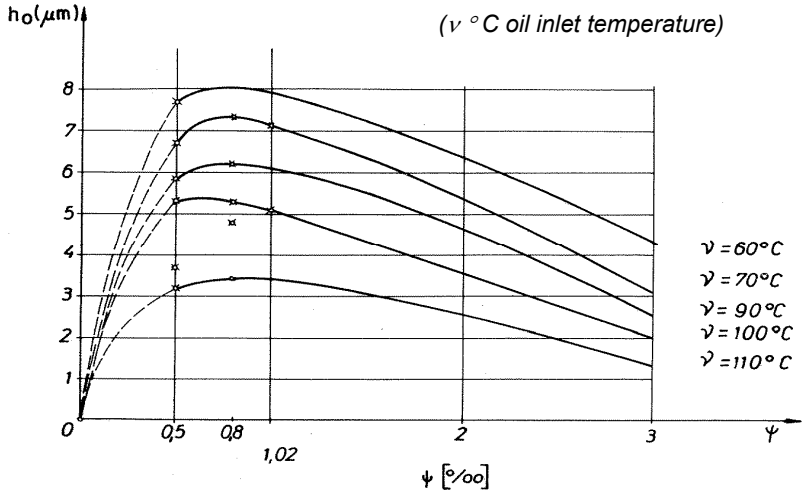

Figure 1 – Minimum thicknesses of the oil film depending on the relative clearance of the bearing
Рисунок 1 – Минимальная толщина масляной пленки в зависимости от относительного зазора подшипника
Слика 1 – Минималне дебљине уљног филма у зависности од релативног зазора лежаја

The parameters that define the vibration process in a plain bearing are: amplitude, phase shift, frequency, attenuation, etc. These parameters can show the wear of the sliding bearing which causes vibrational processes that increase or change when a defect occurs.

During working processes in mechanical and electrical plants, there are variable excitation forces, deformations, variable temperatures, different oil film thicknesses, different stiffness and damping. Consequently, different energies and vibration intensities will occur.

In the case of plain bearings, the reduction of vibration energy is influenced by friction forces. The coefficients of friction change values with the change of the oil temperature in the bearing. The coefficients of friction are significantly influenced by the lubrication conditions and the speed of rotation of the sleeve in the bearing. In real working conditions, damping is nonlinear so that the whole problem of a damping analysis becomes more complicated.

Complex diagnostic objects, such as internal combustion engines, should be evaluated with a large number of structural parameters that change over time and cause system failures. One of the important components in the structure of the vibration signal is its intensity which can be expressed through three quantities: displacement, velocity, and acceleration. Displacement as a vibration parameter is suitable for investigating the complex movement of the bearing sleeve during normal wear, all the way to complete wear when the bearing must be replaced. For measuring points that are further away from the vibration source (bearing - sleeve), speed and acceleration can be used as parameters for describing vibrations.

Vibrations generated in coupled parts cannot be described by exact mathematical models (Fertis, 1973), (Schiffbänker & Gerhard, 1988), (Zhdanovsky et al, 1977). These are non-periodic vibrations in which the rms values of the vibration parameters change by transmission through the system. Vibration signals are modulated. An overview of such changes is given in Figure 2.

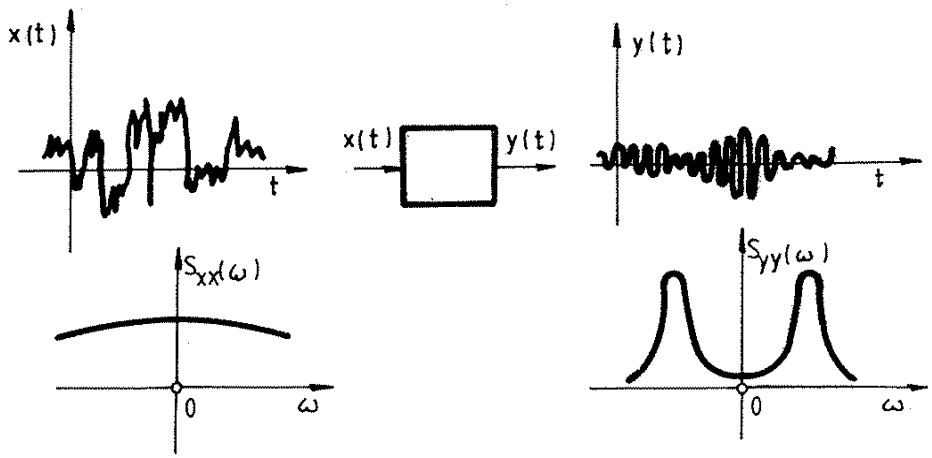

Figure 2 – Changes in the input signal through the system with the corresponding spectra
Рисунок 2 – Изменения во входном сигнале через систему с соответствующими спектрами
Слика 2 – Промене улазног сигнала кроз систем са одговарајућим спектрима

Theoretical settings, calculation of sliding bearing diagnostic parameters and analysis of influencing factors that can cause certain errors in the application of diagnostic methods

In order to examine the influence of the clearance on the dynamics of the sliding bearing, it is necessary to develop a theoretical model of the movement of the sleeve in the bearing with all the influencing factors. The theoretical model of sleeve movement is also a diagnostic model that will contain important settings for diagnostics.

When mathematically describing the theoretical model of backlash movement, it is necessary to give a connection between structural and diagnostic parameters, which represents a scientific contribution in this area.

The theoretical foundations of the calculation of a nonstationarily loaded sliding bearing are described by the Reynolds differential equation (Lang & Steinhilper, 1978). The equation describes the pressure distribution in the direction of bearing volume and width. Considering the problem of lubrication of plain bearings, Reynolds started from several assumptions that greatly simplify the equation:

- along the entire cross section of the bearing there is no change in the viscosity of the observed fluid,
- the observed fluid is an incompressible liquid,
- external forces acting on the fluid can be neglected because they are very small in relation to the tangential forces acting in the fluid layers,
- the fluid flow in the bearing is laminar, the flow rate is constant,
- the curvature of the sliding surfaces can be neglected, since the dimensions of the body between which the oil film is formed are significantly larger compared to the dimensions of the oil film, so that instead of rotation there is a plane motion, and
- the weight and inertia of the fluid are neglected.

These simplifications of the Reynolds equation allow the calculation of the nonstationary force loading the bearing. This force contains the component due to rotation (F_0) and the component due to pressing the sleeve (F_P) in the bearing, (Figure 3).

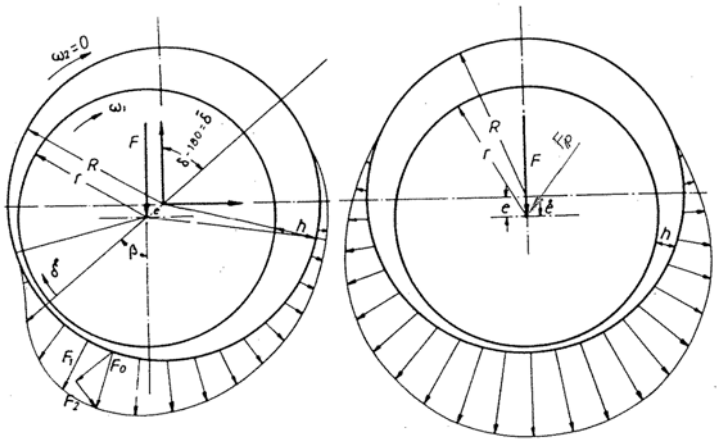

a) rotation *b) pressure*

Figure 3 – Display of a radial bearing with dynamic load forces
Рисунок 3 – Отображение радиального подшипника с динамическими нагрузками
Слика 3 – Приказ радијалног лежаја са динамичким силама оптерећења

This paper presents internal combustion engines as complex diagnostic objects. A special problem is the procedure for determining dynamic forces acting on plain bearings in multy-cylinder engines. For theoretical and experimental research, an in-line marine diesel four-stroke 6-cylinder engine type 6ASL-25D, manufactured by JUGOTURBINA - SULZER, was used.

In the scientific research work, the diagnostics of the main bearings of the engine crankshaft was considered. The load on the sliding bearings of the engine crankshaft is caused by the action of combustion forces and inertial forces. Inertial forces arise from rotating and oscillating masses. In this paper, a detailed analysis of the action of all forces on the engine piston mechanism and on the crankshaft as a whole was performed in a completely new way. Previous calculations have been made on the basis of approximations of quantities, for example that 1/3 of the mass of the connecting rod is in a rectilinear motion and 2/3 of the mass is in a circular motion. It was also not taken into account that the connecting rod makes a complex movement during engine operation. Based on the new procedure for calculating the piston mechanism, kinetostatic and dynamic models were developed and used to determine all kinematic and dynamic quantities (Žegarac, 1989). The deformations of the bearing housing were not taken into account in the calculation, which later turned out to have no special effect.

The calculation of the dynamic parameters was performed for different values of radial clearances in the main bearings: a clearance size of Z = 84 μm when a new clearance bearing was installed in the engine, a clearance size of Z = 124 μm when the engine was running half of the working resource, and a clearance size of Z = 144 μm when the engine ran for the entire working life and the bearing had to be changed.

The time-varying dynamic trajectory of the main sleeve is caused by dynamic non-stationary load. The first computational dynamic model for plain bearings was developed by scientists (Lang & Steinhilper, 1978). Significant improvements have been made according to (Žegarac, 1989).

The method of calculating the dynamic parameters used for the diagnosis of sliding bearings is based on the balance of the external force (F) and the hydrodynamic forces due to the rotation of the sleeve (F_0) and the pressing of the sleeve (F_P). Based on the results of the calculation of dynamic quantities, it was shown that the 5th foundation bearing, located between the 4th and 5th cylinder, is the most loaded on this engine. Figure 4 shows the polar load diagram of that bearing, when the value of the radial clearance is Z = 84 μm.

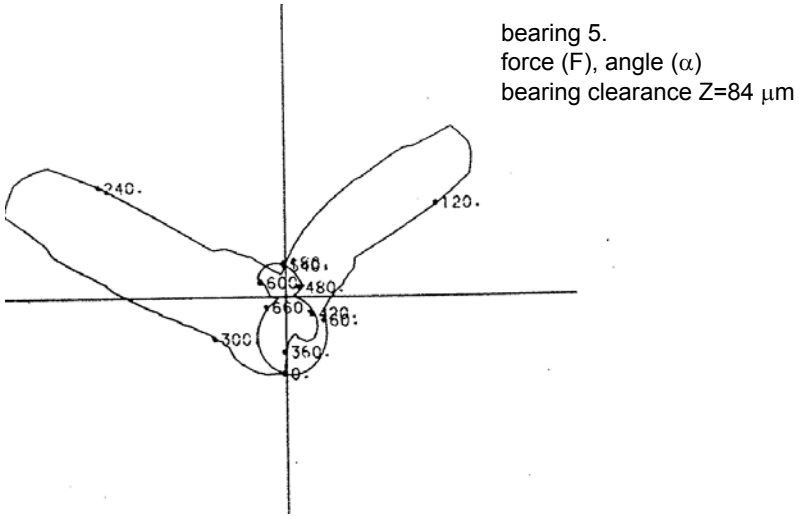

Figure 4 – Polar load diagram of the main sleeve of the 5th bearing depending on the angle of rotation of the engine crankshaft, bearing clearance Z = 84 μm
Рисунок 4 – Схема полярной нагрузки главной втулки 5-го подшипника в зависимости от угла поворота коленчатого вала двигателя, зазора в подшипнике Z = 84 μm
Слика 4 – Поларни дијаграм оптерећења главног рикавца 5. лежаја зависоно од угла заокрета коленастог вратила мотора, зазор лежаја Z = 84 μm

In Figure 5, a graphical representation of the dynamic force (F) loading the bearing is given. Two dynamic pulses originating from the 4th and the 5th cylinder of the engine can be observed.

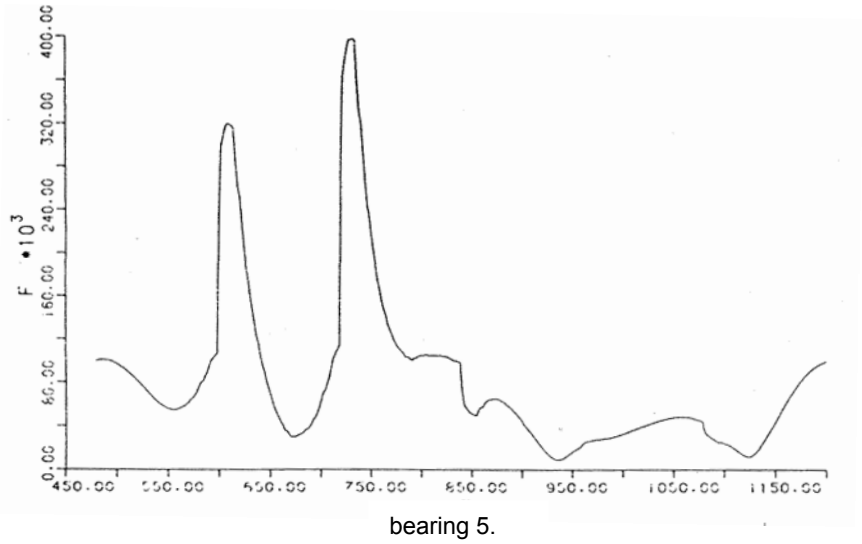

bearing 5.

Figure 5 – Change of the angle ((γ) and the load intensity of the main sleeve of the 5th bearing depending on the angle of rotation of the engine crankshaft
Рисунок 5 – Изменение угла ((γ) и интенсивности нагрузки главного рычага 5-го подшипника в зависимости от угла поворота коленчатого вала двигателя

Слика 5 – Промена угла (γ) и интензитета оптерећења главног рукавца 5. лежаја зависно од угла заокрета коленастог вратила мотора

Figure 6 shows the dynamic trajectory of the main bearing of the 5th bearing, on which the parameters of the dynamic trajectory are most pronounced, since it is the most loaded bearing.

The value of the radial clearance is Z = 144 μm.

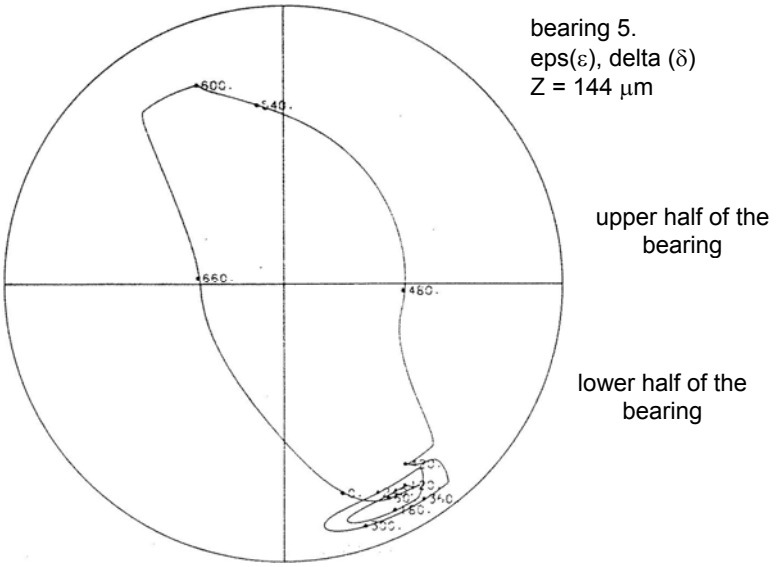

Figure 6 – Dynamic trajectory of the main sleeve of the 5th bearing, the radius of the radial clearance Z = 144 μm

Рисунок 6 – Динамическая траектория главной втулки 5-го подшипника, значение радиального зазора Z = 144 μm

Слика 6 – Динамичка путања главног рукавца 5.лежаја, вредност радијалног зазора Z = 144 μm

Figure 7 shows the parameters of the dynamic trajectory of the main sleeve of the 5th bearing, the value of the eccentricity (e) for various bearing wear values (Z = 84 μm, Z = 124 μm, Z = 144 μm) depending on the crankshaft rotation time. The displayed (e) values differ significantly depending on the bearing wear. The crankshaft rotation angles (α = 0° - 720°) are marked on the dynamic trajectory.

The eccentricity of the sleeve (e), measured in (μm), represents the distance of the center of the sleeve in relation to the geometric center of the bearing. The rotation time is measured in (ms). The eccentricity of the sleeve (e) and the parameter (δ), which represents the angle of the smallest thickness of the oil film (h_{0min}), are the basic parameters for the bearing wear diagnostics.

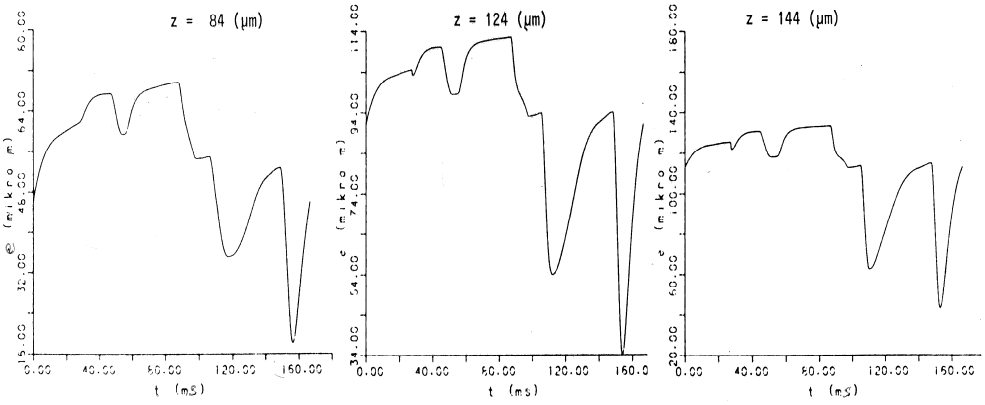

Figure 7 – Changing the eccentricity of the main bearing of the 5th bearing for various bearing wear values, depending on the rotation time of the engine crankshaft
Рисунок 7 – Изменение эксцентриситета основного подшипника 5-го подшипника при различном износе подшипника в зависимости от времени вращения коленчатого вала двигателя
Слика 7 – Промена ексцентрицитета главног рукавца 5. лежаја при разним истрошењима лежаја, зависно од времена ротације коленастог вратила мотора

Experimental research and the analysis of diagnostic parameters of plain bearings

The experimental research and the analysis of the diagnostic parameters related to the wear of plain bearings were performed on a marine diesel engine type 6ASL-25D, manufactured by SULZER - JUGOTURBINA - Karlovac.

The engine is in-line, 6-cylinder, four-stroke, turbocharged and water-cooled. The rated motor power at speed n=720min^{-1} is Pe=927kW.

In the research program, the influence of the clearance of the main sliding foundation bearings of the engine crankshaft was examined. On the same motor, 3 sets of bearings with radial clearance values of Z=84μm, Z=124μm, and Z=144μm were replaced in order to determine exclusively the influence of clearance on dynamic parameters and vibrations on the internal and external surfaces of the engine.

The test program was prepared in detail, setting out the general requirements that had to be met before and during research:

- before the start of the diesel engine, the hydraulic brake was calibrated in the engine test station,

- the crankshaft sleeves of the engine must not have residual magnetism, since non-contact probes for measuring the displacement of the sleeve work on the inductive principle,

- the fuel supply system was set on the engine to have a more even supply of fuel in order to achieve a minimum difference in pressure on the engine cylinders, due to fuel combustion,

- compression pressure was measured in all engine cylinders,

- pressure measurement was performed at the end of the combustion process in all engine cylinders,

- all electronic measuring equipment was calibrated before and during the measurements and the analysis. For this purpose, the characteristics of the measuring equipment and the calibration factors were determined, which were taken into account during the measurement and the analysis, and

- during the measurement, the temperature of oil and water was constantly maintained. The data were entered into measurement protocols. In this way, other influences on the results of measuring diagnostic parameters were eliminated.

The measuring points on the engine were determined and the diagnostic parameters to be measured were defined, which can be seen from the illustration in Figure 8.

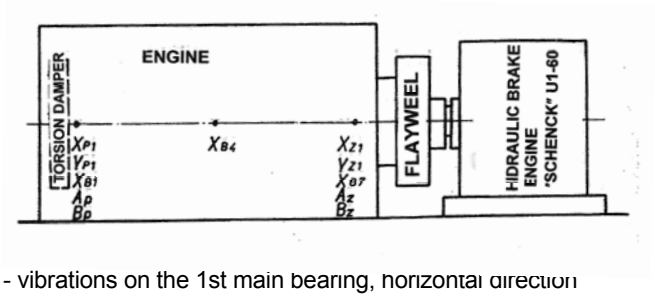

Xp1 - vibrations on the 1st main bearing, horizontal direction
Yp1 - vibrations on the 1st main bearing, vertical direction
Xb1 - vibrations on the side bolt of the 1st main bearing, horizontal direction
Ap, Bp - displacement of the center of the sleeve of the 1st main bearing, direction of the probes Ap and Bp
Xb4 - vibrations on the side screw of the 4th main bearing, horizontal direction
Xz1 - vibrations on the 7th main bearing, horizontal direction
Yz1 - vibrations on the 7th main bearing, vertical direction
Xb7 - vibrations on the side bolt of the 7th main bearing
Az, Bz - displacement of the center of the sleeve of the 7th main bearing, direction of the probes Az and Bz

Figure 8 – Arrangement of the measuring points on the engine 6 ASL-25D
Рисунок 8 – Расположение точек замера на двигателе 6 ASL-25D
Слика 8 – Распоред мерних места на мотору 6 ASL-25D

Figure 9 specifically shows the measuring points on the engine crankshaft on which the probes for measuring the dynamic trajectory of the sleeves on the 1st and 7th main bearings are placed. The dashed line on the cross section of the sleeve ″C - C″ shows the deviation from the circular shape of the sleeve.

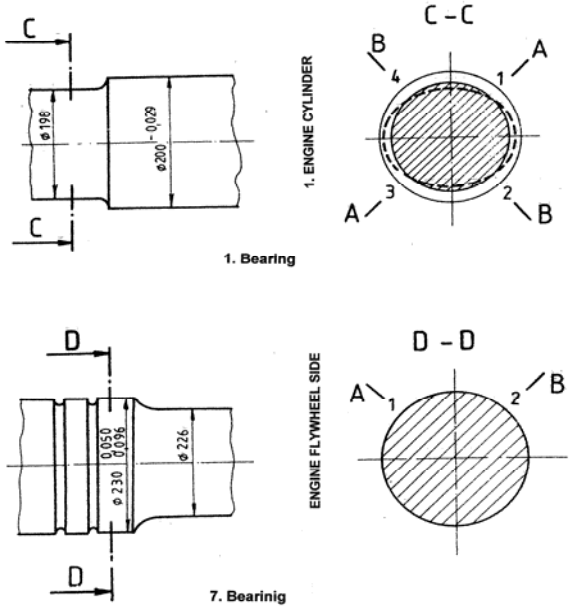

Figure 9 – Display of the measuring points with the positions of the probes for measuring the dynamic paths of the main sleeve
Рисунок 9 – Отображение точек измерения, где расположены датчики для измерения динамических траекторий главных рычагов
Слика 9 – Приказ мерних места на којима су постављене сонде за мерење динамичких путања главних рукаваца

The probes for measuring the dynamic trajectory are centered using a centering device (Žegarac, 1989), (Žegarac, 1993) or using an electronic centering device from the Swedish company Damalini (Easy-Laser, 2020). Centering non-contact probes is very important for the measurement procedure and for obtaining accurate results.

Probes for measuring the temperature of all bearings are placed in the lower covers of the main bearings. An overview of the measuring points is given in Figure 10.

The measuring device Hotinger Boldwin - Messtechnik UPM - 60 and thermometers PT-100 ATM - Zagreb were used for temperature measurement. The symbol (Tu) indicates the coolant temperature at the engine inlet and (Ti) indicates the fluid temperature at the engine outlet.

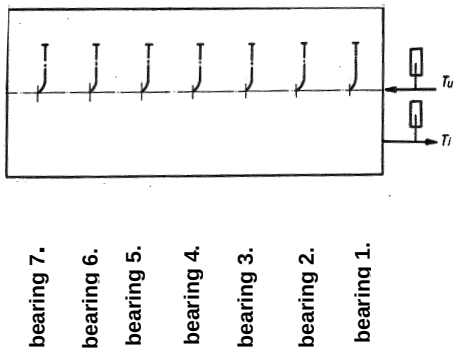

Figure 10 – Overview of the measuring points where the temperature measurement of the main bearings of the engine crankshaft was performed

Рисунок 10 – Обзор точек измерения, где проводилось измерение температуры главных подшипников коленчатого вала двигателя

Слика 10 – Преглед мерних места на којима је извршено мерење температуре главних лежајева коленастог вратила мотора

Temperature was measured on the main bearings in all engine operating modes. In the no-load mode, at various speeds, the temperature values were in the range of 60 - 70 °C, on almost all bearings. In the engine load mode of 20 - 110%, the temperature values were from 65 - 80 °C.

The temperature values in this case were almost the same, even on the busiest 5th main bearing.

The temperature change is shown in Figure 11. The temperature regime of the engine was under strict control, since the engine was tested at the maximum bearing clearance of Z = 144 μm.

bearing 5.

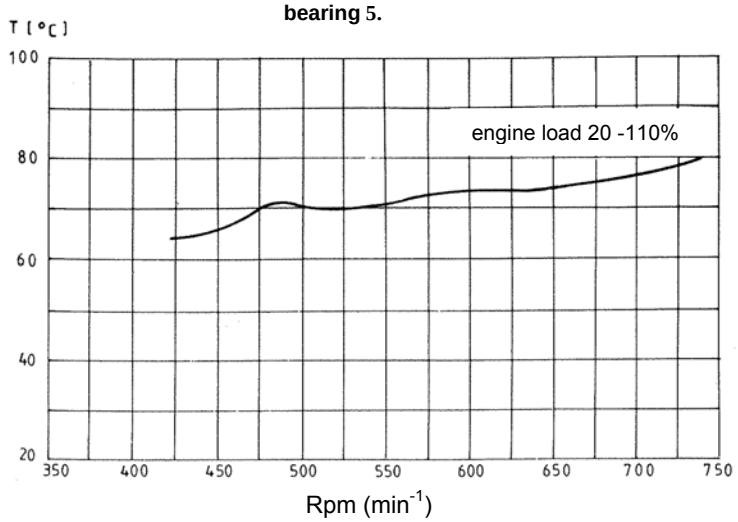

Figure 11 – Temperature change on the 5th main bearing depending on the engine load
Рисунок 11 – Изменение температуры на 5-м главном подшипнике в зависимости от нагрузки двигателя
Слика 11 – Промена температуре на 5. главном лежају зависно од оптерећења мотора

Figure 12 shows a scheme for measuring the vibration characteristics of the engine.

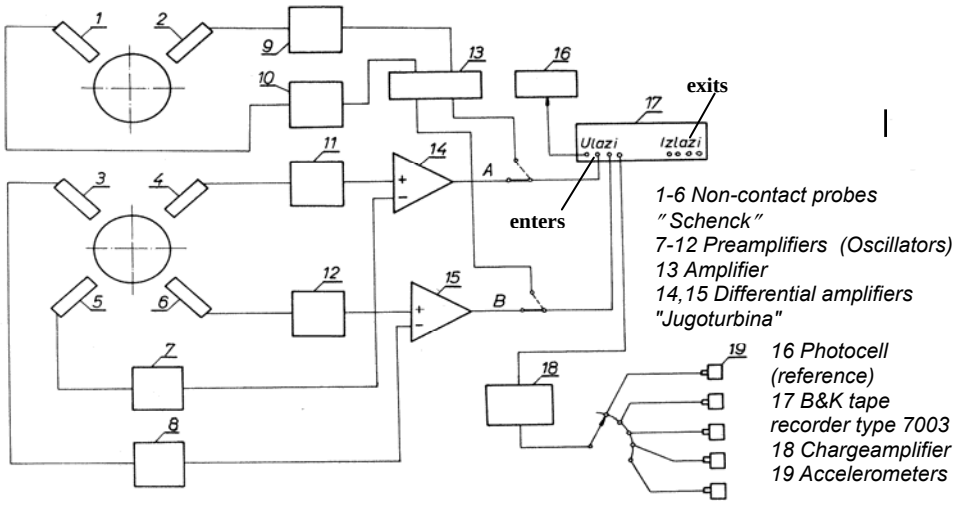

Figure 12 - Scheme of measuring the vibration characteristics of the engine 6ASL -25D
Рисунок 12 - Схема измерения вибрационных характеристик двигателя 6ASL-25D
Слика 12 - Шема мерења вибрацијских карактеристика мотора 6ASL -25D

Figure 13 shows the non-contact probes of the German company *"Schenck"* for measuring the dynamic trajectory of the main sleeve bearing. The probes are of different sizes so that measurements can be carried out depending on the dimensions and the place where they are placed. They can be standard versions or with built-in oscillators.

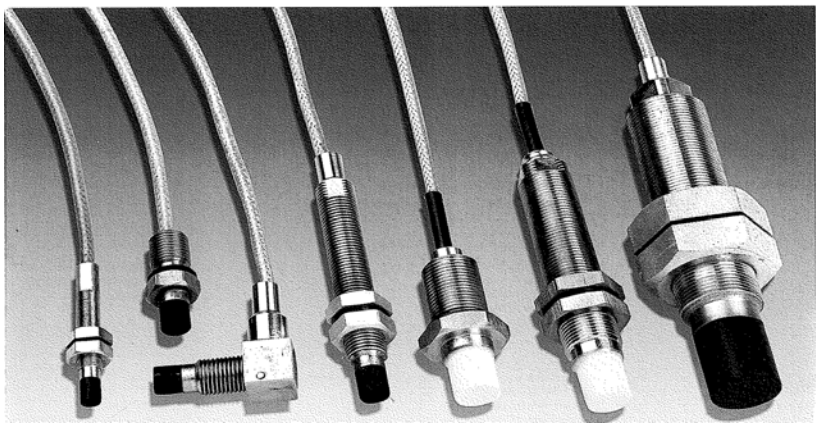

Figure 13 – Non-contact probes for measuring the dynamic paths of the main sleeve
Рисунок 13 – Бесконтактные датчики для измерения динамических траекторий главных рычагов
Слика 13 – Бесконтактне сонде за мерење динамичких путања главних рукаваца

Starting from the theoretical bases, the defined methods of testing and the analysis, the engine tests provided by the program were carried out and the experimental research results were obtained.

In the first moment, no agreement was reached between the measured dynamic trajectory on the 1st main bearing and the calculated trajectory. A detailed analysis was performed, based on which it was concluded that, when measuring and processing the signal, the irregularity of the circular shape of the sleeve, marked in Figure 9 with a dashed line at the cross section of the sleeve "C - C", should be taken into account.

This part of the sleeve is not intended to be machined more precisely during machining, as it is located outside the plain bearing.

The part of the sleeve that is inside the bearing is very precisely processed. Its deviation from the circular shape is 5 μm.

The deviations from the circular shape of sleeve 1 of the main bearing are shown in Table 1, on the basis of which the results of the dynamic trajectory measurements were corrected.

Based on the results of the research, engine manufacturers could be recommended to precisely process these parts of the crankshaft, in order to simplify the procedure of diagnosing the engine.

More precise machining would not make the production process more expensive.

Table 1 – Deviations from the circular shape of the sleeve of the 1st main bearing of the engine crankshaft in (mm)
Таблица 1 – Отклонения от круглой формы втулки 1-го главного подшипника коленчатого вала двигателя в (мм)
Табела 1 – Одступања од кружног облика рукавца 1. главног лежаја коленастог вратила мотора у (mm)

Nominal sleeve size ∅ 198 mm			
Crankshaft rotation angle ($\alpha°$)	Nominal sleeve size	Crankshaft rotation angle ($\alpha°$)	Nominal sleeve size
0*)	+0.001	190	+0.012
10	+0.002	200	+0.035
20	+0.003	210	+0.039
30	+0.004	220	+0.031
40	+0.004	230	+0.031
50	+0.008	240	+0.028
60	+0.013	250	+0.026
70	+0.006	260	+0.020
80	+0.024	270	+0.018
90	+0.027	280	+0.017
100	+0.036	290	+0.011
110	+0.035	300	+0.008
120	+0.015	310	+0.003
130	+0.013	320	0.000
140	+0.035	330	-0.002
150	+0.023	340	-0.005
160	+0.012	350	-0.007
170	+0.013	360	-0.004
180	+0.033	*) The piston of the 1st cylinder of the engine is located in the top dead center (TDC)	

The results of the calculations and the measurements were not particularly affected by crankshaft deformations and additional inertial moments shown in Figure 13.

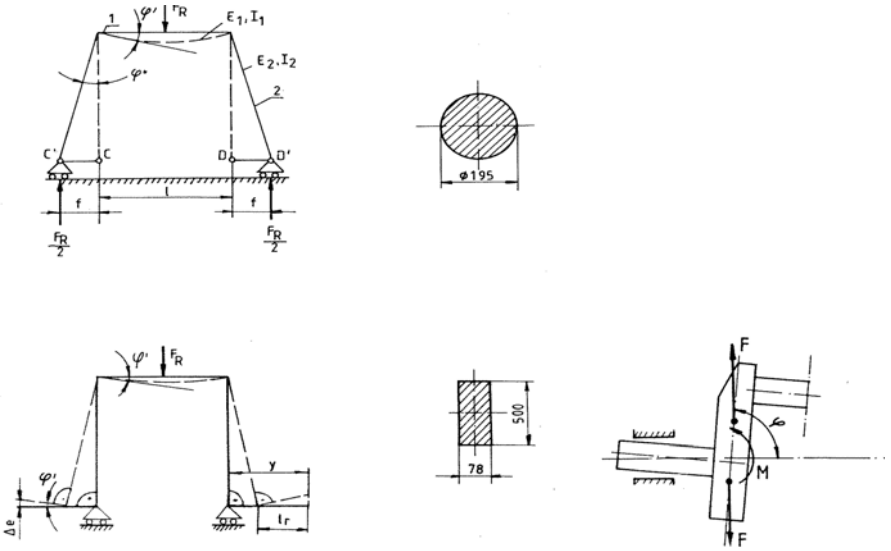

Figure 13 – Deformations of the engine crankshaft and the influence of additional inertial moments

Рисунок 13 – Деформации коленчатого вала двигателя и влияние дополнительных инерционных моментов

Слика 13 – Деформације коленастог вратила мотора и утицај додатних инерционих момената

In Figure 14, the dynamic trajectory of the 1st main bearing is shown.

In the graphical display of the dynamic path, several engine operating cycles are shown.

The paths on the diagram are shown with several lines and the crankshaft rotation angle is indicated (α= 0° – 720°). It can be seen that there is very little difference in paths per engine cycle.

The engine is well tuned, the engine speed is stable.

The agreement of the calculation and measurement results is in the range of 5%.

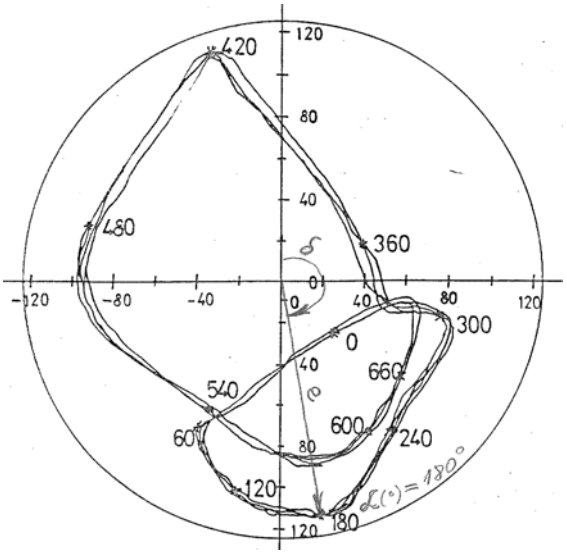

Figure 14 – Display of the measured dynamic sleeve trajectory on the 1st main bearing of the crankshaft, at the engine load of 100%, n = 720 min^{-1}, and the bearing clearance Z=124 (μm)

Рис. 14 – Изображение измеренной динамической траектории рукава в первом главном подшипнике двигателя коленчатого вала, при нагрузке на двигатель (100%), n = 720 мин$^{-1}$, зазор подшипника Z = 124 (μm)

Слика 14 – Приказ измерене динамичке путање рукавца на првом главном лежају мотора коленастог вратила мотора при оптерећењу мотора (100%), n = 720 min^{-1}, зазор лежаја Z=124 (μm)

Based on the measurement results, the dependence of the displacement of the center of the sleeve (e) and the clearance (Z) was determined when driving the engine with and without load in the form (Žegarac, 2020):

$$Z = 1.01 \cdot e + 7{,}48 \pm 4 \qquad (4)$$

Previous research on the wear of vital parts of internal combustion engines has shown that crankshaft bearings wear evenly provided that all

engine lubrication conditions are met (Žegarac, 1989). An indicator of bearing wear is sufficient, if diagnostic parameters are measured on any bearing.

Figure 15 shows the measured dynamic trajectory of the main sleeve on the 7th engine bearing. With increasing clearance, at different speeds and motor loads, differences in dynamic trajectory are observed, but there is no coincidence of the calculation and measurement results.

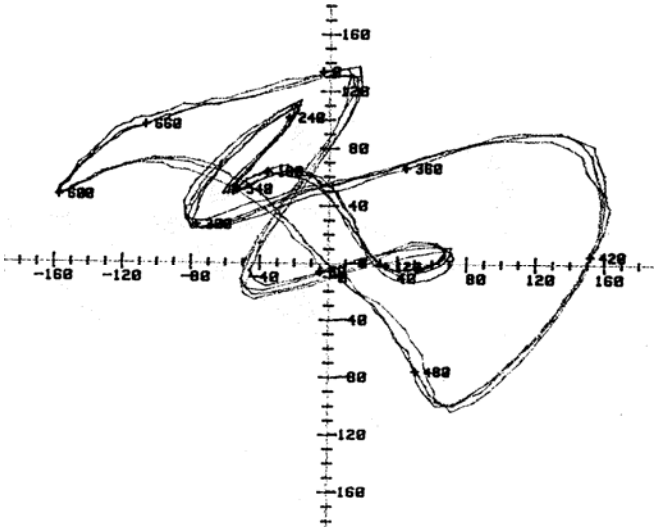

Figure 15 – Dynamic trajectory of the main sleeve on the seventh bearing of the engine crankshaft, engine load 100%, bearing clearance Z = 144 μm, rotation speed n = 720 min^{-1}

Рисунок 15 – Динамическая траектория основного рычага на седьмом подшипнике коленчатого вала двигателя, нагрузка двигателя 100%, зазор подшипника Z = 144 μm, частота вращения n = 720 мин$^{-1}$

Слика 15 – Динамичка путања главног рукавца на седмом лежају коленастог вратила мотора, оптерећење мотора 100%, зазор лежаја Z = 144 μm, брзина вртње n = 720 min^{-1}

The dynamic trajectory was measured on the part of the sleeve located on the outside of the engine block.

The shape of the dynamic trajectory was influenced by static and dynamic deformations of the crankshaft due to the weight of the engine flywheel.

The illustration is given in Figure 16. It would probably be possible to measure dynamic trajectories on this part of the engine crankshaft in multi-cylinder engines that do not have flywheels since such engines are dynamically balanced due to a larger number of engine cylinders.

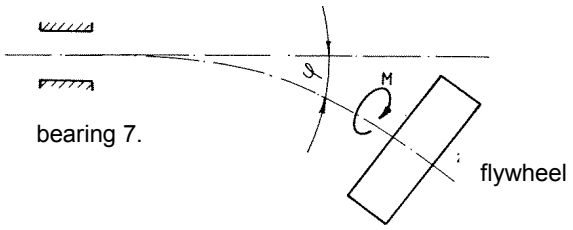

Figure 16 – Deformations of the main sleeve on the 7th bearing of the engine crankshaft

Рисунок 16 – Деформации главного рычага седьмого подшипника коленчатого вала двигателя

Слика 16 – Деформације главног рукавца на 7. лежају коленастог вратила мотора

The vibration parameters were measured at 7 measuring points, on the inner and outer surfaces of the engine (shown in Figure 8):

Xp1 - vibrations on the 1st main bearing, horizontal direction,
Yp1 - vibrations on the 1st main bearing, vertical direction,
Xb1 - vibrations on the side bolt of the 1st main bearing, horizontal direction,
Xb4 - vibrations on the side screw of the 4th main bearing, horizontal direction,
Xz1 - vibrations on the 7th main bearing, horizontal direction,
Yz1 - vibrations on the 7th main bearing, vertical direction, and
Xb7 - vibrations on the side bolt of the 7th main bearing.

Based on the results of measuring the vibration parameters, it was determined that the highest vibration levels are at measuring point 3, (Figure 17), Xb1, horizontal direction, on the side screw that fastens the lower cover of the main bearing in the engine block. Figure 17 shows the

effective values of the vibration velocity Vef (mm/s), harmonic of the 1st order, at different speeds and motor loads, when the bearing clearance is Z= 144 μm. It was concluded that the frequency components (harmonics) of 0.5 and 1. order are most related to bearing wear. The harmonics of 1.5, 2, 2.5, 3 and 3.5 are less pronounced. The intensity of vibrations is related to the variable excitation forces from the bearing to the bearing in the horizontal and vertical planes of the engine. It was found that the higher level of vibration is in the horizontal plane of the engine, on the side of the 1st cylinder of the engine, which is significantly contributed by large weights of the parts located on the engine crankshaft - torsional vibration damper on the front of the engine whose weight is Gp = 3558 (N) and the parts on the side of the 6th engine cylinder - the gear that drives the systems on the engine whose weight is Gzu = 1176 (N) and the engine flywheel weight of Gz = 7106 (N).

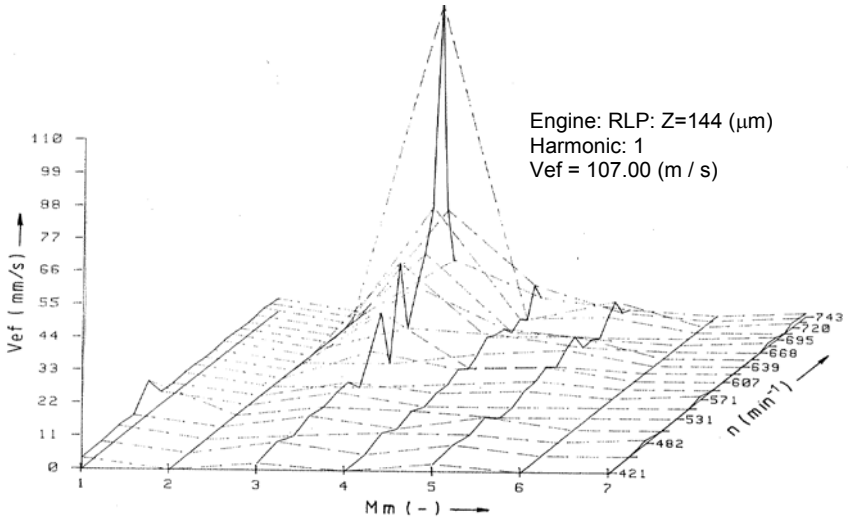

Figure 17 – Effective value of the vibration speed (Vef) for different measuring points at different speeds and motor loads

Рисунок 17 – Эффективное значение скорости вибрации (Vef) для различных точек измерения при разных скоростях и нагрузках двигателя

Слика 17 – Ефективна вредност вибрацијске брзине (Vef) за разна мерна теста при различитим брзинама вртње и оптерћењу мотора

Many reputable companies deal with technical diagnostics of sliding bearings. Some well-known companies are Bently Nevada, Emerson

Electric, Brüel & Kjær and others, whose systems are installed on hydroelectric power plants, thermal power plants and other facilities.

In these systems, a problem is created by the roto group in the system: there is a mechanical, electrical and hydraulic imbalance of the rotor. Figure 18 shows a bearing housing on which non-contact probes for measuring dynamic paths of roto systems are mounted, according to the configuration of Bently Nevada (Bently Nevada Corporation, 1987).

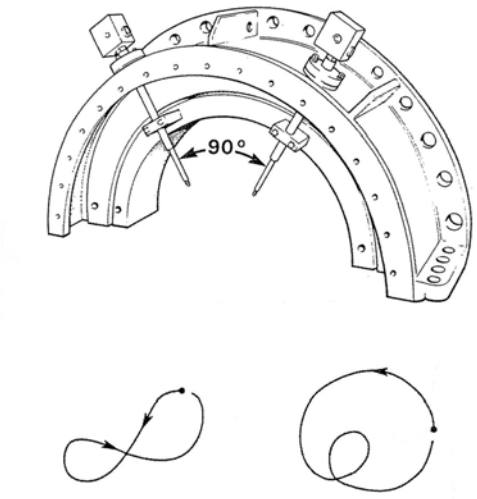

Figure 18 – View of the bearing cover showing the non-contact probes for measuring the dynamic path according to the configuration of the Bently Nevada company

Рисунок 18 –- Вид крышки подшипника, показывающий бесконтактные датчики для измерения динамического пути в соответствии с конфигурацией компании Bently Nevada

Слика 18 – Поглед на поклопац лежаја који приказује бесконтактне сонде за мерење динамичке путање по конфигурацији фирме Bently Nevada

Conclusion

The reliability and durability of internal combustion engines and other engines is a function of correct operation and durability of individual parts, of which plain bearings are especially important. Besides being influenced by construction dimensions and types of lubricating oil, wear intensity of plain bearings is also affected by operating conditions and system maintenance. The mutual influences of the parameters describing

the wear of plain bearings are very complex and cannot be reliably described mathematically. Therefore, simplified mathematical models, used to describe these phenomena, give approximate bearing wear functions.

With the development of the method of calculation of plain bearings, which determines the data on the function and construction parameters of bearings (oil film thickness, forces on the bearing), it was found out which bearing is the most loaded. At this measuring point, the dynamic parameters related to the increase of the clearance in the bearing are most pronounced, although in reality all bearings are worn evenly, if all the conditions for lubrication of plain bearings are met.

The original mathematical formulas that determine the dimensions of clearance in the bearing based on measurements are completely reliable. Lang's approximate formulas for non-stationary bearing loading were used.

Modeling dynamic models of internal combustion engines was used as an example to describe all engine dynamic parameters in a completely new way. Based on that, the results of the calculation and the measurements of the dynamic parameters were verified and the deviations were within the range of 5%.

Experimental methods are the most authoritative for the final assessment of bearing wear. Based on the performed measurements of the dynamic trajectory of the sleeve and the vibration parameters on the inner and outer surfaces, the actual state is determined without disassembling assemblies and detailed inspections.

Measurement of the dynamic trajectories of the bearing sleeve is performed using non-contact probes. Measurements can be made with 1 contactless probe or with 2 and 4 of them. Contactless probes are installed on special supports which are fixed in the immediate vicinity of the measuring point. If access to the bearing is limited (due to small bearing dimensions), probes can be installed in the bearing housing.

It is especially important to measure the vibration parameters on the inner and outer surfaces of the engine that are directly related to the clearance in the sliding bearing. The choice of vibration parameters and measuring points is important. This method has a number of advantages over other diagnostic methods, as it is easy to access the measuring points.

A database related to the degree of bearing wear should be created for each diagnostic case. Engines differ significantly in construction, operating conditions and load. It is important to strictly adhere to the norms set by the system manufacturers regarding when plain bearings

have to be changed, i.e. when bearing wear reaches the wear limit values.

In the final assessment of the technical condition, the vibration standards from the prescribed vibration standards (ISO, 1974, 1995) must be taken into account, due to the fact that drive systems are coupled with other assemblies in mechanical and electrical systems, which can interactively affect the operation of the whole system.

The spectral and correlation analysis of signals obtained on the basis of measuring vibration parameters on internal and external surfaces singles out frequency components related to wear of plain bearings, at different speeds and operating modes without load and with motor load. The diagnostic method does not require special preparations and auxiliary devices for the installation of the measuring system. Measurements are performed very simply and reliably. Repeatability of the measurement results was achieved.

The person performing the diagnosis must have top knowledge and experience in this field in order to qualitatively select diagnostic parameters and measuring points, assess the factors influencing the measurement results and analyze the measured quantities.

New diagnostic methods can determine bearing wear accurately enough. New diagnostic methods and monitoring systems have a wide range of possibilities of application: internal combustion engines, all piston machines, hydroelectric power plants, thermal power plants, process plants, and other plants. The new monitoring system for sliding bearing diagnostics offers hardware and software support to various systems for monitoring and checking the compatibility of devices and equipment of many manufacturers, which are used for plant technical diagnostics.

References

-Bently Nevada Corporation. 1987. *Turbine Supervisory Instrumentation Brochure, L2016, february.* Nevada, US: Bently Nevada Corporation.

Cohn-Sfetcu, S., Smith, M.R., Nichols, S.T. & Henry, D.L. 1975. A digital technique for analyzing a class of multicomponent signals. *Proceedings of the IEEE*, 63(10), pp.1460-1467. Available at: https://doi.org/10.1109/PROC.1975.9975.

-Easy-Laser. 2020. *Laser measurement & alignment systems. Technical documentation.* Damalini, Sweden: Easy-Laser.

Fertis, D.G. 1973. *Dynamics and Vibrations of Structures*. New York: John Wiley & Sons.

Genkin, M.D. & Sokolova, A.G. 1987. *Vibroakusticheskaya diagnostika mashin i mekhanizmov*. Moscow: Mashinostroenie (in Russian). (In the original: Генкин, М.Д., Соколова А.Г. 1987. *Виброакустическая диагностика машин и механизмов.* Машиностроение: Москва).

-ISO. 1974. *ISO 2372:1974 Mechanical vibration of machines with operating speeds from 10 to 200 rev/s - Basis for specifying evaluation standards* [online]. Available at: https://www.iso.org/standard/7212.html [Accessed: 12 June 2020].

-ISO. 1995. *ISO 10816-1:1995 Mechanical vibration - Evaluation of machine vibration by measurements on non-rotating parts - Part 1: General guidelines* [online]. Available at: https://www.iso.org/standard/18866.html [Accessed: 12 June 2020].

Lang, O.R. & Steinhilper, W. 1978. *Gleitlager*. Berlin, Heidelberg: Springer-Verlag (in German). Available at: https://doi.org/10.1007/978-3-642-81225-5.

Miroshnikov, L.V., Boldin, A.P. & Pal, V.I. 1977. *Diagnostirovaniye tekhnicheskogo sostoyaniya avtomobiley na avtotransportnykh predpriyatiyakh*. Moscow: Tehnika (in Russian). (In the original: Мирошников, Л.В., Болдин, А.П., Пал В.И. 1977. *Диагностирование технического состояния автомобилей на автотранспортных предприятиях*. Москва: Транспорт).

Schiffbänker, H. & Gerhard, E.T. 1988. Automatische Gutekontrole an Verbrennungsmotoren auf Basis von Schingungs Informationen. *MTZ - Motortechnische Zeitschrift*, 49(2) (in German).

Thomson, W.T.1983. *Theory of Vibration with Applications, Second edition*. London: George Allen & Unwin Ltd.

Vasilyev, Yu.N., Beskletnyy, M.Ye., Igumentsev, Ye.A. & Khristenzen, V.L. 1987. *Vibratsionnyy kontrol' tekhnicheskogo sostoyaniya gazoturbinnykh gazoperekachivayushchikh agregatov*. Moscow: Nedra (in Russian). (In the original: Васильев, Ю.Н., Бесклетный, М.Е., Игуменцев, Е.А., Христензен, В.Л. 1987. *Вибрационный контроль технического состояния газотурбинных газоперекачивающих агрегатов*. Москва: Недра).

Zhdanovskiy, N.S. 1966. *Bestormoznyye ispytaniya traktornykh dvigateley*. Moscow, Leningrad: Mashinostroenie (in Russian). (In the original: Ждановский, Н.С. 1966. *Бестормозные испытания тракторных двигателей*. Москва, Ленинград: Машиностроение).

Zhdanovskiy, N.S. 1977. *Diagnostika avtotraktornykh dvigateley*. Leningrad: Kolos (in Russian). (In the original: Ждановский, Н.С. 1977. *Диагностика автотракторных двигателей*. Ленинград: Колос).

Žegarac, N. 1989. *Dijagnostika kliznih ležajeva u dizel motoru* (in Serbian). Ph.D. thesis. Zagreb: University of Zagreb, Faculty of Mechanical Engineering and Naval Architecture.

Žegarac, N. 1993. *Postupak dijagnostike ležajeva merenjem dinamičkih putanja glavnih rukavaca, kolenastog vratila* (in Serbian). Serbian Patent number P-640/93.

Žegarac, N. 2020. Development of a method for determining the size of clearance in sliding bearings. *Vojnotehnički glasnik/Military Technical Courier*, 68(3), pp.530-553. Available at: https://doi.org/10.5937/vojtehg68-26107.

АНАЛИЗ ФАКТОРОВ ВЛИЯНИЯ, КОТОРЫЕ МОГУТ ПРИЧИНИТЬ ОШИБКИ ПРИ ПРИМЕНЕНИИ СОВРЕМЕННЫХ МЕТОДОВ ДИАГНОСТИКИ СКОЛЬЗЯЩИХСЯ ПОДШИПНИКОВ НА МАШИНОСТРОИТЕЛЬНЫХ И ЭЛЕКТРОСТАНЦИЯ

Никола П. Жегарац

Сербская академия изобретателей и ученых,
г. Белград, Республика Сербия

РУБРИКА ГРНТИ: 55.00.00 МАШИНОСТРОЕНИЕ:
55.45.00 Судостроение,
44.00.00 ЭНЕРГЕТИКА
ВИД СТАТЬИ: оригинальная научная статья

Резюме:

Введение/цель: В статье представлено применение современных методов диагностики подшипников скольжения и анализ влияющих факторов, которые могут вызвать ошибки в применении. Представлены возможности надежного определения того, когда и где возникнет проблема, возникающая при износе подшипников скольжения при дальнейшей эксплуатации установки.
Определяется, как система будет продолжать функционировать с течением времени, прогнозируются причины сбоев и способы их

устранения, а также время планового технического обслуживания технических систем.

Метод. Новый метод решает проблему диагностики подшипников скольжения путем измерения динамических траекторий муфты в подшипнике скольжения и измерения параметров вибрации на внутренней и внешней поверхностях установки. Измерение динамических траекторий опорной втулки осуществляется с использованием бесконтактных датчиков. Центрирование зондов относительно геометрического центра подшипника очень важно. Параметры вибрации измеряются на внутренней и наружной поверхностях установки, которые непосредственно связаны с зазором в подшипнике скольжения. Выбор параметров вибрации и точек измерения очень важен. Этот метод имеет ряд преимуществ по сравнению с другими методами диагностики, поскольку он имеет легкий доступ к точкам измерения.

Результаты: Путем измерения динамической траектории (траектории) втулок в подшипнике скольжения, параметров вибрации на внутренней и наружной поверхностях определяются размеры зазора в подшипнике, которые характеризуются: нормальным состоянием, начальным размером зазора, его дальнейшим увеличением, размерами зазора в подшипнике, когда параметры состояния близки к верхнему пределы зазора подшипника.

Вывод: новые методы диагностики и системы контроля могут широко применяться: на двигателях внутреннего сгорания, на всех поршневых машинах, гидроэлектростанциях, тепловых электростанциях, технологических установках и многих других установках.

Ключевые слова: техническая диагностика, подшипник скольжения, зазор подшипника, износ подшипника, головка подшипника, динамическая траектория.

АНАЛИЗА УТИЦАЈНИХ ФАКТОРА КОЈИ МОГУ ПРОУЗРОКОВАТИ ГРЕШКЕ У ПРИМЕНИ САВРЕМЕНИХ МЕТОДА ДИЈАГНОСТИКЕ КЛИЗНИХ ЛЕЖАЈЕВА У МАШИНСКИМ И ЕЛЕКТРО ПОСТРОЈЕЊИМА

Никола П. Жегарац
Српска академија изумитеља и научника, Београд, Република Србија

ОБЛАСТ: машинство, енергетика, бродоградња
ВРСТА ЧЛАНКА: оригинални научни рад

Сажетак:

Увод/циљ: У раду је дат приказ примене савремених дијагностичких метода клизних лежајева и анализа утицајних фактора који могу проузрокавти грешке у примени. Приказане су могућности да се поуздано утврди када и где ће се појавити проблем који се јавља при трошењу клизних лежајева у даљој експлоатацији постројења. Утврђује се како ће систем наставити да функционише током времена, предвиђају се узроци кварова и начин њиховог отклањања, као и време за планско одржавање техничких система.

Методе: Нова метода решава проблем дијагностике клизних лежајева, мерењем динамичких путања рукавца у клзном лежају и мерењем вибрацијских параметара на унутрашњим и вањским површинама постројења. Мерење динамичких путања рукавца лежаја врши се помоћу бесконтактних сонди. При томе је веома важна центрација сонди у односу на геометријски центар лежаја. Врши се мерење вибрацијских параметара на унутрашњим и вањским површинама постројења који су у директној вези са зазором у клизном лежају. При томе је веома важан избор вибрацијских параметара и мерних места. Ова метода има низ предности у односу на друге дијагностичке методе, пошто је једноставан приступ мерним местима.

Резултати: Мерењем динамичке путање (трајекторије) рукаваца у клизном лежаји, вибрацијских параметара на унутрашњим и вањским површинама, утврђују се величине зазора лежаја које карактеришу: нормално стање, почетну величину зазора, његово даље повећавање, величине зазора лежаја, када су параметри стања близу горње границе дозвољеног зазора лежаја.

Закључак: Нове дијагностичке методе и мониторниг системи могу се широко применити: на моторима са унутрашњим сагоревањем, на свим клипним машинама, хидроелектранама, термоелектранама, процесним постројењима и многим другим постројењима.

Кључне речи: техничка дијагностика, клизни лежај, зазор лежаја, истрошење лежаја, рукавац лежаја, динамичка путања.

Paper received on / Дата получения работы / Датум пријема чланка: 27.06.2020.
Manuscript corrections submitted on / Дата получения исправленной версии работы / Датум достављања исправки рукописа: 28.09.2020.
Paper accepted for publishing on / Дата окончательного согласования работы / Датум коначног прихватања чланка за објављивање: 30.09.2020.

ADVANCE IN ULTRASONIC SPRAY PYROLYSIS (USP) FOR THE SYNTHESIS OF GOLD NANOPARTICLES

Srećko R. Stopić[a], *Bernd* G. Friedrich[b]
RWTH Aachen University, IME Process Metallurgy and Metal Recycling, Aachen, Federal Republic of Germany
[a] e-mail: sstopic@ime-aachen.de, **corresponding author**, ORCID iD: https://orcid.org/0000-0002-1752-5378
[b] e-mail: bfriedrich@ime-aachen.de, ORCID iD: https://orcid.org/0000-0002-2934-2034

DOI: 10.5937/vojtehg68-27948; https://doi.org/10.5937/vojtehg68-27948

FIELD: Chemical technology
ARTICLE TYPE: Original scientific paper

Summary:

Introduction/purpose: Ultrasonic spray pyrolysis (USP) is usually used for the preparation of submicronic and nanosized gold powders. This is a simple method for a synthesis from an aerosol containing dissolved metallic salts such as gold chloride, gold nitrate, and gold-acetate, obtained in the ultrasonic field using frequencies ranging from 0.8 to 2.5 MHz.

Methods: The USP method combines aerosol formation in an ultrasonic field, transport of an aerosol with a carrier gas to the reactor and final reduction of $HAuCl_4$ with a used gas such as hydrogen and carbon monoxide. The thermal decomposition of gold acetate takes place in a neutral atmosphere such as nitrogen and argon at elevated temperatures. The chemical reduction of $HAuCl_4$ takes place in the aqueous phase using sodium citrate and sodium boride after heating water solution.

Results: Powders of gold were obtained at room temperature using hydrogen reduction in an ultrasonic field at room temperature from $HAuCl_4$ using a frequency of 0.8 MHz. The obtained gold particles were analysed using scanning electron microscopy (SEM) and energy disperse spectroscopy (EDS). The formed particles are round and agglomerated. An increase in temperature to 260°C and 500°C leads to the formation of spherical and cylindrical gold particles.

ACKNOWLEDGEMENT: The author would like to thank Mr. Sava Maksimovic and Prizma Company, Kragujevac, Serbia, for their continuous support in the synthesis of nanosized gold particles and for their permission to use some photos from their deveopment programme focusing on a new ultrasonic generator and a USP horizontal experimental setup.

Conclusion: New improved equipment for an ultrasonic spray pyrolysis synthesis of gold powder from $HAuCl_4$ with hydrogen reduction was offered by PRIZMA, Kragujevac, Serbia, enabling a controlled reduction process with better prevention of piezo transducers in an ultrasonic field and increased aerosol production and its transport to the reaction furnace.

Key words: gold, advancement, ultrasonic spray pyroylsis, synthesis.

Introduction

Various strategies are used for the synthesis of gold nanoparticles. Traditionally, physicochemical techniques have increased environmental concerns due to the reduction of metal ions followed by surface modification, toxic compounds added for stability, and dangerous by-products. The currently used nanoparticle synthesis based on chemical and physical methods at high temperature and pressure values, with reduced introduction of stabilizing agents, asks for a new nanoparticle synthesis based on improved ultrasonic spray pyrolysis of water solutions at a room temperature and atmospheric pressure, in the presence of some additives and stabilizing agents. A green synthesis method provides a faster metallic nanoparticle production by offering an environmentally friendly, simple, economical, and reproducible approach.

Gold as a noble metal has resistance to corrosion and it is mostly used in jewellery and currency. Schmid and Corain (2003, pp.3081-3098) studied the synthesis, structures, electronics, and reactivity of gold nanoparticles. Both physical and chemical methods are usually used in order to produce gold nanoparticles. A decrease in the size of gold nanoparticles had dramatic consequences on their physical and chemical properties.

Gold nanoparticles can accelerate the oxidation processes better than micron-sized ones (Bond, 2008, pp.235-241). Examining the published results and especially the patents granted before 1978 reveals frequent observations of the potential of gold as a catalyst. (Qi, 2008, pp.224-234) reported the production of propylene oxide over nanosized gold catalysts in the presence of hydrogen and oxygen. Polte et al (2010, 1296-1301) reported the mechanism of gold nanoparticle formation in the classical citrate synthesis method derived from coupled in situ XANES and SAXS Evaluation. The same method was used by Turkevich in 1953 (Turkevich et al, pp.670-673). This method confirmed good quality control of the particle size, in the range between 22 and 120 nm. A big disadvantage of the citrate method is that high excess remains in the final solution. The residual citrate and sodium in the solution, acting as a

passivation layer on the surface of nanosized gold, reduce the effectiveness of surface functionalization with other biological markers.

The efficient recovery of scraps and wastes in gold jewellery manufacture is a vital component of a profitable manufacturing business, irrespective of whether it is a large factory or a small, traditional workshop (Corti, 2002, pp.111-130). Possible techniques for gold purification contain: 1) cupellation, 2) Miller chlorination process, Wohlwill electrolytic process, 3) Fizzer cell, 4) solvent extraction, 5) Aqua regia process, and 6) pyrometallurgical process. The process for recovering gold from a chloride solution involves adding finely divided activated carbon to the solution for the reduction of gold metal and subsequent absorption of gold metal by carbon (Piret et al, 1977). The most used methods for the synthesis of gold powder are presented in Table 1.

Table 1 – Most used methods for the synthesis of gold powder
Таблица 1 – Наиболее распространенные методы получения золотого порошка
Табела 1 – Најчешће коришћене методе за синтезу праха од злата

Author	Method	Precursor	Reducing agent	Particle Size (nm)
(Schmid & Corain, 2003, pp.3081-3098)	Reduction	$HAuCl_4$	P	Spherical
(Polte et al, 2010, pp.1296-1301)	Reduction	$HAuCl_4$	$Na_3C_6H_5O_7$	- Spherical - below 100 nm
(Piret et al, 1977)	Reduction, precipitation	Precious metal containing chloride leach	Zn, Fe	- Agglomerated irregular form - above 1000 nm
(Young et al, 2011)	Reduction	$HAuCl_4$	CO	Spherical 2-100 nm
(Tréguer-Delapierre, 2008, pp.195-207)	Reduction	$HAuCl_4$	$NaBH_4$	-Non-spherical -below 100 nm
(Rudolf et al, 2012, pp.595-612)	Ultrasonic spray pyrolysis &reduction	Water solution after dissolution of jewellery scrap in HNO_3/HCl	H_2	- Spherical, cylindrical, triangular - below 100 nm
(Turkevich et al, 1953, pp.670-673)	Reduction in an aqueous phase	$HAuCl_4$	$Na_3C_6H_5O_7$	Spherical 20-150 nm

Young et al (2011) reported on a successful hydrometallurgical production of nanosized gold from $HAuCl_4$ using carbon monoxide gas as

a selective gold precipitating agent. The size of gold nanoparticles is adjustable from 4 and 100 nm by altering the concentration of $HauCl_4$ and the inlet carbon monoxide injection flow rate. Fast synthesis rates at room temperature ease tunability and the absence of cytotoxic by-products allows these CO-based gold nanoparticles to be optimized and readily produced for biomedical and industrial application.

The development of a colloid chemistry route continues to be essential for the synthesis and manipulation of anisotropic gold nanoparticles, with the major requirements already demonstrated by Tréguer-Delapierre et al (2008, pp.195-207), such as the control of the nuclei shape and the growth on specific facets. A key feature of non-spherical nanoparticles is that their optical properties vary dramatically with their physical dimensions. In contrast to gold spherical nanoparticles, their resonance frequency is tuneable over a wide range from blue to near infrared and enables one to set the surface plasmon resonance to a wavelength or spectral region specific to a particular application. Together with a high degree of biocompatibility of gold, these structures show potential in a wide variety of biological applications (Rudolf et al, 2012, pp.595-612). Spherical, round and cylindrical nanosized particles of gold were synthesized by ultrasonic atomization of chloride-nitrate solutions based on gold from jewellery scraps and an alloying element (Cu, Ag, Zn, In, and Ni). A subsequnt decomposition of the obtained solution at temperatures of 300°C and 800°C in hydrogen and nitrogen atmospheres was performed. The aerosols produced by the resulting frequencies of 0.8 and 2.5 MHz were transported by a carrier, mostly a reduction gas, into a hot reactor, where aerosol droplets undergo drying, droplet shrinkage, solute precipitation, thermolysis, and sintering to form particles with different forms.

The gold formation from $HAuCl_4$ takes place in two steps (Stopic et al, 2013, pp.577-583) using ultrasonic spray pyrolysis:

First step: $2\ HAuCl_4 = Au_2Cl_6 + 2\ HCl$ (2)

Second step: $Au_2Cl_6 + 3\ H_2 = 2Au + 6\ HCl$ (3)

Under the spray pyrolysis conditions, hydrogen was passed continuously through the quartz tube (l= 1.0 m, b= 20 mm) at a flow rate of 1 l/min. Then, atomized droplets of the solution from gold auric acid were transported further by hydrogen to the furnace for the subsequent reduction of gold chloride at a different reaction temperature between

260°C and 500°C. After the completed reduction process, the obtained gold nanopowder was collected in a reaction tube and in two bottles with ethanol and water. The presence of triangular, rounded, and irregular particles revealed that the synthesis of gold nanoparticles is possible at temperatures lower than the melting point of gold.

On the other hand, both the methods and the parameters for the synthesis depend on the available equipment capable of supplying suitable conditions for ultrasonic spray pyrolysis and a subsequent treatment of the prepared powder. Kozhukharov and Tchaoushev (2013, pp.111-118) showed a basic construction of the equipment for spray pyrolysis in a vertical chamber, a horizontal chamber and a chamber for film deposition. The horizontal construction permits the separation of drops and particles based on their size. The basic operation units of each spray pyrolysis installation, regardless of its construction, are a spray nozzle or a nebulizer, a heat source and a product collector or a substrate for deposition. The employment of an ultrasonic nebulizer instead of a conventional nozzle enables production of nanomaterials in a form of monodispersive fine powders with easy particle size control by the variation of the ultrasound frequency and the concentration of water solution.

The present work is our attempt to summarize the basic parts and types of equipment as well as the conditions for the preparation of gold nanoparticles using ultrasonic spray pyrolysis. Regarding the very acidic and corrosive properties of a precursor solution such as $HAuCl_4$, the aim is to propose new equipment for an environmental friendly process for the synthesis of gold nanoparticles aiming for a continuous process in laboratory conditions with on-line control of an injection of precursor, level of liquid in an ultrasonic atomizer and improved transport with increased residence time in the reactor.

Laboratory scale horizontal USP equipment without a furnace

The experimental setup for the synthesis of nanogold particles is shown in Figure 1. The proposed equipment contains a gas station for hydrogen (a bottle with hydrogen and a flowmeter with a connection), a thermostat and an ultrasonic spray pyrolysis generator, as shown in Figure 1.

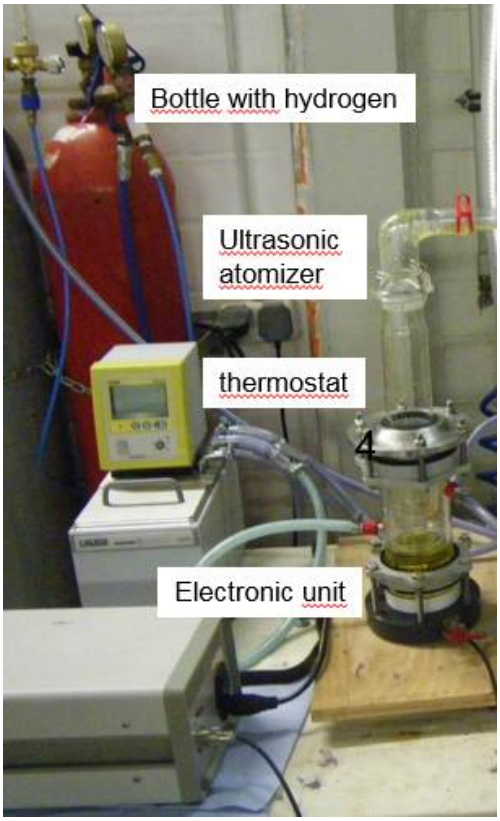

Figure 1 – One step USP lab-scale horizontal equipment
Рис. 1 – Горизонтальное устройство для получения порошка путем одношагового ультразвукового распыления раствора
Слика 1 – Хоризонтална апаратура за синтезу прахова ултразвучним распршивањем раствора у једном кораку

The thermostat is responsible for the prevention of overheating of the piezo transducer. Our first results are related to a new study of the preparation of gold nanoparticles from gold auric acid (1 g/L) by ultrasound-assisted reduction using 0.8 MHz at room temperature in hydrogen (a flow rate of 2 l/min) in the absence of a reaction furnace. These first results have confirmed the formation of gold nanoparticles under the above mentioned conditions, as shown in Figure 2, where a scanning electron microscope (ZEISS DSM 982 Gemini, Carl Zeiss Microscopy GmbH, Oberkochen, Germany) was used for the characterization of the obtained gold powders. The SEM images were used to observe the surface morphology of the particles formed at

different parameter sets. The qualitative characterization of the impurity level was performed by the energy disperse spectroscopy (EDS) analysis with an Si(Bi) X-ray detector connected to the SEM and a multi-channel analyser.

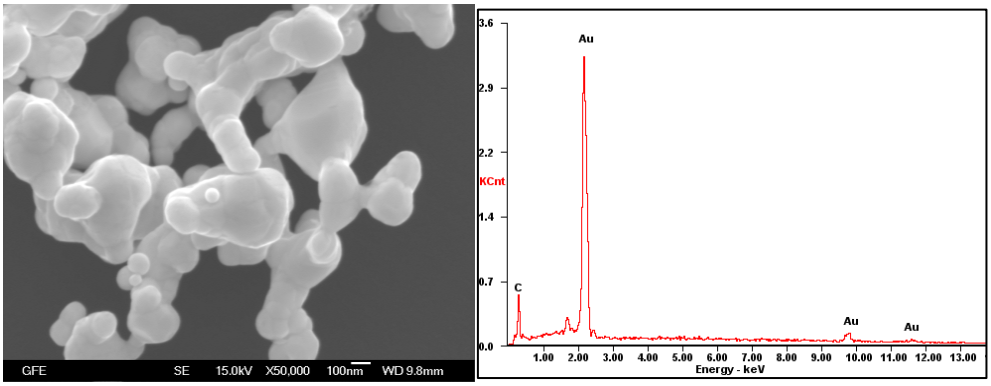

Figure 2 – SEM and EDS analysis of the gold particles obtained in the ultrasound field at room temperature
Рис. 2 – СЭМ и ЭРС анализ золотых порошков, полученных в ультразвуковом поле при комнатной температуре
Слика 2 – Скенирајућа електронска микроскопија и енергетска дисперзивна спектроскопија прахова злата добијених у ултразвучном пољу на собној температури

These results confirm that ultrasound can induce the reduction of $HAuCl_4$ with hydrogen. This study has to establish the current limitations of this induced synthesis. The relationship between the ultrasound frequency and the produced nanoparticles will be investigated in order to explain this phenomenon. Kinetic studies of the reduction of Au(III) complex ions and the gold nanoparticle formation with hydrogen at room temperature will be studied. The rate law and the rate limiting step will be established. The Finke–Watzky Two-Step Nucleation–Autocatalysis Model will be studied for gold nanoparticles. The two-step particle synthesis mechanism, also known as the Finke–Watzky (Watzky & Finke, 1997, pp.10382-10400) mechanism, has emerged as a significant development in the field of nanoparticle synthesis. It explains a characteristic feature of the synthesis of transition of metal nanoparticles, an induction period in the precursor concentration followed by its rapid sigmoidal decrease. The two-step mechanism considers slow continuous nucleation and autocatalytic growth of particles directly from the precursor as its two kinetic steps.

Laboratory scale horizontal USP equipment with a furnace

In order to improve the gold preparation by USP and hydrogen reduction, an additional furnace was used in the experimental set, as shown in Figure 3. With a concentration of gold in auric acid of 1.25 g/L, temperature of 260°C and 500°C, a hydrogen flow rate of (2 L/min), and an ultrasound frequency of 0.8 and 2.5 MHz, the obtained particles have cylindrical and spherical forms, as shown in Figure 4. (Dittrich et al, 2011, pp.1065-1076)

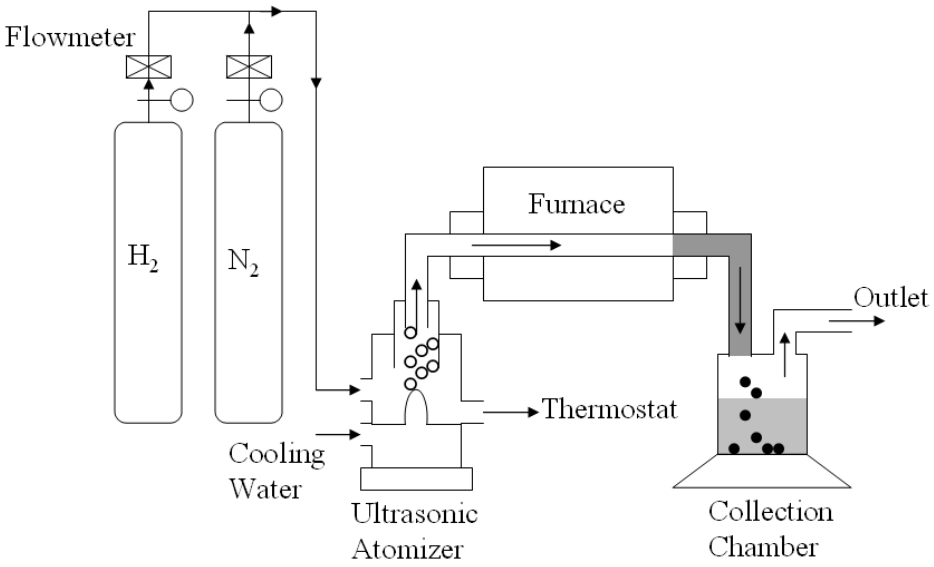

Figure 3 – Schematic drawing of the experimental apparatus for the synthesis of gold nanoparticles from a gold-chloride solution
Рис. 3 – Схема экспериментального устройства для извлечения наночастиц золота из раствора хлорида золота
Слика 3 – Шематски приказ експерименталне апаратуре за синтезу наночестица злата из раствора злато-хлорида

Three most important components of the USP equipment contain: 1) aerosol production in an ultrasonic field, 2) aerosol transport to the reaction furnace and the reduction of $HAuCl_4$ to Au, and 3) collection of gold particles in water and alcohol with its stabilization.

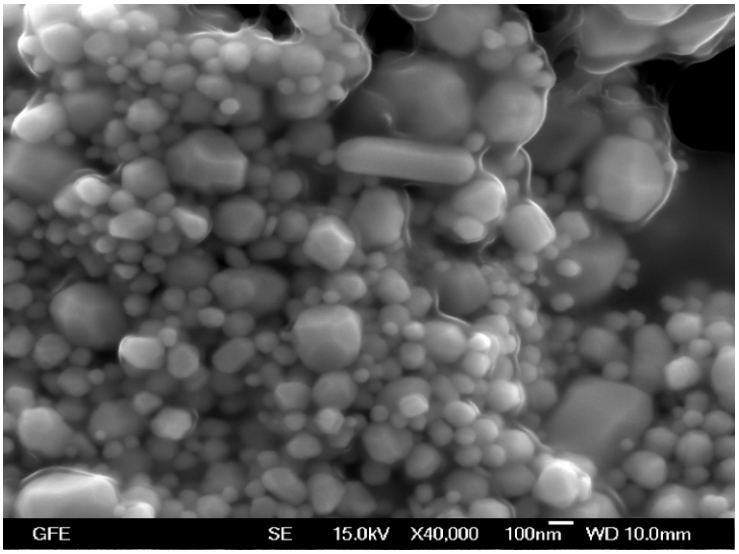

Figure 4 – Gold nanoparticles produced by USP (T=260°C, 2.5 MHz)
Рис. 4 – Наночастицы золота, полученные ультразвуковым распылением раствора (T=260°C, 2.5 MHz)
Слика 4 – Наночестице злата произведене ултразвучним распршивањем раствора (T=260°C, 2,5 MHz)

The big disadvantage of this process is frequent destruction of the piezo-transducer in contact with an acidic solution in the ultrasonic generator during aerosol production. This problem becomes very urgent for the solution obtained from secondary sources based on the dissolution of jewelry scraps in a high acidic solution of aqua regia, where the solution pH-Value is negative and the gold concentration is higher than 20 g/l. The losses of aerosol were detected during aerosol transport to the reactor. A higher flow rate of the carrier gas brings better transport of aerosol to the reactor furnace, but the residence time is shorter. Finally, collection of gold nanoparticles using either an electrofilter or a wet scrubber system is an open question for the future work in order to increase collection efficiency. A fully controlled process with an continuous injection is of the highest challenge in particular.

Improvement of the horizontal USP equipment

Regarding the previously mentioned disadvantages of the USP processes, some improvements are required and achieved firstly for the aerosol production using a new ultrasonic atomizer: PROFI SONIC and

PRIZNano, Kragujevac, Serbia. The main aim is to enable environmentally friendly aerosol production in an ultrasonic generator.

PROFI SONIC ultrasonic generator

Aerosol production from water solution was performed using the ultrasonic nebuliser (power: 55 W), PROFI SONIC, PRIZMA Kragujevac, transmitting the energy of ultrasonic vibrations (ultrasonic frequency of 1.7 MHz) from the vibrator located at the bottom of the water tank into water, as shown in Figure 5. Ultrasonic vibrations are transmitted to the medication cup (volume of 300 ml) through water in the water tank. Ultrasonic vibrations emit medication from the medication cup (like a fountain) and it is dispersed as aerosol. The air from the fan carries this nebulised medication out of the medication cup. The maximum production of aerosol amounts to 3 ml/min with a droplet size between 0.5-5 μm. The operation temperature is between 15 and 40°C. This ultrasonic generator allows the water solution of metallic salt to be separated from the piezo transducer, and protected during this work. This atomizer has also a control unit and a possibility to monitor the required time for the production of an aerosol.

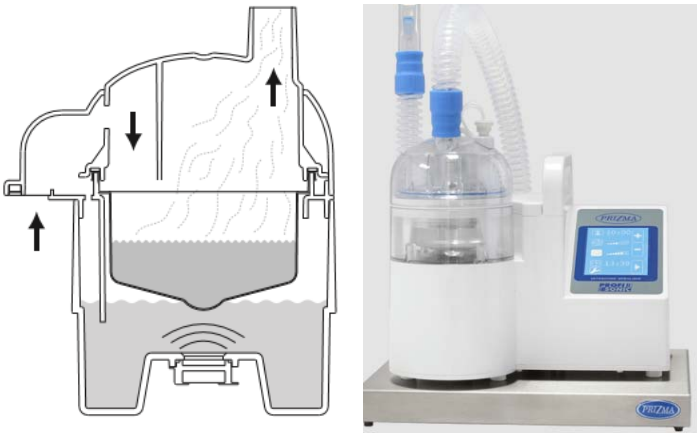

Figure 5 – Principle of aerosol production with an ultrasonic atomizer
Рис. 5 – Принцип получения аэрозоля с помощью ультразвукового распылителя
Слика 5 – Принцип производње аеросола са ултразвучним атомизером

PRIZNano Generator

The usage of three piezo-electric crystals with a frequency of 1.7 MHz guarantees a large atomization capacity up to 1.2 l/h, which provides the production of large quantities of aerosol, ideal for

independent use (humidification of large spaces) or, in a combination with other systems, for the production of nanoparticles, as shown in Figure 6. The result of new development by PRIZMA, Kragujevac, Serbia, is a compact PRIZnano ultrasonic pyrolysis generator with the dimensions of 300x300x450 mm and a weight of 3 kg. The atomizer can be powered from an AC power supply of 110 V to 240 V, 50 Hz or 60 Hz, and the maximum power consumption is 150 W. This generator was successfully used for the synthesis of metallic and oxidic particles at the RWTH Aachen University. Then, this PRIZNano is connected with a control unit as shown in Figure 6, which regulates the operation of each of three transducers. A flow meter is especially installed at an ultrasonic atomizer for the carrier gas. A special sensor is added for monitoring the solution level in the ultrasonic atomizer in order to prevent destruction of piezo transducers through the total consumption of the studied solution. The second sensor is responsible for the continuous injection of the solution in time. This type of generators does not use additional thermostats for cooling the solution in the ultrasonic atomizer. A special electronic unit controls the operations of all three piezo transducers in time, solution injection, and aerosol production power, as shown in Figure 6 (right). In contrast to the most frequently used GAPUSOL, RBI, France, this ultrasonic atomizer has shown many advantages (corrosion resistance, aerosol production and its transport, better control of transducer operation, and continuous solution injection).

Figure 6 – PRIZNano aerosol generator, Kragujevac, with the electronic control unit
Рис. 6 – Генератор аэрозолей ПРИЗНано, г. Крагуевац, с электронным блоком управления
Слика 6 – Генератор ааеросола PRIZnano „Призме" из, Крагујевца, са контролном електронском јединицом

The first measurement of the production and transport of aerosol in a PRIZNano generator from the water solution using different flow rates is shown in Figure 7.

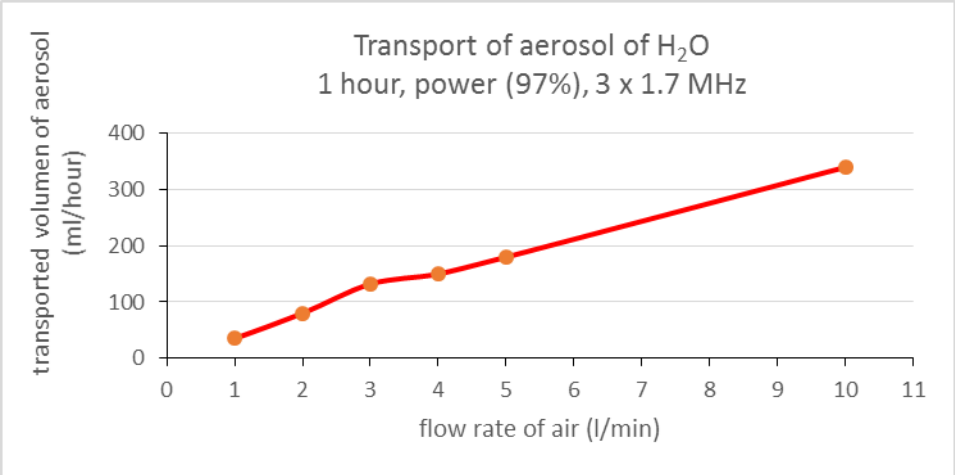

Figure 7 – Transport of aerosol depending on the air flow rate

Рис. 7 – Перемещение аэрозоля в зависимости от расхода воздуха

Слика 7 – Преношење аеросола у зависности од протока ваздуха

As shown in Figure 7, an increase in the flow rate increases the transport of aerosol.

The maximal transport is 330 ml in 60 min using 10 l/min.

Improved horizontal USP setup

Based on the previously mentioned improvements, new horizontal USP equipment was installed at PRIZMA, Kragujevac, Serbia.

Figure 7 – Improved USP Setup: a bottle with $HAuCl_4$ solution (yellow color), a peristaltic pump, an ultrasonic atomizer (f=1.7 MHz), an electronic unit with on-line process control, a quartz tube, a horizontal furnace and a bottle with water for the collection of gold nanoparticles (purple color, particle size approx. 50-80 nm)
Рис. 7 – Улучшенное устройство ультразвукового распылителя: баллон с раствором $HAuCl_4$ (желтый цвет), шланговый насос, ультразвуковой распылитель (f = 1,7 МГц), электронный блок управления, кварцевая трубка, горизонтальная печь и баллон с водой для извлечения наночастиц золота (фиолетовый цвет, размер частиц около 50-80 нм)
Слика 7 – Побољшана опрема за синтезу прахова ултразвучним распршивањем раствора: боца са ратвором $HAuCl_4$, (жута боја), перистатичка пумпа, ултразвучни генератор (фреквенца 1,7 MHz), електронска јединица са непрекидном контролом процеса, кварцна цев, хоризонтална пећ и боца са водом за сакупљање наночестица злата величине приближно између 50 и 80 nm (љубичаста боја)

The advantages of new USP equipment:

- On-line control of the liquid level in the ultrasonic atomizer,
- Continuous injection of the solution into the ultrasonic atomizer,
- Better protection of the piezo transducer, because a separate bottle with $HAuCl_4$ solution prevents contact with the piezo transducer and its destruction,

- Higher aerosol production and its transport to the furnace in order to decrease losses of aerosol,
- Full control of aerosol production using three transducers (f=1.7 Mhz) via the electronic unit,
- Improved collection of powder using a newly constructed electrofilter which is not presented in this work but is available as part of this USP equipment constructed by PRIZMA, Kragujevac, Serbia.

Conclusion

A critical analysis of the state of the art in preparation of nanosized gold particles using different reducing agents such as sodium citrate, sodium boride, zinc and iron powder, carbon monoxide, hydrogen, and phosphorus, producing spherical, cylindric and agglomerated gold particles, has made ultrasonic spray pyrolysis a highly promising method. The use of gaseous reducing agents such as hydrogen and carbon oxide leads to the synthesis of gold particles using reduction at room temperature. An increase in temperature between 260°C and 500°C supports the formation of spherical and cylindrical particles. New horizontal USP equipment offers many advantages in order to obtain one continuous controlled process, which is missing in the production of nanogold particles. Because of their very low production rate, USP processes are not industrially developed in comparison to traditional primary metallurgy for gold production. Therefore, scaling up these USP processes is a big challenge in the future related to the synthesis of nanogold.

References

Bond, G. 2008. The early History of Catalysis by Gold. *Gold Bulletin*, 41(3), pp.235-241. Available at: https://doi.org/10.1007/BF03214875.

Corti, C. 2002. Recovery and refining of gold jewelry scraps and waste. In: *The Santa Fe Symposium - The Premier Conference For Jewelry Makers*, Albuquerque, NM, pp.111-130 [online]. Available at: http://www.santafesymposium.org/2002-santa-fe-symposium-papers/2002-recovery-and-refining-of-gold-jewellery-scraps-and-wastes [Accessed: 10 August 2020].

Dittrich, R., Stopic, S. & Friedrich, B. 2011. Mechanism of nanogold formation by ultrasonic spray pyrolysis. In: *Proceeding of EMC 2011 - European Metallurgical Conference*, Duesseldorf, June 26-29, pp.1065-1076 [online]. Available at: http://www.metallurgie.rwth-aachen.de/new/images/pages/publikationen/emc2011_id_5231.pdf [Accessed: 10 August 2020].

Kozhukharov, S. & Tchaoushev, S. 2013. Spray pyrolysis equipment for various application. *Journal of Chemical Technology and Metallurgy*, 48, pp.111-118 [online]. Available at: https://www.researchgate.net/publication/283826563_Spray_pyrolysis_equipment_for_various_applications [Accessed: 10 August 2020].

Piret, N.L., Hopper, M. & Kudelka, H. 1977. *Process for recovering silver and gold from chloride solutions*. US Patent number 4131454 [online]. Available at: https://patents.google.com/patent/US4131454A/en [Accessed: 10 August 2020].

Polte, J., Ahner, T.T., Delissen, F., Sokolov, S., Emmerling, F., Thünemann, A.F. & Kraehnert, R. 2010. Mechanism of Gold Nanoparticle Formation in the Classical Citrate Synthesis Method Derived from Coupled In Situ XANES and SAXS Evaluation. *Journal of the American Chemical Society*, 132(4), pp.1296-1301. Available at: https://doi.org/10.1021/ja906506j.

Qi, C. 2008. The production of propylene oxide over nanometer Au catalysts in the presence of H_2 and O_2. *Gold Bulletin*, 41(3), pp.224-234. Available at: https://doi.org/10.1007/BF03214874.

Rudolf, R., Friedrich, B., Stopić, S., Anžel, I., Tomić, S. & Čolić, M. 2012. Cytotoxicity of Gold Nanoparticles Prepared by Ultrasonic Spray Pyrolysis. *Journal of Biomaterials Applications*, 26(5), pp.595-612. Available at: https://doi.org/10.1177/0885328210377536.

Schmid, G. & Corain, B. 2003. Nanoparticulated Gold: Syntheses, Structures, Electronics, and Reactivities. *European Journal of Inorganic Chemistry*, 2003(17), pp.3081-3098. Available at: https://doi.org/10.1002/ejic.200300187.

Stopic, S, Rudolf, R., Bogovic, J., Majerič, P., Čolić, M., Tomić, S., Jenko, M. & Friedrich, B. 2013. Synthesis of Au nanoparticles prepared with ultrasonic spray pyrolysis and hydrogen reduction. *Materials and Technology*, 47(5), pp.577-583 [online]. Available at: http://mit.imt.si/izvodi/mit135/stopic.pdf [Accessed: 10 August 2020].

Tréguer-Delapierre, M., Majimel, J., Mornet, S., Duguet, E. & Ravaine, S. 2008. Synthesis of non-spherical gold nanoparticles. *Gold Bulletin*, 41(2), pp.195-207. Available at: https://doi.org/10.1007/BF03216597.

Turkevich, J., Stevenson, P.C. & Hillier, J. 1953. The Formation of Colloidal Gold. *The Journal of Physical Chemistry*, 57(7), pp.670-673. Available at: https://doi.org/10.1021/j150508a015.

Young, J.K., Lewinski, N.A., Langsner, R.J., Kennedy, L.C., Satyanarayan, A., Nammalvar, V., Lin, A.Y. & Drezek, R.A. 2011. Size-controlled synthesis of monodispersed gold nanoparticles via carbon monoxide gas reduction. *Nanoscale Research Letters*, 6(art.numb.428). Available at: https://doi.org/10.1186/1556-276X-6-428.

Watzky, M.A. & Finke, R.G. 1997. ransition Metal Nanocluster Formation Kinetic and Mechanistic Studies. A New Mechanism When Hydrogen Is the Reductant: Slow, Continuous Nucleation and Fast Autocatalytic Surface Growth. *Journal of the American Chemical Society,* 119(43), pp.10382-10400. Available at: https://doi.org/10.1021/ja9705102.

СОВЕРШЕНСТВОВАНИЕ УЛЬТРАЗВУКОВОГО РАСПЫЛЕНИЯ ДЛЯ ИЗВЛЕЧЕНИЯ НАНОЧАСТИЦ ЗОЛОТА

Сречко Р. Стопич, **корреспондент**, *Бернд* Г. Фридрих

Технический университет города Ахен,
Институт металлургических процессов и рециклирования металлов,
г. Ахен, Федеративная Республика Германия

РУБРИКА ГРНТИ: 61.00.00 ХИМИЧЕСКАЯ ТЕХНОЛОГИЯ. ХИМИЧЕСКАЯ ПРОМЫШЛЕННОСТЬ:
61.13.21 Химические процессы
ВИД СТАТЬИ: оригинальная научная статья

Резюме:

Введение/цель: *Ультразвуковое распыление обычно используется для получения субмикронных наночастиц и наночастиц золота с помощью ультразвукового распылителя. Это простой метод спрей-пиролиза, содержащего соли металлов, таких как: хлорид золота, нитрат золота и ацетат золота, которые образуются в ультразвуковом поле с частотами от 0,8 до 2,5 МГц.*

Методы: В ультразвуковом распылении сочетается образование аэрозоля в одном ультразвуковом поле с его перемещением в реактор с использованием газа-носителя USP и окончательное восстановление с использованием водорода или монооксида углерода. Термическое разложение ацетата золота происходит в нейтральной атмосфере, такой как азот и аргон, при повышенных температурах. Повышение температуры восстановления до 260 и 500 ° C приводит к образованию цилиндрических и сферических частиц. Химическое восстановление происходит в водной фазе с использованием цитрата натрия и борида натрия после нагревания раствора.

Результаты: Золотые порошки были получены при комнатной температуре восстановлением водородом в ультразвуковом поле при комнатной температуре из раствора $HAuCl_4$ с частотой ультразвука 0,8 МГц. Полученные частицы золота анализировались с помощью сканирующей электронной микроскопии (СЭМ) и энергодисперсионной рентгеновской спектроскопии (ЭРС). Образованные агломерированные частицы имеют сферическую форму. Повышение температуры до 260 ° C и 500 ° C приводит к образованию сферических и цилиндрических частиц золота.

Выводы: Новое усовершенствованное оборудование для извлечения золота путем ультразвукового распыления раствора $HAuCl_4$ и восстановления водородом было предложено компанией PRIZMA, г. Крагуевац, Республика Сербия, что позволяет контролировать процесс с лучшей защитой

пьезопреобразователя в ультразвуковом поле и увеличивать образование аэрозоля и его перемещение в реакционную печь.

Ключевые слова: золото, совершенствование, ультразвуковое распыление, синтез.

НАПРЕДАК У УЛТРАЗВУЧНОМ РАСПРШИВАЊУ ЗА СИНТЕЗУ НАНОЧЕСТИЦА ЗЛАТА

Срећко Р. Стопић, **аутор за преписку**, *Бернд* Г. Фридрих

Технички универзитет у Ахену, Институт за процесну металургију и рециклирање метала, Ахен, Савезна Република Немачка

ОБЛАСТ: хемијске технологије
ВРСТА ЧЛАНКА: оригинални научни рад

Сажетак:

Увод/циљ: Ултразвучно распршивање обично је коришћено за припрему субмикронских и наночестица злата. То је једноставна метода синтезе из аеросола која садржи металне соли као што су злато-хлорид, злато-нитрат и злато-ацетат, који су формирани у ултразвучном пољу са фреквенцијама између 0,8 и 2,5 MHz.

Методе: Ултразвучно распршивање комбинује формирање аеросола у једном ултразвучном пољу са његовим транспортом у реактор коришћењем носећег гаса USP и завршном редукцијом помоћу водоника или угљен-моноксида. До термичког разлагања злато-ацетата долази у неутралној атмосфери као што је азот и аргон на повишеним температурама. Увећање температуре редукције до 260°C и 500°C води до добијања цилиндричних и сферних честица. Хемијска редукција дешава се у воденој фази коришћењем натријум-цитрата и натријум-борида након загревања раствора.

Резултати: Прахови злата добијени су на собној температури коришћењем редукције водоником у једном ултразвучном пољу на собној температури из раствора $HAuCl_4$ при фреквенци ултразвука од 0,8 MHz. Добијене честице злата анализиране су скенирајућом електронском микроскопијом (СЕМ) и енергетски дисперзивном спектроскопијом (ЕДС). Образоване честице су сферне и агломерисане. Увећање температуре до 260°C и 500°C води до формирања сферних и цилиндричних честица злата.

Закључак: Нову побољшану опрему за синтезу злата ултразвучним распршивањем раствора $HAuCl_4$ и редукцијом водоником понудила је „Призма" из Крагујевца (Србија). Она омогућава контролисан процес са бољом затититом претварача

Stopić, S. et al, Advance in ultrasonic spray pyrolysis (USP) for the synthesis of gold nanoparticles, pp.877-894

у ултразвучном пољу и увећаном производњом аеросола и његовим транспортом у реакциону пећ.

Кључне речи: злато, напредак, ултразвучно распршивање, синтеза.

Paper received on / Дата получения работы / Датум пријема чланка: 12.08.2020.
Manuscript corrections submitted on / Дата получения исправленной версии работы / Датум достављања исправки рукописа: 06.10.2020.
Paper accepted for publishing on / Дата окончательного согласования работы / Датум коначног прихватања чланка за објављивање: 08.10.2020.

ПРЕГЛЕДНИ РАДОВИ
ОБЗОРНЫЕ СТАТЬИ
REVIEW PAPERS

ZETA FUNCTION AND SOME OF ITS PROPERTIES

Nicola Fabiano

Independent researcher, Rome, Italy,
e-mail: nicola.fabiano@gmail.com,
ORCID iD:ORCID ID: https://orcid.org/0000-0003-1645-2071

DOI: 10.5937/vojtehg68-28535; https://doi.org/10.5937/vojtehg68-28535

FIELD: Mathematics
ARTICLE TYPE: Review paper

Abstract:

Introduction/purpose: Some properties of the zeta function will be shown as well as its applications in calculus, in particular the "golden nugget formula" for the value of the infinite sum $1+2+3+\cdots$. *Some applications in physics will also be mentioned.*

Methods: Complex plane integrations and properties of the Gamma function will be used from the definition of the function to its analytic extension.

Results: From the original definition of the $\zeta(s)$ *function valid for* $s>1$ *a meromorphic function is obtained on the whole complex plane with a simple pole in* $s=1$.

Conclusion: The relevance of the zeta function cannot be overstated, ranging from the infinite series to the number theory, regularization in theoretical physics, the Casimir force, and many other fields.

Key words: Zeta function, analytic continuation, complex plane integration.

Definition of the Zeta Function and its generalization

Consider the complex variable $s=\sigma+it$ with σ and t being real. For $\sigma>1$ the series

$$\zeta(s)=\sum_{n=1}^{+\infty}\frac{1}{n^s} \tag{1}$$

is convergent. This defines the zeta function, already known to Euler (Euler, 1738), (Euler, 1740), the properties of which were discovered by Riemann (Riemann, 1859) more than 100 years after Euler's works.

One generalization of this function is the following function

$$\zeta(s,a)=\sum_{n=0}^{+\infty}\frac{1}{(n+a)^s} \tag{2}$$

with $a>0$ due to Hurwitz (Hurwitz, 1932). For $a=1$ one recovers the zeta function. Working with the Hurwitz zeta allows us to obtain more general results that can immediately be translated for the zeta function in the case $\zeta(s,1)$.

By considering the definition of the Γ function

$$\Gamma(s)=\int_0^{+\infty}x^{s-1}e^{-x}dx \tag{3}$$

and by applying the substitution $x\to(n+a)x$, where n is an integer, we get

$$\Gamma(s)=\int_0^{+\infty}x^{s-1}(n+a)^s e^{-x(n+a)}dx\ , \tag{4}$$

that is

$$\Gamma(s)\frac{1}{(n+a)^s}=\int_0^{+\infty}x^{s-1}e^{-x(n+a)}dx\ . \tag{5}$$

Summing of n on both sides of (5) and using (2) leads to

$$\Gamma(s)\zeta(s,a)=\int_0^{+\infty}x^{s-1}\sum_{n=0}^{+\infty}e^{-x(n+a)}dx=\int_0^{+\infty}\frac{x^{s-1}e^{-ax}}{1-e^{-x}}dx\ , \tag{6}$$

the integral converges for $\sigma>1$. This formula furnishes us with an integral expression for $\zeta(s,a)$ that will be useful to analytically extend the zeta function even for $\sigma<1$. (2) could be rewritten as

$$\zeta(s,a)=\frac{1}{\Gamma(s)}\int_0^{+\infty}\frac{x^{s-1}e^{-ax}}{1-e^{-x}}dx\ , \tag{7}$$

which bears resemblance to the Γ function itself (3).

The integral on the complex plane

From formula (7) we will consider the integral

$$I_a(s) = \int_{\mathcal{C}} \frac{(-z)^{s-1}e^{-az}}{1-e^{-z}}dz \tag{8}$$

extended over the complex plane, $z \in \mathbb{C}$, on the contour $\mathcal{C}$. When observing the integrand we see that there is a branch point at $z = 0$ and that there exist simple poles for $z = \pm 2n\pi i$, where $n = 1, 2, 3, \ldots$. Assuming there is a cut on the real positive axis, we will make use of a Hankel's type of contour for the integral (Hankel, 1869). It comes from $+\infty$ just above the real positive axis, goes around the origin and returns back to $+\infty$ this time below the real positive axis, so it does not contain any of the above mentioned poles, and does not pass through the branch point $z = 0$. We conclude that such an integral (8) provides us with an analytical function for *all values of* s. We can write the relation

$$\int_{\mathcal{C}} \frac{(-z)^{s-1}e^{-az}}{1-e^{-z}}dz = [e^{\pi i(s-1)} - e^{-\pi i(s-1)}] \int_0^{+\infty} \frac{(-x)^{s-1}e^{-ax}}{1-e^{-x}}dx =$$
$$2i\sin[\pi(s-1)] \int_0^{+\infty} \frac{(-x)^{s-1}e^{-ax}}{1-e^{-x}}dx = -2i\sin(\pi s) \int_0^{+\infty} \frac{(-x)^{s-1}e^{-ax}}{1-e^{-x}}dx \,. \tag{9}$$

Remembering the reflection property of the Γ function, for which

$$\Gamma(1-s)\Gamma(s) = \frac{\pi}{\sin(\pi s)}, \tag{10}$$

combining with the result of (9) and plugging all back in (7), we end up with an expression for Hurwitz's ζ from an integral on the complex plane

$$\zeta(s,a) = -\frac{\Gamma(1-s)}{2\pi i} \int_{\mathcal{C}} \frac{(-z)^{s-1}e^{-az}}{1-e^{-z}}dz = -\frac{\Gamma(1-s)}{2\pi i} I_a(s) \,. \tag{11}$$

Now, we have already noticed that the last integral $I_a(s)$ gives an analytical function for *all* values of s on the complex plane. Therefore the only possible poles of $\zeta(s,a)$ could be given by the $\Gamma(1-s)$ function, that is at the points $1, 2, 3, \ldots$.

On the other hand, from definition (2), we already know that $\zeta(s,a)$ converges for $\sigma > 1$. We, therefore, conclude that the only possible pole for $\zeta(s,a)$ is to be found at the point $s = 1$, and it is a simple pole, because the Γ function has only simple poles for negative integers, of the form

$$\Gamma(x) = \frac{(-1)^n}{n!(x+n)} + \frac{(-1)^n \psi(n+1)}{n!} + \mathcal{O}(x+n) \ , \tag{12}$$

where $\psi(x) = d/dx[\ln(\Gamma(x))]$. For $s = 1$, $I_a(1)$ is written as

$$I_a(1) = \int_{\mathcal{C}} \frac{e^{-az}}{1-e^{-z}} dz = 2\pi i \operatorname*{Res}_{z=0} \left(\frac{e^{-az}}{1-e^{-z}} \right) = 2\pi i \ , \tag{13}$$

because for $a > 0$ the integrand is zero at infinity, and its residue is +1. Hence, from (11) we obtain that

$$\lim_{s \to 1} \frac{\zeta(s,a)}{\Gamma(1-s)} = -1 \ . \tag{14}$$

Equation (12) tells us that $\Gamma(1-s)$ has a single pole for $s = 1$ with the residue of -1. It, therefore, follows that $\zeta(s,a)$ has $s = 1$ as the only singularity, which is a single pole with the residue of +1.

Functional equation

Formula (11) provides an expression for the Hurwitz zeta function $\zeta(s,a)$ which is valid for all values of $s \in \mathbb{C}\backslash\{1\}$ by means of an expression containing a complex integral (8) $I_a(s)$ (Hurwitz, 1932).

Consider now the real positive point $(2N+1)\pi$, N being an integer, and define the Hankel's contour $\mathcal{C}_N$ in analogy to the previous one encountered. The path runs from the point $(2N+1)\pi$ towards 0 just above the positive real axis, goes around the origin $z = 0$ in a counterclockwise direction without intersecting it, and returns to the original point just below the real positive axis, and does not contain any of the simple points $\pm 2n\pi i$ of the integrand. Consider then a circle $\mathcal{C}'_N$ centered in the origin with the radius $(2N+1)\pi$, ending at the beginning of $\mathcal{C}_N$. The full path $\mathcal{C}_N + \mathcal{C}'_N$ is closed, and the origin lies outside of it, therefore we obtain

$$-\frac{1}{2\pi i}\int\limits_{\mathcal{C}_N+\mathcal{C}'_N}\frac{(-z)^{s-1}e^{-az}}{1-e^{-z}}dz=\sum_{n=1}^{N}(R_n^+ + R_n^-)\,, \tag{15}$$

where R_n^+ and R_n^- are the residues of the integrand at the points $+2n\pi i$ and $-2n\pi i$ respectively, for $n=1,\dots,N$. This is true because all the poles are inside the above defined contour, and the minus sign is necessary as this contour runs clockwise. The residues at points $\pm 2\pi i n$ are given by

$$R_n^{\pm}=(2\pi n)^{s-1}e^{\mp\frac{i}{2}\pi(s-1)}e^{\mp 2\pi i n a}\,, \tag{16}$$

hence

$$R_n^+ + R_n^- = (2\pi n)^{s-1}\,2\sin\left(\frac{\pi}{2}s+2\pi n a\right)=\frac{2\sin\left(\frac{\pi}{2}s\right)}{(2\pi)^{1-s}}\frac{\cos(2\pi a n)}{n^{1-s}}+ \\ \frac{2\cos\left(\frac{\pi}{2}s\right)}{(2\pi)^{1-s}}\frac{\sin(2\pi a n)}{n^{1-s}}\,. \tag{17}$$

For a large N, the first part of the contour, $\mathcal{C}_{\mathcal{N}}$, becomes the Hankel's contour already encountered in (8), $\lim_{N\to+\infty}\mathcal{C}_{\mathcal{N}}=\mathcal{C}$. The integral on the circle $\mathcal{C}'_N$ does not contribute in the limit $N\to+\infty$. In fact, parametrizing the variable on the circle path $z=(2N+1)\pi e^{i\theta}$, $-\pi\le\theta\le+\pi$ and for $a>0$ one has

$$\left|\int\limits_{\mathcal{C}'_N}\frac{(-z)^{s-1}e^{-az}}{1-e^{-z}}dz\right|\le\int_{-\pi}^{+\pi}[(2N+1)\pi]^s e^{-(2N+1)\pi}d\theta= \\ 2\pi[(2N+1)\pi]^s e^{-(2N+1)\pi}, \tag{18}$$

and this expression clearly goes to zero for $N\to+\infty$.

In the limit $N\to+\infty$ applied to (15), we therefore obtain

$$\lim_{N\to+\infty}-\frac{1}{2\pi i}\int\limits_{\mathcal{C}_N}\frac{(-z)^{s-1}e^{-az}}{1-e^{-z}}dz=-\frac{1}{2\pi i}\int\limits_{\mathcal{C}}\frac{(-z)^{s-1}e^{-az}}{1-e^{-z}}dz= \\ \frac{2\sin\left(\frac{\pi}{2}s\right)}{(2\pi)^{1-s}}\sum_{n=1}^{+\infty}\frac{\cos(2\pi a n)}{n^{1-s}}+\frac{2\cos\left(\frac{\pi}{2}s\right)}{(2\pi)^{1-s}}\sum_{n=1}^{+\infty}\frac{\sin(2\pi a n)}{n^{1-s}}\,, \tag{19}$$

Fabiano, N., Zeta function and some of its properties, pp.895–906

and with the aid of (11) we can eventually write the converging series

$$\zeta(s,a) = \frac{\Gamma(1-s)}{(2\pi)^{1-s}} \left[2\sin\left(\frac{\pi}{2}s\right) \sum_{n=1}^{+\infty} \frac{\cos(2\pi a n)}{n^{1-s}} + 2\cos\left(\frac{\pi}{2}s\right) \sum_{n=1}^{+\infty} \frac{\sin(2\pi a n)}{n^{1-s}} \right] . \tag{20}$$

By writing $a = 1$ in (20) we obtain the functional equation linking the values of $\zeta(s)$ and $\zeta(1-s)$ discovered by Riemann

$$\zeta(s) = (2\pi)^s \frac{\Gamma(1-s)}{\pi} \sin\left(\frac{\pi}{2}s\right) \zeta(1-s) , \tag{21}$$

and by making use of the Γ function reflection property (10), we obtain the alternative expression for the ζ function reflection property

$$2^{1-s}\Gamma(s)\zeta(s)\cos\left(\frac{\pi}{2}s\right) = \pi^s \zeta(1-s) . \tag{22}$$

Some special values of ζ

In the previous section, we have seen that $\zeta(s)$ is a meromorphic function on the complex plane, with a simple pole for $s = 1$. We will now discuss some notable values of this function.

$\zeta(2)$: the Basel problem

Historically, the first who posed the problem of the values of $\sum_{n=1}^{+\infty} 1/n^2$ was Mengoli in 1650 (Mengoli, 1650). Euler solved this problem in the years after 1730, and he named it after his hometown (Euler, 1740).

Consider the series

$$\sin(x) = x - \frac{x^3}{3!} + \frac{x^5}{5!} - \frac{x^7}{7!} + \cdots \tag{23}$$

and divide this expression by x, obtaining the infinite polynomial

$$\frac{\sin(x)}{x} = 1 - \frac{x^2}{3!} + \frac{x^4}{5!} - \frac{x^6}{7!} + \cdots . \tag{24}$$

This function is well defined for all $x \in \mathbb{R}$ and has its zeroes at the points $\pm n\pi$, for $n = 1, 2, 3, \ldots$. Hence, this polynomial can be written as an infinite product of the factors

$$\frac{\sin(x)}{x} = \left(1-\frac{x}{\pi}\right)\left(1+\frac{x}{\pi}\right)\left(1-\frac{x}{2\pi}\right)\left(1+\frac{x}{2\pi}\right)\left(1-\frac{x}{3\pi}\right)\left(1+\frac{x}{3\pi}\right)\cdots$$
$$= \left(1-\frac{x^2}{\pi^2}\right)\left(1-\frac{x^2}{4\pi^2}\right)\left(1-\frac{x^2}{9\pi^2}\right)\cdots = \prod_{n=1}^{+\infty}\left(1-\frac{x^2}{n^2\pi^2}\right) . \quad (25)$$

That has to be compared with $\zeta(2)$, namely

$$\zeta(2) = \sum_{n=1}^{+\infty}\frac{1}{n^2} = \left(1+\frac{1}{4}+\frac{1}{9}+\cdots\right) . \quad (26)$$

Consider the coefficient of the polynomial (25) in x^2. It is obtained by picking exactly once each x^2 term in the factors, multiplyng it with all the constant terms and then adding together all those terms. An analogy that helps would be with the characteristic polynomial of a matrix, where the coefficient of the lowest term of the polynomial (in our case, x^2) is given by the trace of the matrix that is the sum of all eigenvalues. This gives for the x^2 term in (25)

$$-x^2\left(\frac{1}{\pi^2}+\frac{1}{4\pi^2}+\frac{1}{9\pi^2}+\cdots\right) = -\frac{x^2}{\pi^2}\left(1+\frac{1}{4}+\frac{1}{9}+\cdots\right) = -\frac{x^2}{\pi^2}\zeta(2) . \quad (27)$$

Comparing this result with the x^2 term of (24), one obtains

$$-\frac{x^2}{3!} = -\frac{x^2}{\pi^2}\zeta(2) \quad (28)$$

giving eventually the required value for ζ

$$\zeta(2) = \frac{\pi^2}{6} \approx 1.6449 . \quad (29)$$

Notice that, even though this brilliant procedure leads to the correct value, it is wrong. In fact, one could multiply (25) by an arbitrary positive function, say $\exp(x)$, and retain the same result, because the roots of the polynomial will not change. Yet the series expansion of this new function would be quite different from (24). The culprit is that it is not valid to treat an infinite product or sum expecting it to behave like a finite one.

Fabiano, N., Zeta function and some of its properties, pp.895–906

$\zeta(-1)$

The infinite sum

$$1+2+3+4+5+\cdots=\sum_{n=1}^{+\infty}\frac{1}{n^{-1}} \tag{30}$$

is equivalent to $\zeta(-1)$. By writing $s=-1$ in (21), we get

$$\zeta(-1)=\frac{1}{2\pi}\frac{\Gamma(2)}{\pi}\sin\left(-\frac{\pi}{2}\right)\zeta(2) \tag{31}$$

remembering the properties of the Γ function and eq. (29) for the value of $\zeta(2)$ we have

$$\zeta(-1)=-\frac{1}{12}=1+2+3+4+5+\cdots\,, \tag{32}$$

so we end up with an astonishing result: the sum of all positive integers is not only finite, but also negative! Of course this does not mean that the usual addition rules turned out to be magically spoiled. In fact, consider the finite sum

$$1+2+3+\cdots+N=\sum_{n=1}^{N}n=\frac{N(N+1)}{2}\,, \tag{33}$$

and this expression becomes infinite when $N\to+\infty$.

What it really means is that the definition of ζ given in (1) is no longer valid whenever $\sigma\leq 1$, like in our case of $s=-1$. The $\zeta(s)$ that obeys to (21) is the analytical continuation on the whole complex plane of the one defined in (1), and they do coincide only when $\sigma>1$.

One could also think of equation (30) as an equivalence to a so–called regularized ζ function defined in (1). This technique is used very often in theoretical physics and lays on a rigorous basis, too vast to be described here. Loosely speaking, it is like considering the behavior of a function near a pole, then discarding the divergent part while retaining the finite part. The latter assigns the value of the function on the pole.

For instance, by considering the behavior of the Γ function close to negative integers described in (12), near the origin we have

$$\lim_{x\to 0}\Gamma(x) = \frac{1}{x} - \gamma + \frac{6\gamma^2+\pi^2}{12}x + \mathcal{O}(x^2) \tag{34}$$

so that a regularized Γ function should assume the value

$$\mathrm{Reg}[\Gamma(0)] = -\gamma \approx -0.5772\ . \tag{35}$$

It is worth noticing that the value of $\zeta(-1)$ appears in physics when computing the Casimir force in one dimension, that arises as a fluctuation of the vacuum energy when quantizing the electromagnetic field, or when computing the ground state energy of the bosonic string theory, a model which was an attempt to unify gravitational with other fundamental forces.

$\zeta(0)$

The infinite sum

$$1+1+1+1+1+\cdots = \sum_{n=1}^{+\infty}\frac{1}{n^0} \tag{36}$$

is equivalent to $\zeta(0)$. By writing $s=0$ in (21), we get

$$\zeta(0) = \lim_{s\to 1}\frac{1}{\pi}\Gamma(1)\sin\left(\frac{\pi}{2}s\right)\zeta(1-s)\ , \tag{37}$$

and, remembering that ζ has a simple pole with residue +1 in $s=1$, we have

$$\lim_{s\to 1}\sin\left(\frac{\pi}{2}s\right)\zeta(1-s) = -\frac{\pi}{2} \tag{38}$$

Thus, by putting all the values in (37) we obtain

$$\zeta(0) = -\frac{1}{2} = 1+1+1+1+1+\cdots\ , \tag{39}$$

obtaining once again a negative value for an infinite sum of positive terms.

The same considerations given for the case of $\zeta(-1)$ apply here.

Other useful information on complex functions could be found for instance in (Denjoy, 1926), (Wolff, 1926), (Došenović, 2018), (Todorčević, 2019).

References

Denjoy, A. 1926. Sur l'itération des fonctions analytiques. *C.R. Acad. Sci. Paris*, 182, pp.255-257 (in French).

Došenović, T., Kopellaar, H. and Radenović, S. 2018. On some known fixed point results in the complex domain: Survey. *Vojnotehnički glasnik/Military Technical Courier*, 66(3), pp.563-579. Available at: https://doi.org/10.5937/vojtehg66-17103.

Euler, L. 1738. De summatione innumerabilium progressionum. *Euler Archive - All Works*, 20 (in Latin) [online]. Availabe at: https://scholarlycommons.pacific.edu/euler-works/20 [Accessed: 15 September 2020].

Euler, L. 1740. De summis serierum reciprocarum. *Euler Archive - All Works*, 41 (in Latin) [online]. Availabe at: https://scholarlycommons.pacific.edu/euler-works/41 [Accessed: 15 September 2020].

Hankel, H. 1869. Die Cylinderfunctionen erster und zweiter Art. *Math. Ann.*, 1, pp.467-501 (in German).

Hurwitz, A. 1932. Einige Eigenschaften der Dirichlet'schen Funktionen $F(s) = \sum(D/n) \cdot 1/(n^s)$, die bei der Bestimmung der Klassenanzahlen binärer quadratischer Formen auftreten. In: *Abteilung für Mathematik und Physik der Eidgenössischen Technischen Hochschule (eds) Mathematische Werke.* Basel: Springer (in German). Available at: https://doi.org/10.1007/978-3-0348-4161-0_3.

Mengoli, P. 1650. *Novæ Quadraturæ Arithmeticæ.* Bononiæ: ex Typographia Iacobi Montij (in Latin).

Riemann, B. 1859. Ueber die Anzahl der Primzahlen unter einer gegebenen Grösse. *Monatsberichte der Berliner Akademie* (in German) [online]. Available at: http://www.emis.mi.sanu.ac.rs/EMIS/classics/Riemann/Zeta.pdf [Accessed: 15 September 2020].

Todorčević, V. 2019. *Harmonic Quasiconformal Mappings and Hyperbolic Type Metrics*. Springer Nature Switzerland AG. ISBN: 978-3-030-22591-9.

Wolff, J. 1926. Sur l'itération des fonctions bornées. *C. R. Acad. Sci.*, 182, pp.200-201.

Fabiano, N., Zeta function and some of its properties, pp.895–906

ДЗЕТА-ФУНКЦИЯ И ЕЕ ОСОБЕННОСТИ

Никола Фабиано
независимый исследователь, Рим, Италия

РУБРИКА ГРНТИ: 27.00.00 МАТЕМАТИКА:
27.25.17 Метрическая теория функций,
27.33.00 Интегральные уравнения,
27.39.29 Приближенные методы функционального анализа
ВИД СТАТЬИ: обзорная статья

Резюме:

Введение/цель: В данной статье представлены некоторые особенности дзета-функции, а также ее применение в математическом анализе, особое внимание уделено формуле «golden nugget» при вычислении бесконечной суммы 1 + 2 + 3 + • • •. В статье также приводятся примеры ее применения в физике.

Методы: Интеграция в комплексной плоскости и свойства гамма-функции используются на всех этапах: от определения функции до ее аналитического расширения.

Результаты: Из первоначального определения функции ζ (s), относящейся к s> 1, выводится мероморфная функция на всей комплексной плоскости с простым полюсом в s = 1.

Выводы: Дзета-функция безусловно играет важнейшую роль во многих областях, начиная от бесконечных рядов и заканчивая теорией чисел, регуляризации в теоретической физике, силе Казимира и пр.

Ключевые слова: дзета-функция, аналитическое продолжение, интеграция в комплексной плоскости.

ЗЕТА-ФУНКЦИЈА И НЕКЕ ЊЕНЕ ОСОБИНЕ

Никола Фабиано
независни истраживач, Рим, Италија

ОБЛАСТ: математика
ВРСТА ЧЛАНКА: прегледни рад

Сажетак:

Увод/циљ: У раду су приказане неке особине зета-функције, као и њена примена у математичкој анализи, нарочито формула „golden nugget" за вредност бесконачног збира 1+2+3+…. Такође, поменуте су и неке њене примене у физици.

Методе: Интеграције комплексне равни и особине гама-функције биће искоришћене од дефиниције функције до њене аналитичке екстензије.

Резултати: Од оригиналне дефиниције функције ζ(s) валидне за s >1, добија се мероморфна функција на целој комплексној равни са простим полом на s = 1.

Закључак: Изузетан значај зета-функције је несумњив, од бесконачних низова до теорије бројева, регуларизације у теоријској физици, Казимирове силе и многих других области.

Кључне речи: зета-функција, аналитичка континуација, интеграција комплексне равни.

Paper received on / Дата получения работы / Датум пријема чланка: 24.09.2020.
Manuscript corrections submitted on / Дата получения исправленной версии работы / Датум достављања исправки рукописа: 09.10.2020.

Paper accepted for publishing on / Дата окончательного согласования работы / Датум коначног прихватања чланка за објављивање: 11.10.2020.

Доминација борбених возила пешадије[1]

Борбена возила пешадије (БВП) добијају на значају због новог тржишта поткомпоненти, новог наоружања и активних система одбране.

Мада основни борбени тенкови остају основно оружје на бојном пољу, свестрани БВП освајају све већи део тржишта. па се и проценат средстава предвиђених за набавку овог наоружања повећава.

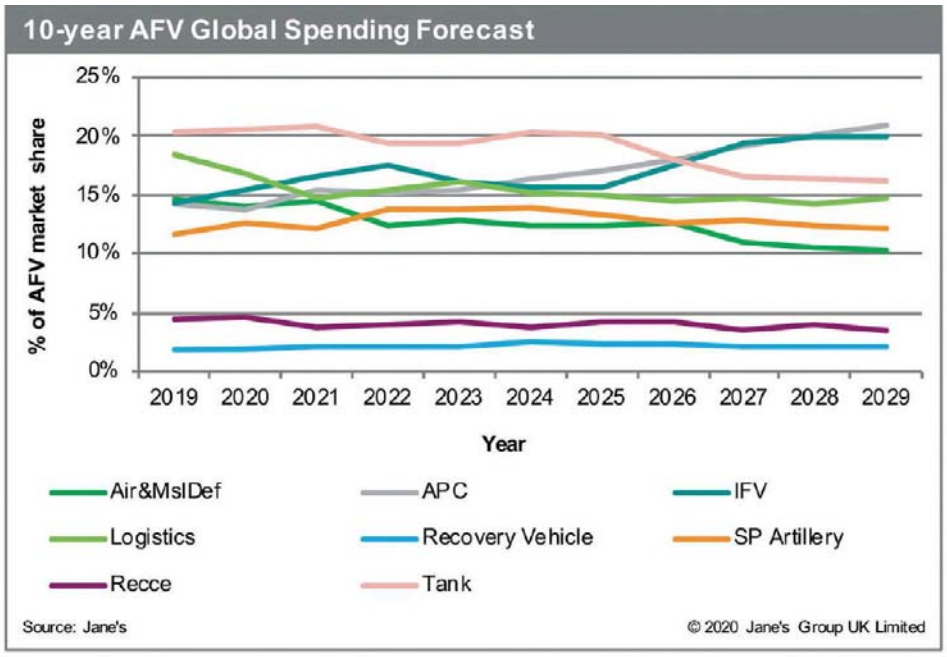

Пројекција глобалних трошкова набавке БВП

Велики број земаља инвестирао је значајна средства у модернизацију тенкова или у развој нових тенковских пројеката. Основни борбени тенк је и даље на првом месту у многим земљама, укључујући Француску, Немачку и Русију, у којима се развијају или уводе у оперативну употребу нове генерације основног борбеног тенка. Русија је започела производњу тенка Т-14 Armata, чији је број ограничен. За то време приводи се крају пројектовање француско-немачког основног копненог борбеног система (Main Ground Combat System – MGCS) који би требало да буде уведен у

[1] Jane's Defence International May 2020

оперативну употребу до 2035. године. Међутим, подаци Jane's Market Forecast наводе да би се средства намењена за развој основних борбених тенкова могла преусмерити на развој БВП и оклопних транспортера пешадије (ОТП).

Разлог повећаног улагања представљају бројни програми чији је циљ замена застарелих БВП новом генерацијом возила, док се замена основних борбених тенкова планира за период после 2030. године.

Разлози повећане тражње за БВП су различити. Поред релативних предности у односу на тенкове, БВП имају флексибилнији оперативни профил, мању масу, већу стратешку и оперативну мобилност, амфибијски потенцијал, нижу цену по возилу, као и јефтиније одржавање, а и једноставнија су за развијање и производњу. Фактор који додатно утиче на доминацију БВП представља и све већи број борбених дејстава која се све чешће дешавају у урбаним зонама, раст индустријског екосистема који води ка развоју БВП и ОТП, повећана убојитост наоружања БВП, глобална доступност противтенковских вођених ракета и развој нових активних система заштите.

Рачунање трошкова

Неколико промена на бојиштима и ван њих током последње деценије утицало је на војно планирање и потребе.

Нова купола руских БВП приказана у децембру 2019. године.

Прва промена односи се на буџет, трошкове и вештине. У доба када су многи војни буџети под притиском обезбеђивања максималне вредности у односу на утрошак средстава, корисници настоје да што више уједначе развој система који би могли бити коришћени на различитим платформама. Стандардизација заједничке платформе је нарочито остварљива са БВП с

обзиром на то да највећи број модерних пројеката за БВП може бити искоришћен у фамилији разних ОТП, заменом куполе са даљински управљаном оружаном станицом и додавањем места за седење у унутрашњости транспортера. Они могу лако бити оспособљени и за друге улоге, као што су носачи минобацача, санитетска возила, инжињерска возила и возила за извлачење. И основни борбени тенкови могу бити адаптирани за друге улоге, али је тај процес много скупљи, унутрашњи простор мањи, а ниво заштите непотребан у улози БВП. Због тога је једноставније адаптирати БВП и ОТП.

Користи компатибилних платформи упућују кориснике да прихвате компатибилне флоте фокусиране на ОБВ и ОТП које би користиле исту основну платформу као основ механизоване формације. Такав пример представља фамилија лаких оклопних возила *(LAV)/Piranha,* а повећана модуларност модерних оклопних возила олакшава овај процес.

Резултат овакве модуларности довео је до стварања екосистема снабдевача који нуде компоненте као што су куполе, даљински управљани оружни системи, ракете, топови односно митраљези, активни системи заштите, нишанске справе и системи за управљање ватром.

Корисници су искористили предности овог екосистема, а резултати су видљиви на тржишту ОБВ у виду јефтинијих производа. Један од примера представља литвански ОБВ *Boxer* (локални назив *Vilkas*), који користи шасију ОБВ Boxer и борбени модул са израелском даљински управљаном куполом *Rafael Samson Mk II* наоружаном аутоматским топом 30 mm Mk44 *Bushmaster* и контејнером са две противтенковске вођене ракете *Spike-LR*.

Уз повећану компатибилност дошло је до раста трошкова производње оклопних борбених возила где предњаче основни борбени тенкови који су и најскупљи за производњу и одржавање. Спирала трошкова приморала је многе земље да одређују приоритете у производњи средстава одбране и да производе делове у својим земљама кад год је то могуће. То значи повећање домаће радне снаге, трансфер знања и инжињеријских способности.

Локална производња

Поред набројаних погодности, многи корисници преферирају домаћу производњу као облик заштите своје земље од могућих санкција или потреса на тржишту. Ради се о озбиљним политичким и економским разлозима, па се произвођачи све чешће оријентишу на домаћу производњу ради добијања наруџби.

Ипак, домаћа производња често не представља идеалну солуцију , јер произвођачи морају рачунати на трошкове успостављања домаће фабрике. Она може имати негативне реперкусије и за корисника, јер домаћа индустрија можда нема неопходне вештине или ланац снабдевања за пуну серијску производњу софистицираног система. Међутим, ови проблеми су ипак решиви када се ради о БВП и ОТП, јер се они и наручују у већим количинама.

Слика куполе Epokha на платформи Kurganets-25

Пример успешне домаће производње БВП представља пољски *Rosomak 8×8*, домаћа варијанта возила *Patria AMV 8×8,* где је произведено близу 1000 возила у најмање 10 варијанти. Компанија која производи возило *Patria* потписала је уговор са Јужном Африком за домаћу производњу програма Badger, што је ипак довело до великих застоја у реализацији.

Возило *ARTEC Boxer 8×8* је развијено као кооперативни програм и производи се у Немачкој и Холандији. Компанија *Rheinmetall* је, такође, показала да прихвата овакву врсту сарадње и успоставила је домаћу производњу у Аустралији у оквиру програма *Land 400 Phase 2,* као и у Алжиру. Компанија *RBSL,* британски огранак компаније *Rheinmetall,* успоставила је и домаћу производњу возила *Boxer* у Великој Британији у оквиру програма *Mechanised Infantry Vehicle (MIV) requirement.* Други произвођачи, као што је компанија *General Dynamics,* такође су покренули домаћи производни програм за породицу британских возила *Ajax,* где ће првих 100 возила бити произведено у Шпанији, а остатак од 489 возила у Великој Британији.

Домаћа производња основних борбених тенкова ипак је много тежа. Композитни оклопи и одговарајући производни процеси спадају у строго чуване индустријске и државне тајне и, сходно томе, производња основних борбених тенкова тражи много већа финансијска улагања, као и велико искуство у производњи тешких возила.

С друге стране, при производњи БВП нема таквих проблема, јер ова возила могу бити на точковима или гусеницама, што дозвољава већу лепезу могућих дизајна. БВП точкаши могу се производити у фабрикама које имају искуство у производњи тешких камиона, што повећава број земаља које их могу производити. Стога се све чешће појављују нови модели оклопних точкаша у свету.

Прототип возила EFV наоружаног аутоматским топом Bushmaster Mk44 30 мм

Смртоносна бојишта

Будући БВП мораће се бранити од све већих калибара аутоматских топова, односно њихове муниције, као што су 40 мм CTAS, 50 мм *Super Shot* и две различите врсте метака 57 мм. Ова муниција пробија све оклопе са заштитом *STANAG 4569* Level 6.

Поред аутоматских топова, вођене противтенковске ракете имају све већу даљину дејства и прецизност. Оваква унапређења довела су до великог броја уништених оклопних возила у Либану, Сирији и нарочито у Јемену. Вођене противтенковске ракете развијене су до таквог степена да чак и модерни основни борбени тенкови својим пасивним оклопом не могу избећи уништење.

Израелски војни стручњаци изнели су тврдње да ниједно модерно оклопно борбено возило не може издржати удар противтенковске вођене ракете *Kornet* против свог пасивног оклопа. Очекује се да ће вођене противтенковске ракете убудуће представљати већу опасност од мина и импровизованих експлозивних средстава.

Са друге стране, вођене противтенковске ракете омогућују БВП ангажовање противничког оклопа на даљинама већим од радијуса дејства тенковског топа и то већом прецизношћу, нарочито против покретних мета. Неке противтенковске вођене ракете могу гађати циљеве и ван визуелног домета, што омогућава нападачком возилу дејство из заклона.

Већина вођених противтенковских ракета има малу масу, што значи да могу бити монтиране на БВП, што представља једноставно решење за ангажовање против непријатељевих оклопних возила. У случају када се вођене ракете додају уз конвенционално наоружање, као што су аутоматски топ и митраљез, БВП могу бити коришћени против највећег броја циљева. Вођене противтенковске ракете, за разлику од топова, могу бити и демонтиране уколико се не очекује налет непријатељевих оклопних возила.

Преживљавање

Убојитост модерног оружја захтева превенцију удара на сам оклоп возила, што се постиже употребом модерних активних система заштите, као и умањењем одраза возила.

Приказ истовремене употребе пумпи са воденим млазом и гусеница за савладавање коралних гребена

Активне системе заштите много је лакше инсталирати на БВП него на тенкове који имају много већу масу. На тај начин се скоро изједначава способност БВП у смислу преживљавања напада противтенковском вођеном ракетом. Ипак, то не утиче на могућност преживљавања од удара поткалибарне гранате испаљене са тенкова или аутоматских топова. У том

смислу овај недостатак може бити компензован безбедном даљином напада БВП помоћу противтенковске вођене ракете.

Ипак, тенкови нису и највећа претња БВП, јер је њихова висока цена знатно утицала на смањење њиховог укупног броја од престанка хладног рата.

Од брода ка обали

У прошлости је амерички произвођач, компанија *General Dynamics,* експериментисала са тежим прототиповима БВП за амерички маринси корпус. Радило се о возилу *Expeditionary Fighting Vehicle (EFV),* које је било способно да кроз воду плови брзином од 25 чворова и да врши операције на даљини до 40 км од обале. Међутим, програм је угашен 2011. године, делом због цене возила које је тада требало да кошта читавих 24 милиона долара.

Приказ поткалибарне муниције за топ 57 мм на куполи Epokha и две противтенковске вођене ракете – Bulat (мања) и larger Kornet (већа).

Јапан је недавно изразио интересовање за сличан концепт својим пројектом „Будуће амфибијско возило" (*Future Amphibious Vehicle (FAV*)). Изгледа да ће доћи до трансфера технологије од угашеног програма EFV, а циљ је развијање транспортера пешадије носивости 40 тона који ће имати способност брзог пловљења и савладавања коралних гребена.

Јапанска агенција (*Acquisition, Technology and Logistics Agency (ATLA*)) при јапанском министарству одбране развила је мотор од 3000 КС, чији је први прототип приказан 2019. године. Он обезбеђује пролаз преко гребена гусеницама уз погон водених млазница, што је условљено географским положајем Јапана. Наиме, ова земља има 6847 острва од којих су многа окружена коралним гребенима.

У случају сукоба са Кином у вези са удаљеним острвима, *FAV* је намењен обезбеђивању острва преко искрцане пешадије. Кинески маринци

Vučković, D., SAVREMENO NAORUŽANJE I VOJNA OPREMA / MODERN WEAPONS AND MILITARY EQUIPMENT, pp.907-920

располажу великом флотом амфибијских возила од којих је најзаступљенији БВП *ZBD-05*. Ово возило опремљено је мотором и уређајима који побољшавају брзину и пловност, омогућавајући амфибијске карактеристике, тј. пловност на морима по степену 4 и брзини пловљења од 13,5 чворова.

Поред Јапана, и амерички маринski корпус биће потенцијални корисник развоја БВП *FAV*. Маринski корпус биће смањен на 12 000 маринаца, биће редукована авијација и артиљерија, као и тенковска флота. Ове промене биће реализоване до 2030. године.

Имајући у виду острвску географију и бројне коралне гребене очекује се да ће маринци имати задатак да обезбеђују бројна острва у Јужном кинеском мору. Зато ће им бити потребна варијанта FAV и то вероватно кроз пројекат ACV 2.0 који, за разлику од пројекта ACV 1.1/1.2, предвиђа и пловност великом брзином и савладавање коралних гребена.

Кинески ZBD-05 у маринској камуфлажи

Нова руска купола Epoch

Године 2015. Русија је приказала нову генерацију оклопних возила, укључујући и варијанте БВП тенка Armata, као што су *Kurganets-25* и *Bumerang*. Док су ова возила била у процесу производње и тестова, Русија је испитивала и различите начине јефтине модернизације своје велике флоте БВП која је састављена од платформи BMP-2 и BMP-3. Поред осталих унапређења, флота BMP-2 је модернизована на стандард BMP-2M *Berezhok* која је опремљена куполом *B05Ya01 Berezhok*. Ова купола представља модерну али скромну модернизацију постојећих БВП BMP-2, која обезбеђује унапређени систем за управљање ватром, дневно-ноћну

термалну нишанску справу и дневно-ноћну панорамску нишанску справу командира.

У смислу ватрене моћи, купола *Berezhok* задржава примарни топ 30 мм 2А42, али јој се додаје и аутоматски бацач граната 30 мм АГ-30 који се налази на врху куполе, као и четири вођене противтенковске ракете Kornet, по две са сваке стране куполе. Иако се ради о скромној модернизацији, БМР-2 може бити коришћен у борби против непријатељевих оклопних возила.

Амбициознији програм је ипак даљински управљана купола *Epokha* која је била примећена током јула 2019. године и на возилима типа *Kurganets-25* у марту 2020. године.

Вођена противтенковска ракета Kornet показала се врло ефикасном против тешко оклопљених оклопних возила током сукоба прошле деценије

Купола *Epokha* замењује универзални борбени модул који је претходно приказан на возилима *B-11 Kurganets-25* и *K-17 Bumerang,* виђених на паради 2015. године. Као и *Berezhok*, купола *Epokha* је опремљена независном дневно-ноћном термалном нишанском справом за нишанџију и командира, али је оружани систем на куполи *Epokha* скоро потпуно нов. Примарно наоружање куполе *Epokha* чини топ *LShO-57 (Light Assault Weapon)* 57 мм AGL који је модификован за употребу у директном гађању. Топ има домет до 6000 м, а користи муницију HE-FRAG и APFSDS. Употреба APFSDS муниције сугерише да је топ *LShO-57* модификован за рад са већим притиском коморе. Поред топа, купола је опремљена и коаксијалним митраљезом 7,62 мм ПКТ.

Купола *Epokha* опремљена је са два типа противтенковских вођених ракета *Bulat* и *Kornet*. Ракета *Bulat* предвиђена је за напад на лако оклопљене циљеве, а има их укупно осам на куполи. Нема много

информација о овој ракети, али она делује као мање и једноставније решење у односу на ракету *Kornet*. Обе ракете наводе се ласерским снопом путем полуаутоматског начина вођења (*SACLOS*). Бојеве главе су вероватно типа тандем кумулативне и термобаричне.

Претпоставља се да је ракета *Bulat* намењена нападу на теже БВП и ОТП који су опремљени слабијим пасивним оклопом од тенкова или за уништавање утврђених положаја. За напад на тешко оклопљене циљеве купола је опремљена са четири ракете типа *Kornet* које су монтиране у пару, по две са сваке стране куполе.

Купола *Epokha* располаже великом ватреном моћи, надмашајући и модерне основне борбене тенкове. Само возило *Kurganets-25* је интересантно. Опремљено је модификованом верзијом оклопа *Afghanit* са активним системом заштите преузетог са фамилије возила *Armata*, који се састоји од аеросолних бацача димних кутија повезаних са детекторима ласерског озрачивања и електрооптичким сензорима повезаним са бацачима парчадно-фугасних граната који су повезани са радарима.

Када су инсталирани одговарајући модули, возило *Kurganets-25* може достићи брзину до 10 км/ч у води. Сваки модул тежи око 30 кг, тако да уколико је један одељак оштећен у води, она се не шири по другим одељцима. Оклопни модули повећавају масу возила и ширину до 4 м, али су они одвојиви и могу се уклонити за време транзита или када нису потребни.

Коначно, возило *Kurganets-25* опремљено куполом *Epokha* одлично илуструје како би будући БВП могли бити употребљени као замена за основне борбене тенкове. Ово возило мале масе и амфибијских способности у стању је да напада различите циљеве, па чак и модерне основне борбене тенкове. Инклузија активног система заштите значи да БВП поседује заштиту против вођених противтенковских ракета и других пројектила већег калибра. Возило ће носити ознаку В-18 или В-19, у зависности од тога да ли се ради о *Kurganets-25* са куполом *Epokha*, док ће друго возило бити ВМР-3, такође опремљено куполом *Epokha.*

Будући развој

Забринутост у вези с лимитом пасивне заштите основних борбених тенкова отворило је нов концептуални простор за развој оклопних возила. Израелски програм *Carmel* представља пример таквог размишљања.

Иако је израелски програм тек започет и тренутно није откривен пројекат возила, претпоставља се да је реч о платформи на бази борбеног возила са типичним оружаним комплетом БВП у форми аутоматског топа и вођених противтенковских ракета, опремљеном увезаним сензорима за ефикасније деловање посаде. Возило се претежно ослања на активни систем заштите.

Поред активног система заштите и експлозивно реактивни оклоп ЕРО је знатно напредовао, па су се на тржишту појавили нови заштитни пакети као што су хибридни ЕРО/активни систем заштите као што је систем

Protection Systems SMART-PROTech компаније *Rheinmetall*. У комбинацији са активним системом заштите, пакети EPO обезбеђују возило и од претњи напада пројектилима великог калибра.

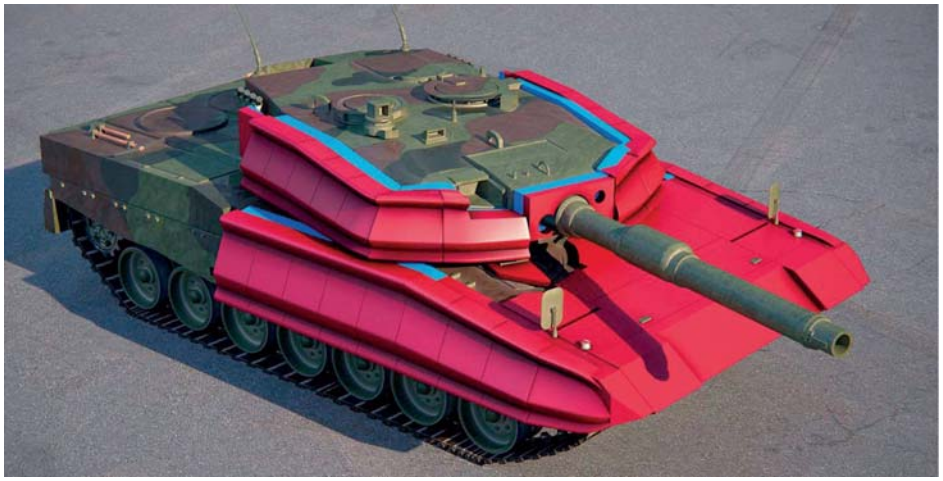

Рендерована слика оклопног пакета SMART-PROTech на тенку Leopard 2. Реактивни модули су приказани црвеном бојом, а керамички оклоп плавом. Иако је овај оклоп приказан на основном борбеном тенку, такав пакет се може инсталирати и на возила средње тежине као што су БВП.

Са развитком активних система заштите и пакета EPO, постаје могућа одбрана и од пројектила већих калибара и од вођених противтенковских ракета. Ипак, у средњој категорији, заштита од аутоматских топова већег калибра, као што су 40 мм, 50 мм и 57 мм, и даље остаје велики проблем.

Тренутно, решење се састоји од додавања још масивнијег пасивног оклопног пакета или прихватања да опасност постоји и развијања ситуационих стратегија као што су ограничења емисија, наоружање за гађање циљева на великим даљинама и умрежени сензори.

И Србија је недавно приказала пакет модернизације БВП М-80А. Возило је добило куполу нове конструкције са топом 30 мм и аутоматским бацачем граната истог калибра, нови систем са термовизијском камером великог домета, већи ниво балистичке заштите, радио-вођене противтенковске ракете 2Т5 и жицом вођене модернизоване противтенковске ракете *Maljutka 2F* и *2T*.

БВП М-80А

Ради подизања балистичке заштите оклопног дела БВП урађена је комплетна реорганизација унутрашњег простора и елемената, а повећана је и снага мотора.

Драган М. Вучковић (*Dragan* M. Vučković),
e-mail: draganvuckovic64@gmail.com,
ORCID iD: http://orcid.org/0000-0003-1620-5601

Средњи тенк *Kaplan*[2]

Током фебруара 2020. године индонезијско министарство одбране објавило је да су завршена финална испитивања средњег тенка *Kaplan* и да је спреман за серијску производњу. Захтеви индонежанске војске су јединствени. Наиме, тражена је платформа која обезбеђује директно ватрено дејство, а која може пролазити у тешким теренским условима у неразвијеној инфраструктурној мрежи, што је немогућа мисија за основни борбени тенк *Leopard 2A4RI* од 62 тоне који се налази у наоружању индонежанске војске.

Поред терена Индонезије, тенк *Kaplan* би могао бити ефикасан и у урбаним борбама, у срединама које карактеришу уски простори, високе зграде и осетљива инфраструктура.

[2] Jane's Defence International May 2020

Средњи тенк Kaplan

Kaplan покреће дизел мотор *Caterpillar C13* који обезбеђује 711 КС и има однос снаге/тежине од 24 КС по тони. Поред тога, највећи обртни моменат је 2700 Нм при 1300 окретаја у минуту. Највећи обртни моменат се креће од 1300 до 1500 окретаја у минуту, што значи да возило има велико убрзање. Гусенице и описана снага мотора чине га врло погодним за напредовање кроз рушевине, али и кроз зидове.

Наоружање се састоји од топа 105 мм *Cockeril* са комором високог притиска у куполи *John Cockerill Defence C3105* коју опслужују два члана посаде. Топ пуни аутоматски пуњач, а спрегнут је коаксијалним митраљезом 7,62 мм. Испаљује стандардну НАТО муницију 105 мм.

Тенкови који дејствују у урбаном окружењу могу бити лимитирани дужином топа, која износи 5,546 м, што је дуже од топовске цеви америчког тенка *M1 Abrams* од 5,28 м, па цев прилично штрчи у односу на тело тенка.

Наоружање тенка *Kaplan* је резултат компромиса. Наиме, дужина топа омогућава велику почетну брзину зрна и кинетичку енергију потребну за уништавање оклопних циљева, али, с друге стране, ограничава могућност возила да изводи операције у строго урбаним зонама за разлику од возила са краћом топовском цеви. Међутим, елевација топовске цеви се креће од -10 до 42 степена, што омогућава гађање циљева на високим зградама.

Поређења ради, топ на америчком тенку М1 има елевациони радијус од -10 до 20 степени.

Индонежански извори наводе да средњи тенк *Kaplan* издржава удар муниције митраљеског калибра у свој чеони део, као и да је опремљен и заштитом против импровизованих експлозивних направа или вођених противтенковских ракета употребом активног система заштите *Pulat*.

Командир располаже широкоугаоном панорамском нишанском справом, а нишанџија фиксним нишаном са десне стране топа. Обе нишанске справе имају другу или трећу генерацију термалних камера којима могу откривати скривене циљеве у урбаним зонама. Поред тога, у компанији *Cockerill* тврде да је могуће додати и контролисати беспилотну летелицу *Spy'Ranger* из куполе тенка, као и да посада може лоцирати циљеве користећи беспилотне летелице и напасти их индиректном ватром преко координата добијених од беспилотне летелице.

Драган М. Вучковић (*Dragan* M. Vučković),
e-mail: draganvuckovic64@gmail.com,
ORCID iD: http://orcid.org/0000-0003-1620-5601

Платформа „Corner Shot”

Кризне ситуације у урбаним срединама врло често, услед сложености услова, захтевају ангажовање високообучених професионалаца, припадника полицијских, војних, односно војнополицијских јединица за специјалне намене. Анализирањем великог броја интервенција у урбаним срединама (енг. close quarters battle – CQB), са освртом на специфичност окружења (на пример, мноштво објеката различитих врста и намена, прозора, врата, уских ходника, мањих просторија, степеница, спратова и др.), односно начин организовања и дејствовања непријатеља, дошло се до закључка да је изложеност оперативаца дејству непријатеља приликом извођења интервенција у овим условима висока, и поред уобичајене заштитне опреме која се користи у овим ситуацијама.

У вези с тим, у развоју специјалистичке опреме могу се приметити бар два приступа. Први подразумева увећавање укупне балистичке заштите, како појединца, тако и борбене групе, односно тима, на уштрб покретљивости. Специјалисти се опремају балистичким шлемовима на које за потребе *CQB* монтирају балистичке визире, док се торза штите габаритнијим балистичким прслуцима – панцирима (енг. body armor), често у конфигурацији са заштитом за рамена, односно препоне.[12] Масивна балистичка опрема је прилично тешка, те осетно успорава кретање појединца, групе или тима, чинећи их тако изложенијим за противника. Стога је додатна групна заштита при кретању императив и остварује се тактичким балистичким штитовима различитих величина и конструкција. Други приступ развија се услед основног недостатка првог – умањене покретљивости, захваљујући усавршавању електронске опреме. Зато су се, почетком новог миленијума, појавиле бројне иновације конструктора чији је циљ био повећање оперативности припадника приликом извођења специјалних дејстава, а истовремено увећање њихове безбедности, како се не би нужно излагали непријатељевој ватри.

Почетком двехиљадитих, на основу размене искустава и заједничког рада на пројекту израелских и америчких конструктора и искусних оперативаца, представљен је нови систем – платформа „Corner Shot”. У тиму инжењера и специјалаца две земље био је идејни творац пројекта Амос Голан, бивши командант једне израелске антитерористичке јединице, који тврди да поменута платформа штити животе оперативаца и увећава њихове шансе за преживљавање, олакшавајући им да осматрају окружење, преносе информације и ангажују мете, без директног контакта са њима.

[1] Важно је уочити разлике између балистичког панцира и тзв. носача плоча (енг. plate carrier). Носачи плоча су знатно мањих димензија, осетно мање масе и углавном штите витални органе торза. Другим речима, површина заштите се жртвује ради мање масе и увећања покретљивости припадника.

[2] Овакав приступ у опремању за потребе *CQB* може се, на пример, данас уочити код елитних јединица француске (нпр. *RAID*) и немачке (нпр. *GSG9*) полиције.

Намена и детаљи конструкције

Сврха система „Corner Shot" јесте да омогући стрелцу осматрање и дејствовање иза угла (тј. заклона), без излагања непријатељевој ватри. У питању је платформа футуристичког дизајна, која се састоји од два основна дела: задњег – фиксног са кундаком, рукохватом, камером и основним командама и предњег – носача који се може померати у углу од 180 степени и у који се монтира оружје, најчешће пиштољ.[3] Ради рационализације укупне масе, платформа „Corner Shot" је израђена од композитних материјала, док су најважнији делови израђени од квалитетног челика.

Пример употребе платформи „Corner Shot" при извођењу специјалних дејстава. Фото: cornershot.com

На задњем делу платформе смештен је преклопиви кундак, а са горње стране налази се батерија којом се остварује рад камере, односно екрана на којем се понавља слика са камере.

Ергономски рукохват је шупаљ, а изнад њега постављен је регулатор паљбе који у горњем положају блокира обарач који је смештен одмах испред рукохвата платформе. На горњој страни платформе интегрисане су стандардне „Picatinny" шине које омогућавају монтирање тактичких додатака, зависно од потреба интервенције. Екран *LCD* је преклопив и

[3] Произвођач нуди и моделе који су компатибилни са различитим системима за личну одбрану (енг. personal defense weapon).

постављен бочно. Са доње стране, испред браника обарача, налази се мобилна хоризонтална полуга коју корисник такође може користити приликом употребе и њоме мењати положај носача оружја на предњој страни платформе.[4]

Предњи преклопиви носач оружја може се померати у углу од 180 степени. У складу са захтевима купаца, предњи носач може се опремити и ласерским обележивачем циља (ЛОЦ), који је постављен одмах испод цеви оружја.[5]

Упадни тим Специјалне полицијске јединице ФУП БиХ увежбава упад у барикадирану просторију. Фото: Велија Хасанбеговић

Кућиште тактичке лампе постављено је испод места за ЛОЦ, док се кућиште са видео-камером налази испод тактичке лампе.[6] Систем може да снима и звук, а видео-камера је погодна и за употребу у условима смањене видљивости. Такође, видео-камера и *LCD* екран повезани су специфичним системом ласерског обележавања мете који се може подесити тако да самостално помаже при нишањењу, односно приликом употребе ласерског обележивача циља. Поред тога, подешавањима на *LCD* екрану корисник платформе може омогућити понављање слике и на другим екранима који су повезани са главним екраном. Конструкција платформе омогућава једноставно скидање и монтирање ласерског обележивача, лампе и видео-

[4] Полугу је могуће померати у страну.
[5] Ласерски уређај произвођача има два канала – један у видљивом спектру и, други, инфрацрвени (енг. infrared) за дејствовање у ноћним условима.
[6] Видео-камера снима у резолуцији 1080 p (Full HD).

камере, па корисник може мењати конфигурацију оптоелектронских уређаја, зависно од потреба интервенције.

Купцима се нуде платформе компатибилне са пиштољима, затим модели компатибилни са бацачем граната 40 mm, као и са пушчаним системима „Colt M4", односно „АК-47".

Недостаци и предности

У вези са тактичко-борбеном употребом „Corner Shot" платформе, отежавајућу околност за стрелца може представљати нетрадиционалан начин нишањења, јер најчешће ангажује мету коју не опажа непосредно. Неуобичајен правац преноса силе трзаја приликом паљбе из оружја монтираног на носач платформе умањује брзину паљбе стрелца. Додатно, нишањење се не реализује остваривањем нишанске линије помоћу механичких или других нишана на оружју, већ помоћу „кончанице" пројектоване на *LCD* екрану. Такође, зависно од природног и/или вештачког осветљења и специфичности окружења, за стрелца може бити компликовано да ваљано и правовремено опази мету, ангажује је, или о томе извести остатак снага. На основу претходних чињеница може се извести неколико закључака:

- када је прецизност паљбе у питању, задовољавајућа прецизност поготка је, најчешће, реална само на веома малим дистанцама, много мањим у односу на ситуације са уобичајеним радњама нишањења,
- сложеност система, специфичност осматрања, нишањења и паљбе захтевају темељну претходну обуку и период навикавања припадника.

Основна предност ове платформе је у већој безбедности припадника током интервенције, јер се осматрање непосредног окружења, пренос информација у реалном времену и евентуално ангажовање мете могу реализовати иза заклона. То је уједно и *differentia specifica* ове платформе у односу на различите телескопске штапове или савитљиве каблове са видео-камерама који, иако практични, омогућавају само осматрање. Иако није реално очекивати прецизност паљбе као при традиционалном нишањењу, сама могућност паљбе иза заклона, заједно са безбедним осматрањем и преносом информација у реалном времену чине платформу „Corner Shot" корисним елементом специјалистичке опреме, посебно за полицијске елитне јединице. Потенцијал овог система за увећање оперативних капацитета препознало је и руководство Федералне управе полиције Федерације БиХ, опремивши одређеним контингентом елитну Специјалну полицијску јединицу (СПЈ), подижући тако ефективност специјалиста при извођењу високоризичних хапшења, односно динамичких упада у објекте.

Милош М. Јевтић (*Miloš* M. Jevtić),
уредник сајта specijalne-jedinice.com,
e-mail: info@specijalne-jedinice.com,
ORCID iD: http://orcid.org/0000-0002-1305-7618

ПОЗИВ И УПУТСТВО АУТОРИМА
ПРИГЛАШЕНИЕ И ИНСТРУКЦИЯ ДЛЯ АВТОРОВ РАБОТ
CALL FOR PAPERS AND INSTRUCTIONS FOR AUTHORS

ПОЗИВ И УПУТСТВО АУТОРИМА О НАЧИНУ ПРИПРЕМЕ ЧЛАНКА

Упутство ауторима о начину припреме чланка за објављивање у *Војнотехничком гласнику* урађено је на основу Акта о уређивању научних часописа, Министарства за науку и технолошки развој Републике Србије, евиденциони број 110-00-17/2009-01, од 09. 07. 2009. године. Примена овог Акта првенствено служи унапређењу квалитета домаћих часописа и њиховог потпунијег укључивања у међународни систем размене научних информација. Засновано је на међународним стандардима ISO 4, ISO 8, ISO 18, ISO 215, ISO 214, ISO 18, ISO 690, ISO 690-2, ISO 999 и ISO 5122, односно одговарајућим домаћим стандардима.

Војнотехнички гласник / Vojnotehnički glasnik / Military Technical Courier (втг.мо.упр.срб, www.vtg.mod.gov.rs, ISSN 0042-8469 – штампано издање, e-ISSN 2217-4753 – online, UDC 623+355/359, DOI: 10.5937/VojnotehnickiGlasnik; https://doi.org/10.5937/VojnotehnickiGlasnik), јесте мултидисциплинарни научни часопис Министарства одбране и Војске Србије. Часопис објављује научне и стручне чланке из области основних истраживања (математике, рачунарских наука и механике) и технолошког развоја (електронике, телекомуникација, информационих технологија, машинства, материјала и хемијских технологија), као и техничке информације о савременим системима наоружања и савременим војним технологијама. Часопис прати јединствену интервидовску техничку подршку Војске на принципу логистичке системске подршке, области основних, примењених и развојних истраживања, као и производњу и употребу средстава наоружања и војне опреме. Часопис објављује и остала теоријска и практична достигнућа која доприносе усавршавању свих припадника српске, регионалне и међународне академске заједнице, а посебно припадника војски и министарстава одбране.

Уређивачка политика Војнотехничког гласника заснива се на препорукама Одбора за етичност у издаваштву (COPE Core Practices), као и на најбољим прихваћеним праксама у научном издаваштву. Војнотехнички гласник је члан COPE (Committee on Publication Ethics) од 2. маја 2018. године.

Министарство просвете, науке и технолошког развоја Републике Србије, сагласно одлуци из члана 27. став 1. тачка 4), а по прибављеном мишљењу из члана 25. став 1. тачка 5) Закона о научноистраживачкој делатности („Службени гласник РС”, бр. 110/05, 50/06-испр. и 18/10), утврдило је категоризацију Војнотехничког гласника, за 2019. годину:

за област технолошки развој:

– на листи часописа за електронику, телекомуникације и информационе технологије:

категорија водећи научни часопис националног значаја **(М51)**,

– на листи часописа за материјале и хемијске технологије:

категорија научни часопис националног значаја **(М52)**,

– на листи часописа за машинство:

категорија научни часопис националног значаја **(М52)**,

за област основна истраживања:

– на листи часописа за математику, рачунарске науке и механику:

категорија научни часопис **(М53)**.

Усвојене листе домаћих часописа за 2019. годину могу се видети на сајту Војнотехничког гласника, страница *Категоризација часописа* (Министарство просвете, науке и технолошког развоја Републике Србије још увек није објавило званичну категоризацију научних часописа за 2020. годину).

Детаљније информације могу се пронаћи и на сајту Министарства просвете, науке и технолошког развоја Републике Србије.

Подаци о категоризацији могу се пратити и на сајту КОБСОН-а (Конзорцијум библиотека Србије за обједињену набавку).

Категоризација часописа извршена је према Правилнику о поступку и начину вредновања и квантитативном исказивању научноистраживачких резултата истраживача, који је прописао Национални савет за научни и технолошки развој (Службени гласник РС, број 38/2008).

У складу са овим правилником и табелом о врсти и квантификацији индивидуалних научноистраживачких резултата (у саставу Правилника), објављени рад у Војнотехничком гласнику вреднује се са 2 бода (категорија М51), 1,5 бод (категорија М52) и 1 бод (категорија М53).

Часопис се прати у контексту Српског цитатног индекса – СЦИндекс (база података домаћих научних часописа) и Руског индекса научног цитирања (РИНЦ). Подвргнут је сталном вредновању (мониторингу) у зависности од утицајности (импакта) у самим базама и, посредно, у међународним (Clarivate Analytics) цитатним индексима. Детаљи о индексирању могу се видети на сајту Војнотехничког гласника, страница *Индексирање часописа*.

Војнотехнички гласник омогућава и примењује Creative Commons (CC BY) одредбе о ауторским правима. Детаљи о ауторским правима могу се видети на сајту часописа, страница *Ауторска права и политика самоархивирања*.

Радови се предају путем онлајн система за електронско уређивање АСИСТЕНТ, који је развио Центар за евалуацију у образовању и науци (ЦЕОН).

Приступ и регистрација за сервис врше се на сајту www.vtg.mod.gov.rs, преко странице *АСИСТЕНТ* или *СЦИНДЕКС*, односно директно на линку aseestant.ceon.rs/index.php/vtg.

Детаљно упутство о регистрацији и пријави за сервис налази се на сајту www.vtg.mod.gov.rs, страница *Упутство за АСИСТЕНТ*.

Потребно је да се сви аутори који подносе рукопис за објављивање у Војнотехничком гласнику региструју у регистар ORCID (Open Researcher and Contributor ID), према упутству на страници сајта *Регистрација за добијање ORCID идентификационе шифре*.

Војнотехнички гласник објављује чланке на српском, руском и енглеском језику (arial, српска ћирилица или српска латиница, величина слова 11 pt, проред Single).

Поступак припреме, писања и уређивања чланка треба да буде у сагласности са *Изјавом о етичком поступању* (http://www.vtg.mod.gov.rs/izjava-o-etickom-postupanju.html).

Чланак треба да садржи сажетак са кључним речима, увод, разраду, закључак, литературу и апстракт са кључним речима на енглеском и руском језику (без нумерације наслова и поднаслова). Обим чланка треба да буде око једног ауторског табака (16 страница формата А4 са проредом Single), а највише 24 странице.

Чланак треба да буде написан на обрасцу за писање чланка, који се у електронској форми може преузети са сајта на страници *Образац за писање чланка*.

Наслов

Наслов треба да одражава тему чланка. У интересу је часописа и аутора да се користе речи прикладне за индексирање и претраживање. Ако таквих речи нема у наслову, пожељно је да се придода и поднаслов. Наслов треба да буде преведен и на енглески и руски језик.

Ови наслови исписују се испред сажетка на одговарајућем језику.

Текући наслов

Текући наслов се исписује са стране сваке странице чланка ради лакше идентификације, посебно копија чланака у електронском облику. Садржи презиме и иницијал имена аутора (ако аутора има више, преостали се означавају са „et al.“ или „и др.“), наслове рада и часописа и колацију (година, волумен, свеска, почетна и завршна страница). Наслови часописа и чланка могу се дати у скраћеном облику.

Име аутора

Наводи се пуно име и презиме (свих) аутора. Веома је пожељно да се наведу и средња слова аутора. Имена и презимена домаћих аутора увек се исписују у оригиналном облику (са српским дијакритичким знаковима), независно од језика на којем је написан рад.

Назив установе аутора (афилијација)

Наводи се пун (званични) назив и седиште установе у којој је аутор запослен, а евентуално и назив установе у којој је аутор обавио истраживање. У сложеним организацијама наводи се укупна хијерархија (нпр. Универзитет одбране у Београду, Војна академија, Катедра природно-математичких наука). Бар једна организација у хијерархији мора бити правно лице. Ако аутора има више, а неки потичу из исте установе, мора се, посебним ознакама или на други начин, назначити из које од наведених установа потиче сваки од наведених аутора. Афилијација се исписује непосредно након имена аутора. Функција и звање аутора се не наводе.

Контакт подаци

Адреса или е-адреса свих аутора даје се поред имена и презимена аутора.

Категорија (тип) чланка

Категоризација чланака обавеза је уредништва и од посебне је важности. Категорију чланка могу предлагати рецензенти и чланови уредништва, односно уредници рубрика, али одговорност за категоризацију сноси искључиво главни уредник.

Чланци у *Војнотехничком гласнику* класификују се на научне и стручне чланке.

Научни чланак је:

– оригиналан научни рад (рад у којем се износе претходно необјављени резултати сопствених истраживања научним методом);

– прегледни рад (рад који садржи оригиналан, детаљан и критички приказ истраживачког проблема или подручја у којем је аутор остварио одређени допринос, видљив на основу аутоцитата);

– кратко или претходно саопштење (оригинални научни рад пуног формата, али мањег обима или прелиминарног карактера);

– научна критика, односно полемика (расправа на одређену научну тему, заснована искључиво на научној аргументацији) и осврти.

Изузетно, у неким областима, научни рад у часопису може имати облик монографске студије, као и критичког издања научне грађе (историјско-архивске, лексикографске, библиографске, прегледа података и сл.), дотад непознате или недовољно приступачне за научна истраживања.

Радови класификовани као научни морају имати бар две позитивне рецензије.

Ако се у часопису објављују и прилози ваннаучног карактера, научни чланци треба да буду груписани и јасно издвојени у првом делу свеске.

Стручни чланак је:

– стручни рад (прилог у којем се нуде искуства корисна за унапређење професионалне праксе, али која нису нужно заснована на научном методу);

– информативни прилог (уводник, коментар и сл.);

– приказ (књиге, рачунарског програма, случаја, научног догађаја, и сл.).

Језик рада

Језик рада може бити српски, руски или енглески.

Текст мора бити језички и стилски дотеран, систематизован, без скраћеница (осим стандардних). Све физичке величине морају бити изражене у Међународном систему мерних јединица – SI. Редослед образаца (формула) означава се редним бројевима, са десне стране у округлим заградама.

Сажетак

Сажетак јесте кратак информативан приказ садржаја чланка који читаоцу омогућава да брзо и тачно оцени његову релевантност. У интересу је уредништава и аутора да сажетак садржи термине који се често користе за индексирање и претрагу чланака. Саставни делови сажетка су увод/циљ истраживања, методи, резултати и закључак. Сажетак треба да има од 100 до 250 речи и треба да се налази између заглавља (наслов, имена аутора и др.) и кључних речи, након којих следи текст чланка.

Кључне речи

Кључне речи су термини или фразе које адекватно представљају садржај чланка за потребе индексирања и претраживања. Треба их додељивати ослањајући се на неки међународни извор (попис, речник или тезаурус) који је најшире прихваћен или унутар дате научне области. За нпр. науку уопште, то је листа кључних речи Web of Science. Број кључних речи не може бити већи од 10, а у интересу је уредништва и аутора да учесталост њихове употребе буде што већа. Кључне речи дају се на језику на којем је написан чланак (сажетак) и на енглеском језику. У чланку се пишу непосредно након сажетка.

Систем АСИСТЕНТ у ту сврху користи специјалну алатку KWASS: аутоматско екстраховање кључних речи из дисциплинарних тезауруса/речника по избору и рутине за њихов одабир, тј. прихватање односно одбацивање од стране аутора и/или уредника.

Датум прихватања чланка

Датум када је уредништво примило чланак, датум када је уредништво коначно прихватило чланак за објављивање, као и датуми када су у међувремену

достављене евентуалне исправке рукописа наводе се хронолошким редоследом, на сталном месту, по правилу на крају чланка.

Захвалница

Назив и број пројекта, односно назив програма у оквиру којег је чланак настао, као и назив институције која је финансирала пројекат или програм, наводи се у посебној напомени на сталном месту, по правилу при дну прве стране чланка.

Претходне верзије рада

Ако је чланак у претходној верзији био изложен на скупу у виду усменог саопштења (под истим или сличним насловом), податак о томе треба да буде наведен у посебној напомени, по правилу при дну прве стране чланка. Рад који је већ објављен у неком часопису не може се објавити у Војнотехничком гласнику (прештампати), ни под сличним насловом и измењеном облику.

Табеларни и графички прикази

Пожељно је да наслови свих приказа, а по могућству и текстуални садржај, буду дати двојезично, на језику рада и на енглеском језику.

Табеле се пишу на исти начин као и текст, а означавају се редним бројевима са горње стране. Фотографије и цртежи треба да буду јасни, прегледни и погодни за репродукцију. Цртеже треба радити у програму word или corel. Фотографије и цртеже треба поставити на жељено место у тексту.

За слике и графиконе не сме се користити снимак са екрана рачунара програма за прикупљање података. У самом тексту чланка препоручује се употреба слика и графикона непосредно из програма за анализу података (као што су Excel, Matlab, Origin, SigmaPlot и други).

Навођење (цитирање) у тексту

Начин позивања на изворе у оквиру чланка мора бити једнообразан.

Војнотехнички гласник за референцирање (цитирање и навођење литературе) примењује Харвардски систем референци, односно Харвардски приручник за стил (Harvard Referencing System, Harvard Style Manual). У самом тексту, у обичним заградама, на месту на којем се врши позивање, односно цитирање литературе набројане на крају чланка, обавезно у обичној загради написати презиме цитираног аутора, годину издања публикације из које цитирате и, евентуално, број страница. Нпр. (Petrović, 2012, pp.10–12).

Детаљно упутство о начину цитирања, са примерима, дато је на страници сајта *Упутство за Харвардски приручник за стил*. Потребно је да се позивање на литературу у тексту уради у складу са поменутим упутством.

Систем АСИСТЕНТ у сврху контроле навођења (цитирања) у тексту користи специјалну алатку CiteMatcher: откривање изостављених цитата у тексту рада и у попису референци.

Напомене (фусноте)

Напомене се дају при дну стране на којој се налази текст на који се односе. Могу садржати мање важне детаље, допунска објашњења, назнаке о коришћеним изворима (на пример, научној грађи, приручницима), али не могу бити замена за цитирану литературу.

Листа референци (литература)

Цитирана литература обухвата, по правилу, библиографске изворе (чланке, монографије и сл.) и даје се искључиво у засебном одељку чланка, у виду листе референци. Референце се не преводе на језик рада и набрајају се у посебном одељку на крају чланка.

Војнотехнички гласник, као начин исписа литературе, примењује Харвардски систем референци, односно Харвардски приручник за стил (Harvard Referencing System, Harvard Style Manual).

Литература се обавезно пише на латиничном писму и набраја по абецедном редоследу, наводећи најпре презимена аутора, без нумерације.

Детаљно упутство о начину пописа референци, са примерима, дато је на страници сајта *Упутство за Харвардски приручник за стил*. Потребно је да се попис литературе на крају чланка уради у складу са поменутим упутством.

Нестандардно, непотпуно или недоследно навођење литературе у системима вредновања часописа сматра се довољним разлогом за оспоравање научног статуса часописа.

Систем АСИСТЕНТ у сврху контроле правилног исписа листе референци користи специјалну алатку RefFormatter: контрола обликовања референци у складу са Харвардским приручником за стил.

Изјава о ауторству

Поред чланка доставља се *Изјава о ауторству* у којој аутори наводе свој појединачни допринос у изради чланка. Такође, у тој изјави потврђују да су чланак урадили у складу са *Позивом и упутством ауторима* и *Изјавом о етичком поступању часописа*.

Сви радови подлежу стручној рецензији.

Списак рецензената Војнотехничког гласника може се видети на страници сајта *Списак рецензената*. Процес рецензирања објашњен је на страници сајта *Рецензентски поступак*.

Адреса редакције:
Војнотехнички гласник
Вељка Лукића Курјака 33
11042 Београд
e-mail: vojnotehnicki.glasnik@mod.gov.rs.

Главни и одговорни уредник
мр *Небојша* Гаћеша, дипл. инж.
nebojsa.gacesa@mod.gov.rs,
https://orcid.org/0000-0003-3217-6513,
тел: војни 40-260 (011/3603-260),
066/8700-123

ПРИГЛАШЕНИЕ И ИНСТРУКЦИЯ ДЛЯ АВТОРОВ О ПОРЯДКЕ ПОДГОТОВКИ СТАТЬИ

Инструкция для авторов о порядке подготовки статьи к опубликованию в журнале «Военно-технический вестник» разработана в соответствии с Актом о редактировании научных журналов Министерства науки и технологического развития Республики Сербия, № 110-00-17/2009-01 от 09.07.2009 г. Применение этого Акта способствует повышению качества отечественных журналов и их более полному вовлечению в международную систему обмена научной информацией. Инструкция соответствует международным стандартам ISO 4, ISO 8, ISO 18, ISO 215, ISO 214, ISO 18, ISO 690, ISO 690-2, ISO 999, ISO 5122 и соответствующим стандартам Республики Сербия.

Военно-технический вестник (**Vojnotehnički glasnik / Military Technical Courier**), втг.мо.упр.срб, www.vtg.mod.gov.rs/index-ru.html, ISSN 0042-8469 – печатное издание, e-ISSN 2217-4753 – online, UDK 623+355/359, DOI: 10.5937/VojnotehnickiGlasnik; https://doi.org/10.5937/VojnotehnickiGlasnik, является мультидисциплинарным научным журналом Министерства обороны и Вооруженных сил Республики Сербия.. В журнале публикуются научные и профессиональные статьи, исследующие такие области как: математика, компьютерные науки и механика, а также области технологического развития: электроника, телекоммуникации, информационные технологии, машиностроение, материалы и химические технологии, в журнале также публикуется: техническая информация о современных системах вооружения и современных военных технологиях. Журнал следит за единой межвидовой технической поддержкой вооруженных сил, основанной на принципах системной логистики, за прикладными и инновационными научными исследованиями, в том числе, в области производства вооружения и военной техники. В журнале публикуются и прочие теоретические и практические достижения, которые способствуют повышению квалификации представителей сербского, регионального и международного академического сообщества, особенно военнослужащих Министерства Обороны и Вооружённых сил.

Редакционная политика журнала «Военно-технический вестник» основана на рекомендациях Комитета по этике научных публикаций (COPE Core Practices), а также на лучшей практике в научно-издательской деятельности. «Военно-технический вестник» является членом COPE со 2 мая 2018 года.

Министерство образования, науки и технологического развития Республики Сербия, согласно решению принятому в соотвествии со ст. 27 абзац 1, пункт 4 и на основании толкования ст. 25 абзац 1 пункт 5 Закона о научно-исследовательской деятельности («Службени гласник РС», № 110/05, утвердило категоризацию «Военно-технического вестника» за 2019 год:

Категории в области технологического развития:

– Область электроники, телекоммуникаций и информационных технологий:

ведущий научный журнал национального значения **(M51)**,

– Область материалов и химической технологии:

научный журнал национального значения **(M52)**,

– Область механики:

научный журнал национального значения **(M52)**.

Категории в области основных исследований:

– Область математика, компьютерные науки, технические науки:

научный журнал **(M53)**.

С информацией относительно категоризации за 2019 год можно ознакомиться на странице сайта «Военно-технического вестника» *Категоризация Вестника* (Министерством просвещения, науки и технологического развития Республики Сербия пока не произведено официального ранжирования научных журналов за 2020 год).

Более подробную информацию можно найти на сайте Министерства образования, науки и технологического развития Республики Сербия.

С информацией о категоризации можно ознакомиться и на сайте КОБСОН (Консорциум библиотек Республики Сербия по вопросам объединения закупок).

Категоризация Вестника проведена согласно Положению о порядке и способе категоризации научно-исследовательских результатов, утверждённого Национальным комитетом по науке и технологиям (Службени гласник РС, № 38/2008).

В соответствии с вышеуказанным Положением и таблицей с показателями классификации и категоризации индивидуальных научно-исследовательских результатов, являющейся неотъемлемой частью Положения, научная статья, опубликованная в «Военно-техническом вестнике», оценивается следующим способом: 2 балла (категория М51), 1,5 балла (категория М52) и 1,5 балл (категория М53).

Журнал соответствует стандартам Сербского индекса научного цитирования (СЦИндекс/SCIndeks) – наукометрической базы данных научных журналов Республики Сербия, а также Российского индекса научного цитирования (РИНЦ). Журнал постоянно подвергается мониторингу и оценивается количественными наукометрическими показателями, отражающими его научную ценность, в т.ч. опосредованно в международных индексах цитирования (Clarivate Analytics).

С информацией об индексировании можно ознакомиться на странице сайта журнала *Индексирование Вестника*.

«Военно-технический вестник» обеспечивает читателям возможность открытого доступа, в соответствии с положениями об авторских правах, утверждёнными Creative Commons (CC BY). С инструкцией об авторских правах можно ознакомиться на странице *Авторские права и политика самоархивирования*, перейдя по ссылке http://www.vtg.mod.gov.rs/index-ru.html.

Рукописи статей направляются в редакцию журнала с использованием online системы ASSISTANT, запущенной Центром поддержи развития образования и науки (ЦПРОН).

Регистрация в системе и оформление прав доступа выполняется по адресу http://www.vtg.mod.gov.rs/index-ru.html, через страницу *ASSISTANT* или *СЦИНДЕКС* (aseestant.ceon.rs/index.php/vtg).

С инструкцией по регистрации и правам доступа можно ознакомиться по адресу http://www.vtg.mod.gov.rs/index-ru.html, на странице *Инструкция по ASSISTANT*.

Все авторы, предоставляющие свои рукописи для публикации в редакцию журнала «Военно-технический вестник» должны пройти предварительную регистрацию в реестре ORCID (Open Researcher and Contributor ID). Эта процедура осуществляется в соответствии с инструкцией, размещенной на странице сайта *Регистрация в реестре ORCID для присвоения идентификационного кода*.

«Военно-технический вестник» публикует статьи на сербском, русском или английском языках (Arial, шрифт 11 pt, пробел Single).

Процесс подготовки, написания и редактирования статьи должен осуществляться в соответствии с принципами *Этического кодекса* (http://www.vtg.mod.gov.rs/etichyeskiy-kodyeks.html).

Статья должна содержать резюме с ключевыми словами, введение, основную часть, выводы, список использованной литературы и резюме с ключевыми словами на английском языке (без нумерации заголовков и подзаголовков). Объём статьи не должен превышать один авторский лист (16 страниц формата А4 с пробелом Single).

Статья должна быть набрана на компьютере с использованием специально подготовленного редакцией макета, который можно скачать на странице сайта *Правила и образец составления статьи*.

Заголовок

Заголовок должен отражать тему статьи. В интересах журнала и автора необходимо использовать слова и словосочетания, удобные для индексации и поиска. Если такие слова не содержатся в заголовке, то желательно их добавить в подзаголовок. Заголовок должен быть переведён на английский язык. Название заголовка (подзаголовка) пишется перед резюме на соответствующем языке.

Текущий заголовок

Текущий заголовок пишется в титуле каждой страницы статьи с целью упрощения процесса идентификации, в первую очередь копий статьей в электронном виде. Заголовок содержит в себе фамилию и инициал имени автора (в случае если авторов несколько, остальные обозначаются с «et al.» или «и др.»), название работы и журнала (год, том, выпуск, начальная и заключительная страница). Заголовок статьи и название журнала могут быть приведены в сокращенном виде.

ФИО автора

Приводятся полная фамилия и полное имя (всех) авторов. Желательно, чтобы были указаны инициалы отчеств авторов. Фамилия и имя авторов из Республики Сербия всегда пишутся в оригинальном виде (с сербскими диакритическими знаками), независимо от языка, на котором написана работа.

Наименование учреждения автора (аффилиация)

Приводится полное (официальное) наименование и местонахождение учреждения, в котором работает автор, а также наименование учреждения, в котором автор провёл исследование. В случае организаций со сложной структурой приводится их иерархическая соподчинённость (напр. Военная академия, кафедра военных электронных систем, г. Белград). По крайней мере, одна из организаций в иерархии должна иметь статус юридического лица. В случае если указано несколько авторов, и если некоторые из них работают в одном учреждении, нужно отдельными обозначениями или каким-либо другим способом указать в каком из приведённых учреждений работает каждый из авторов. Аффилиация пишется непосредственно после ФИО автора. Должность и специальность по диплому не указываются.

Контактные данные

Электронный адрес автора указываются рядом с его именем на первой страницы статьи.

Категория (тип) статьи

Категоризация статьей является обязанностью редакции и имеет особое значение. Категорию статьи могут предлагать рецензенты и члены редакции, т.е.

редакторы рубрик, но ответственность за категоризацию несет исключительно главный редактор. Статьи в журнале распределяются по следующим категориям:

Научные статьи:

– оригинальная научная статья (работа, в которой приводятся ранее неопубликованные результаты собственных исследований, полученных научным методом);

– обзорная статья (работа, содержащая оригинальный, детальный и критический обзор исследуемой проблемы или области, в который автор внёс определённый вклад, видимый на основе автоцитат);

– краткое сообщение (оригинальная научная работа полного формата, но меньшего объёма или имеющая предварительный характер);

– научная критическая статья (дискуссия-полемика на определённую научную тему, основанная исключительно на научной аргументации) и научный комментарий.

Однако, в некоторых областях знаний научная работа в журнале может иметь форму монографического исследования, а также критического обсуждения научного материала (историко-архивного, лексикографического, библиографического, обзора данных и т.п.) – до сих пор неизвестного или недостаточно доступного для научных исследований. Работы, классифицированные в качестве научных, должны иметь, по меньшей мере, две положительные рецензии.

В случае если в журнале объявляются и приложения, не имеющие научный характер, научные статьи должны быть сгруппированы и четко выделены в первой части номера.

Профессиональные статьи:

– профессиональная работа (приложения, в которых предлагаются опыты, полезные для совершенствования профессиональной практики, но которые не должны в обязательном порядке быть обоснованы на научном методе);

– информативное приложение (передовая статья, комментарий и т.п.);

– обзор (книги, компьютерной программы, случая, научного события и т.п.).

Язык работы

Работа может быть написана на сербском, русском или английском языке.

Текст должен быть в лингвистическом и стилистическом смысле упорядочен, систематизирован, без сокращений (за исключением стандартных). Все физические величины должны соответствовать Международной системе единиц измерения – СИ. Очередность формул обозначается порядковыми номерами, проставляемыми с правой стороны в круглых скобках.

Резюме

Резюме является кратким информативным обзором содержания статьи, обеспечивающим читателю быстроту и точность оценки её релевантности. В интересах редакции и авторов, чтобы резюме содержало термины, часто используемые для индексирования и поиска статьей. Составными частями резюме являются введение/цель исследования, методы, результаты и выводы. В резюме должно быть от 100 до 250 слов, и оно должно находится между титулами (заголовок, ФИО авторов и др.) и ключевыми словами, за которыми следует текст статьи.

Ключевые слова

Ключевыми словами являются термины или фразы, адекватно представляющие содержание статьи, необходимые для индексирования и поиска. Ключевые слова необходимо выбирать, опираясь при этом на какой-либо международный источник (регистр, словарь, тезаурус), наиболее используемый внутри данной научной области. Число ключевых слов не может превышать 10. В интересах редакции и авторов, чтобы частота их встречи в статье была как можно большей. Ключевые слова даются на языке, на котором написана статья (резюме), и на английском языке. В статье они пишутся непосредственно после резюме.

Программа ASSISTANT предоставляет возможность использования сервиса KWASS, автоматически фиксирующего ключевые слова из источников/словарей по выбору автора/редактора.

Дата получения статьи

Дата, когда редакция получила статью; дата, когда редакция окончательно приняла статью к публикации; а также дата, когда были предоставлены необходимые исправления рукописи, приводятся в хронологическом порядке, как правило, в конце статьи.

Выражение благодарности

Наименование и номер проекта, т.е. название программы благодаря которой статья возникла, совместно с наименованием учреждения, которое финансировало проект или программу, приводятся в отдельном примечании, как правило, внизу первой страницы статьи.

Предыдущие версии работы

В случае если статья в предыдущей версии была изложена устно (под одинаковым или похожим названием, например, в виде доклада на научной конференции), сведения об этом должны быть указаны в отдельном примечании, как правило, внизу первой страницы статьи. Работа, которая уже была опубликована в каком-либо из журналов, не может быть напечатана в «Военно-техническом вестнике» ни под похожим названием, ни в изменённом виде.

Нумерация и название таблиц и графиков

Желательно, чтобы нумерация и название таблиц и графиков были исполнены на двух языках (на языке оригинала и на английском). Таблицы подписываются таким же способом как и текст и обозначаются порядковым номером с верхней стороны. Фотографии и рисунки должны быть понятны, наглядны и удобны для репродукции. Рисунки необходимо делать в программах Word или Corel. Фотографии и рисунки надо поставить на желаемое место в тексте. Для создания изображений и графиков использование функции снимка с экрана (скриншота) не допускается. В самом тексте статьи рекомендуется применение изображений и графиков, обработанных такими компьютерными программами, как: Excel, Matlab, Origin, SigmaPlot и др.

Ссылки (цитирование) в тексте

Оформление ссылок на источники в рамках статьи должно быть однообразным. «Военно-технический вестник» для оформления ссылок, цитат и списка использованной литературы применяет Гарвардскую систему (Harvard Referencing System, Harvard Style Manual). В тексте в скобках приводится фамилия цитируемого автора (или фамилия первого автора, если авторов несколько), год издания и по необходимости номер страницы. Например: (Petrović, 2010, pp.10-20). Рекомендации

о способе цитирования размещены на странице сайта *Инструкция по использованию Гарвардского стиля*. При оформлении ссылок, цитат и списка использованной литературы необходимо придерживаться установленных норм. Программа ASSISTANT предоставляет при цитировании возможность использования сервиса CiteMatcher, фиксирующего пропущенные цитаты в работе и в списке литературы.

Примечания (сноски)

Примечания (сноски) к тексту указываются внизу страницы, к которой они относятся. Примечания могут содержать менее важные детали, дополнительные объяснения, указания об использованных источниках (напр. научном материале, справочниках), но не могут быть заменой процедуры цитирования литературы.

Литература (референции)

Цитированной литературой охватываются, как правило, такие библиографические источники как статьи, монографии и т.п. Вся используемая литература в виде референций размещается в отдельном разделе статьи.

Названия литературных источников не переводятся на язык работы.

«Военно-технический вестник» для оформления списка использованной литературы применяет Гарвардскую систему (Harvard Style Manual). В списке литературы источники указываются в алфавитном порядке фамилий авторов или редакторов. Рекомендации о способе цитирования размещены на странице сайта *Инструкция по использованию Гарвардского стиля*. При оформлении списка использованной литературы необходимо придерживаться установленных норм.

При оформлении списка литературы программа ASSISTANT предоставляет возможность использования сервиса RefFormatter, осуществляющего контроль оформления списка литературы в соответствии со стандартами Гарвардского стиля.

Нестандартное, неполное и непоследовательное приведение литературы в системах оценки журнала считается достаточной причиной для оспаривания научного статуса журнала.

Авторское заявление

Авторское заявление предоставляется вместе со статьей, в нем авторы заявляют о своем личном вкладе в написание статьи. В заявлении авторы подтверждают, что статья написана в соответствии с *Приглашением и инструкциями для авторов*, а также с *Кодексом профессиональной этики журнала*.

Все рукописи статей подлежат профессиональному рецензированию.

Список рецензентов журнала «Военно-технический вестник» размещён на странице сайта *Список рецензентов*. Процесс рецензирования описан в разделе *Правила рецензирования*.

Почтовый адрес редакции:
«Војнотехнички гласник»
ул. Велька Лукича Куряка 33
11042 Белград, Республика Сербия
e-mail: vojnotehnicki.glasnik@mod.gov.rs.

Главный и ответственный редактор
Кандидат технических наук *Небойша* Гачеша
nebojsa.gacesa@mod.gov.rs
https://orcid.org/0000-0003-3217-6513
тел: +381 11 3603 260, +381 66 8700 123

CALL FOR PAPERS AND ARTICLE FORMATTING INSTRUCTIONS

The instructions to authors about the article preparation for publication in the *Military Technical Courier* are based on the Act on scientific journal editing of the Ministry of Science and Technological Development of the Republic of Serbia, No 110-00-17/2009-01 of 9th July 2009. This Act aims at improving the quality of national journals and raising the level of their compliance with the international system of scientific information exchange. It is based on international standards ISO 4, ISO 8, ISO 18, ISO 215, ISO 214, ISO 18, ISO 690, ISO 690-2, ISO 999 and ISO 5122 and their national equivalents.

The Military Technical Courier / Vojnotehnički glasnik (www.vtg.mod.gov.rs/index-e.html, втг.мо.упр.срб, ISSN 0042-8469 – print issue, e-ISSN 2217-4753 – online, UDC 623+355/359, DOI: 10.5937/VojnotehnickiGlasnik; https://doi.org/10.5937/VojnotehnickiGlasnik) is a multidisciplinary scientific journal of the Ministry of Defence and the Serbian Armed Forces. The journal publishes scientific and professional papers covering fundamental research (mathematics, computer science and mechanics) and technological development (electronics, telecommunications, information technologies, mechanical engineering, material science and chemical technologies) as well as technical data on modern weapon systems and military technologies. The journal covers inter-service technical support to the Army on the principle of logistic system support; fundamental, applied and development research; production and use of weapons and military equipment. Also, the journal publishes other theoretical and practical achievements leading to professional development of all members of Serbian, regional and international academic communities as well as members of the military and ministries of defence in particular.

The editorial policy of the Military Technical Courier is based on the COPE Core Practices and the journal articles are consistent with accepted best practices in their subject areas. As of 2 May 2018, the Military Technical Courier is a member of COPE (Committee on Publication Ethics).

Pursuant to the decision given in Article 27, paragraph 1, point 4, and in accordance with the acquired opinion given in Article 25, paragraph 1, point 5 of the Act on Scientific and Research Activities (Official Gazette of the Republic of Serbia, No 110/05, 50/06-cor and 18/10), the Ministry of Education, Science and Technological Development of the Republic of Serbia classified the Military Technical Courier for the year 2019

in the field technological development:
– on the list of periodicals for electronics, telecommunications and IT,
category: leading scientific periodical of national interest **(M51)**,
– on the list of periodicals for materials and chemical technology,
category: scientific periodical of national interest **(M52)**,
– on the list of periodicals for mechanical engineering,
category: scientific periodical of national interest **(M52)**,
in the field fundamental research:
– on the list of periodicals for mathematics, computer sciences and mechanics,
category: scientific periodical **(M53)**.

The approved lists of national periodicals for the year 2019 can be viewed on the website of the Military Technical Courier, page *Journal categorization* (The Ministry of Education, Science and Technological Development of the Republic of Serbia has not yet published the official evaluation of scientific journals for 2020).

More detailed information can be found on the website of the Ministry of Education, Science and Technological Development of the Republic of Serbia.

The information on the categorization can be also found on the website of KOBSON (Consortium of Libraries of Serbia for Unified Acquisition).

The periodical is categorized in compliance with the Regulations on the procedure and method of evaluation and quantitative formulation of scientific and research results of researchers, stipulated by the National Council for Scientific and Technological Development (*Official Gazette of RS*, No 38/2008). More detailed information can be found on the website of the Ministry of Education, Science and Technological Development.

In accordance with the Regulations and the table about types and quantification of individual scientific and research results (as a part of the Regulations), a paper published in the *Military Technical Courier* scores 2 (two) points (category M51), 1,5 (one and a half) point (category M52) and 1 (one) point (category M53).

The journal is in the Serbian Citation Index – SCIndex (data base of national scientific journals), in the Russian Index of Science Citation/Российский индекс научного цитирования (RINC/РИНЦ) and is constantly monitored depending on the impact within the bases themselves and indirectly in the international (e.g. Clarivate Analytics) citation indexes. More detailed information can be viewed on the website of the Military Technical Courier, page *Journal indexing*.

Manuscripts are submitted online, through the electronic editing system ASSISTANT, developed by the Center for Evaluation in Education and Science – CEON.

The access and the registration are through the Military Technical Courier site http://www.vtg.mod.gov.rs/index-e.html, on the page *ASSISTANT* or the page *SCINDEKS* or directly through the link (aseestant.ceon.rs/index.php/vtg).

The detailed instructions about the registration for the service are on the website http://www.vtg.mod.gov.rs/index-e.html, on the page *Instructions for ASSISTANT*.

All authors submitting a manuscript for publishing in the Military Technical Courier should register for an ORCID ID following the instructions on the web page *Registration for an ORCID identifier*.

The Military Technical Courier publishes articles in Serbian, Russian or English, using Arial and a font size of 11pt with Single Spacing.

The procedures of article preparation, writing and editing should be in accordance with the *Publication ethics statement* (http://www.vtg.mod.gov.rs/publication-ethics-statement.html).

The article should contain the abstract with keywords, introduction, body, conclusion and references (without heading and subheading enumeration). The article length should not exceed 24 pages of A4 paper format.

The article should be formatted following the instructions in the Article Form which can be downloaded from website page *Article form*.

Title

The title should be informative. It is in both Journal's and author's best interest to use terms suitable for indexing and word search. If there are no such terms in the title, the author is strongly advised to add a subtitle. The title should be given in English as well.

The titles precede the abstract and the summary in an appropriate language.

Letterhead title

The letterhead title is given at a top of each page for easier identification of article copies in an electronic form in particular. It contains the author's surname and first name initial (for multiple authors add "et al"), article title, journal title and collation (year, volume, issue, first and last page). The journal and article titles can be given in a shortened form.

Author's name

Full name(s) of author(s) should be used. It is advisable to give the middle initial. Names are given in their original form (with diacritic signs if in Serbian).

Author's affiliation

The full official name and seat of the author's affiliation is given, possibly with the name of the institution where the research was carried out. For organizations with complex structures, give the whole hierarchy (for example, University of Defence in Belgrade, Military Academy, Department for Military Electronic Systems). At least one organization in the hierarchy must be a legal entity. When some of multiple authors have the same affiliation, it must be clearly stated, by special signs or in other way, which department exactly they are affiliated with. The affiliation follows the author's name. The function and title are not given.

Contact details

The postal addresses or the e-mail addresses of the authors are given in the first page.

Type of articles

Classification of articles is a duty of the editorial staff and is of special importance. Referees and the members of the editorial staff, or section editors, can propose a category, but the editor-in-chief has the sole responsibility for their classification.

Journal articles are classified as follows:

Scientific articles:

– Original scientific papers (giving the previously unpublished results of the author's own research based on scientific methods);

– Review papers (giving an original, detailed and critical view of a research problem or an area to which the author has made a contribution demonstrated by self-citation);

– Short communications or Preliminary communications (original scientific full papers but shorter or of a preliminary character);

– Scientific commentaries or discussions (discussions on a particular scientific topic, based exclusively on scientific argumentation) and opinion pieces.

Exceptionally, in particular areas, a scientific paper in the Journal can be in a form of a monograph or a critical edition of scientific data (historical, archival, lexicographic, bibliographic, data survey, etc.) which were unknown or hardly accessible for scientific research.

Papers classified as scientific must have at least two positive reviews.

If the journal contains non-scientific contributions as well, the section with scientific papers should be clearly denoted in the first part of the Journal.

Professional articles:

– Professional papers (contributions offering experience useful for improvement of professional practice but not necessarily based on scientific methods);

– Informative contributions (editorial, commentary, etc.);

– Reviews (of a book, software, case study, scientific event, etc.)

Language

The article can be in Serbian, Russian or English.

The grammar and style of the article should be of good quality. The systematized text should be without abbreviations (except standard ones). All measurements must be in SI units. The sequence of formulae is denoted in Arabic numerals in parentheses on the right-hand side.

Abstract and summary

An abstract is a concise informative presentation of the article content for fast and accurate evaluation of its relevance. It contains the terms often used for indexing and article search. A 100- to 250-word abstract has the following parts: introduction/purpose of the research, methods, results and conclusion.

Keywords

Keywords are terms or phrases showing adequately the article content for indexing and search purposes. They should be allocated heaving in mind widely accepted international sources (index, dictionary or thesaurus), such as the Web of Science keyword list for science in general. The higher their usage frequency is, the better. Up to 10 keywords immediately follow the abstract and the summary, in respective languages.

For this purpose, the ASSISTANT system uses a special tool KWASS for the automatic extraction of key words from disciplinary thesauruses/dictionaries by choice and the routine for their selection, i.e. acceptance or rejection by author and/or editor.

Article acceptance date

The date of the reception of the article, the dates of submitted corrections in the manuscript (optional) and the date when the Editorial Board accepted the article for publication are all given in a chronological order at the end of the article.

Acknowledgements

The name and the number of the project or programme within which the article was realised is given in a separate note at the bottom of the first page together with the name of the institution which financially supported the project or programme.

Article preliminary version

If an article preliminary version has appeared previously at a meeting in a form of an oral presentation (under the same or similar title), this should be stated in a separate note at the bottom of the first page. An article published previously cannot be published in the *Military Technical Courier* even under a similar title or in a changed form.

Tables and illustrations

All the captions should be in the original language as well as in English, together with the texts in illustrations if possible. Tables are typed in the same style as the text and are denoted by Arabic numerals at the top. Photographs and drawings, placed appropriately in the text, should be clear, precise and suitable for reproduction. Drawings should be created in Word or Corel.

For figures and graphs, proper data plot is recommended i.e. using a data analysis program such as Excel, Matlab, Origin, SigmaPlot, etc. It is not recommended to use a screen capture of a data acquisition program as a figure or a graph.

Citation in the text

Citation in the text must be uniform. The Military Technical Courier applies the Harvard Referencing System given in the Harvard Style Manual. When citing sources within your paper, i.e. for in-text references of the works listed at the end of the paper, place the year of publication of the work in parentheses and optionally the number of the page(s) after the author's name, e.g. (Petrovic, 2012, pp.10-12). A detailed guide on citing, with examples, can be found on Military Technical Courier website on the page *Instructions for Harvard Style Manual*. In-text citations should follow its guidelines.

For checking in-text citations, the ASSISTANT system uses a special tool CiteMatcher to find out quotes left out within papers and in reference lists.

Footnotes

Footnotes are given at the bottom of the page with the text they refer to. They can contain less relevant details, additional explanations or used sources (e.g. scientific material, manuals). They cannot replace the cited literature.

Reference list (Literature)

The cited literature encompasses bibliographic sources such as articles and monographs and is given in a separate section in a form of a reference list.

References are not translated to the language of the article.

In compiling the reference list and bibliography, the Military Technical Courier applies the Harvard System – Harvard Style Manual. All bibliography items should be listed alphabetically by author's name, without numeration. A detailed guide for listing references, with examples, can be found on Military Technical Courier website on the page *Instructions for Harvard Style Manual*. Reference lists at the end of papers should follow its guidelines.

In journal evaluation systems, non-standard, insufficient or inconsequent citation is considered to be a sufficient cause for denying the scientific status to a journal.

Authorship Statement

The Authorship statement, submitted together with the paper, states authors' individual contributions to the creation of the paper. In this statement, the authors also confirm that they followed the guidelines given in *the Call for papers* and the *Publication ethics and malpractice statement of the journal*.

All articles are peer reviewed.

The list of referees of the Military Technical Courier can be viewed at website page *List of referees*. The article review process is described on the *Peer Review Process* page of the website.

Address of the Editorial Office:
Vojnotehnički glasnik / Military Technical Courier
Veljka Lukića Kurjaka 33
11042 Belgrade, Republic of Serbia
e-mail: vojnotehnicki.glasnik@mod.gov.rs.

Editor in chief
Nebojša Gaćeša MSc
nebojsa.gacesa@mod.gov.rs
https://orcid.org/0000-0003-3217-6513
tel.: +381 11 3603 260, +381 66 8700 123

ОБАВЕШТЕЊА САРАДНИЦИМА И ЧИТАОЦИМА
СООБЩЕНИЯ ДЛЯ АВТОРОВ И ЧИТАТЕЛЕЙ
INFORMATION FOR CONTRIBUTORS AND READERS

Додељена признања најбољим рецензентима за 2020.

Српски цитатни индекс завршио је вредновање рецензената за 2020. годину. Свечана додела награде и признања најбољим рецензентима одржана је у просторијама ЦЕОН-а у Београду, у петак, 25. септембра. Извештај о томе доступан је сајту ЦЕОН-а на страници https://www.ceon.rs/index.php?option=com_content&view=article&id=630&catid=114&Itemid=482&lang=sr.

Војнотехнички гласник са задовољством истиче да је наш дугогодишњи члан уређивачког одбора и рецензент др Срећко Стопић добио признање као истакнути рецензент за област инжењерства и технологије.

ЦЕОН подсећа да се за избор носилаца признања према Правилнику (https://www.ceon.rs/images/pdf/RR_pravilnik_sr.pdf) не расписује посебан конкурс, већ у њему учествују сви они који рецензирају рукописе приспеле на објављивање у око стотину СЦИндекс часописа који се уређују онлајн посредством платформе СЦИндекс Асистент.

ЦЕОН ће и у будућности настојати да програм вредновања и награђивања рецензената учини још успешнијим.

Вручение наград за лучшую работу рецензентов за 2020 год

Сербский индекс научного цитирования завершил оценку работы рецензентов за 2020 год. Торжественная церемония вручения наград за лучшую работу рецензентов состоялась в помещениях ЦЕОН в Белграде в пятницу 25 сентября 2020 года. С более подробной информацией можно ознакомиться на сайте ЦЕОН на странице https://www.ceon.rs/index.php?option=com_content&view=article&id=631:2020-award-and-acknowledgments-for-the-best-reviewers&catid=170&lang=en&Itemid=574.

Редакция журнала «Военно-технический вестник» с удовольствием отмечает, что постоянный член нашего Редакционного совета и рецензент Сречко Стопич был признан выдающимся рецензентом в областях: инженерное дело и технологии.

ЦЕОН напоминает, что в соответствии с Регламентом (https://www.ceon.rs/images/pdf/RR_pravilnik_sr.pdf) при выборе лучшего рецензента не проводится специальный конкурс, в нем участвуют все

рецензенты рукописей, поступивших к публикации в журналах, охватываемых СИНЦ Ассистент.

ЦЕОН и впредь будет совершенствовать программу оценивания и награждения рецензентов.

2020 Award and acknowledgments for the best reviewers

The Serbian citation index has completed the evaluation of reviewers for 2020. The award ceremony for the best reviewers was held at the CEON office in Belgrade, on Friday, September 25. The report is available on the CEON website on the page https://www.ceon.rs/index.php?option=com_content&view=article&id=631:2020-award-and-acknowledgments-for-the-best-reviewers&catid=170&lang=en&Itemid=574.

The Military Technical Courier is pleased to point out that our longtime member of the editorial board and reviewer Dr. Srećko Stopić received recognition as an outstanding reviewer in the field of engineering and technology.

CEON emphasizes that there are no special calls for nominations for the award according to their Rulebook (https://www.ceon.rs/images/pdf/RR_pravilnik_sr.pdf), but all those who review manuscripts submitted for publication in about one hundred of SCIndeks journals edited online through the platform SCIndeks Assistant are eligible to be nominees.

CEON will continue to strive to make the reviewer evaluation and reward program even more successful.

Ликовно-графички уредник
мр *Небојша* Кујунџић,
e-mail: nebojsa.kujundzic@mod.gov.rs

Техничко уређење
мр *Небојша* Гаћеша, e-mail: nebojsa.gacesa@mod.gov.rs,
https://orcid.org/0000-0003-3217-6513

Лектор
Добрила Милетић, професор,
e-mail: miletic.dobrila@gmail.com

Превод на енглески
Јасна Вишњић, професор,
e-mail: jasnavisnjic@yahoo.com, https://orcid.org/0000-0003-1728-4743

Превод на руски
др Карина Авагјан,
e-mail: karinka2576@mail.ru

Превод на немачки
Гордана Богдановић
e-mail: gordana.bogdanovic@yahoo.com

Превод на француски
Драган Вучковић,
e-mail: draganvuckovic64@gmail.com, https://orcid.org/0000-0003-1620-5601

ЦИП – Каталогизација у публикацији:
Народна библиотека Србије, Београд

623+355 / 359
355 / 359

ВОЈНОТЕХНИЧКИ гласник : научни часопис Министарства одбране Републике Србије = Military Technical Courier : scientific periodical of the Ministry of Defence of the Republic of Serbia / одговорни уредник Небојша Гаћеша. - Год. 1, бр. 1 (1953) - - Београд (Браће Југовића 19) : Министарство одбране Републике Србије, 1953- (Београд : Војна штампарија). - 24 cm

Доступно и на: http://www.vtg.mod.gov.rs
Тромесечно. - Друго издање на другом медијуму: Vojnotehnički glasnik (Online) = ISSN 2217-4753
ISSN 0042-8469 = Војнотехнички гласник
COBISS.SR-ID 4423938

Цена: 600,00 динара,
Тираж: 100 примерака

На основу мишљења Министарства за науку, технологију и развој Републике Србије, број 413-00-1201/2001-01 од 12. 9. 2001. године,
часопис „Војнотехнички гласник“ је публикација од посебног интереса за науку.

УДК: Народна библиотека Србије, Београд

Художественный редактор
Магистр дизайна, *Небойша* Куюнджич,
e-mail: nebojsa.kujundzic@mod.gov.rs

Технический редактор
Кандидат технических наук *Небойша* Гачеша, e-mail: nebojsa.gacesa@mod.gov.rs,
https://orcid.org/0000-0003-3217-6513

Корректор
Добрила Милетич,
e-mail: miletic.dobrila@gmail.com

Перевод на английский язык
Ясна Вишнич,
e-mail: jasnavisnjic@yahoo.com, https://orcid.org/0000-0003-1728-4743

Перевод на русский язык
Д.филол.н. *Карина* Кареновна Авагян,
e-mail: karinka2576@mail.ru

Перевод на немецкий язык
Гордана Богданович,
e-mail: gordana.bogdanovic@yahoo.com

Перевод на французский язык
Драган Вучкович,
e-mail: draganvuckovic64@gmail.com, https://orcid.org/0000-0003-1620-5601

CIP – Каталогизация в публикации: Национальная библиотека Сербии, г. Белград

623+355 / 359
355 / 359

ВОЕННО-ТЕХНИЧЕСКИЙ вестник: научный журнал
Министерства обороны Республики Сербия=
Military Technical Courier : scientific
periodical of the Ministry of Defence of the
Republic of Serbia / главный редактор
Небойша Гачеша. – Первый выпуск (1953) –
г. Белград (ул. Браче Юговича, д. 19): Министерство
обороны Республики Сербия, 1953- (Белград:
Военная типография). - 24 см
Размещено на сайте:
http://www.vtg.mod.gov.rs
Ежеквартально - Издание в электронном виде:
Военно-технический вестник (Online) = ISSN2217-4753
ISSN 0042-8469 = Военно-технический вестник
COBISS.SR-ID 4423938

Цена: 600,00 динаров
Тираж: 100 экземпляров

На основании решения Министерства науки и технологий Республики Сербия,
№ 413-00-1201/2001-01 от 12. 9. 2001 года, журнал «Военно-технический вестник»
объявлен изданием, имеющим особое значение для науки.

УДК: Национальная библиотека Сербии, г. Белград

Graphic design editor
Nebojša Kujundžić MA,
e-mail: nebojsa.kujundzic@mod.gov.rs

Copy editing
Nebojša Gaćeša MSc, e-mail: nebojsa.gacesa@mod.gov.rs,
https://orcid.org/0000-0003-3217-6513

Proofreader
Dobrila Miletić BA,
e-mail: miletic.dobrila@gmail.com

English translation and polishing
Jasna Višnjić BA,
e-mail: jasnavisnjic@yahoo.com, https://orcid.org/0000-0003-1728-4743

Russian translation and polishing
Karina Avagyan PhD,
e-mail: karinka2576@mail.ru

German translation and polishing
Gordana Bogdanović,
e-mail: gordana.bogdanovic@yahoo.com

French translation and polishing
Dragan Vučković,
e-mail: draganvuckovic64@gmail.com, https://orcid.org/0000-0003-1620-5601

CIP – Catalogisation in the publication: National Library of Serbia, Belgrade

623+355 / 359
355 / 359

ВОЈНОТЕХНИЧКИ гласник : научни часопис Министарства одбране Републике Србије = Military Technical Courier : scientific periodical of the Ministry of Defence of the Republic of Serbia / одговорни уредник Небојша Гаћеша. - Год. 1, бр. 1 (1953) - - Београд (Браће Југовића 19) : Министарство одбране Републике Србије, 1953-(Београд : Војна штампарија). - 24 cm

Доступно и на:
http://www.vtg.mod.gov.rs
Тромесечно. - Друго издање на другом медијуму:
Vojnotehnički glasnik (Online) = ISSN 2217-4753
ISSN 0042-8469 = Војнотехнички гласник
COBISS.SR-ID 4423938

Price: 600.00 RSD
Printed in 100 copies

According to the Opinion of the Ministry of Science and Technological Development No 413-00-1201/2001-01 of 12th September 2001, the *Military Technical Courier* is a publication of special interest for science.

UDC: National Library of Serbia, Belgrade

ГОДИНА

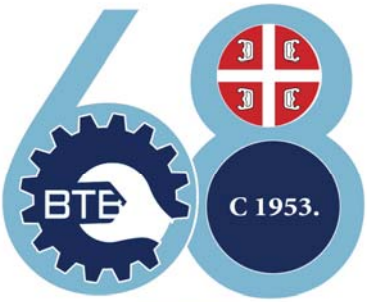

ЛЕТ

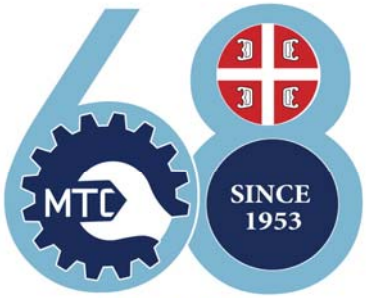

YEARS